Vol. 129, August 1, 1981
Complete in one issue

ISSN 0003-2670

ANALYTICA CHIMICA ACTA

International journal devoted to all branches of analytical chemistry

ELSEVIER SCIENTIFIC PUBLISHING COMPANY

ANALYTICA CHIMICA ACTA

International journal devoted to all branches of analytical chemistry
Revue internationale consacrée à tous les domaines de la chimie analytique
Internationale Zeitschrift für alle Gebiete der analytischen Chemie

PUBLICATION SCHEDULE FOR 1981 (incorporating the section on Computer Techniques and Optimization).

	J	F	M	A	M	J	J	A	S	O	N	D
Analytica Chimica Acta	123	124/1	124/2	125	126	127	128	129	130/1	130/2	131	132
Section on Computer Techniques and Optimization		133/1			133/2			133/3			133/4	

Scope. *Analytica Chimica Acta* publishes original papers, short communications, and reviews dealing with every aspect of modern chemical analysis, both fundamental and applied. The section on *Computer Techniques and Optimization* is devoted to new developments in chemical analysis by the application of computer techniques and by interdisciplinary approaches, including statistics, systems theory and operation research. The section deals with the following topics: Computerized acquisition, processing and evaluation of data. Computerized methods for the interpretation of analytical data including chemometrics, cluster analysis, and pattern recognition. Storage and retrieval systems. Optimization procedures and their application. Automated analysis for industrial processes and quality control. Organizational problems.

Submission of Papers. Manuscripts (three copies) should be submitted as designated below for rapid and efficient handling:

Papers from the Americas to: Professor Harry L. Pardue, Department of Chemistry, Purdue University, West Lafayette, IN 47907, U.S.A.

Papers from all other countries to: Dr. A. M. G. Macdonald, Department of Chemistry, The University, P.O. Box 363, Birmingham B15 2TT, England.

For the section on *Computer Techniques and Optimization:* Dr. J. T. Clerc, Universität Bern, Pharmazeutisches Institut, Sahlistrasse 10, CH-3012 Bern, Switzerland.

American authors are recommended to send manuscripts and proofs by INTERNATIONAL AIRMAIL.

Submission of an article is understood to imply that the article is original and unpublished and is not being considered for publication elsewhere. Upon acceptance of an article by the journal, the author(s) resident in the U.S.A. will be asked to transfer the copyright of the article to the publisher. This transfer will ensure the widest dissemination of information under the U.S. Copyright Law.

Information for Authors. Papers in English, French and German are published. There are no page charges. Manuscripts should conform in layout and style to the papers published in this Volume. Authors should consult Vol. 121, p. 353 for detailed information. Reprints of this information are available from the Editors or from: Elsevier Editorial Services Ltd., Mayfield House, 256 Banbury Road, Oxford OX2 7DE (Great Britain).

Reprints. Fifty reprints will be supplied free of charge. Additional reprints (minimum 100) can be ordered. An order form containing price quotations will be sent to the authors together with the proofs of their article.

Advertisements. Advertisement rates are available from the publisher.

Subscriptions. Subscriptions should be sent to: Elsevier Scientific Publishing Company, P.O. Box 211, 1000 AE Amsterdam, The Netherlands. The section on *Computer Techniques and Optimization* can be subscribed to separately.

Publication. *Analytica Chimica Acta* (including the section on *Computer Techniques and Optimization*) appears in 11 volumes in 1981. The subscription for 1981 (Vols. 123–133) is Dfl. 1639.00 plus Dfl. 198.000 (postage) (total approx. U.S. $942.00). The subscription for the *Computer Techniques and Optimization* section only (Vol. 133) is Dfl. 149.00 plus Dfl. 18.00 (postage) (total approx. U.S. $89.00). Journals are sent automatically by airmail to the U.S.A. and Canada at no extra cost and to Japan, Australia and New Zealand for a small additional postal charge. All earlier volumes (Vols. 1–121) except Vols. 23 and 28 are available at Dfl. 164.00 (U.S. $84.00), plus Dfl. 13.00 (U.S. $6.50) postage and handling, per volume.

Claims for issues not received should be made within three months of publication of the issue, otherwise they cannot be honoured free of charge.

Customers in the U.S.A. and Canada who wish to obtain additional bibliographic information on this and other Elsevier journals should contact Elsevier/North Holland Inc., Journal Information Center, 52 Vanderbilt Avenue, New York, NY 10017. Tel: (212) 867-9040.

More and more primary literature? Less and less time to read it?

take TrAC

trends in analytical chemistry

A monthly publication of short, critical reviews and news on trends and developments in analytical chemistry

How much better informed you could be if only you had the time to keep up with the latest developments.

Time we cannot give you, but we can give you concise, critical information on what is going on in the analytical sciences. Every month, as it happens.

It's all in TrAC – Trends in Analytical Chemistry – new for the 1980's from Elsevier and yours now at a low introductory rate.

Introductory Offer

SIXTEEN ISSUES FOR THE PRICE OF TWELVE!

Volume 1 – 1981/82 – of **Trends in Analytical Chemistry** will have sixteen issues: March 1981 and monthly from October 1981 to December 1982. Order the **Personal Edition** before December 1981 and receive all sixteen issues for US $42.50 (USA and Canada), £20.00 (UK), 91.50 Dutch guilders (Europe), 95.50 Dutch guilders (elsewhere). Or order the **Library Edition** for US $133.25 or 260.00 Dutch guilders throughout the world.

All issues of both editions are sent by air worldwide.

*) The Dutch guilder price is definitive.

Take just a minute to order either edition now – you will enjoy the time it saves you later.

ELSEVIER

TrAC is your opportunity to learn from researchers in related fields, to get first-hand, detailed reports on important developments in methodology and instrumentation. **TrAC** brings you current information on trends and techniques from laboratories all over the world.

Lab managers will find in **TrAC** evaluations of new methods and techniques which will enable them to make better-informed purchasing decisions. As a training aid **TrAC** is more up-to-date than any textbook.

TrAC is written in clear, jargon-free language, avoiding highly specialized terminology and provides you with a working knowledge of related methodology and techniques.

In every issue you will find:

- **short critical reviews written for an interdisciplinary audience**
- **feature articles**
- **insights into the function, organization and operation of industrial, government or research laboratories**
- **news on topics of general interest**
- **teaching aids – TrAC is more up-to-date than any textbook**
- **articles on the history of analytical chemistry**
- **reports on meetings and book reviews**

Trends in Analytical Chemistry comes in either the monthly **Personal Edition** or the special **Library Edition** which includes the monthly issues plus a hardbound volume containing all the review articles published over the year and indexed for easy retrieval.

Order Form

Special Introductory Offer for the Personal Edition valid until December 31, 1981

To **ELSEVIER Dept. TrAC. AP**

P.O. Box 330
1000 AH Amsterdam
The Netherlands

52 Vanderbilt Avenue
New York, NY 10017

US residents may call (212) 867 9040 and charge their American Express, Master Charge or Visa/Bankamericard account

Yes! Please enter my subscription now – Volume 1 – 1981/82

☐ Personal Edition ☐ Library Edition

I enclose my ☐ personal cheque ☐ bankcheque

Orders from individual subscribers must be prepaid.

☐ Please send me a free sample copy first.

Name: Position: Date:

Address:

City: State: Postal Code

7198

New Horizons in Catalysis

Proceedings of the 7th International Congress on Catalysis, Tokyo, Japan, 30 June – 4 July, 1980

edited by T. SEIYAMA, *Kyushu University and* K. TANABE, *Hokkaido University, Japan*

STUDIES IN SURFACE SCIENCE AND CATALYSIS 7

Unparalleled interest in the science and technology of catalysis has arisen largely due to the essential role of catalysts in pollution control, the use of natural resources and the problems of energy conservation. This quadrennial conference attracted over 1000 delegates from 38 countries and during the course of the meeting 5 plenary lectures, 101 contributed papers and 63 communications were presented with the result that the range of topics covered was as wide as the science of catalysis itself.

In two volumes the text comprises the complete manuscripts, comments and responses, emerging as an invaluable guide to the results of much illuminating research leading directly to developments not only in fundamental theory and understanding of heterogeneous catalysts, but also in the application of catalysis in industry. At a time when catalysis is so vitally important, these proceedings provide a most thorough and comprehensive survey of, for example, catalyst design and preparation, and the development of new catalytic processes of technological importance. The studies encompass a broad variety of adsorption and catalysis by metals, alloys, metal oxides, zeolites and supported catalysts, with many examples of various surface science techniques which have been successfully applied to energy related subjects. Arguably the world's foremost conference on catalysis, these volumes will be essential in libraries and all research laboratories seriously concerned with catalysis research.

CONTENTS: **Plenary Lectures.** Molecular Shape Selective Catalysis *(P. B. Weisz)*. Surface Science and Catalysis *(G. Ertl)*. Coordination Chemistry of Metal Surfaces and Metal Complexes *(E. L. Muetterties)*. Recent Progress in Elucidating the Mechanism of Heterogeneous Catalysis *(K. Tamaru)*. Anchored Complexes in Fundamental Catalytic Research *(Y. I. Yermakov)*.

1981 1586 pages
(in 2 volumes)
US $170.75 / Dfl. 350.00
D-444-99750-4

P.O. Box 211,
1000 AE Amsterdam,
The Netherlands.

52 Vanderbilt Ave.,
New York. N.Y. 10017.

The Dutch guilder price is definitive US $ prices are subject to exchange rate fluctuations.

ELSEVIER

ANALYTICA CHIMICA ACTA
VOL. 129 (1981)

ANALYTICA CHIMICA ACTA

International journal devoted to all branches of analytical chemistry

ELSEVIER SCIENTIFIC PUBLISHING COMPANY

Anal. Chim. Acta, Vol. 129 (1981)

Analytica Chimica Acta, 129 (1981) 1—17
Elsevier Scientific Publishing Company, Amsterdam — Printed in The Netherlands

THE PRINCIPLES AND THEORY OF HIGH-SPEED TITRATIONS BY FLOW INJECTION ANALYSIS

A. U. RAMSING, J. RŮŽIČKA* and E. H. HANSEN

The Technical University of Denmark, Chemistry Department A, Building 207, DK-2800 Lyngby (Denmark)

(Received 11th March 1981)

SUMMARY

The highly reproducible concentration gradients formed between an injected sample zone and the carrier stream in flow injection analysis are exploited for titrations based on measuring the time span between points of identical gradient dispersion. Comparison of the experimental data with theoretical models, has made it possible to locate the position and physical dimension of a single mixing stage, which at medium dispersion of the sample zone allows the entire titration cycle, including sampling and washout periods, to be completed within less than 30 s. The capability of this high-speed titration technique is demonstrated for acid—base, complexometric and iodimetric titration procedures.

The importance of controlling the dispersion of a sample zone in a system for flow injection analysis (f.i.a.) is now well recognized [1]. Depending on the type of system to be automated, the use of limited, medium or large dispersion has been suggested [2]. The dispersion (D) has been defined as the ratio of the original sample concentration C^0 to the concentration of the dispersed sample zone in that section of the carrier solution from which the analytical readout is being taken

$$D = C^0/C^{max} \quad \text{and} \quad D_g = C^0/C^{grad} \qquad (1\,a, b)$$

Here, C^{max} is the concentration corresponding to the top of a peak, while C^{grad} is the concentration within a section of the dispersed zone situated on the ascending, or descending part of the peak, thus defining the so-called gradient dispersion D_g. While direct methods, like spectrophotometry, flame methods, fluorimetry, etc., rely on measurement of peak height, to which D is related, the gradient techniques such as flow injection titrations are based on the concept of gradient dispersion (Figs. 1 and 2).

The general concept of these titrations can be illustrated by considering a sample of an acid to be titrated, which has been injected into a carrier stream of a base serving as a titrant. Such a sample zone will disperse on its way towards the detector through different stages (A—C, Fig. 1), while neutralization takes place at the interfaces between the acid and the base. If the injected material is more concentrated than the carrier stream, then it is self-

0003—2670/81/0000—0000/$02.50

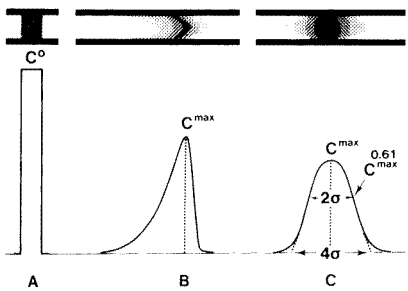

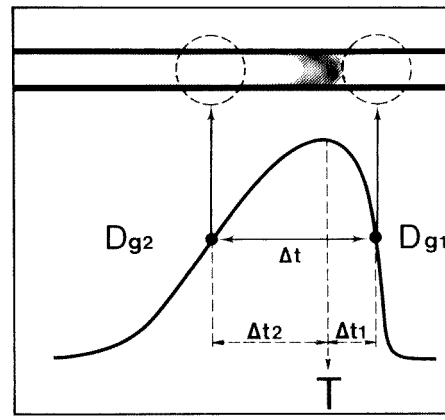

Fig. 1. Dispersion of an injected sample zone of original concentration C^0 as a function of length (time) travelled. (A) Injected sample zone; (B) zone after moderate dispersion; (C) zone after reaching Gaussian distribution.

Fig. 2. Dispersed sample zone and corresponding recorder output. To each element of fluid on the rising curve of gradient dispersion D_{g_1} corresponds an element of fluid on the falling curve of identical D_g value (D_{g_2}). In flow injection titrations this concept is exploited by locating those two elements of fluids where equivalence is achieved between carrier stream and sample. The time span Δt ($=\Delta t_1 + \Delta t_2$) between these two points is related to the concentration of analyte.

evident that at the front as well as at the tailing sections of the peak a point must exist where the acid is exactly neutralized by the base. These two equivalence points form a pair, having the same D_g value and their physical distance (measured in time units for a constant pumping rate Q) will increase with the concentration of the acid to be titrated. Therefore, the time span Δt (Fig. 2) will be proportional to the concentration of the analyte (C_A^0) and inversely proportional to the concentration of titrant (C_B^0). In order to obtain a straightforward mathematical relationship between Δt, C_A^0 and C_B^0, a simple single-channel system was designed comprising a peristaltic pump, a sample injection valve, a mixing chamber, and a spectrophotometric detector [2]; the main feature is a mixing chamber of such a large volume (compared to the rest of the system) that the dispersion in it dominates the performance of the whole system. Therefore, the concentration profile is exponential in time and

$$\Delta t = (V_m/Q) \ln 10 \log (C_A^0/C_B^0 n) + (V_m/Q) \ln 10 \log (S_v/V_m) \quad (2)$$

where V_m is the volume of the mixing chamber, S_v is the injected volume, and n is the molar ratio of the reacting components. In other words, the time span, Δt, measured by means of a spectrophotometric or potentiometric indicator increases linearly with the logarithm of the analyte concentration.

Compared to the conventional approach, these flow injection titrations are faster and require a simpler experimental set-up. Furthermore, the f.i.a.

system is self-adjusting because the analytical channel is continuously washed by the titrant; therefore a sample can be injected immediately after the preceding sample zone has cleared the detector, and the signal has reached the baseline. Flow injection titrations have been included for several years as an exercise in the undergraduate training at this Department [3], where their reliability and simplicity have been appreciated. Stewart et al. [4] have included similar titrations in their research programs. Pardue and Fields [5] have discussed in great detail various continuous flow titrations, and suggested that the above system should be applied with very diluted carrier stream solutions (or even in pure water streams) in order to increase sensitivity. The titration systems described by Pungor et al. [6] are interesting but are not considered further here because their principles are quite different; dispersion of sample zones is not involved.

With regard to flow injection titrations [1, 2], the use of a mixing chamber is a rather clumsy method to create an exponential concentration gradient. Not only are the mechanics of a mixing chamber with the magnetic stirrer objectionable, but the large volume of the chamber is undesirable because it results in a large dilution of the sample material causing loss of sensitivity as well as a low sample throughput rate, if a moderate reagent consumption is to be maintained. For example, with a typical V_m = 1 ml and Q = 1.5 ml min^{-1} the purely physical process of decreasing C_A to one half requires 28 s ($t_{1/2}$) and reaching the baseline within 4% requires as much as 6 $t_{1/2}$, i.e. 2.8 min. This is the worst case possible, as during titration a chemical reaction takes place, which depending on the C_A^0/C_B^0 ratio will decrease the above values perhaps as much as five times.

It is the purpose of this work to dismiss these drawbacks by eliminating the mixing chamber and designing a simpler flow channel. This will be done by comparing the experimental data obtained by dispersion measurements with the theoretical models which describe the dispersion of material during its movement through a tubular reactor. This makes it possible to locate the position and physical dimensions of a single mixing stage which is capable of providing the same function as the mixing chamber did in the previous design. The performance of the new f.i.a. system designed on this basis is tested by acid—base, redox and complexometric titrations with colour indicators and spectrophotometric detection.

THE INJECTION PROCESS

The first insight into the nature of the injection process is offered by the well verified dependence of the D value on the injected sample volume [1]

$$1/D = 1 - \exp(-kS_v) \tag{3}$$

where $k = 0.693/S_{1/2}$, $S_{1/2}$ being the sample volume necessary to reach D = 2 (Fig. 3). It is also well established that $S_{1/2}$ increases with the volume of the tubular reactor V_r, through which the sample zone passes on its way towards the detector, yet $S_{1/2}$ and V_r have not so far been exactly related.

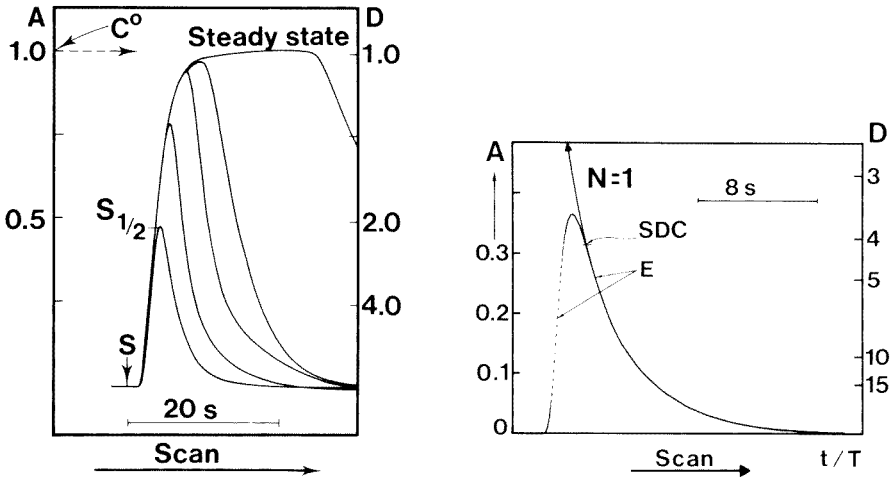

Fig. 3. Response curves as a function of injected volume. The peak height increases with the volume injected into the f.i.a. system until the steady-state signal is reached; the sample volume needed to achieve 50% of this signal is $S_{1/2}$, corresponding to $D = 2$.

Fig. 4. Dispersion of a sample zone in a short tubular reactor. (E) Experimental curve; ($N = 1$) is the curve simulated from the experimental data collected after point SDC (Start of Data Collection).

As the injection process seems to be well described by eqn. (3), it will be useful to investigate it further by means of the tanks-in-series model based on the expression

$$C_\theta = [N(N\theta)^{N-1}/(N-1)!] \exp(-N\theta) \quad (4)$$

where N is the number of mixing stages (tanks), θ is the reduced time $\theta = t/\bar{T}$ and $\bar{T}$ is the overall mean residence time in the system; the corresponding value of the variance is $\sigma_\theta^2 = 1/N$ ($=\sigma_t^2/\bar{T}^2$). In its simplest form ($N = 1$), this model describes the curve form for one mixing stage, i.e., the concentration profile of a sample of volume S_v and of initial concentration C^0, injected into a mixing stage of volume V_m, will be

$$C = (C^0 S_v/V_m) \exp(-t/\bar{T}) = (C^0 S_v/V_m) \exp(-tQ/V_m) \quad (5)$$

from which the volume of the mixing stage V_m can be computed.

Thus by collecting the C values experimentally at fixed real time intervals at the descending part of the dispersion curve (Fig. 4, from the level marked as Start of Data Collection), obtained by injecting a dye of definite concentration (C^0) into a colourless carrier stream and measuring the absorbance of the carrier stream, extrapolation could be made to an imaginary point in time ($\theta = t/\bar{T} = 0$) when the dispersion process started. At the same time, the curves obtained experimentally were compared to eqn. (5) and this enabled V_m to be computed from known values of S_v and Q. This was done by means of a computer program [7] for numerical evaluation of factors A and

B in the equations Y = A exp (Bt) and $V_m = -Q/B$ derived from eqn. (5). By using a constant length of tubing between the injection valve and the detector (L = 23 cm of 0.55 mm i.d.), and always injecting the same sample volume (S_v = 30 μl) of a definite dye concentration (C^0), while varying the pumping rate Q in each experiment, the volume of the mixing stage (V_m) was computed (Table 1). Except for the lowest pumping rate (6.17 μl s^{-1}), the regression coefficient (r^2) was higher than 0.99 and the mean computed volume of the mixing stage was found to be V_m = 73 μl. The volume of the connecting tube between the injection port and the flow cell was 55 μl (as measured by a Hamilton syringe) and the difference of 18 μl between this reactor volume, V_r, and the above mean V_m, is close to half the sample volume actually injected. Thus it is logical to assume that the mixing stage is partially accommodated in the injector volume and that $V_m \approx 50\%\ S_v + V_r$. This relationship is depicted schematically in Fig. 5.

TABLE 1

Calculation of the volume of a mixing stage, V_m, for an injected volume of 30 μl[a]

Q[b] (μl s^{-1})	D	−B	Regression coefficient	V_m (μl)
(6.17	3.2	0.0964	0.988	64.0)
11.8	—	0.1602	0.999	73.7
17.5	3.3	0.2482	—	70.5
22.5	3.6	0.3057	0.999	73.6
24.3	—	0.3300	—	73.6
28.3	3.9	0.3782	1.000	74.8
34.2	4.2	0.4704	0.997	72.7
			Mean =	73.2[c]

[a]From Y = A exp (Bt) and $V_m = -Q/B$. Although V_m can be calculated from factor A as well as B only the latter was used here. [b]Flow rates in the range 0.37—2.05 ml min^{-1}. [c]Relative standard deviation (excluding one measurement), 2.0%.

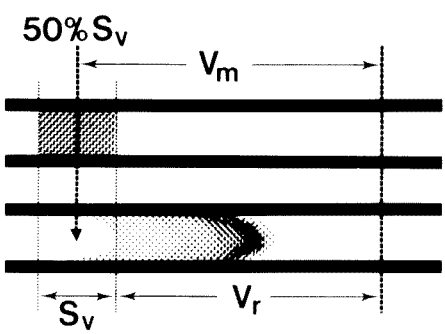

Fig. 5. Schematic representation of the relationship between mixing stage volume (V_m), sample volume (S_v) and reactor volume (V_r) for short reactor lengths.

To verify this concept of V_m the above experiment was repeated using the same V_r and two constant Q values, but this time S_v was varied over a wide range; V_m and B were computed as above. Again, except for the very large sample volumes (resulting in $D < 2$), a reactor volume value close to 55 μl was found (Table 2).

Thus several conclusions can be drawn. First, the mixing stage occupies the whole length of the tubular reactor and 50% of the injector volume. Therefore, the starting point of the dispersion process can be located formally to the middle of the sample zone prior to its injection. In other words, one may visualize that the concentration gradient between the sample and carrier stream solution is established when half the sample volume has been expelled from the injector by the carrier solution. It should be noted that, as the linear velocity in the centre of the stream is twice the mean linear velocity, the carrier stream would then have reached right through the injector at the core. Further, when the D values of Table 2 were plotted as a function of the sample volume (S_v) an exponential curve was found, conforming with eqn. (3), from which an $S_{1/2}$ value of 54 μl was found. Therefore, $S_{1/2} \approx V_r$; this, together with the good regression coefficients in Table 2, supports the finding that the tubular injector volume followed by a short tube of equally narrow diameter accommodates one mixing stage ($N = 1$), so that the dispersed sample zone detected by an optical flow cell will be recorded as a peak, the rising and falling edges of which will have purely exponential form.

To summarize, the data in Tables 1 and 2 suggest that very fast flow injection titrations may be performed with a flow channel of 0.55 mm i.d. at pumping rates between 0.7 and 2.1 ml min^{-1} with a S_v/V_r ratio ranging from ca. 1:2 ($D \approx 2$) to 1:4 ($D \approx 4$), i.e., at medium or even somewhat limited

TABLE 2

Calculation of reactor volume V_r[a]

S_v (μl)	Q (μl s^{-1})	D	—B	Regression coefficient	V_m (μl)	V_r (μl)
7.7	19.2	—	0.3255	—	59.0	55.2
26.6	19.2	4.5	0.2902	0.9987	66.2	52.9
26.6	29.2	4.5	0.4204	0.9997	69.5	56.2
35.3	19.2	3.5	0.2796	0.9993	68.7	51.1
35.3	29.2	3.5	0.3878	0.9995	75.3	57.7
62.8	19.2	2.3	0.2253	0.9916	85.2	53.8
62.8	29.2	2.3	0.3462	0.9964	84.3	52.9
75	19.2	1.4	0.2177	0.9996	88.2	51
100	19.2	1.2	0.1907	0.9977	100.7	51
150	19.2	1.1	0.1612	0.9935	119.1	(44)
200	19.2	1.1	0.1311	0.9884	146.5	(47)
					Mean =	53.5

[a]From the equations Y = A exp (Bt), $V_m = -Q/B$, and $V_m = 50\% S_v + V_r$.

dispersion. Before the practical impact of such a miniature mixing stage could be explored further, the further transformation of the sample zone through stages B towards C (Fig. 1) had to be investigated. On the assumption that at this stage the flow has stabilized, so that it is not being influenced further by the boundary conditions, another flow model can be applied.

THE DISPERSION MODEL

When the stream moves through an open narrow tube with a constant linear flow velocity $F = QL/V_r$ then the dispersion of the sample zone can be viewed as a statistical process and can be described formally by Fick's second law of diffusion [8]. The solution of the corresponding differential equations is

$$C = [2(\pi\ \theta\ \delta)]^{-1/2} \exp[-(1-\theta)^2/4\theta\delta] \quad (6)$$

where $\theta = t/\bar{T}$ and $\delta = D_f/LF$; D_f is the axial dispersion coefficient, L is the reactor length, F is the mean linear flow velocity, t is the time and $\bar{T}$ is the mean residence time. Depending on the value of the dispersion number δ (which is the reciprocal of the Peclet number), the curves obtained vary from a symmetrical (Gaussian) to an extremely skewed shape (Fig. 6). Thus for small dispersion numbers ($\delta \rightarrow 0$) plug flow is achieved, while at the other extreme ($\delta \rightarrow \infty$) mixed flow corresponding to the most skewed curves is obtained. In this way, by changing a single parameter δ, the various stages of sample zone dispersion (cf. Fig. 1) may be described and compared with the experimental values. It is only the curve shape which can be compared at this stage; because of normalization, the curves in Fig. 6 increase in height (in order to maintain the same area), whereas the height of real f.i.a. curves decreases with increasing L (or t, at constant pumping rate). Because it is the peak height, and so the D value which is of primary interest in f.i.a., the maximum value of C has to be found from eqn. (6). This is done by differen-

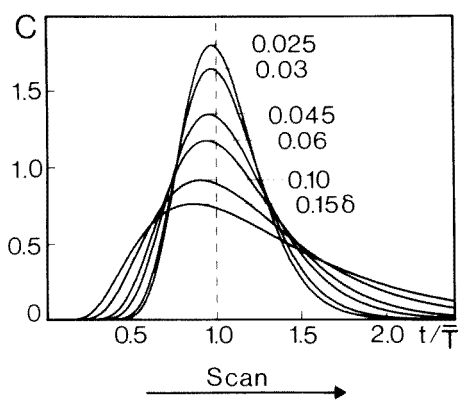

Fig. 6. Shape of C curves as a function of dispersion number δ (eqn. 6). Dispersion number is indicated on the curves. The peak maxima always occur at $\theta = t/\bar{T} < 1$.

tiation, which results [9] in

$$\theta = [(\delta^2 + 1)^{1/2} + \delta]^{-1} \tag{7}$$

This shows that the maximum on the C curve will always occur at a mean residence time $\theta < 1$ and that this difference will increase with increasing δ (cf. Fig. 6). In other words, for low δ values, say 0.001, $\theta = 0.999$ and therefore the curve maximum will practically coincide with $\bar{T}$. With such an approximation, eqn. (6) describes a Gaussian curve for which the variance is $\sigma^2 = 2\delta$ and $2\sigma = 2(2\delta)^{1/2}$ while $C^{max} = [2(\pi\delta)]^{-1/2}$.

In this section the coloured zone has so far been considered as an ideal impulse (of zero width, infinite height and area = 1) which cannot be achieved experimentally. A further step is therefore to accommodate a real impulse of concentration C^0 and volume S_v. Then

$$C^{max} = C^0 S_v / V_r 2(\pi\delta)^{1/2} \tag{8}$$

$$\text{or } D = C^0/C^{max} = 2V_r(\pi\delta)^{1/2}/S_v \tag{9}$$

Furthermore, because $V_r = \pi r^2 L$ and $F = L/\bar{T}$, eqn. (9) can be rearranged to

$$D = 2\pi^{3/2} r^2 D_f^{1/2} \bar{T}^{1/2}/S_v \tag{10}$$

which, in agreement with previous work [1], predicts that dispersion will increase with the second power of the tube radius and the square root of the mean residence time (at constant Q). It should be noted that the dispersion as a function of S_v will decrease nearly linearly up to $D = 2$ (cf. eqn. 3 and Fig. 3), i.e., for $S_v < S_{1/2}$.

Unfortunately, the above equations describe stage C (Fig. 1) which is seldom reached in f.i.a. (unless, a single bead string reactor [10] is used). For the usual, more skewed f.i.a. curves, the simple expressions for variance indicated above must be replaced [9] by $\sigma^2 = 8\delta^2 + 2\delta$, which may be rewritten as $\delta = \frac{1}{8}[(8\sigma^2 + 1)^{1/2} - 1]$. This relation between σ and δ can then be used for computation of δ from the experimental σ^2 value with the aim of generating a model curve based on eqn. (6) and comparing it with the experimental curve. (It must be recalled that the higher the δ value, the more skewed the curve will be.) For this purpose the variance may be found by collecting the C values at regular time intervals by scanning the entire peak obtained by a dispersion experiment

$$\sigma_t^2 = (\sum t_i^2 C_i)/C_i - [(\sum t_i C_i)/C_i]^2 \tag{11}$$

where C_i are concentrations measured at certain t_i intervals, the starting point being the time of injection (S).

The experimental curve obtained with $S_v = 30$ µl and $Q = 1.20$ ml min^{-1} and with a 120-cm coiled reactor (0.55 mm i.d.) is shown in Fig. 7 (curve E) together with the computer-generated curve based on eqn. (6) and a δ value of 0.035 (curve D), and a computer-generated curve (curve T) based on the same numerical value of the variance ($\sigma^2 = 0.081$) but using the tank-in-series

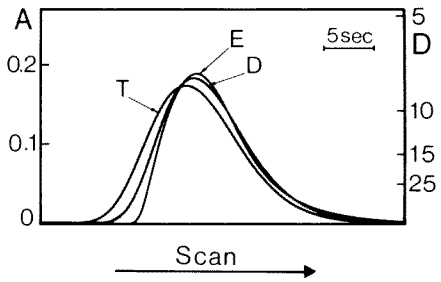

Fig. 7. Experimental and computer-generated f.i.a. response curves. The experimental curve (E) was obtained with S_v = 30 μl, Q = 1.20 ml min^{-1} and with a 120-cm coiled reactor (0.55 mm i.d.). From this curve the variance (σ^2) was determined and then used to compute curve D on the basis of the dispersion model and curve T on the basis of the tank-in-series model.

model (eqn. 4). As one would expect, the dispersion in the long coiled reactor is better described by the dispersion model and therefore curve D fits the experimentally recorded curve (E) better than curve T, while the tanks-in-series model is preferable for describing the events in very short reactors ($N \simeq 1$).

Finally, δ values were computed from experimental σ^2 values obtained with various reactor lengths (V_r from 74 μl to 318 μl) under otherwise the same conditions (Table 3). These data were used to compute D by means of eqn. (10). The computed D values are in very good agreement with the D values obtained by simple peak height measurements (cf. eqn. 1) and thus confirm the validity of eqn. (10). As pointed out previously [1], the D value must not be too low as the conditions of the instant pulse will not be met and the reactor volume V_r must be larger than S_v. Thus the limit of the

TABLE 3

Comparison of calculated (D_c) and measured (D_m) dispersion values

δ	Q (μl s^{-1})	T[a] (s)	V_r[b] (μl)	S_v (μl)	D_c	D_m	Error (%)
0.024	20.9	15.0	314	26	6.6	6.6	0
0.035	20.0	15.9	318	30	7.1	6.9	3
0.048	20.3	7.2	146	26	4.4	4.3	2
0.056	20.6	7.2	148	26	4.8	4.8	0
0.056	20.3	9.0	183	26	5.9	5.6	5
0.076	20.3	5.1	104	26	3.9	3.9	0
0.077	20.6	4.8	99	26	3.8	3.5	8
0.191	20.2	3.9	79	30	4.1	3.5	15
0.212	20.5	3.6	74	30	4.0	3.5	13

[a]Residence time in f.i.a., i.e., time elapsed between sample injection and appearance of peak maximum. [b] $V_r = QT$.

present model is $D \geqslant 4$ as otherwise the above condition is not met and the sample would travel too short a distance to be affected by dispersion whether by diffusion or by other processes which could, through radial movement, change the concentration profile established by the injection process.

DESIGN OF A FLOW INJECTION SYSTEM FOR HIGH-SPEED TITRATIONS

It can be concluded from the foregoing that the function of a mixing chamber of the original f.i.a. design for titrations [1, 2] can be fulfilled by a single mixing stage which is partially located in the injector volume and further located in an open narrow (and preferably) straight tube leading to a flow-through detector (Fig. 8a). The optimum volume of the tube reactor is equal to, or in the vicinity of, $V_r \approx S_{1/2}$ which will yield $D \approx 2$, thus allowing D_{g_1} and D_{g_2} to be close to 4 (Fig. 2). This is roughly fulfilled for $S_v = 30$ µl and $L = 25$ cm (at 0.5 mm i.d.). Naturally, this is not a rigid requirement as depending on practical conditions (such as concentration of sample material) D can be increased or even slightly decreased. It should be kept in mind, however, that the relationship $S_{1/2} \approx V_r$ has been found valid only for a short straight reactor, and that for longer tubes (120 cm or more) this condition was shown not to hold. Therefore, a tube length of 0.25–0.5 m seems to be the optimum (for 0.5 mm i.d. tubing).

The practical consequences of performing titrations at medium D_g using a miniaturized mixing stage are far-reaching. First, the titration cycle, including the washout period, can be made as short as 12 s with an equivalence period Δt of 2.2 s (Table 4). Secondly, when medium dispersion is used the sensitivity of titration is at least as good as that of conventional batch procedures. Thirdly, the sample volume is low (e.g., 50 µl) and therefore the reagent consumption is also low. Of these statements, only the first requires a short explanation. By constructing a system where $S_v = V_r$ (by using 25 cm of 0.5-mm i.d. tubing), an injected volume of 50 µl will result in $D = 2$ (cf. the above-mentioned relationship $S_{1/2} \approx V_r$). In this way the length of the titration cycle is fixed in terms of $t_{1/2}$ and can be varied in real time units by

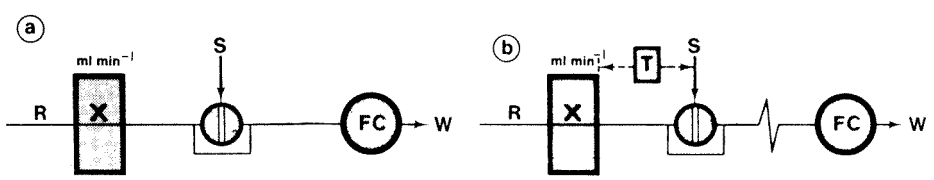

Fig. 8. Single-line flow injection titration manifolds. (a) Configuration used for acid–base, complexometric and redox titrations; the tube connecting the injection port and the flow-through detector (FC) is 25 cm long, 0.5 mm i.d.; $S_v = 30$ µl. (b) Configuration used for stopped-flow titrations; the timer (T) is activated by a microswitch on the injection valve, and by a preset timing program the sample can be stopped either outside or inside the flow cell for any length of time.

TABLE 4

Length of titration time (Δt) and titration cycle (t_c) as functions of gradient dispersion, reactor volume and pumping rate[a]

Q (ml min^{-1})	t_r[b] (s)	Δt			
		$D_g = 4$ ($1.5\ t_{1/2}$) (s)	$D_g = 8$ ($2.75\ t_{1/2}$) (s)	$D_g = 16$ ($3.88\ t_{1/2}$) (s)	t_c[c] (s)
0.7	4.45	6.68	12.23	17.27	35.60
2.1	1.48	2.22	4.07	5.74	11.84

[a]All values for $D = 2$, in absence of chemical reaction, where $V_m = 75\ \mu l$, $S_v = 50\ \mu l$ and $V_r = 50\ \mu l$ (0.5 mm i.d.). [b]$t_r = V_r/Q' \simeq V_m \ln 2/Q' = t_{1/2}$ ($Q' = 1000\ Q/60$). [c]$t_c = t_r + t_{1/2} + 6\ t_{1/2} \simeq 8\ t_{1/2}$.

the choice of Q (Table 4). Within these time limits, the Δt can be varied by the choice of D_g, this being the level at which the usual equivalence condition $C_A^0 v_A = C_B^0 v_B\ n$ for the reaction $nA + B = A_nB$ is fulfilled. As $D_g = C_A^0/C_A$ and therefore $C_B = C_B^0\ (D_g - 1)/D_g$ (where $C_A = C_A^0 \exp(-kt)$ or $t = 1/k \ln 10 \log D_g$), the time, Δt, elapsed between the two points D_{g_1} and D_{g_2} (Fig. 2), in each of which the equivalence condition $C_A = nC_B$ is met, is given by

$$\Delta t = 1/k \ln 10 \log C_A^0/C_B^0 + 1/k \ln 10 \log D_g/(D_g - 1)n \qquad (12)$$

where $k = V_m/Q$. It should be noted that Δt consists of two contributions Δt_1 and Δt_2 (Fig. 2), but as these originate from exponential relationships, characterized by the same k value, the sum of the individual contributions results in the relation given by eqn. (12). Like eqn. (2), eqn. (12) predicts the dependence of the time interval, Δt, on the logarithm of the analyte concentration C_A^0. It is interesting to observe that for large D_g values, eqn. (12) will reduce to eqn. (2) (i.e., for $S_v \approx V_m$) which was originally derived for titrations done at high dispersion values.

So far only the physical aspects of high-speed flow injection titrations have been dealt with; an equally important problem, the rate of the chemical reactions involved, has not been considered. Although experience with direct f.i.a. methods indicates that the chemical reactions on which many analytical procedures are based are fast enough to be accommodated within a 10—20-s reaction period, it is doubtful at this stage how much can be achieved under the conditions of a titration, in which not the reagent (as in the case of a direct measurement), but the analyte is in excess during a certain part of the titration cycle. Furthermore, the time during which the chemical reaction, including the indication of the equivalence points must take place, is severely restricted in the present case (Table 4).

Fortunately, an alternative scheme to continuous flow titrations (Fig. 8a) can be designed, where the reaction time can be prolonged to any desired

value. In the same way as all other stopped-flow f.i.a. methods [1], titrations can also be done by means of intermittent pumping (Fig. 8b), in which case the titration cycle will consist of three periods: (a) injection of the sample and formation of the dispersed zone profile; (b) a stopped-flow period during which the reactions can take place; and (c) resumed pumping during which the reacted zone will be scanned while passing through the detector. It is important to realize that even a very short stop period, say 5 s, will be very effective, as during that time the chemical reaction will take place within the mixed zone along the dispersed profile, thus yielding a continuum of measuring points. In contrast, the conventional batch titration method, even if automated, would require waiting periods of 5 s after each discrete addition of titrant, in order to allow for the same reaction time. Another use of the stopped-flow technique is the investigation of how far chemical reactions have progressed at any given time, so that one may estimate whether chemical equilibrium has been reached.

At present, it is difficult to predict all the types of titrations which might be performed at high speed. Therefore only a few examples, i.e. neutralization, compleximetric and redox titrations have been chosen and tested in the newly designed titration system.

EXPERIMENTAL

Apparatus

The flow injection systems used were essentially similar to those described previously [11] (for manifold configurations, see Fig. 8). Reagents were pumped by a four-channel peristaltic pump, Ismatec Model Mini-S 840. Optical measurements were made with a Varian Varichrom UV-VIS spectrophotometer furnished with an 8-μl flow cell, the original leads to and from which were replaced by 0.5 i.d. tubing; or with a Corning Model 256 spectrophotometer, equipped with an 18-μl Hellma flow cell (type OS 178.12).

The computer used (Commodore PET 2001 Model 16N), combined with a printer (Commodore Tractor Printer Model 3022) and a floppy disk (Commodore CBM Model 2040 Dual Drive Floppy Disk), was connected via an active interface (constructed in this laboratory) to the flow injection system (via a microswitch on the injection valve), to the spectrophotometer and to a recorder. For the actual titration experiments, the recorder was a Radiometer REC 80, furnished with a high-sensitivity unit (REA 112), while for the dispersion-model experiments, an X-Y recorder was used (Brüel & Kjær, Type 2308).

Reagents

All reagents were of analytical-reagent grade. Distilled and degassed water was used throughout.

The bromothymol blue indicator stock solution was prepared by dissolving 0.400 g of indicator (Merck) in 25 ml of 96% ethanol and diluting to 100

ml with distilled water. The xylenol orange indicator stock solution (Merck) was made by dissolving 0.5 g of the indicator in 100 ml of water. The aqueous starch stock solution was 1%.

High-speed titrations

A single line manifold (Fig. 8a) with a line length of 25 cm (0.5 mm i.d. tube) and a photometric flowthrough detector (volume 8 μl) was used. A sample volume of 30 μl was injected in all cases.

Neutralization titrations. The model system chosen was the titration of hydrochloric acid by 1×10^{-3} M NaOH using bromothymol blue as indicator added directly to the sodium hydroxide carrier stream (at a level of 0.2% of the indicator stock solution). As the carrier stream was blue, the detector, when tuned to 600 nm, would detect a steady absorbance level at approximately 0.5, which was then chosen as the baseline (Fig. 9). Thus, during any titration cycle, when the indicator went through two transitions (blue/yellow/blue), a peak-shaped curve was recorded, the width of which increased with the concentration of the injected acid (1×10^{-2}, 2×10^{-2}, 4×10^{-2}, 6×10^{-2} and 1×10^{-1} M HCl). In the example shown in Fig. 9, the recorder chart was returned after each run so that all five titration cycles were recorded from the same starting point (S). It is important to realize that once the indicator has turned either completely blue, or yellow, the detector reaches a limiting level and therefore all recorded curves have a common baseline as well as a common top level, regardless of the concentration of the titrated analyte. This is analogous to classical batch titrations where the colour change of the indicator at its transition point is all that is needed to establish the end-point of a titration. In the present experiments, an absorbance of 0.25 was chosen as the transition level (Eq.), corresponding to the pK value of the indicator (7.1). At this level, the individual curves are spaced both at the leading as well as on the tailing edge in a pattern which much resembles that of the dispersion experiment in Fig. 4, indicating the logarithmic dependence between Δt and the concentration of hydrochloric acid. Because of the high titration speed (the longest titration cycle lasts 15 s), a graphical evaluation of Δt would not have been sufficiently precise. Therefore, during these tests (at Q = 1.46 ml min^{-1}) as well as during three other series of tests (when the carrier stream was pumped at 1.06, 1.72 and 2.13 ml min^{-1}) the peak widths were read out by means of the PET computer. The Δt values thus obtained plotted versus the logarithm of the acid concentrations (Fig. 10), confirm the validity of eqn. (12). The reproducibility of this type of titration is seen from Table 5; the regression coefficient for these results was r^2 = 0.9989, and the mean relative standard deviation was 0.9%.

Compleximetric titrations. The titration of zinc by an EDTA solution of pH 4.69, with xylenol orange as indicator [12] was taken as an example. The composition of the carrier stream was 1×10^{-3} M EDTA in 0.1 M acetate buffer, containing 0.5% (v/v) of the xylenol orange indicator stock

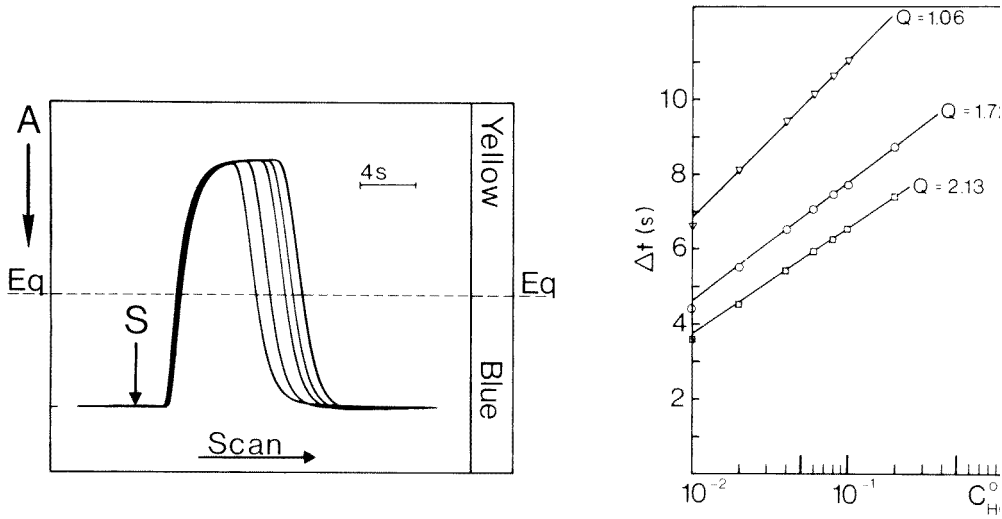

Fig. 9. Titration of strong acid with strong base in manifold Fig. 8(a), using bromothymol blue as indicator added to the alkaline carrier stream (1×10^{-3} M NaOH) pumped at a rate of 1.46 ml min^{-1}. All samples (C^{o}_{HCl} = 0.01, 0.02, 0.04, 0.06 and 0.1 M, respectively) were injected at point S, and the Δt values were read at the Eq. level (cf. Table 5).

Fig. 10. Calibration plots for acid—base titration (Figs. 8(a) and 9) obtained for different pumping rates (Q, ml min^{-1}).

TABLE 5

Titration of strong acid with strong base
(Carrier solution 2×10^{-3} M NaOH containing bromothymol blue indicator; Q = 1.46 ml min^{-1}; S_v = 30 μl; reactor length 25 cm 0.5 mm i.d.)

C^{o}_{HCl} (M)	$-\ln 10 \log C^{o}_{HCl}$	Δt [a] (s)	R.s.d. (%)
0.008	4.83	3.13	3.4
0.010	4.61	3.59	0.3
0.020	3.91	5.11	0.2
0.040	3.22	6.39	0.2
0.060	2.81	7.06	1.6
0.080	2.53	7.71	0.2
0.100	2.30	8.13	0.3
0.200	1.61	9.27	1.4
0.400	0.92	10.55	1.1
0.600	0.51	11.40	0.1

[a]Mean of six injections.

solution. The carrier stream, which was pumped at a rate of 1.5 ml min^{-1}, was monitored by the spectrophotometer adjusted to 575 nm so that the recorder baseline was at zero absorbance when the yellow carrier stream was passing though the flow cell. The Eq. level was at 0.5 absorbance so that the indicator transition was monitored when about 50% of the indicator was bound by zinc as the red complex. This time the chart paper was run continuously at a speed of 10 s cm^{-1} (Fig. 11), while the peak width was read out by means of the PET microcomputer. Each sample was injected in triplicate, the analyte concentrations lying in the range 5×10^{-3}—10^{-1} M $ZnSO_4$. The plot of Δt vs. log C^0_{Zn} had a regression coefficient of 0.9999 and the relative standard deviation of the individual measurements was 1.2%.

Redox titrations. The titration of iodine by thiosulphate with starch as indicator was examined. The carrier stream consisted of 5×10^{-5} M thiosulphate containing 5% by volume of the starch stock solution, and was pumped at a rate of 1.35 ml min^{-1} through the spectrophotometer tuned to 610 nm. The colourless carrier solution had zero absorbance and this served as the recorder baseline (Fig. 12). The Eq. level was set arbitrarily to absor-

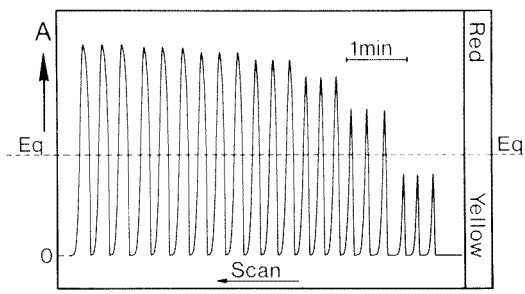

Fig. 11. Complexim etric titration of zinc(II) by EDTA with xylenol orange as indicator added to the carrier stream (1×10^{-3} M EDTA in 0.1 M acetate buffer, pH 4.69), employing the manifold depicted in Fig. 8(a); Q = 1.5 ml min^{-1}. All samples (C^0 = 0.005, 0.01, 0.02, 0.04, 0.06, 0.08, and 0.10 M $ZnSO_4$) were injected in triplicate, and the Δt values were read at the Eq. level, i.e., the most dilute sample did not give rise to any Δt signal.

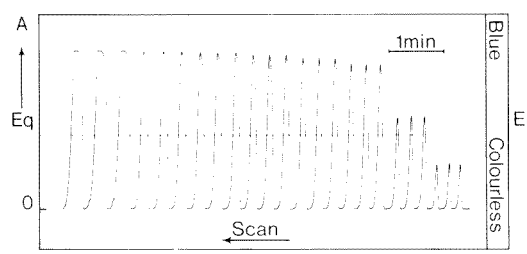

Fig. 12. Titration of potassium triiodide by thiosulphate (manifold, Fig. 8a) with starch as indicator added to the carrier stream (5×10^{-5} M sodium thiosulphate), pumped at a rate of 1.35 ml min^{-1}. All samples (C^0 = 0.001, 0.002, 0.004, 0.005, 0.006, 0.008, 0.010, and 0.050 M KI_3) were injected in triplicate, and the Δt values read off at the Eq. level.

bance 1.2 so that the presence of the blue starch—iodine complex was detected, and the titration curves were recorded in exactly the same manner as in the case of complexiметry. The iodine standards, injected in triplicate, were in the range 1×10^{-3}—5×10^{-2} M KI_3. Again, the plot of Δt vs. the logarithm of analyte concentration was linear, with a regression coefficient of 0.9921, while the relative standard deviation of the individual measurements was 1.1%.

DISCUSSION AND CONCLUSIONS

The above results confirm that the flow injection titrations, done in this novel and very simple way, allow unprecedented sampling rates to be achieved. The titration cycle varied in these experiments between 15 and 30 s, thus allowing up to 240 titrations to be done per hour. It is, however, not so much the real hourly sampling capacity which is of practical value, as the fact that the titration result is available within seconds after sample injection and that the flow injection titrator is self-restoring, being immediately ready for the next assay. It is conceivable that the present system could be operated at even higher sampling rates. The only reason why this possibility was not tested was the inability of the cheap computing system used, and especially the interface, to collect the data more frequently than at a rate of 10 s^{-1}. Obviously, an inexpensive dedicated microprocessor, designed for these titrations, should be capable of collecting data at a rate of 200 s^{-1}, thus permitting the actual limits of the system to be investigated with sufficient precision of measurement. The average relative standard deviation (1%) found for the above examples is very probably to be attributed to the data collection system.

It is rather surprising that the rates of the chemical reactions, on which the above experiments were based, were fast enough to achieve equilibrium. This was checked by doing each of the above titrations in a stopped-flow mode where the sample zone was stopped on its way to the detector for 30 s (using manifold Fig. 8b), or by using the stopped-flow technique to monitor a selected section of the response curve (in the vicinity of Eq.) within the flow cell [1]. The Δt values obtained in this way did not differ from those registered by the continuous mode and the absorbance values did not change more than 10% during the 1-min monitoring period. Naturally, these observations are valid only for the above three examples, but they give grounds for optimistic evaluation of the potential of these high-speed flow injection titrations.

Some questions remain to be answered. Firstly, how many other types of titration can be accommodated within that short titration cycle? The rate of some chemical reactions may well be too slow to come close to equilibrium. Yet over the centuries during which titrations have been developed [13], there has been a natural selection of those chemical systems which do not require long waiting periods after each addition of titrant, especially at the end-point of titration.

Secondly, it will be of interest to establish if stepwise titrations are possible, through two or several equivalence points, either of the same species or a mixture of two or three components, as is done in batch titrations. The principal obstacle would be the logarithmic dependence of Δt on the concentration of analyte. Yet again, this has been overcome in the case of ion-selective electrodes (which also yield a logarithmic dependence for concentration vs. potential), and indeed it is far easier to measure reproducibly a volume or a time (Δt) rather than an electrode potential. The use of other modes of detection, such as potentiometry, voltammetry or conductometry, may be less successful than colorimetry. The material monitored must reach the electrode surface in order to be detected, so that endpoint indication by electrochemical detectors may be too slow, unless proper transport of the species to be monitored can be ensured.

A further problem, in practical analyses, may arise if the titrated solution differs in its physical properties (viscosity, inherent colour, presence of minute amounts of colloidal matter) or in its chemical composition (e.g., pH), from the standards by means of which the flow injection titrator is calibrated. The extent to which such differences may influence results has not yet been studied. In batch titrations, the extensive dilution of the analyte nearly always reduces these factors to negligible levels. Yet, exactly the same can be done in a f.i.a. system where dilution prior to injection, or the use of a two-line f.i.a. system [1], will reduce the difference in composition between the standard and the assayed material.

The present work has shown that, in many respects at least, the highly sophisticated and mechanically complex automated batch titrators now commercially available can be replaced by a simple tubing system through which the analyte flows, whilst being titrated, to a detector.

The authors express their appreciation to the Danish Council for Scientific and Industrial Research for partial financial support.

REFERENCES

1 J. Růžička and E. H. Hansen, Flow Injection Analysis, J. Wiley, New York, 1981.
2 J. Růžička, E. H. Hansen and H. Mosbæk, Anal. Chim. Acta, 92 (1977) 235.
3 E. H. Hansen and J. Růžička, J. Chem. Educ., 56 (1979) 677.
4 K. K. Stewart, J. F. Brown and B. M. Golden, Anal. Chim. Acta, 114 (1980) 119.
5 H. L. Pardue and B. Fields, Anal. Chim. Acta, 124 (1981) 39 and 65.
6 G. Nagy, Zs. Fehér, K. Tóth and E. Pungor Anal. Chim. Acta, 91 (1977) 87, 97; 100 (1978) 181.
7 A. U. Ramsing, Ph.D. thesis, Technical University of Denmark, 1981 (in Danish).
8 O. Levenspiel, Chemical Reaction Engineering, 2nd edn., J. Wiley, New York, 1972.
9 O. Levenspiel and W. H. Smith, Chem. Eng. Sci., 6 (1957) 227.
10 J. M. Reijn, W. E. van der Linden and H. Poppe, Anal. Chim. Acta, 123 (1981) 229.
11 J. Růžička and E. H. Hansen, Anal. Chim. Acta, 114 (1980) 19.
12 E. Bishop, Indicators, Pergamon, Oxford, 1972, p. 358.
13 E. Rancke-Madsen, The Development of Titrimetric Analysis till 1806, C.E.C. Gad, Copenhagen, 1958.

Analytica Chimica Acta, 129 (1981) 19—27
Elsevier Scientific Publishing Company, Amsterdam — Printed in The Netherlands

PHOTOACOUSTIC STUDIES OF COMPLEXATION OF COPPER(II) WITH AN ETHYLENEDIAMINE ANALOG IMMOBILIZED ON SILICA GEL

L. W. BURGGRAF, D. S. KENDALL, D. E. LEYDEN* and F.-J. PERN
Department of Chemistry, University of Denver, Denver, CO 80208 (U.S.A.)
(Received 9th March 1981)

SUMMARY

Photoacoustic spectroscopy and solid—solution distribution measurements are used to study complexation of copper(II) with N-2-aminoethyl-3-aminopropyltrimethoxysilane immobilized on silica gel. Nearly consecutive formation of bis and mono complexes occurs on the surface with increasing copper(II) concentration. Evidence for conversion of bis sites to mono sites with increasing copper(II) concentration was not found. Heterogeneous distribution measurements fit well with a model which assumes two independent types of binding sites. An approximately 2.5:1 ratio of mono to bis sites was found.

Silanes have been used widely to modify surfaces for chemical application [1]. The specific applications of chemically modified surfaces which are of particular interest here are the preconcentration of trace metals for x-ray fluorescence (x.r.f.) determinations and metal—ion chromatography. Prediction of the affinity of a particular immobilized ligand for metal ions by extrapolating from analogous solution-phase equilibria ignores the influence of the surface on the heterogeneous equilibria. For example, the distribution of immobilized ligands on the surface determines the possible metal—ligand stoichiometries. This paper illustrates a method by which comparisons of solution-phase equilibria with corresponding heterogeneous equilibria may be made.

The complexation of copper(II) by the immobilized ethylenediamine analog was chosen for study for two reasons. First, this immobilized ligand has practical application for preconcentration of trace species. In addition to complexing a variety of transition metal cations [2], the immobilized ethylenediamine analog can bind a number of anions [3]. Secondly, our experience with this system suggests that the immobilized ligand behaves similarly to its solution-phase counterpart. The uptake of copper(II) by immobilized ethylenediamine as a function of pH has been studied [2], as has the ratio of immobilized material to copper loading [4]. Both studies suggest that the bis chelate is an important species on the surface. Pinnavaia et al. [5] applied e.s.r. to the study of immobilized ethylenediamine—copper(II) complexes on silica gel with a very low surface density of immobilized ethylenediamine analog (8.3 molecules/10^4 Å^2). Mono and bis

complexes were found at all copper—ligand ratios studied with mono complexes predominant at high copper loading (2.3:1 maximum mono-to-bis ratio). The aim of this study was to investigate this heterogeneous equilibrium as a function of copper concentration. Confirmation of the utility of photoacoustic spectroscopy (p.a.s.) as a tool for monitoring the surface species was of prime interest.

EXPERIMENTAL

Silylation

The silica gel (Baker column chromatography grade, 60—200 mesh) was dried overnight at 110°C in an evacuated oven. The surface area of the silica gel was found to be 300 $m^2\ g^{-1}$ as measured by nitrogen adsorption using a Quantachrome Monosorb Surface Area Analyzer. N-2-Aminoethyl-3-aminopropyltrimethoxysilane (Dow Corning Z-6020; abbreviated here to AEAPS) was vacuum-distilled before use. A 5% solution of AEAPS in dried toluene was prepared. The silica gel was refluxed for 2 h in the silane solution (15 ml per g of silica gel) or, alternatively, the silica gel was stirred with silane solution at room temperature for 2 h. No differences were discerned between the products of these methods other than small differences in capacities. After silylation, the silylated silica gel was washed thoroughly with toluene and ethanol. The silylated silica gel was cured for several hours at 80°C. These conditions lead to an approximately monolayer coverage of the surface [6]. From a carbon determination (Huffmann Laboratory, Wheatridge, CO), the average surface coverage was calculated to be 1.4 molecules/10^2 $Å^2$.

Photoacoustic spectroscopic study

Solutions of copper(II) were prepared covering the concentration range 1.0×10^{-1}—2.0×10^{-5} mol l^{-1}. The solutions were made 0.10 mol l^{-1} in acetate buffer (pH 5.0). Other selected copper(II) solutions were adjusted to pH 5.0 with nitric acid. Portions of silylated silica gel weighing 0.20 g were equilibrated with 25.0-ml aliquots of the copper(II) solutions. After separation of the silica gel by filtration, the silica gel was air-dried. The copper loading was determined by using a United Scientific Spectrace 440 energy dispersive x-ray fluorescence spectrometer equipped with a Tracor Northern 880 spectrum analyzer. Dried samples of the copper-loaded silica gel were ground for 1 min in a miniature stainless-steel ball mill. Photoacoustic spectra were measured by techniques described elsewhere [7]. Visible spectra of copper(II)—AEAPS solutions were recorded on a Cary 219 double-beam spectrophotometer.

Binding studies

Binding studies were conducted both with and without acetate buffer. The most reproducible results were obtained with the buffer present. A

copper(II) stock solution was standardized by EDTA titration. Dilutions of the copper(II) stock solution were made 0.10 mol l^{-1} in acetate buffer (pH 5.0), or were adjusted to pH 5.0 with acid. Portions of the silylated silica gel weighing 0.200 g were stirred with 50.0 ml of the copper(II) solutions. The contact time was limited to 15 min to minimize removal of the immobilized AEAPS by hydrolysis. The silica gel and copper solutions were separated by filtration. The bound copper was stripped from the silica gel with a 10% HCl solution. Both the filtrate and the solution containing the stripped copper were diluted and copper was quantified using a Perkin-Elmer model 2380 atomic absorption spectrophotometer.

RESULTS AND DISCUSSION

Solution-phase equilibrium

The solution-phase equilibrium of copper(II) and AEAPS is expected to be similar to that for other substituted ethylenediamines. Large stability constants are observed for mono and bis copper(II) complexes with substituted ethylenediamine compounds, while tris complexes are formed only weakly, if at all [8]. For example, the stability constants for successively formed copper—ethylenediamine complexes are: $\log K_1 = 10.7$, $\log K_2 = 9.3$, and $\log K_3 = -1$.

The result of a classical Job continuous variations experiment for the aqueous copper(II)—AEAPS system with total concentration equal to 5.0×10^{-3} mol l^{-1} is presented in Fig. 1. Very stable mono and bis complexes are formed. In the visible region, the mono and bis complexes exhibit broad absorption bands with maxima at 658 nm and 556 nm, respectively. These spectra are shown in Fig. 2. Spectra of solutions with 99:1 AEAPS—copper(II) molar ratio were indistinguishable from that of the bis copper(II)—AEAPS complex. It is concluded that the solution-phase equilibrium for this system is that of a substituted ethylenediamine ligand.

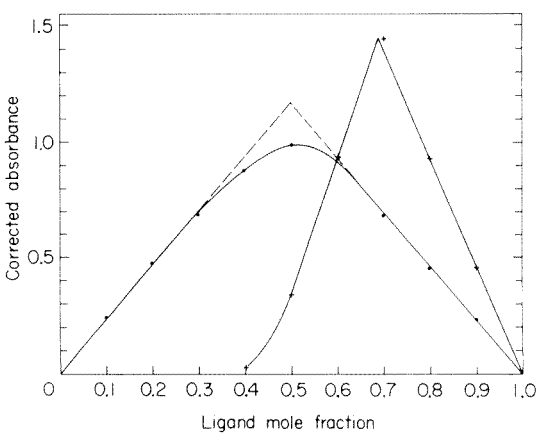

Fig. 1. Corrected absorbance versus AEAPS mole fraction at 556 nm (•) and 656 nm (+).

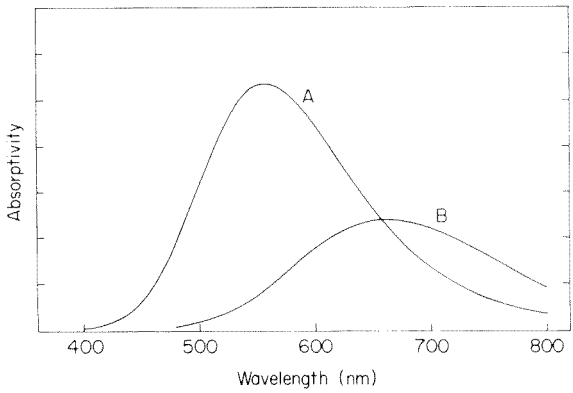

Fig. 2. Visible spectra of bis Cu(II)—AEAPS (A) and mono Cu(II)—AEAPS (B) in aqueous solution.

Photoacoustic spectroscopy results

The copper loading, as determined by x.r.f., and the wavelength of maximum absorption of the surface-bonded species are plotted versus the initial copper concentration in the acetate-buffered solutions in Fig. 3. The copper loading curve has the appearance of two consecutive sigmoidal waves. During the second wave, the visible absorption band broadens and the wavelength maximum shifts to longer wavelengths. These data are interpreted as representing nearly consecutive formation of predominantly bis then mono copper(II) complexes on the surface. At very low copper concentrations, formation of the bis complex is favored because of its greater stability. Throughout the region of high initial copper concentration, the mono complex makes an increasing contribution to the absorption spectrum.

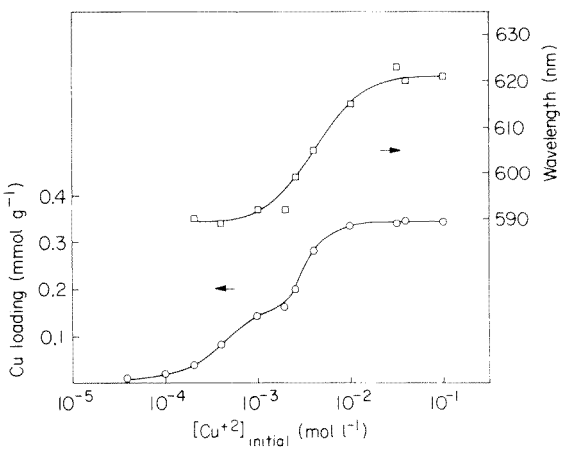

Fig. 3. Copper loading and wavelength of absorption maximum for AEAPS-modified silica gel versus initial Cu(II) concentration in 0.10 mol l^{-1} acetate buffer.

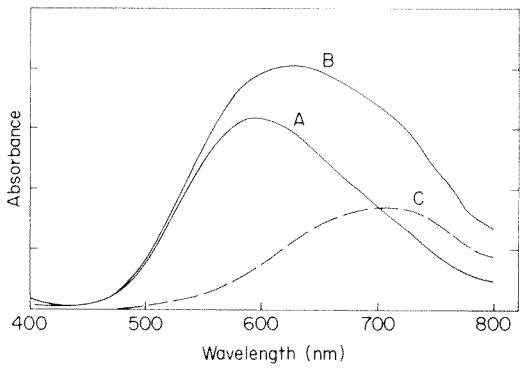

Fig. 4. Scaled p.a.s. absorption spectra for AEAPS-modified silica gel loaded with Cu(II) at an initial Cu(II) concentration of (A) 1×10^{-3} mol l^{-1} and (B) 1×10^{-1} mol l^{-1} in 0.10 mol l^{-1} acetate buffer. (C) Spectrum of mono species found by difference.

The photoacoustic absorption spectrum of the surface species formed at low copper concentration with nitrate counter-ion is identical to the solution-phase of the bis copper(II)—AEAPS complex shown in Fig. 2. The absorption spectrum of the surface species formed at low copper concentration with acetate counter-ion is shifted to longer wavelength (590 nm absorption maximum) while the shape of the absorption spectrum remains unchanged. This shift is due to the weakened ligand field caused by the association of the acetate ion with the bis copper(II)—AEAPS complex. The absorption spectra for samples at the beginning and at the end of the high concentration wave in Fig. 3 are presented in Fig. 4. The spectrum of the mono complex was obtained by stripping out the predominantly bis component from the spectrum obtained at high copper loading. Here also, the association of the acetate ion produces a shift to longer wavelength (710 nm absorption maximum) relative to the mono spectrum with nitrate counter-ion.

The immobilized AEAPS is expected to form a bis copper complex at binding sites for which this conformation is possible. For the present experimental conditions, the following scheme describes this process

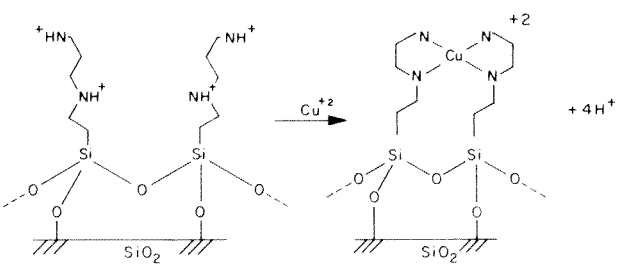

(1)

This scheme is not meant to describe the details of bonding to the surface.

At least two mechanisms can contribute to the formation of mono complexes on the surface at high copper concentrations. First, an immobilized

ligand not physically adjacent to another uncomplexed ligand could produce only a mono complex. Isolated ligands might be expected to be dominant for substrates with very low surface coverage as in the work of Pinnavaia et al. [5]. Also, the microdistribution of ligands on the surface may limit the possibility of bis copper(II) complex formation. Consider, for example, a trimeric site on the surface. A tris copper(II) complex is unlikely, not only because of the small formation constant, but also because of the conformational constraints introduced by ligand bonding to the surface. So, once two ligands of the trimer are involved in a bis copper(II) complex, the third ligand can only bind in a mono complex. The second mechanism involves the bis copper(II) complex being forced to two mono complexes at high copper concentration by mass action analogous to the solution-phase equilibrium. The very high local "concentration" of surface-bonded ligand and the stability of the bis chelate must be overcome for this process to be important.

The photoacoustic data presented in Fig. 5 argue against the second mechanism. The absorbance of the immobilized copper species at 535 nm is plotted versus the copper loading as measured by x.r.f. At 535 nm the absorptivity of the bis copper(II) complex is approximately ten times greater than the absorptivity of the mono copper(II) complex. If replacement of a bis copper complex by two mono complexes were important, the slope of the line would turn negative during the mono formation. Instead, the slope becomes less positive as predicted by the hypothesis of independent mono and bis sites. The linearity of the photoacoustic absorbance versus copper loading was confirmed in the region of the isosbestic point (690 nm).

Binding study results

It is instructive to consider the type of binding curve expected for metal binding at a single type of site on the surface. The heterogeneous equilibrium can be described by the following equations

$$M + L \overset{K_L}{\rightleftharpoons} ML \; ; \; LH_n^{+n} \overset{K_a}{\rightleftharpoons} L + n\,H^+$$

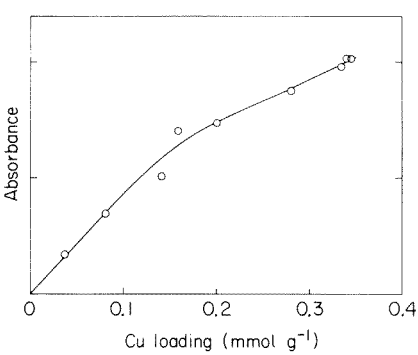

Fig. 5. Absorbance of AEAPS-modified silica gel at 535 nm versus total copper loading.

In these equations M is a metal cation, L is an available binding site on the surface, ML is an occupied binding site, and K_a is the acid dissociation constant for the protonated binding site. The equilibrium between the bound cation and the mobile cation at constant pH can be represented by an operational equilibrium constant

$$K = K_L K_a / [H^+]^n = (ML)/[M]\ (LH_n^{+n}) \quad (2)$$

where $(LH_n^{+n}) = \{C - (ML)\}$. Here, (ML) and (LH_n^{+n}) are measures of the quantity of occupied and unoccupied sites on the surface in units of millimoles per gram of substrate and C represents the maximum capacity of the chemically modified substrate in the same units. Equation (2) can be rearranged to give the linear equation

$$1/(ML) = 1/KC\ [M] + 1/C \quad (3)$$

Thus, the reciprocal of the quantity of bound metal is a linear function of the reciprocal of the copper concentration with an intercept equal to the reciprocal of the maximum capacity. This type of analysis has been applied to the evaluation of equilibrium constants by affinity chromatography [9].

The results of the binding studies were displayed as reciprocal concentration plots which invariably showed two linear regions in the limit of very low and very high copper(II) concentration. For example, the reciprocal concentration plot for the binding of copper(II) to immobilized AEAPS in acetate buffer is shown in Fig. 6. The precision of the data is limited, not by the measurement technique error, but by the irreproducibility of silane hydrolysis from the surface. The presence of the acetate buffer reduces the effective copper concentration causing the reciprocal concentration plots to be compressed while the extrapolated intercepts remain unchanged.

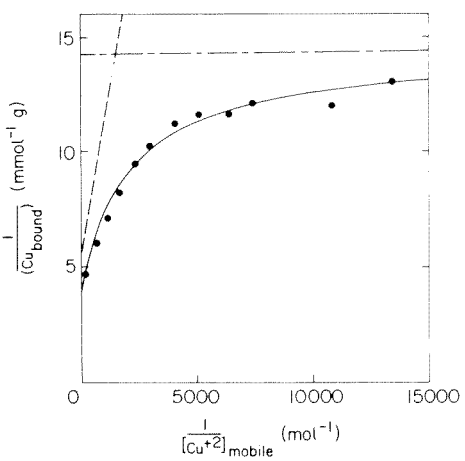

Fig. 6. Reciprocal of amount of bound copper versus reciprocal of solution-phase Cu(II) concentration (•). Solid curve results from iterative fit of two-site model: bis binding (— · —) and mono binding (— — —).

The reciprocal concentration plot correlates well with the p.a.s. result. The transition from regions of predominantly bis to predominantly mono binding occurs at the same solution concentration in both studies. The data from the binding study were fitted iteratively to a model which assumes two independent types of sites each of which is characterized by an operational equilibrium constant as in eqn. (3). This model generates the fit shown in Fig. 6, substantiating the two-site model. The values of K and C for this system are 5.8×10^2 mol^{-1} l and 0.18 mmol g^{-1}, respectively, for mono binding and $\gtrsim 10^6$ mol^{-1} l and 0.07 mmol g^{-1}, respectively, for bis binding. The ratio of mono-to-bis sites on the surface is approximately 2.5:1.

The agreement of this mono-bis-ratio with that found by Pinnavaia et al. [5] is remarkable, considering that the average surface coverage in this study was more than an order of magnitude greater than in the earlier study. This agreement may be explained by the stability of oligomeric silanes bound to the surface as suggested by the work of Waddell et al. [10]. The nature of the surface "template" may promote condensation of especially stable oligomeric binding sites. Condensation of silane triols to oligomeric silanols in aqueous solution is known [11].

Conclusions

Evidence for independent mono and bis binding sites for immobilized AEAPS on silica gel was obtained by using photoacoustic spectroscopy and heterogeneous distribution measurements. In the concentration range studied, no evidence was found for conversion of bis sites to mono sites with increasing copper(II) concentration. Plots of the reciprocal of amount of immobilized metal versus the reciprocal of the mobile metal concentration offer a convenient way of describing the heterogeneous metal distribution as a function of concentration of metal ion. They also provide a basis for comparison with the corresponding solution-phase equilibria. For the ethylenediamine analog immobilized on silica gel, the heterogeneous distribution measurements were well fitted by a model which assumes two independent types of binding sites.

The authors acknowledge B. B. Jablonski for the construction of our initial photoacoustic spectrometer. L. W. B. thanks the Air Force Institute of Technology for their support. This research was supported in part by research grant CHE-78-23123 from the National Science Foundation and by a grant from the AMAX Foundation.

REFERENCES

1 D. E. Leyden and W. Collins (Eds.), Silylated Surfaces, Midland Macromolecular Monographs, Vol. 7, Gordon and Breach, New York, 1980.
2 D. E. Leyden and G. H. Luttrell, Anal. Chem., 47 (1975) 1612.
3 D. E. Leyden, G. H. Luttrell, W. K. Nonidez and D. B. Werho, Anal. Chem., 48 (1976) 67.

4 D. E. Leyden, M. Steel, B. B. Jablonski and R. Somoano, Anal. Chim. Acta, 100 (1978) 545.
5 T. J. Pinnavaia, J. G. Lee and M. Abedeni, in D. E. Leyden and W. Collins (Eds.), Silylated Surfaces, Gordon and Breach, New York, 1980, p. 333.
6 D. F. Untereker, J. C. Lennox, L. M. Wier, P. R. Moses and R. W. Murray, J. Electroanal. Chem., 81 (1977) 309.
7 L. W. Burggraf and D. E. Leyden, Anal. Chem., 53 (1981) 759.
8 M. T. Beck, Chemistry of Complex Equilibria, Van Nostrand Reinhold, New York, 1970, p. 260.
9 L. W. Nichol, A. G. Ogston, D. J. Winzor and W. H. Sawyer, Biochem. J., 143 (1974) 435.
10 T. G. Waddell, D. E. Leyden and M. DeBello, J. Am. Chem. Soc., 103 (1981) 0000.
11 E. P. Plueddemann, in D. E. Leyden and W. Collins (Eds.), Silyated Surfaces, Gordon and Breach, New York, 1980, pp. 37, 38.

Analytica Chimica Acta, 129 (1981) 29—47
Elsevier Scientific Publishing Company, Amsterdam — Printed in The Netherlands

SYNTHETIC ASPECTS OF THE CHARACTERIZATION OF SOME SILICA-BOUND COMPLEXING AGENTS

CINDY FULCHER, MARTHA A. CROWELL, ROBERT BAYLISS, KEVIN B. HOLLAND and JOHN R. JEZOREK*

Department of Chemistry, University of North Carolina at Greensboro, Greensboro, NC 27412 (U.S.A.)

(Received 8th October 1980)

SUMMARY

A number of synthetic aspects of silica-bound complexing agents are considered. Modifications of the procedure for amidization of bound amines and of the diazotization-coupling sequence are discussed. The amidization of aminopropyl silica gel appears to be complete while that of ethylenediamine silica gel is less so. Loss of activity of the dried, bound diazonium salt appears to result from return to the Ar—NH_2 form, while a decrease in metal—ion complexation capacity for 8-quinolinol silica gel compared to the aminopropyl or ethylenediamine silica gel seems to be related to steric clogging of the matrix pores by bound organic moieties. A method of stripping the azo-coupled ligand from the appendage is examined, and some infrared and thermogravimetric characterizations are presented.

In recent years, surface modification of various supports has become an increasingly important technique in disciplines as diverse as heterogeneous catalysis [1], gas and liquid chromatographic separation of organic substances [2], enzyme—substrate reactions [3], and electrode studies [4, 5]. Numerous reports have also been published describing the use of immobilized complexing agents for solvent cleanup purposes [6], and for preconcentrating trace metals and anions [7, 8]. These materials have also shown promise as the stationary phase in the liquid chromatographic separation of trace metal ions [9]. Given the many actual and potential uses of bound ligands, it is important that their behavior, in both synthetic and analytical contexts, be understood well. Accordingly, during chromatographic studies in this laboratory, acid—base information for various bound ligands and possible improvements to the preparation of these materials are also being examined, so that optimum and controlled surface coverage by the ligand can be achieved.

In the preparation of bound ligands, the procedures of Weetall et al. [10—12] and Hill [13] were followed; various modifications of these methods are described below and their utility is assessed.

The first step in the synthesis usually involves the immobilization of an alkylamine on the surface of a silica gel matrix. Additional organic groups are subsequently attached, terminating in an organic ligand such as 8-quinoli-

nol (oxine). This first reaction and the properties of the bound amine are of interest for several reasons. The amount of chelating ligand finally attached to the matrix seems to depend directly on the absolute amount of the amine bound to the surface, as well as on the chemical and physical state of the amine. Furthermore, incompleteness of any subsequent reaction will also result in a reduced surface density of the terminal-bound chelating ligand. Therefore, several ways to obtain more complete reactions for the intermediate steps, as well as the initial silylation of the surface, were investigated. Also briefly discussed, are the use of infrared spectroscopy and thermogravimetry in the characterization of these materials.

EXPERIMENTAL

Reagents and solutions

All aqueous solutions were prepared with doubly-distilled deionized water. Organic solvents were dried over appropriate molecular sieves. Except as noted, all reagents were ACS grade and were used as received. Triethylamine (Eastman) was distilled before use.

Most glass and plastic ware was soaked overnight in (1 + 1) nitric acid solution, rinsed, and then soaked in a dilute EDTA solution at pH 8—9 to remove metal contaminants. Most solutions were stored in plastic containers.

The following silanes were used as received: 3-aminopropyltriethyloxysilane (Pierce, Rockford, IL); 3-(2-aminoethylamino)propyltrimethoxysilane (Dow-Corning Z-6020); and trimethylchlorosilane (both from PCR, Gainesville, FL). All were stored under refrigeration.

Silica gel was t.l.c. grade (HR extra pure; Merck) with 6-nm pore size, 550 $m^2\ g^{-1}$ surface area and 10—50 μm size range. This material was crudely sized before derivatization by stirring about 100 g into 500 ml of water, decanting the fine particles after about 5 min, and repeating five times. The resulting particle size range is estimated to be 30—50 μm.

Apparatus

Atomic absorption measurements were made on a Beckman Model 1301-DB. Infrared measurements were performed with a Perkin-Elmer Model 457 spectrometer, and thermal studies with a Perkin-Elmer DSC-1 with TGS-1 thermobalance.

Infrared pellet preparation. Both sample and die were heated (120—250°C) for several hours. About 150 mg of sample was placed into the die, which was again heated. The die was assembled while still hot, and the pellet pressed for 1—15 h at 15—25000 psi (Carver Laboratory press). The sample compartment of the spectrometer was flushed with nitrogen and the pellet was removed from the die in the nitrogen stream and inserted into a Wilkes Mini-Cell using fiber washers as spacers to hold it in place. The nitrogen stream was maintained while the spectrum was recorded.

Preparation of aminopropyl silica gel (APSG) and ethylenediamine silica gel (EDSG)

Preparation of the bound amines utilized Hill's procedure [13] in which a 4—10% solution of the silane in dry acetone was allowed to incubate with the silica gel for several hours in a sealed flask. In later work, refluxing toluene was used as the solvent with a 3—4-h reaction time. From 0.2 to 0.4 ml of the silane was used per gram of silica gel. In all cases the silica gel was first dried at about 120—150°C, either under vacuum in the reaction vessel or in an oven, and transferred to the vessel that was sealed quickly. Dry-box procedures were used in some cases, as noted below. After the reaction was complete, the modified silica gel was transferred quickly to a filter funnel, the reaction mixture was filtered, and the solid was washed with dry acetone (for the acetone preparation) or sequentially with toluene, methanol, and acetone for the toluene procedure. In all cases, the solid was then cured at 70—80°C for several hours under vacuum.

Amidization procedures

Initial work followed that of Weetall et al. [10—12] and Hill [13]. To the amine silica gel was added a solution of *p*-nitrobenzoyl chloride in chloroform containing triethylamine to absorb hydrogen chloride. The bound amine, acid chloride, and triethylamine were present in an approximately 1:3:4 mole ratio. This mixture was incubated in a sealed flask for 2—3 days at 30—50°C. The *p*-nitrobenzamide silica gel (NBSG) was filtered and washed with chloroform, and in later procedures also with methanol and acetone. The color of the final product was anywhere from beige to yellow—orange.

One modification of the above procedure involved vacuum degassing of the EDSG prior to reaction followed by the use of 10 mol % pyridine (with respect to total bound amine present) as a catalyst and a very large excess of the acid chloride to force the amidization of the amine to completion (1:15:20 bound amine:acid chloride:triethylamine). The resulting NBSG was rust-brown.

A second modification used 10 mol % pyridine with the normal 1:3:4 ratio of bound amine:acid chloride:triethylamine. The resulting amide was a light peach color.

Capping procedure. If a deactivated or "capped" material was desired, it was obtained at the NBSG stage in the reaction sequence. Residual hydroxyl or amine groups were deactivated by treating the solid material with a 10% solution of trimethylchlorosilane in toluene. The mixture was refluxed for 3—4 h, filtered, and washed with toluene, or with toluene, methanol, and acetone sequentially.

Preparation of p*-aminobenzamide silica gel (ABSG)*

The procedures of Weetall et al. [10—12] and Hill [13] were again used. Hill's method involved overnight reaction of a sodium dithionite solution with the NBSG at about 50°C while that of Weetall et al. required reaction

for 30—60 min with a boiling dithionite solution. It was noted early on that the more vigorous conditions were superior (see discussion) and the latter procedure was used exclusively thereafter. In both cases, an approximately 3-fold molar excess of dithionite to original amine was used, resulting in a 3—5% dithionite solution. In later work, the NBSG was vacuum-degassed prior to reduction with dithionite.

In some runs, sulfur was obtained as a dithionite decomposition product in this reaction and hot ethanol was used to dissolve the sulfur from the ABSG. A final water rinse was used in all cases.

Diazotization and coupling procedure

The typical procedure utilized a mix of the ABSG with a 2% sodium nitrite solution in 2 M HCl at 0—3°C. The bound diazonium salt (DS) was filtered, washed with cold water, and immediately added to an ethanolic 2% solution of 8-quinolinol. Both the DS preparation and coupling reaction were run for 0.5 h. The red 8-quinolinol silica gel (QSG) was filtered and washed with ethanol, 0.1 M hydrochloric acid, and water.

A modification of the above coupling procedure was employed in which the 8-quinolinol was added directly to the DS preparation mixture, and the pH raised with dilute sodium hydroxide or ammonia solution until the red product formed (pH 7.5—11). The QSG was filtered and washed with water. When this modified coupling procedure was used with the DS derived from EDSG (in which a large absolute amount of acid chloride was used in the amidization procedure because of the relatively large amine coverage), a deep red filtrate formed during the coupling step.

Reduction of the azo bond by dithionite. When it was of interest to strip off the coupled ligand for any reason, the material was boiled with a 3-fold excess (vs. original amine) of sodium dithionite in water for 0.5 h [13]. The resulting ABSG was then filtered and washed with water. The DS formation—coupling procedure was repeated if desired.

Capacity determinations

Carbon was determined in the aminated silica gels by Galbraith Laboratories, Knoxville, TN.

Copper-uptake studies were used as one measure of the amount of active amine or 8-quinolinol present. About 200 mg of the bound ligand species was shaken with 1 mmol of copper(II) nitrate for 30 min in a screw- or friction-cap vial [7]. This represented an approximately 10-fold or greater excess of metal to ligand. The solid was filtered and residual metal was washed away with 30—50 ml of water. The extracted copper(II) was then stripped off with 10—20 ml of 0.1 M hydrochloric acid followed by 20—30 ml of water. The combined washings were neutralized with 1 M ammonia and the copper was titrated with EDTA to a murexide end-point. Alternately, the copper content of the combined washings was quantified by atomic absorption.

In some cases, aqueous pH titrations were also performed as a measure of active base groups. The bound ligand (0.2—1 g) was placed in a minimum volume of water (25—50 ml) and the ligand group was titrated with 0.1 M HCl. As most of the bound ligands reacted slowly in this titration procedure [14], 5—45 min was allowed before each pH reading was taken, with the time lapse depending on the material involved and the region of the titration curve.

RESULTS AND DISCUSSION

Both the 3-aminopropyl- and 3-(2-aminoethylamino)propyl- (a substituted ethylenediamine) were employed as the original group attached to the silica gel by the usual silylation reaction. The aminopropyl silica gel (APSG) and ethylenediamine silica gel (EDSG) were also studied to obtain acid—base information, as reported elsewhere [14]. The next step in the sequence used to prepare a bonded chelating agent is preparation of the *p*-nitrobenzamide silica gel (NBSG); this is then reduced to the *p*-aminobenzamide silica gel (ABSG) with sodium dithionite; the diazonium salt is prepared from the ABSG in the usual way. The weakly electrophilic diazonium salt can then be coupled with nucleophilic ligands via the azide linkage, yielding an immobilized chelating agent. This is the basic scheme used by many workers [9—13]. Because improved efficiency in both the high-performance liquid chromatographic (h.p.l.c.) and preconcentration uses of these bound ligands is realized with higher surface coverage by the complexing group, various modifications of the usual reaction scheme were tried. The assumption was that the greater the surface coverage by the amine silane, the greater the amount of bound ligand that can be coupled in the last step of the sequence. Therefore, optimizing the original amine attachment was deemed important. Furthermore, it was observed that the amount of azide-coupled ligand resulting was substantially smaller in all cases compared to that of the original amine, and it was therefore desirable to optimize each step in the sequence leading to the coupled species.

Silylation reaction

Of the reactions discussed here, silylation has been the most studied [2] because in the majority of cases the original attached moiety is the desired species. Examples include attachment of $-C_8$ or $-C_{18}$ groups for non-polar reverse phase liquid chromatography, other organic species for gas chromatography [15], or amine or amine-derived dithiocarbamates for metal complexing [7].

Both mild acetone conditions and refluxing toluene were used as solvent for the silane, and the silica gel was degassed when toluene was used. As seen in Table 1, degassing plus the more vigorous toluene conditions appears to yield greater surface coverage for both APSG and EDSG. In this context, it is interesting that Unger reported twice the coverage by phenyltrichlorosilane

TABLE 1

Surface coverages of some typical amino silica gels

Product	Preparation method	Surface coverage (μmol g^{-1}) calculated from		
		pH	Cu^{2+a}	% C
APSG	Acetone, not degassed	250[b]	250[b]	336[b]
APSG	Acetone, not degassed	306	280	360
APSG	Acetone, not degassed	—	300	—
APSG	Acetone, not degassed	—	230	—
APSG	Acetone, not degassed	—	290	—
APSG	Refluxing toluene, degassed	—	470	—
EDSG	Acetone, not degassed	315[b]	340[b]	495[b]
EDSG	Refluxing toluene, degassed	660	680	997
EDSG	Refluxing toluene, degassed	—	514	—

[a]Based on ML_2 stoichiometry, see [14]. [b]Glove box used.

at 100 than at 50°C, and that maximum surface density is reached only after about 20 h [2, 16], while Little et al. [17] claim that reaction with various chlorosilanes is rapid and complete in a short time.

Efforts to keep the system dry using dry-box techniques were made in some cases, and essentially the same capacity results were obtained as when the silylation reaction was done simply with dry solvents and sealed reaction flasks. Significant amounts of water in the system can lead to siloxane polymer formation and reasonable dryness must be maintained.

In this reaction, it is helpful to remove air trapped in the pores of the silica gel so that the reaction mixture can contact all parts of the surface [18, 19]. Indeed, higher coverages of both APSG and EDSG were obtained when the silica gel was vacuum-degassed before the silylation mixture was added, and refluxing conditions were used to maintain air-free pores in the solid matrix. Whether degassing or the higher temperature, or both, resulted in the greater coverage is uncertain. Murray et al. [4, 5] used milder non-refluxing conditions to prevent siloxane polymer formation on their metal oxide electrode surfaces. However, with porous silica gel, more rigorous conditions and longer reaction times may be necessary to effect complete reaction in the pores. No evidence of polymer formation was observed when these more vigorous conditions were used. Exact duplication of results for silica gel and metal-oxide electrode surfaces obviously cannot be expected, as the surfaces are so different, chemically and physically. Still, the parallels that occur are informative.

It is worth noting that in the four cases for which surface coverage based on carbon determination is reported, the results are higher than those obtained by copper uptake and potentiometric acid—base titration. Leyden et al. [20] reported similar data for a series of aminosilylated silica gels. Murray [4] speculated that the silane solutions may contain deaminated, but

nitrogen-containing, material which still bonds to the surface, reducing the active amine content. This bound material would of course contribute to the carbon determined in the aminated silica gels.

In accord with established procedures [4, 5, 7, 20], the freshly prepared aminosilica gels were cured to condense water out of the residual —SiOH groups to form siloxane bridges between silylamine appendages. The unbound chloro, methoxy, or ethoxy groups probably are hydrolyzed to —SiOH during the reaction and filtering steps [2]. The curing step strengthens the surface network and minimizes etching of these groups from the surface. Murray et al. [4, 5] often found it beneficial to cure the metal oxide electrodes, but not in all cases. In the present study, this precautionary step was usually taken, although in some cases similar capacities and stabilities were obtained without curing. Occasionally, if the curing was prolonged or the vacuum was not good, a yellowish material resulted which is probably some sort of oxidation product of the amine; this has been reported by other groups [7, 21]. No significant reduction of the metal-uptake capacity of the material was found when this happened, implying that the extent of reaction was not large. Infrared (i.r.) measurements on this yellow material revealed virtually no absorption in the $-NO_2$ regions (1535 cm^{-1}, 1360 cm^{-1}, see below) nor any other unidentifiable peaks, further indicating very little oxidation to $-NO_2$.

Amide formation

Several different procedures were used in attempts to maximize the reaction of *p*-nitrobenzoyl chloride with the amine groups of APSG and EDSG; results are given in Table 2. The basic procedure of Weetall et al. [10—12] and Hill [13] utilizes a 2—3-fold excess of the acid chloride over the bound amine. In an attempt to ensure complete reaction of the terminal amine of EDSG and to encourage reaction of the secondary amine, the amidization procedure was modified to include 10 mol % pyridine as a catalyst with a

TABLE 2

Results from various amidization procedures for EDSG

Origin	Method	Resulting QSG Cu^{2+} uptake capacity (μmol g^{-1})
400 μmol g^{-1} EDSG	Usual method, 2—3-fold acid chloride excess	100, 95[a,b]
400 μmol g^{-1} EDSG	15-fold excess of acid chloride, plus 10% pyridine catalyst	50, 51[a,c]
800 μmol g^{-1} EDSG	Usual method	122[d]
800 μmol g^{-1} EDSG	10% pyridine, 2—3-fold acid chloride excess	102

[a]Two runs from the same amide. [b]Deep red filtrate from the DS coupling reaction when 8-quinolinol was added to the DS reaction mixture. [c]The filtrate was only slightly yellow when 8-quinolinol in ethanol was coupled with DS. [d]Coupled with 8-quinolinol in ethanol.

15—20-fold excess of the acid chloride. The product of this modified procedure was darker yellow—brown than that of the unmodified method, and it appeared that the reaction was more complete. However, the QSG which resulted from this product had about 50% lower copper-uptake capacity than that prepared with the unmodified amidization method.

One more modification was attempted: the pyridine catalyst was retained but the 2—3-fold acid chloride excess was used again. This procedure, however, again resulted in QSG with smaller capacity than that prepared in the usual way. Apparently, a large excess of the acid chloride or a pyridine catalyst is a liability rather than an advantage.

Because of the large absolute amounts of *p*-nitrobenzoyl chloride needed with the more highly aminated EDSG, it appeared as if significant amounts of this reagent were adsorbed on or covalently bound to the silica matrix, perhaps on unreacted silanol sites, and took part in the subsequent reaction sequence. This was manifested in the coupling of the 8-quinolinol with the diazonium salt, by the appearance of a deep red filtrate with the same color as QSG. When the less densely covered APSG was the starting material, less acid chloride was used, and little or no red filtrate was observed in the coupling reaction.

To determine if any of the original amine groups were unreacted with the acid chloride, copper-uptake studies were performed on the NBSG derivatives of APSG and the NBSG and ABSG derivative of EDSG (Table 3). The former (APSG) apparently contained little unreacted copper-active amine, as copper uptake was negligible. However, there was considerable metal uptake by the NBSG and ABSG derivatives of EDSG. Whether this was due to reaction of metal with unreacted terminal primary amine, the inner secondary amine, or some of each, is not known. However, as it is possible that these metal-active sites could interfere in extraction or chromatographic studies using the azo-coupled ligands derived from the EDSG species, it was desirable to "cap" these reactive sites, as well as any unreacted silanol sites, with tri-

TABLE 3

Copper uptake by NBSG and ABSG

Substrate	Origin	Capacity (μmol Cu^{2+} g^{-1})
NBSG 1	APSG, original Cu^{2+} capacity 150 μmol g^{-1} (300 μmol of amine/g)	3
NBSG 2	EDSG, amine coverage 800; amidization by standard method	56
NBSG 3	EDSG as above, amidization with large excess of acid chloride plus 10% pyridine	56
Capped NBSG 2	NBSG 2, degassed, refluxed 4 h with trimethylchlorosilane in toluene	3
ABSG	NBSG 2	50

methylchlorosilane at the NBSG stage of the reaction sequence. After this treatment, however, the copper uptake by the NBSG derivative of EDSG was reduced almost to zero (Table 3). It is important to note that "capping" does not destroy the groups already bound to the surface. This was demonstrated with two parallel batches of APSG-derived QSG, one "capped" at the NBSG stage and one not capped. Copper(II) uptake results for both were nearly identical, about 70 μmol g^{-1}.

In their study of metal-oxide electrode silanization reactions, Murray et al. [4, 5] found that not all surface-bound amine was active in amidization reactions; indeed only 6—30% (for propylamine-modified metal-oxide electrodes) formed the benzamide. However, they claimed that the ethylenediamine derivatives were more reactive toward amide formation than the propylamine derivatives and that up to 50% amidization occurred (100% if the terminal primary amine is considered the only reaction site). It was suggested [4] that the γ-amine sites (terminal $-NH_2$ for propylamine, inner —NH for ethylenediamine derivatives) hydrogen-bond to nearly —SiOH or —MOH sites, interfering in the amidization reaction. This probably also occurs when silica gel is the matrix [14]. However, as noted above, copper-uptake studies on APSG and its derivative NBSG imply that nearly all copper-active amine is active toward amidization. The different results found for the electrodes are due in part to surface differences between the two matrices, and in part to different amidization conditions. The excess of triethylamine always present in the method used here served not only to scavenge by-product hydrogen chloride, but possibly also to neutralize protonated amine, and perhaps to hydrogen-bond to —SiOH sites, thus freeing bound amine for reaction with acid chloride. The less than total amidization of the copper-active amine of EDSG may be due to the lower reactivity of the secondary amine as compared to the primary amine [4, 5]. Steric clogging of the 6-nm pores is also a possible hindrance to complete reaction with bulky groups such as the nitrobenzoyl chloride [2, 22], a problem not present to the same extent for the metal oxide electrodes, and more a factor for EDSG than APSG because of the longer chain. Obviously, total correspondence between metal-oxide electrodes and porous silica gel cannot be expected.

Reduction of NBSG to ABSG

The procedure used by Hill [13] to reduce the nitro group to the aniline involves overnight incubation at 50°C with sodium dithionite, while that of Weetall et al. [10—12] uses á shorter reaction time in boiling dithionite. The results of the present study imply that the more rigorous conditions are preferable. Taking the copper-uptake capacity of the QSG derived from these intermediates as a yardstick, it was found that reductions done in boiling dithionite gave values 50% higher than those done using overnight incubation. There may be two reasons for this: the higher temperatures probably assist reduction, and the shorter reaction time may minimize decomposition of the dithionite, which can undergo various disproportiona-

tion and oxidation reactions [23]. In fact, freshly prepared dithionite solutions should be used; even on standing for a few hours, cloudiness from elemental sulfur is visible. When this sulfur is filtered along with the modified silica gel, it is difficult to remove, carbon disulfide or hot ethanol being the best solvents.

It should be noted that the EDSG derived ABSG which was prepared in a large excess of the acid chloride and pyridine was still more highly colored than that prepared in the usual way.

Diazonium salt preparation and ligand coupling

In the overall reaction scheme, the preparation of the diazonium salt (DS), its handling until use, and ultimate coupling with a ligand provide the greatest opportunity for loss in capacity. Accordingly, various modifications of these last two reaction steps were investigated. In all comparative studies, 8-quinolinol was coupled to the diazonium salt, and the QSG metal-uptake capacity was used as an indicator of differences in the previous reaction efficiencies (Table 4).

Both acetic and hydrochloric acids have been used with sodium nitrite to produce the nitrous acid necessary to convert the aniline group to the diazonium salt. No difference was found between these two acids in terms of preparation and immediate coupling of the diazonium salt.

The DS preparation in hydrochloric acid was allowed to proceed for 30—150 min, and no advantage to the longer reaction time was observed. It was shown that there was no advantage to degassing the ABSG before forming the DS; the same capacity was obtained for QSG whether or not the ABSG was degassed. Possibly, by the time the bound appendage is built up to the ABSG stage, it is no longer "hidden" in the pores of the silica gel, but more or less fills them, excluding air, or this final reaction occurs only at the top edge of the pores (see below).

The diazonium salts formed with the bound organic species are similar in terms of reactivity to their homogeneous solution counterparts, and this is true also for their chemical stability. If the chloride or acetate DS is allowed to become dry, loss of activity begins almost immediately, as evidenced by the extent of reaction with 8-quinolinol (intensity of red color exhibited by the QSG). Some activity remains the next day, but within 2—3 days no reaction with 8-quinolinol occurs. Bauman et al. [24] have observed that a DS immobilized on cellulose can be stored as a damp cake in the freezer for at least a week without loss of activity. This mode of storage was investigated for filtered, washed, silica-bound DS, and the QSG copper-uptake capacity obtained after one month of storage was the same as observed initially (122 μmol Cu^{2+} g^{-1}).

The mode of activity loss of the bound DS has not been reported, but several possibilities exist, including loss of nitrogen as N_2 and replacement by —OH as the DS warms up, or creation of some neutral or electrophobic species. For example, in homogeneous solution the diazonium cation can be converted to non-coupling azo species by hydroxide [25].

TABLE 4

Formation and coupling for diazonium salts[a]

Synthetic aspect	Resultant QSG copper-uptake capacity (μmol g^{-1})	Comments
30-min DS reaction time[b]	62	Method 1
150-min DS reaction time[b]	58	Method 1
150-min DS reaction time[b]	65, 61	Method 2
ABSG degassed before DS reaction[b]	53	Method 2; no need to degas
30-min DS reaction time[c]	138	Method 1
30-min DS reaction time[c]	100, 133	Method 2; very red filtrate during coupling[d]
Dry DS[b] stood one week, then diazotized with 2% $NaNO_2$ in 1% acetic acid	45	Original capacity when coupled immediately was 56 (80—90% activity return)
Dry, inactive "DS"[b] reacted with $S_2O_4^{2-}$; $HClO_4$; HOAc; H_2O_2 (separately)	0	No reversal of inactivation
Bound 8-quinolinol stripped in boiling 1% $Na_2S_2O_4$, diazotization and coupling run again	70	Originally 50 with overnight reduction in $Na_2S_2O_4$; permits re-use for same or other ligands

[a]Two coupling methods were used: (1) filtered, washed (cold) DS was added to ethanolic 8-quinolinol solution; (2) solid 8-quinolinol was added directly to DS reaction mixture and the pH was adjusted with NaOH or NH_3 until reaction occurred (red coupled product) at pH 8—10. [b]Derived from APSG, which had 300 μmol amine g^{-1} (120—150 μmol g^{-1} Cu^{2+} uptake). [c]Derived from EDSG, which had 450 μmol en g^{-1} (200 μmol g^{-1} Cu^{2+} uptake); NBSG prepared in the usual way. [d]See text.

$$Ar{-}N{\equiv}N^{+}OH^{-} \underset{H^{+}}{\overset{OH^{-}}{\rightleftharpoons}} Ar{-}N{=}N{-}OH \underset{H^{+}}{\overset{OH^{-}}{\rightleftharpoons}} Ar{-}N{=}N{-}O^{-}Na^{+} \quad (1)$$

If a reaction other than displacement occurs, such as the above, one might be able to reverse the reaction or somehow regenerate the diazonium group. However, washing the inactive material with acetic or perchloric acid (3°C) then ice water, and immediately reacting it with 8-quinolinol produced no coupling with the ligand, despite the implication of the above reaction. As it is possible that some type of oxidation of the DS occurs on standing, the inactive material was treated with a 5% sodium dithionite solution at 3°C. Cold water washing and immediate reaction with 8-quinolinol again failed to produce coupling. Similar failure occurred with 30% hydrogen peroxide. However, when the inactive species was treated with a 2% sodium nitrite solution

(3°C), washed in cold water, and then treated with 8-quinolinol, some coupling occurred (orange—red product). When the sodium nitrite reaction was done in the presence of 1% acetic acid, 90% or more of the original activity (QSG copper uptake) could be restored. It appears that since the nitrous acid is needed to restore activity, decomposition to the $Ar—NH_2$ had occurred, and the $Ar—N{\equiv}N^+$ is then regenerated in the nitrous acid medium. The primary route of inactivation of the DS seems therefore to be conversion to the $Ar—NH_2$.

Still, in the presence of the acid, displacement by hydroxide can occur if the temperature is allowed to rise; and if base is present the inactive Ar—N=N—OH can form during the coupling procedure. Therefore, most coupling reactions are done in either weakly acidic or basic solution. For phenolic compounds, basic conditions are needed to deprotonate the hydroxyl group of the ligand and yield a species more reactive toward electrophilic aromatic substitution; however, danger of the above side-reaction is greater.

Coupling of the DS in both aqueous and nonaqueous ligand solutions has been reported. Weetall et al. [10—12] coupled several ligands with DS bound to controlled-pore glass in sodium carbonate solution, using a 24-h reaction time, and Hill [13] reported the reaction of an ethanolic solution of 8-quinolinol with silica-bound DS. In both these procedures, the bound diazonium salt was filtered and washed with ice water before reaction with the ligand. In the present study, ethanolic 8-quinolinol solutions were used successfully. The coupling is rapid as evidenced by the immediate change of the material to a burgundy red when the reactants are mixed. Typically, 30-min reaction times were employed, as longer standing did not provide greater chelating capacity. Other less reactive ligands may require increased reaction periods. Because it was felt that some DS reactivity could be lost in the filtering and washing step, a modified procedure involved adding 8-quinolinol directly to the DS reaction mixture (containing hydrochloric acid and excess of sodium nitrite) and adjusting the pH to about 10 at which point the burgundy QSG appeared. As seen in Table 4, there appears to be no significant difference in the yield of the QSG between these two methods. However, there is a danger of etching the organic appendage from the silica surface under the more basic conditions.

As mentioned above, some *p*-nitrobenzoyl chloride may have been adsorbed on the silica gel, reduced, diazotized, coupled with 8-quinolinol and washed off the silica gel as a deep crimson filtrate. The only time this was observed was when the EDSG derivatives were used, necessitating a larger absolute amount of the acid chloride to achieve the proper acid chloride: amine ratio for the EDSG, which had a higher surface coverage than the APSG series. Further, this colored filtrate appeared only when the 8-quinolinol was added directly to the diazotization reaction mixture, but not when ethanolic solutions of 8-quinolinol were used as the coupling medium. In two instances, a reddish-black gelatinous precipitate formed when the pH of the 8-quinolinol—diazotization mixture was increased with ammonia or sodium hydrox-

ide. The precipitate ultimately was washed away from the bound 8-quinolinol with methanol. Presumably, the appearance of the crimson species can be prevented or minimized by scrupulous washing or extraction of the products of the amidization reaction to remove adsorbed acid chloride.

One last feature of these coupled ligands should be mentioned. Hill [13] noted that the terminal ligand can be stripped off by reducing the azo species back to the $Ar—NH_2$ with sodium dithionite, but gave no details of the reaction. In this study it was found that several minutes in boiling 1% dithionite was sufficient for this reduction ($Ar—N=N—L \rightarrow Ar—NH_2$). If desired, the arylamine can be diazotized again and coupled to the same or a different ligand. The bond to the surface of the silica gel remains intact in this procedure, so that silylated derivatives can be recycled again and again. This procedure also affords the opportunity to repeat the diazotization and coupling reactions for practice or as a check on the preceding capacity value. In fact, an increased QSG capacity was often obtained the second time through, presumably because of the reduction of initially unreacted $Ar—NO_2$ groups, especially if the milder overnight incubation with dithionite were used the first time.

All QSG prepared in this study exhibited a copper-uptake capacity significantly less than that of the initial APSG or EDSG. Reduction in copper uptake of typically 50—75% was found. For example, several different batches of APSG with an amine coverage of about 250—400 μmol g^{-1} (125—200 μmol Cu^{2+} g^{-1} uptake, ML_2 stoichiometry [14]) yielded QSG derivatives with an 8-quinolinol coverage of 50—100 μmol g^{-1} (copper uptake capacity is also 50—100 μmol g^{-1} as 1:1 M:Q stoichiometry obtains [14]), a loss in uptake of about 75% or more. The same phenomenon was observed by Hill [13], as a loss of about two-thirds of the capacity occurred on going from the APSG to the bound 8-quinolinol. For EDSG-derived QSG, similar results were obtained. Two batches of material yielded 400—120 and 700—150 μmol g^{-1} uptake in the EDSG and QSG forms, respectively, again using 2:1, and 1:1 ligand-to-metal stoichiometry for the amine and 8-quinolinol species [14]. When it is considered that there are two amine sites that can lead to eventual coupling to 8-quinolinol, even though amidization of the inner —NH may not be as likely as at the terminal $—NH_2$, these data for 8-quinolinol coverage are even more disappointing. These results may be due to incomplete chemical reactions or to some physical phenomenon. However, the amidization reaction seems to convert most of the active amine to the amide (Table 3) and the i.r. evidence cited below shows that $ArNO_2$ reduction is complete. Therefore, the most likely chemical troublespot is the diazotization—coupling sequence, because there are so many possible side-reactions and because the weakly electrophilic DS may not couple completely even in the larger excess of ligand. However, as discussed above, several variations of the coupling reaction yielded similar capacity values. The limited pore size of the silica-gel matrix may also have an effect, so that reactions subsequent to the initial silylation are hindered sterically once the silylamine is covalently

bound to the surface inside a pore. In fact, Unger [2] postulated steric hindrance as the reason for substitution of bound groups being lesser than in homogeneous solutions. Most of the surface area of porous silica is within the pores, and these may "fill up" with bound species which cannot then react extensively with further groups. Perhaps, once the benzamide is formed on the attached moieties, the pores are close to being filled; or once diazonium salt at the pore mouth is coupled to bulky ligands, further reaction with inner-pore sites is precluded. Roumeliotis and Unger [26] found that the pore diameter and pore volume were reduced by up to 50% and 40% respectively, after reaction with hexadecyldimethylchlorosilane. Roumeliotis [27] also found decreased coverage of the surface as the area of bound groups increased in the series from trimethylchlorosilane to triphenylchlorosilane. Thus, steric blocking of the pores may well be a factor in the inability to achieve surface coverage of the coupled ligand comparable to that of the silylamine. Indeed, when the bulkier 4,7-dihydroxyphenanthroline was used in place of 8-quinolinol, significantly lower coverage resulted (20—50 μmol g^{-1}). Likewise, performing the same series of reactions leading to the coupled 8-quinolinol, on silica with a high surface area (700 $m^2\ g^{-1}$) but smaller pore size (2.2 nm) gave an 8-quinolinol coverage of only about 10 μmol g^{-1}; this experiment was not repeated, and must be confirmed. In addition, these partially filled pores can exclude certain metal ions, especially the more highly hydrated ones [28], and this could adversely affect metal—ion uptake studies. In any case, there appears to be a limit of about 150 μmol of 8-quinolinol per gram of silica gel (0.3 μmol m^{-2}), even for EDSG with varying coverages (0.7—1.3 μmol m^{-2}); steric crowding of the pores because of the bulk of the phenyl-azo-oxine linkage is strongly implied. It is also possible that pore size is not a significant factor, and that the sheer bulk of the ligands (8-quinolinol and 4,7-dihydroxyphenanthroline) precludes complete coupling to unreacted DS sites. In an attempt to sort out these possibilities, a number of bound species are being prepared on a series of silicas of different pore sizes.

Infrared characterization

Another aspect of these silica-bound ligands that bears mention in the synthetic context is their infrared spectra. It would be extremely useful to monitor specific functional groups after preparation of a particular bound species or intermediate in the reaction sequence leading to the azo-coupled ligand. Silica gel itself has been extensively studied by i.r. methods [2], but not much has been done with chemically modified silicas. Considerable effort was made in this study to explore this problem, with moderate success.

Some significant difficulties are involved in obtaining a useful i.r. spectrum; included among them are the affinity of silica gel for water vapor, the somewhat low absolute amount of organic material bound to the surface, and light-scattering problems with larger particles [2]. Both mineral oil mulls and pellet sampling were tested. The mulls protected the sample from

moisture to a greater extent, but considerably better resolution was obtained with pellets. In order to obtain spectra with absorption bands of useful amplitude, it was necessary to prepare the pellet without any inert binder material such as potassium bromide. Mechanically, this was not a problem as the silica gel provides relatively strong pellets. However, because of the adsorbed water vapor and the —Si—O bands, much of the i.r. spectrum is obscured by matrix absorptions. Between 2800 and 3800 cm^{-1}, H—OH and Si—OH stretching vibrations produce a broad deep band; significant absorption occurs at 2000 and 1870 cm^{-1} from Si—O skeletal combinations, and at 1630 cm^{-1} from H—OH bending vibrations. Nothing short of putting the spectrophotometer in a dry box, or building a special cell, could completely eliminate the water vapor problem, and this did not seem a reasonable approach for routine application. Further, the region below 1400 cm^{-1} is completely obscured by strong absorption, possibly arising from light scattering by the silica gel matrix [2]. Therefore the ranges that are useful are about 2800—2000 cm^{-1} and 1750—1350 cm^{-1}.

The spectra obtained for the bound amine species are of little use analytically. Only —CH and —NH vibrations can be present besides those of the silica gel matrix, and these are inherently weak. A weak —CH band was observed, but no reliable peak for —NH was present. When additional organic functional groups were introduced onto the bound species, more information became available. The useful bands observed are given in Table 5. The carbonyl, nitro group, and aromatic C=C bands were strong enough to be useful, especially the $-NO_2$ stretching vibrations, and the latter were a good indicator of the success of the dithionite reduction of the aromatic $-NO_2$ to $-NH_2$. For example, the use of overnight incubation of NBSG with dithionite often produced a product that exhibited residual $-NO_2$ bands, perhaps 10—30% of the original. Boiling for 30 min with fresh dithionite caused complete disappearance of the $-NO_2$ band signaling completion of the reduction reaction. The —C=O stretch and —C=C— aromatic skeletal vibrations of NBSG lie 45—50 cm^{-1} apart, and appear as a split band. In ABSG, however, the bands are shifted toward each other and are often not resolved. Less single bond character between carbon atoms in the ring results in carbon—carbon vibrations at slightly higher frequency, and a less polarized —C=O bond yields vibrations at a lower frequency [29, 30].

Spectra of QSG exhibited all the features of those of ABSG as well as another somewhat weak, broad band at 1380 cm^{-1}, which has been tentatively assigned to the phenolic —OH vibrations of the bound 8-quinolinol.

The spectra exhibit several other bands which are weak and difficult to assign, but those discussed above appeared to be most useful. Attempts to quantify these various spectra so as to evaluate critically the efficacy of various synthetic procedures proved frustrating. Light-scattering and moisture-pickup problems reduced reproducibility to unacceptably low levels.

TABLE 5

Main infrared bands for silica gel and bound species

Sample	Frequency (cm^{-1}) and characteristics	Assignment
Silica gel	3700, medium, f, sharp, some H-bonding indications	Si—OH
	3400, v. broad[a]	H—OH
	2000, 1870, moderate, broad	Si—O skeletal combinations
	1630, moderate, broad	HOH bend
	1300—250, complete absorption in pellets	—
APSG	2960, v. weak	C—H stretch
NBSG	1650, f. intense	—C=O stretch
	1605, moderate, sharp	Aromatic ring skeletal vibration
	1540, intense, f. sharp	Asymmetric $-NO_2$ stretch
	1495, weak—moderate, sharp	Aromatic ring vibration
	1360, moderate, sharp	Symmetric $-NO_2$ stretch
ABSG	1630, f. intense	—C=O stretch
	1615, moderate	Aromatic ring skeletal vibration
	1510, weak	Aromatic ring vibrations
	1420, weak	$-CH_2$ scissoring
QSG	1380, weak	Phenol —OH band
	(all ABSG peaks present also)	

[a]Intensity depends on amount of adsorbed water; in pellets these two bands merge into one very broad intense band at 2800—3800.

Thermal measurements

Because an elevated temperature may be useful to dry the surface-modified silicas, to drive off volatile impurities, or to perform reactions under more vigorous conditions, it was desirable to have some idea of the temperature stability of these materials. Thermogravimetry was therefore applied.

In Fig. 1, thermogravimetric profiles are shown for silica gel, APSG, EDSG, and QSG. The results for silica gel conform to what is known about this material [2]. Most of the physically adsorbed water is lost by 150°C and an essentially stable situation obtains up to 250—300°C, when neighboring —SiOH groups begin to release water to form siloxane bridges (—Si—O—Si—). The APSG displays virtually the same temperature profile as silica gel (Fig. 1), which agrees with Grushka's statement of stability up to about 300°C [15]. This behavior is also found for unsubstituted ≡Si—O—Si—R species such as octadecylsilane (ODS) modified silica [2, 15]. Up to 200°C, EDSG appears to have similar stability, but at higher temperatures, it loses relatively more weight than APSG, possibly because the EDSG contains a longer and heavier organic chain and greater surface coverage. On a weight basis, there is almost twice as much organic matter in the EDSG system as the APSG. Therefore, the larger relative weight loss between 300 and 500°C for EDSG than APSG (2.5 vs. 1.3%) may result from loss of a similar number of organic fragments.

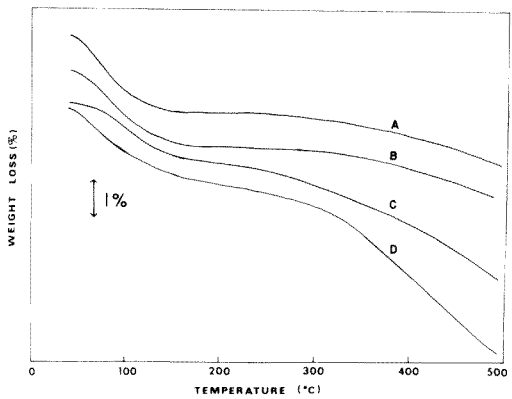

Fig. 1. Thermogravimetric curves of silica gel and some modified silicas: (A) silica gel; (B) APSG; (C) EDSG; (D) QSG. Curves were redrawn on a relative basis from the original traces. QSG was derived from APSG.

To be more quantitative than this is difficult as it is not known where the molecules break off the silica gel matrix; also, the APSG and EDSG may not break in the same place.

The QSG exhibits a considerably larger relative weight loss (4%) between 300 and 500°C than the amine derivatives, but again, the absolute mass of organic matter on the surface has increased substantially. Although the surface coverage of 8-quinolinol groups is only about 25% that of APSG, there may be a mixture of incompletely derivatized or coupled molecules present, so that the results for QSG may represent weight loss from a number of possible species, including ABSG, inactive diazonium salt, etc. A likely breaking point for this material, however, is at the azo linkage. An approach which would sort out some of these situations would be to route the thermogravimetric decomposition products directly to a mass spectrometer. Such experiments will be initiated shortly.

The important feature of the present results, however, is that these silica-bound materials seem to be stable to between 200 and 250°C. The thermogravimetric experiment is run rather quickly of course, and is not definitive about long-term stability at these temperatures; nor can it give information about reactions that do not involve a large weight change. The fact that the relatively minor weight changes in the organic portion of the material are superimposed on any changes which result from the dehydration of the residual silanol groups of the silica matrix, further complicates quantitative comparison of the results.

Conclusion

While there are clearly many parallels between the chemistry of these various bound species and their homogeneous solution counterparts, many aspects of their reactions and behavior will probably eventually be traced to

the matrix bearing them. For example, the porous nature of the silica seems to play a large part in the extent of the various reactions involved, and exclusion of air from the pores is helpful in obtaining a larger amine coverage. It further seems likely that reduced coverage by the azo-coupled ligand can be traced to filling of the pores by bulky reaction products. Where these steric factors are not important, the chemistry of the bound moieties appears to mimic that in homogeneous solution. These complexities are being understood gradually and further work will lead to heightened comprehension and more interesting and useful results.

This work was supported by grants from the Research Corporation and the University of North Carolina at Greensboro Research Council, for which the authors are grateful. The National Science Foundation is acknowledged for funds supporting two of us (C. F., Western Carolina University; R. B., Wake Forest University) in the Undergraduate Research Participation program at UNC—Greensboro. The authors also thank James Lyon and George Shahwan for preparing some of the materials discussed here.

REFERENCES

1 K. G. Allum, R. D. Hancok, I. V. Howell, S. McKenzie, R. C. Pitkethly and P. J. Robinson, J. Organomet. Chem., 87 (1975) 203.
2 K. K. Unger, Porous Silica, Elsevier, New York, 1979.
3 L. D. Bowers and P. W. Carr, Anal. Chem., 48 (1976) 544A.
4 P. R. Moses, L. M. Wier, J. C. Lennox, H. O. Finklea, J. R. Lenhard and R. W. Murray, Anal. Chem., 50 (1978) 576.
5 R. W. Murray, Acc. Chem. Res., 13 (1980) 135.
6 M. M. Guedas da Mota, F. G. Roemer and B. Griepink, Fresenius Z. Anal. Chem., 287 (1977) 19.
7 D. E. Leyden and G. H. Luttrell, Anal. Chem., 47 (1975) 1612.
8 D. E. Leyden, G. H. Luttrell, W. K. Nonidez and D. B. Werho, Anal. Chem., 48 (1976) 67.
9 J. R. Jezorek and H. Freiser, Anal. Chem., 51 (1979) 366.
10 H. H. Weetall, Biochim. Biophys. Acta, 212 (1978) 1.
11 K. F. Sugawara, H. H. Weetall and G. D. Schucker, Anal. Chem., 46 (1974) 489.
12 G. D. Schucker, K. F. Sugawara and H. H. Weetall, U.S. Patent 3886080, 1975.
13 J. M. Hill, J. Chromatogr., 76 (1973) 455.
14 J. R. Jezorek, C. Fulcher, M. A. Crowell, R. Bayliss, B. Greenwood and J. Lyon, Anal. Chim. Acta, submitted.
15 E. Grushka, Bonded Stationary Phases in Chromatography, Ann Arbor Science, Ann Arbor, 1974.
16 K. K. Unger, K. Berg and E. Gallei, Kolloid Z. Z. Polym., 234 (1969) 1108.
17 C. J. Little, A. D. Dale, D. A. Whatley and M. B. Evans, J. Chromatogr., 171 (1978) 431, 435.
18 D. E. Leyden, private communication, 1979.
19 Pierce Chemical Company, Handbook and General Catalog, Rockford, IL, 1979—80.
20 D. E. Leyden, M. L. Steele, B. B. Jablonski and R. B. Somoano, Anal. Chim. Acta, 100 (1978) 545.
21 K. T. Den Bleyker and T. R. Sweet, Chromatographia, 13 (1980) 114.
22 F. Eisenbeiss and K. F. Krebs, Pittsburgh Conference, Cleveland, OH, 1977, paper No. 311.

23 F. A. Cotton and G. Wilkinson, Advanced Inorganic Chemistry, Interscience, New York, 1962, p. 430.
24 A. J. Bauman, H. H. Weetall and N. Weliky, Anal. Chem., 39 (1967) 932.
25 R. T. Morrison and R. N. Boyd, Organic Chemistry, Allyn and Bacon, Boston, 1959, p. 579.
26 P. Roumeliotis and K. K. Unger, J. Chromatogr., 149 (1978) 211.
27 P. Roumeliotis, Thesis, Technische Hochschule, Darmstadt, 1977.
28 B. L. McConnell, K. C. Williams, J. L. Daniel, J. H. Stanton, B. N. Irby, D. L. Dugger and R. W. Maatman, J. Phys. Chem., 68 (1964) 2941.
29 R. T. Conley, Infrared Spectroscopy, Allyn and Bacon, Boston, 1966, p. 88.
30 L. J. Bellamy, Advances in Infrared Group Frequencies, Methuen, London, 1968, pp. 136—137.

Analytica Chimica Acta, 129 (1981) 49—56
Elsevier Scientific Publishing Company, Amsterdam — Printed in The Netherlands

HIGH-PERFORMANCE LIQUID CHROMATOGRAPHY OF ELECTROLYSIS SOLUTIONS: A STUDY OF THE REDUCTION OF CARBON DISULFIDE IN N,N-DIMETHYLFORMAMIDE

JOSEPH C. LODMELL, WILLIAM C. ANDERSON, MICHAEL F. HURLEY and JAMES Q. CHAMBERS*

Department of Chemistry, University of Tennessee, Knoxville, TN 37916 (U.S.A.)

(Received 18th July 1980)

SUMMARY

High-performance liquid chromatographic (h.p.l.c.) and mass spectral studies of CS_2/N,N-dimethylformamide/tetrabutylammonium iodide electrolysis solutions have shown that trithiocarbonate is not formed initially in the electrochemical reduction of CS_2. The h.p.l.c. separation on a Partisil 10-ODS column indicated the presence of at least six products or intermediates in this electrode process. A major chromatographic peak is assigned to the tetrathiooxalate dianion ($C_2S_4^{2-}$) which demonstrates the importance of this species as an intermediate in the CS_2 reduction process.

Often the organic electrode reactions which hold the most promise from a synthetic viewpoint are those which lead to electrolysis solutions of complex mixtures of intermediates and products. In order to optimize electrolysis conditions for maximum yield of the key product(s), a rapid and convenient identification method is required. Many electrolysis solutions are sufficiently complex that conventional voltammograms or electronic spectra do not give the resolution necessary for meaningful interpretation of the results. In these cases, a chromatographic separation can be a useful complement to other methods.

In this report, a high-performance liquid chromatographic (h.p.l.c.) study of N,N-dimethylformamide (DMF) electrolysis solutions is described. The method is a routine application of h.p.l.c. but it has been found useful for the separation and identification of the complex mixture of carbon—sulfur species produced on the reduction of CS_2, and the method should be applicable to many nonaqueous electrolyses.

The method (h.p.l.c.) is faster and more easily made quantitative than thin-layer chromatography (t.l.c.) which has been used with success on the CS_2 reduction solutions. Furthermore, DMF/tetraalkylammonium halide (NR_4X) solutions are not readily flash-evaporated, which is a usual preliminary step in a gas—liquid chromatographic separation of electrolysis solutions. In the procedure described below, the electrolysis solution, after treatment with an alkylating agent, is injected directly onto the h.p.l.c.

column. As shown below, some of the products of the CS_2 reduction are thermally unstable, some have modestly high molecular weights (≈300 daltons), some are oligomeric, and some are intensely colored. Since h.p.l.c. is well suited to separation and detection of samples with these properties, an attempt was made to extend the conditions of the t.l.c. determinations to an h.p.l.c. column operating with an ultraviolet–visible spectrophotometer as detector.

The reduction of carbon disulfide

The electrochemical reductions of CS_2 [1—10] and CSe_2 [11] have been studied by several research groups, and while a variety of products and intermediates have been reported, the following stoichiometry can be realized under suitable conditions. Wawzonek and Heilmann [1] were the first to identify 4,5-dimercapto-1,3-dithiole-2-thione (I) as a product of this reduction

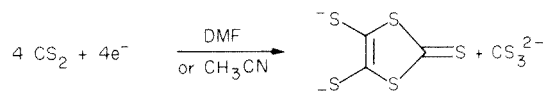

(1)

(I) (II)

This dianion, which is the species of synthetic interest in this reaction, can be produced in almost quantitative yield, according to the stoichiometry in eqn. (1) either by alkali metal reduction [12] or by electrochemical reduction in DMF or acetonitrile solutions at a platinum cathode [13].

The cyclic voltammetry of carbon disulfide in DMF at a platinum electrode is unexceptional and reveals only a broad ($E_{p/2} - E_p \approx 0.2$ V) irreversible wave with $E_p = -2.0$ V vs. the saturated calomel electrode (s.c.e.). Poorly defined product oxidation waves are evident in typical cyclic voltammograms around —0.5 to 0.0 V (vs. s.c.e.) and other anodic currents are evident at more positive potentials. Tentative evidence indicates that oxidation of the electrolysis products films and passivates the platinum surfaces which renders voltammetry a poor technique for following electrolysis products. The complex nature of the electrolysis solutions, not revealed by the voltammograms, is disclosed by the h.p.l.c. chromatograms which show peaks for at least six products or intermediates which are dependent on potential, time, and concentration.

EXPERIMENTAL

Electrochemical procedures

The CS_2 electrolyses were done in a three-compartment cell in which two fine-porosity frits (20-mm diameter) separated the working and counter electrode compartments from the middle compartment. The working electrode was a rectangular platinum gauze of ca. 20 cm^2 surface area fused to a heavy-gauge platinum wire.

All compartments of the cell were filled with 0.4 M tetrabutylammonium iodide (NBu_4I) in DMF. The working electrode compartment (ca. 150 ml) was flushed with nitrogen or argon throughout an electrolysis. Typically, pre-electrolysis was carried out at −1.9 V vs. s.c.e., then the potential was set at −1.8 V vs. s.c.e., and 0.5—1.0 ml of CS_2 was added to the working electrode compartment. The potential selected for this study was on the rising segment of the voltammetric wave. Periodically, additional CS_2 was added, usually a few drops at a time throughout the electrolysis. The solution temperature was in the range 60—90°C. The electrolyses were discontinued after the desired amount of electricity had been passed through the cell, usually 10—30 mF. For this study, conditions were not selected so as to maximize the yield of I; these have been reported elsewhere [13].

A P.A.R. Model 173 potentiostat equipped with a P.A.R. Model 179 digital coulometer was employed.

Liquid chromatography

The h.p.l.c. system used consisted of two Constametric I and II dual-piston pumps with a control module (Laboratory Data Control Co.), a Gradient Master Model 1601 control module (L.D.C.), a precolumn packed with 30—38 μm Partisil octadecylsilane (ODS; Whatman), a six-port rotary sample injector (Rheodyne Model 7120), a 25 cm × 4.6 mm i.d. analytical column packed with 10-μm Partisil 10-ODS (Alltech Associates), and a SpectroMonitor II Model 1202 variable-wavelength u.v.-visible detector (L.D.C.). The solvent was methanol/water, usually in the range 50:50 to 75:25 volume %.

Liquid-chromatographic-grade methanol (Burdick and Jackson) and doubly-distilled water which had been filtered through a 4.5-μm Millipore filter (XX10-047-00) was used as the mobile phase.

The procedure for h.p.l.c. separation of the DMF electrolysis solution involves alkylation of the anionic products and intermediates in a 1-ml syringe prior to injection onto the sample loop of the injector valve. Methyl iodide was found to react rapidly with the mercapto anionic groups formed in the CS_2 reduction process

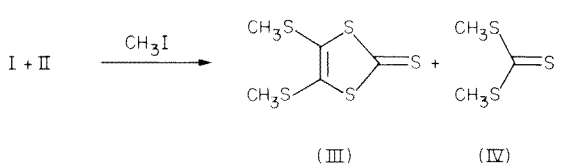

(III) (IV) (2)

For a determination, a fraction of a milliliter of electrolysis solution was drawn into the barrel of a glass syringe via a 6-in. stainless steel needle. Then the needle was replaced, an excess of methyl iodide was drawn into the syringe, and the contents were mixed. Then the sample loop (20 μl) was filled with the contents of the syringe. Qualitative control experiments with DMF solutions of K_2CS_3 (Alfa Inorganics) indicated that the alkylation

reaction was complete under these conditions (30—60 s). An authentic sample of compound III [2] was used as a reference standard to correct for small changes in retention times that were noted on a day-to-day basis.

Mass spectrometry

Mass spectrometry was also used to identify the syringe contents after evaporation of the solution. The spectra were obtained with a Hewlett-Packard Model 5980A mass spectrometer using electron impact ionization (70 eV). The mass spectra were complex, exhibiting many ions which could be assigned to fragments of III or related compounds [14]. For example, a typical mass spectrum obtained on a directly alkylated portion of the electrolysis solution contains a base peak at m/z = 91 [$CS(SCH_3)^+$], and peaks at m/z = 388 [$C_6S_4(SCH_3)_4^+$, 6.4% of base peak], 368 [$C_7S_3(SCH_3)_4^+$, 6.0%], 332 [$C_4S_3(SCH_3)_4^+$, 6.7%], 300 [$C_4S_2(SCH_3)_4^+$, 21.4%], 285 [$C_4S_3(SCH_3)_3^+$, 30.1%], 274 [$C_3S_2H(SCH_3)_3^+$, 16.4%], 226 [$(III)^+$ or $C_3S_3(SCH_3)_2^+$, 82.6%], 182 [$C_2S_2(SCH_3)_2^+$, 16.4%], 150 [$C_2S(SCH_3)_2^+$, 31.4%], 149 [$C_3S_2(SCH_3)^+$, 14.4%], 135 [$C_2S_2(SCH_3)^+$, 36.8%], 103 [$C_2S(SCH_3)^+$, 33.1%], 88 [$C_2S_2^+$, 47.8%], as well as many others with m/z less than 100.

Preparation of 4,5-dimercapto-2-oxo-1,3-dithiole (VII)

The procedure of Kissel et al. [15] was used to prepare compound VII (see below). To a solution of 2.26 g of III (10.0 mmol) in 50 ml of dichloromethane was added 150 ml of anhydrous acetic acid followed by 9.6 g of $Hg(C_2H_3O_2)_2$ (30 mmol). This solution was warmed on a hot plate and stirred for 48 h, then 150 ml of water was added, and after another 24 h the solution was extracted with three 100-ml portions of chloroform. The product is obtained in 30% yield as bright yellow needles after recrystallization from warm hexane. The melting point was 63—64°C and the mass spectrum and ultraviolet—visible absorption spectrum were consistent with the literature and structure VII.

Photolysis of VII was carried out by dissolving approximately 20 mg of VII in 40 ml of dichloromethane and irradiating with an Ace-Hanovia 450-W medium-pressure mercury arc lamp for 15 min [15]. The photolysis product was separated by h.p.l.c. as described in the text.

RESULTS AND DISCUSSION

A typical chromatogram of an electrolysis solution sampled during electrolysis is shown in Fig. 1. The immediate observation is that the electrolysis solution is more complicated than indicated by eqn. 1 since at least six products or intermediates are detected.

Where possible, assignment of the peaks in the chromatograms was made by comparison with the retention times of known compounds. Peaks 1—3 are readily identified as being due to DMF, methyl iodide, and CS_2, respectively. Peak 4 is assigned to dimethyltrithiocarbonate (IV) which is a major

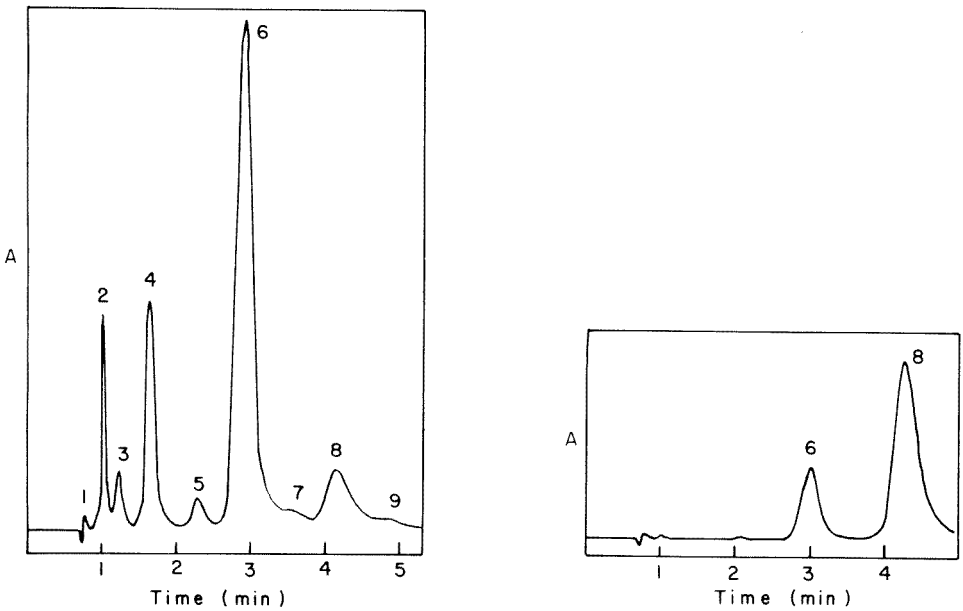

Fig. 1. Chromatogram of CS_2/DMF electrolysis solution. Flow rate, 5.0 ml min^{-1}; solvent, 50 : 50 methanol/water; 0.64 absorbance full scale at 330 nm. Electrolysis at −1.8 V vs. s.c.e., platinum cathode.

Fig. 2. Chromatogram of CS_2 electrolysis solution. Conditions same as Fig. 1; ca. 0.25 absorbance full scale at 412 nm.

electrolysis product at more negative potentials and longer electrolysis times, but which is not present in the solutions which are sampled in the first part of the electrolysis. For the chromatogram of Fig. 1, the detector was set at 330 nm which is the wavelength maximum of IV. At 412 nm which is the wavelength maximum for III, peak 8 corresponding to III dominates the chromatogram (see Fig. 2). The species which gives rise to peak 6 in the chromatograms of Figs. 1 and 2 is evidently a major, and perhaps the principal, electrolysis product under these conditions. Assignment of the species responsible for this peak is discussed below.

Several likely species could be ruled out as electrolysis products. Neither methyldisulfide or dimethylsulfide gave rise to peaks which matched those of Figs. 1 and 2. The latter compound was prepared by treating a Na_2S/DMF solution with methyl iodide. This result eliminates S^{2-} or S_2^{2-} as possible electrolysis products under these electrolysis conditions. Also, elemental sulfur, which would be reduced at the electrolysis potential [16], was not detected in the chromatograms, although some S_8 is usually obtained in the work-up of preparative scale electrolysis solutions [13].

Further information is obtained from chromatograms of electrolysis solutions obtained over a period of hours after disconnecting the working

electrode. Figure 3 shows a chromatogram of the same electrolysis solution of Fig. 1 more than 24 h after the electrolysis. Peak 6 has disappeared completely and peak 4 assigned to compound IV has increased. This indicates that the trithiocarbonate dianion is not formed directly in the electrode reaction, but arises from a slow reaction of the species which gives rise to peak 6 in the chromatograms. Reactions such as those shown in scheme (3) have been suggested previously [1, 5] and are consistent with this behavior.

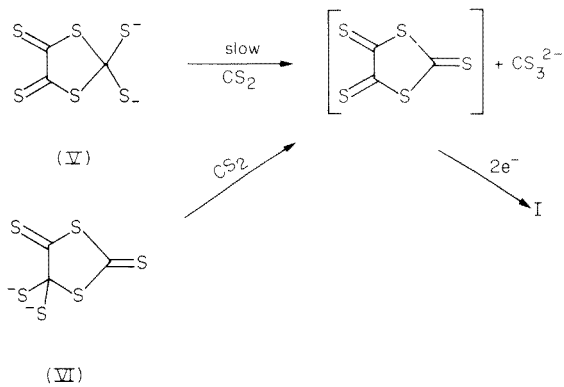

(3)

This result is not consistent with the suggested mechanisms for the electrochemical reduction of CS_2 put forth by Jeroschewski [6] or Bontempelli et al. [3].

The dimethyl ester of tetrathiooxalic acid (VIII) is assigned to peak 6 in the chromatograms. This was established by independent synthesis of VIII by photolysis (reaction 4) of the 2-oxo hydrolysis product of III (compound VII) following the procedure recently reported by Kissel et al. [15].

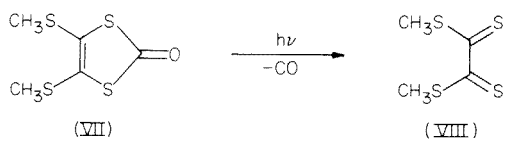

(4)

A chromatogram of the photolysis product obtained at the wavelength maximum of VIII is shown in Fig. 4. The retention volume (V_R) for the major peak in this chromatogram is within 2% of V_R for peak 6 relative to an internal standard of compound III. (The small peak at $V_R \cong 5$ min in Fig. 4 is due to III.) This assignment is supported further by chromatograms of the electrolysis solutions run at different wavelengths which indicate that peak 6 has a λ_{max} in the region of 350 nm in agreement with the known absorption spectrum of VIII [15]. This assignment is also consistent with the mass spectra of the CS_2 electrolysis solution/methyl iodide mixtures which exhibit a strong peak at $m/z = 182$.

Mass spectra also indicated that the electrolysis solutions contained significant amounts of carbon sulfide anions larger than I. Specifically, a relatively intense peak at $m/z = 300$ was routinely found in the mass spectra

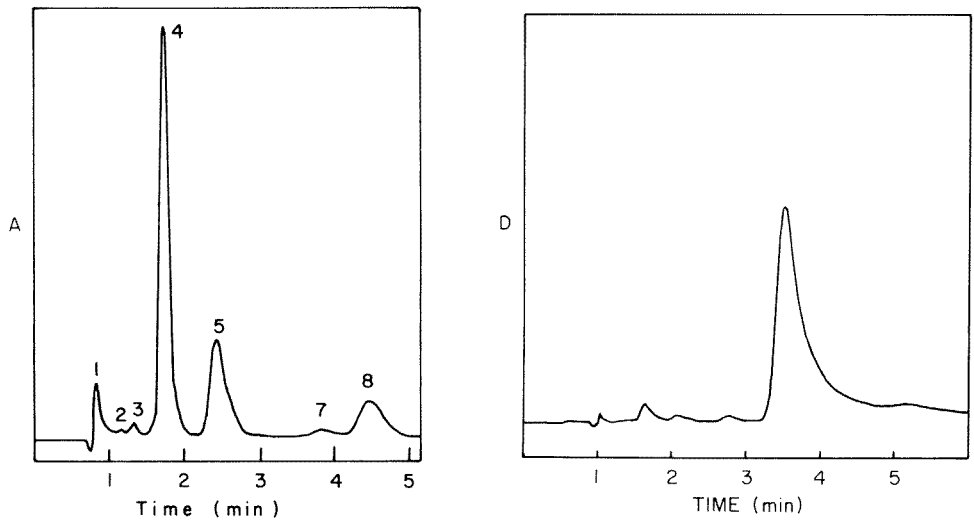

Fig. 3. Chromatogram of CS_2 electrolysis solution. Conditions same as Fig. 1, more than 24 h after electrolysis, ca. 0.5 absorbance full scale at 330 nm.

Fig. 4. Chromatogram of photolysis product of VII. Flow rate, 4.0 ml min^{-1}; solvent, 50 : 50 methanol/water; 0.384 absorbance full scale at 362 nm.

of the electrolysis solution/methyl iodide mixtures. This indicates a $C_4S_6^{4-}$ electrolysis product for which the tetraanion IX is a possible structure.

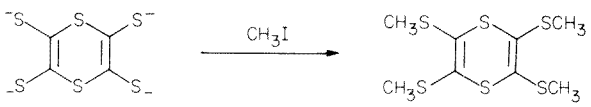

(IX) (5)

Furthermore, the tetraanion X is suggested by the small peak at m/z = 388. Alkylated derivatives of IX or X have not been reported in the literature and corroborative evidence for these assignments has not been obtained at present.

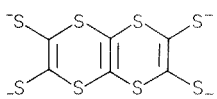

(X)

These results demonstrate the intermediacy of the tetrathiooxalate dianion in the CS_2 reduction process, which strongly suggests that the electrode reaction proceeds via coupling of the $CS_2^{\cdot-}$ radical anion:

$$2\ CS_2 \xrightarrow{2e^-} 2\ CS_2^{\cdot-} \xrightarrow{\text{fast}} C_2S_4^{2-} \qquad (6)$$

The $C_2S_4^{2-}$ species is not stable, but reacts further to give the trithiocarbonate dianion and other species of undetermined nature. The sequence of steps

leading to compound I in the reduction process remain to be elucidated, but it can be inferred from Fig. 3, which shows that the peak corresponding to III does not increase when peak 4 disappears, that decomposition of $C_2S_4^{2-}$ does not lead directly to the 1,3-dithiole ring system of I.

It is interesting that more than fifty years ago in the original work on the CS_2 reduction by alkali metals, the tetrathiooxalate structure was incorrectly assigned to compound III [17]. Radical anion coupling of $CS_2^{\cdot-}$ was also suggested as an intermediate step in the electrochemical reduction by Wawzonek and Heilmann [1], in analogy to $CO_2^{\cdot-}$ which couples to give the oxalate dianion in nonaqueous solvents [18]. The combination of electrochemical and h.p.l.c. methods has now allowed the demonstration of the existence of the elusive $C_2S_4^{2-}$ species in the electrolysis solutions.

This research was supported by the University of Tennessee and the National Science Foundation.

REFERENCES

1 S. Wawzonek and S. M. Heilmann, J. Org. Chem., 39 (1974) 511.
2 P. R. Moses and J. Q. Chambers, J. Am. Chem. Soc., 96 (1974) 945.
3 G. Bontempelli, F. Magno, G. A. Mazzocchin and R. Seeber, J. Electroanal. Chem., 63 (1975) 231.
4 U. Reuter and G. Gattow, Z. Anorg. Allg. Chem., 421 (1976) 143.
5 G. Steimecke, R. Kirmse and E. Hoyer, Z. Chem., 15 (1975) 28.
6 P. Jeroschewski, Z. Chem., 18 (1978) 27.
7 P. R. Moses, R. M. Harnden and J. Q. Chambers, J. Electroanal. Chem., 84 (1977) 187.
8 L. Syper and A. Sucharda-Sobczyk, Bull. Acad. Pol. Sci., Ser. Sci. Chim., 23 (1975) 563.
9 W. P. Krug, A. N. Bloch and D. O. Cowan, J. Chem. Soc., Chem. Commun., (1977) 660.
10 M. Mizuno, M. P. Cava and A. F. Garito, J. Org. Chem., 41 (1976) 1484.
11 E. M. Engler, D. C. Green and J. Q. Chambers, J. Chem. Soc., Chem. Commun., (1976) 149.
12 G. Steimecke, H. J. Sieler, R. Kirmse and E. Hoyer, Phosphorus and Sulfur, 7 (1979) 49.
13 M. F. Hurley and J. Q. Chambers, J. Org. Chem., 46 (1981) 775.
14 J. C. Lodmell, M. S. Thesis, University of Tennessee, Knoxville, TN, 1980.
15 T. Kissel, R. Matusch and K. Hortke, Z. Chem., 16 (1976) 318.
16 R. P. Martin, W. H. Doub, Jr., J. L. Roberts, Jr. and D. T. Sawyer, Inorg. Chem., 12 (1973) 1921.
17 B. Fetkenheuer, H. Fetkenheuer and H. Lecus, Chem. Ber., 60B (1927) 2528.
18 D. A. Tysee, J. H. Wagenknecht, M. M. Baizer and J. L. Chruma, Tetrahedron Lett., (1972) 4809.

Analytica Chimica Acta, 129 (1981) 57—67
Elsevier Scientific Publishing Company, Amsterdam — Printed in The Netherlands

APPLICATION OF CAPILLARY GAS CHROMATOGRAPHY MASS SPECTROMETRY/COMPUTER TECHNIQUES TO SYNOPTIC SURVEY OF ORGANIC MATERIAL IN BED SEDIMENT

THOMAS R. STEINHEIMER*, WILFRED E. PEREIRA and SHARON M. JOHNSON

U.S. Geological Survey, Box 25046, MS 407, Denver Federal Center, Denver, CO 80225 (U.S.A.)

(Received 26th February 1981)

SUMMARY

A bed sediment sample taken from an area impacted by heavy industrial activity was analyzed for organic compounds of environmental significance. Extraction was effected on a Soxhlet apparatus using a freeze-dried sample. The Soxhlet extract was fractionated by silica gel micro-column adsorption chromatography. Separation and identification of the organic compounds was accomplished by capillary gas chromatography/mass spectrometry techniques. More than 50 compounds were identified; these include saturated hydrocarbons, olefins, aromatic hydrocarbons, alkylated polycyclic aromatic hydrocarbons, and oxygenated compounds such as aldehydes and ketones. The role of bed sediments as a source or sink for organic pollutants is discussed.

The Water Resources Division of the U.S. Geological Survey is concerned with providing the hydrologic information required for optimum utilization and management of water resources. This is accomplished by conducting analytical investigations which describe the physical and chemical properties of surface and ground water. Comprehensive water-quality assessment must include examination of the particulate phase, whether it is suspended in the water column or settled out as bed material.

Interest in definitive analysis of environmental samples for trace organic materials continues to increase rapidly. This is due, in part, to monitoring requirements which have been mandated by federal legislation [1] and which are complemented by advances in sophisticated analytical instrumentation. Water-quality assessment requires increasingly complex and multidisciplinary approaches to problem solving. Historically, such evaluations have been based on the nature and concentration of chemical species found in solution. These efforts, which dealt mostly with inorganic chemical species, did not fully recognize that only a small fraction of the total chemical load transported by a stream may be present in the dissolved phase. The bulk of the material may be carried along in a "piggyback" fashion, which is determined largely by the nature and concentration of suspended sediment [2]. Indeed, the availability of large surface areas on suspended sediment may provide the major transport mechanism for many chemical species.

Many of the organic compounds which have been identified in environmental samples can be characterized as non-ionic, low in water solubility, and somewhat suspect in their environmental compatibility and impact. These synthetic materials, which are not ubiquitous to the environment, occur as a result of human activities; thus, they become potential pollutants. Naturally occurring organic material, such as fulvic acids, by virtue of their surfactant properties, can bind hydrophobic organic pollutants and increase their affinity for the aqueous phase [3]. It has been reported that the solubility of DDT in aqueous 0.5% sodium humate solution is 20 times greater than in water [4]. Fulvic acids serve as vehicles for transport of water-insoluble organic compounds [5, 6]. Bed sediments, which consist of humic material adsorbed to the surface of clay minerals, can also bind hydrophobic organic pollutants [7]. Binding to hydrophobic surfaces of sediment particles in lakes and rivers constitutes a major, natural, short-term concentration mechanism. However, sediment particles do not serve as a permanent sink for these organic pollutants; the bound organics are available for later release [8, 9]. Certain hydrophobic pollutants such as polychlorinated biphenyls (PCB) are taken up by invertebrate organisms that either live or feed in the sediments, and are passed along in the food chain to primary carnivores. This process of bioaccumulation results in an eventual increase in the concentration of PCB in carnivorous fish, and is eventually passed on to man [10]. Following dissipation of stream energy and particle settling, organic constituents associated with bed sediments may be considered to be historical descriptors of the chemical quality of water [2]. As such, they become useful as indicators of potential pollution problem areas.

In view of the importance of bed sediments as related to pollution problems, a synoptic survey was undertaken to characterize organic pollutants in an area impacted by heavy industrial activity. A bed sediment sample was taken at Vincent Landing on the Calcasieu River in Louisiana some 4.5 miles south of Hollywood, and approximately 5 miles southwest of Port of Lake Charles. A "stovepipe dredge" bed material sampler was used to collect the bed sediment, which was taken in November of 1979. The dredge was pulled by rope along the bed of the stream, scooping up bed sediment as it moved.

The hydrologic environment south of Lake Charles, Louisiana, and around the Calcasieu River is extremely complex. South of Lake Charles, the Calcasieu River enters a flat coastal environment of indeterminate drainage. The flow in the river is confined to the ship channel portion of the stream. There are, however, numerous outlets from the channel into the marsh areas adjacent to the river. The flow is tidal-affected and virtually impossible to gauge. Attempts to measure the flow continuously have been largely unsuccessful; an experiment conducted by the Louisiana District, U.S. Geological Survey, which involved injection of a fluorescent dye to monitor movement of the water, suggested that the net movement is of the order of a few miles per week. The water in the Calcasieu River south of Lake Charles is not

suitable for most industrial or municipal purposes because of its high salt content. Most of the industries in the area use ground water or obtain surface water from the Houston River or the Calcasieu River some miles upstream north of Lake Charles. Numerous chemical facilities are located in the area. These include manufacturing and processing of such diverse materials as petroleum, sodium hydroxide, chlorine, teflon, butadiene, and synthetic rubber. Wastes from these plants are stored in holding ponds, some of which are known to leach into the river. Drainage from nearby oil and gas fields may also discharge into the Calcasieu River, although it seems unlikely that these fields would be a major contributor to organic pollution in the river bed.

The variability and complexity of the sample matrix outlined above demanded highly efficient extraction and clean-up procedures, coupled with the use of sophisticated analytical instrumentation. The instrumentation best suited for this application was computerized capillary column gas chromatography/mass spectrometry (g.c./m.s.). Glass capillary columns provided greater compound resolution and sharper peaks than conventional packed columns. When interfaced to a mass spectrometer and interactive data system, the combined technique is extremely powerful for the characterization of trace organic compounds. With the development of the Mass Spectral Search System (MSSS) [11], and data bases such as the National Bureau of Standards (NBS) mass spectral library and minicomputer software to permit simultaneous data acquisition in the foreground mode and data reduction in the background mode, it is possible rapidly to identify many new classes of organic environmental pollutants.

EXPERIMENTAL

A bed sediment sample (28.2 gm kg^{-1} organic carbon, dry weight basis) was collected as outlined above, chilled in ice, delivered to the laboratory, and analyzed upon receipt. The sample was mixed and a 137-g portion taken for analysis. Water was removed by lyophilization overnight. The dried material (35.35 g) was sonicated with benzene—methanol (2:1) and then extracted in a Soxhlet apparatus for 24 h. The extract was concentrated to 1 ml in a Kuderna-Danish apparatus. A silica adsorption micro-column was prepared containing 1 g of activated neutral silica gel packed in a chromatography column (6 mm i.d. × 150 mm length, providing a bed depth of 10 cm) and prewashed with 20 ml of hexane. A portion of the concentrated extract was charged to the column for fractionation. Three fractions were collected: (1) 10 ml of hexane; (2) 10 ml of dichloromethane; and (3) 10 ml of dichloromethane—methanol (1:1).

Each fraction was concentrated to 1 ml using a Kuderna-Danish apparatus and analyzed by capillary column g.c./m.s. The Finnigan Model 4023 g.c.—m.s.—data system used was equipped with a 30 m × 0.25 mm i.d. glass capillary column coated with SE-54. The gas chromatographic conditions were as

follows: injection technique, splitless; initial temperature, 50°C; initial time, 4.0 min; programming rate, 6°C min^{-1}; final temperature, 260°C; final time, 40 min; and injector temperature, 250°C. The mass spectrometer was operated in the EI mode using an ionizing voltage of 70 eV and an ionization current of 250 uA.

RESULTS AND DISCUSSION

The purpose of this study was to carry out a synoptic survey of organic substances in the bed sediment. All reported results are qualitative. No attempts were made to quantify individual components, because of compositional complexity, inadequate knowledge of the degree of isomerism, and lack of suitable reference standard materials. The organic compounds identified in the Calcasieu River sediment are listed in Table 1. Tentative identifications were based upon computerized matching of mass spectra in the sample with that of spectra contained in the NBS library, and from a knowledge of mass spectral fragmentation patterns. In addition, retention times of ten components, for which pure standards were available, were matched against sample components to within less than 0.1 min. Special precautions were taken throughout the analysis to avoid introduction of artifacts or other contaminants. These included the baking of glassware, use of high-purity solvents (organic residue analysis grade), and heat-treated chromatographic grade adsorbents.

TABLE 1

Organic pollutants identified in Calcasieu River bed sediment

Fraction 1	Fraction 2	Fraction 3
n-$C_{11}H_{24}$-n-$C_{31}H_{64}$	Toluene	Methylpentanol isomer
Methylcyclohexane	α-Methylstyrene	3-Hexanone
Dimethyloctane isomer	Acetophenone	3-Hexanol
Ethylheptane isomer	Nonanal	Methylpentanol isomer
Ethylmethylhexane isomer	Dodecanal	Methylcyclopentanol isomer
Ethylmethylheptane isomer	Biphenyl	1-Hexanol
Trimethylheptane isomer	Trimethylindane isomer	2-Cyclohexene-1-one
Trimethylnonene isomers	Dimethylnaphthalene isomers	Phenol
Tetramethylhexane isomer	Trimethylnaphthalene isomers	Methylpentenone isomers
Dimethylhexene isomer	Methylisopropylnaphthalene isomer	6-Methyl-2-heptanone
Dimethyloctane isomer	Trimethylphenylindane isomer	Methyl undecanoate
Butylnonane isomer	Methylphenanthrene isomers	Methyl tetradecanoate
Methyldecane isomer	Methylanthracene	Methyl palmitoleate
Dimethylundecane isomer	Methoxyanthracene	Methyl palmitate
Methyltridecane isomer	Dimethylphenanthrene isomers	Diisooctyl phthalate
2,6,10,14-Tetramethylpentadecane (pristane)	Trimethylphenanthrene isomers	
	Methylpyrene isomers	
Trimethyldodecane isomer	Tetramethylphenanthrene isomers	
Trimethyltridecane isomer	Terphenyl isomers	
2,6,10,14-Tetramethylhexadecane (phytane)	Δ1,1-Biindan	
	Benz(a)anthracene	
	Methylbenz(a)anthracene isomer	
	Benzonaphthothiophene isomer	

In the sample preparation and workup, Soxhlet extraction was chosen because of its efficiency and simplicity. After overnight refluxing, the extract assumed a dark-green to black appearance. These colored materials probably result from natural decay and/or synthesis processes involving organic compounds contained in all living matter. To simplify the mixture prior to gas chromatography and remove naturally occurring high-molecular-weight organic compounds, further cleanup of the extract was necessary. Silica gel micro-column chromatography has previously been reported for clarification of sediment or soil extracts [12].

The composition of Fraction 1 of the sediment extract indicates a very complex mixture of normal and branched chain alkanes and alkenes, suggesting a multiplicity of sources. Figure 1 shows a reconstructed ion chromatogram

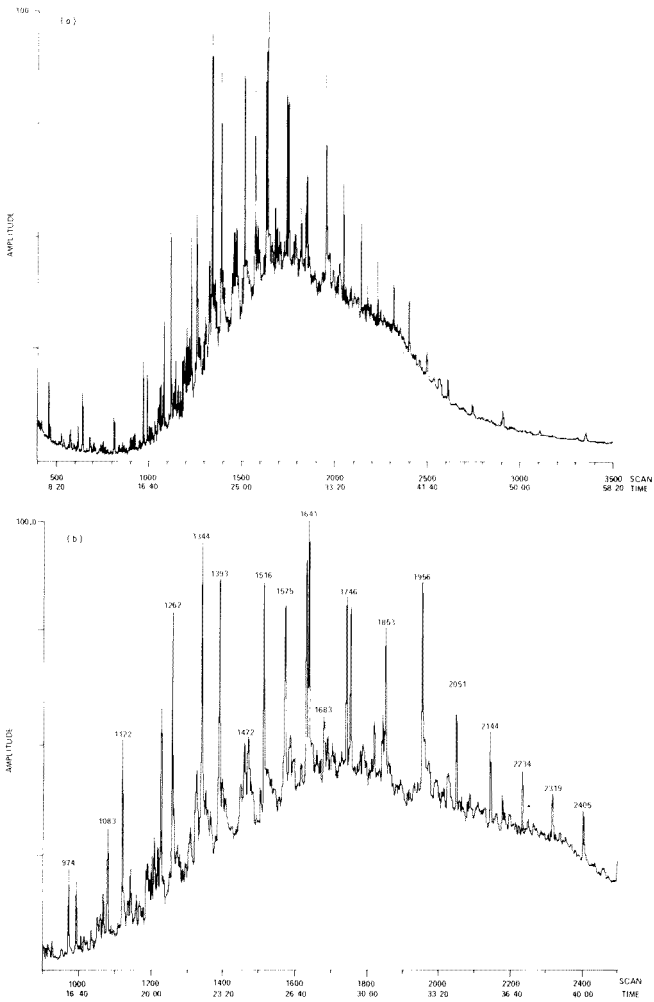

Fig. 1. (a) Reconstructed ion chromatogram of Fraction 1 from the bed sediment. (b) Expanded portion of (a).

of Fraction 1, clearly demonstrating the effectiveness of small bore capillary columns in resolving components of very complex mixtures. Each compound of the homologous series of n-alkanes between C_{11} and C_{31} was identified. The absence of an odd/even carbon number predominance attests to input from sources other than higher plants. Pristane and phytane were also identified in Fraction 1, with the pristane concentration approximately double that of phytane. The occurrence and relative ratios of these two isoprenoid skeleton-containing hydrocarbons are probably determined by the nature of the indigenous biota. Figure 2 is a spectrochromatic map displaying mass chromatograms characteristic of the alkanes identified in Fraction 1.

The large envelope beneath the peaks in Figs. 1 and 2, also referred to as the "hydrocarbon hump", attests to the large number of unresolved components yet to be separated and identified. Similar chromatographic features are apparently not seen in biota samples [13]. It is likely that such a complex hydrocarbon assemblage is not of biogenic origin. Possible sources of such complexity are limited to contamination by petroleum-derived hydrocarbons, input from combustion processes, or contribution from fossil hydrocarbons present in surrounding ancient sediments [13].

Figure 3 shows a reconstructed ion chromatogram of Fraction 2. Most of the compounds identified in Fraction 2 were either cyclic or aromatic in character. The alkylated benzenes and naphthalenes probably result from industrial activities. Similar compounds have been reported to be components of an aromatic and naphthenic oil used to extend and soften rubber formulations [14]. Several alkylated polycyclic aromatic hydrocarbons (PAH) were also identified in Fraction 2; PAH homologs of more than four rings were not identified. Geochemical formation, biosynthesis by algae or higher plants, and incomplete combustion of organic material are among the mechanisms proposed for the formation of PAH [13]. Thermal PAH formation can occur over a wide range of temperatures and with many source materials.

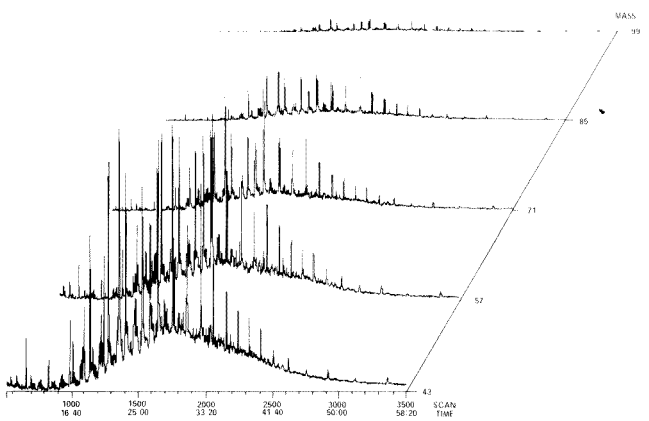

Fig. 2. Spectrochromatic map displaying mass chromatograms characteristic of n-alkanes in Fraction 1.

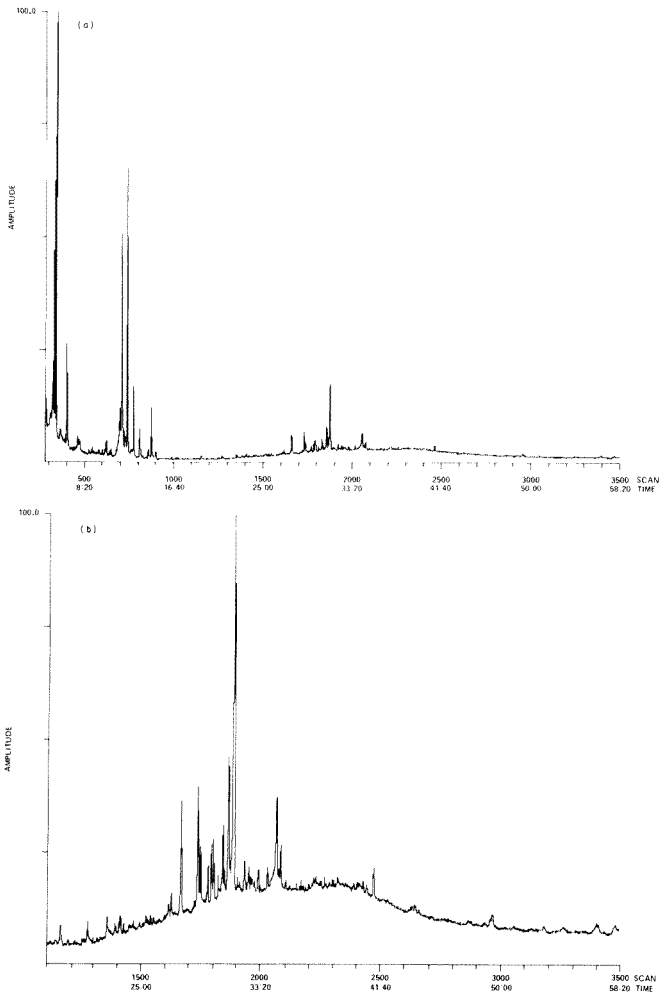

Fig. 3. (a) Reconstructed ion chromatogram of Fraction 2 from the bed sediment. (b) Expanded portion of (a).

Lower formation temperatures preserve a higher degree of alkylation. Thus, the slow formation of petroleum may lead to complex and highly alkylated PAH assemblages [15]. The predominance of alkylated PAH in Fraction 2 suggests that the primary source of these compounds is from petroleum processing, particularly as several large refineries operate in the area. Polycyclic aromatic hydrocarbons and their alkyl derivatives were reported to be the most abundant class of organic compounds identified in sediment taken from the Charles River near Boston [16]. Other compounds identified in that study included aliphatic and olefinic hydrocarbons.

Figure 4 shows a spectrochromatic map of characteristic masses corresponding to the molecular ions of several alkylated aromatic and polycyclic

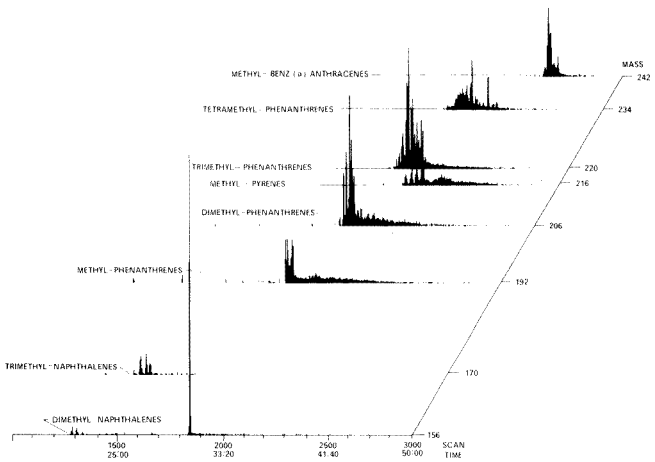

Fig. 4. Spectrochromatic map of alkylated aromatic and polycyclic aromatic hydrocarbons.

aromatic hydrocarbons. These mass chromatograms [17], which are plots of the absolute intensity of one mass versus scan time, are useful as a means of detecting a specific compound or class of compounds. The spectrochromatic map or three-dimensional orthogonal display is an extremely powerful tool for accentuating specific compounds in a complex sample matrix. The number of isomers suggested by the fine structure within a peak cluster further attested to the complexity of the mixture. The spectrochromatic map shown in Fig. 5 for *m/z* 242 clearly indicates the presence of at least five isomers of methylbenz(a)anthracene.

In addition to the PAH biphenyl and all three terphenyl isomers were identified in Fraction 2. Biphenyl has been reported to be a common dye carrier [18]. When mixed with the colorant during the dyeing process, these compounds serve as accelerators, and promote a uniform colored appearance. The spectrochromatic map shown in Fig. 6 indicated the presence of three terphenyl isomers. The accompanying reconstructed ion chromatogram does not indicate the presence of these isomers. The terphenyls are used as starting materials for the synthesis of polychlorinated terphenyls (PCT), such as the Aroclor series 25, 44, and 54, or can be formed by the photolysis of PCT [19]. A terphenylol isomer was also identified in Fraction 2. This compound is believed to be a photochemical degradation product of the PCT. The only hetero-atom-substituted PAH identified in Fraction 2 was a benzonaphthothiophene isomer. The mass spectrum of this compound showed a very intense molecular ion (*m/z* 234, base peak), M − 32 ion, and M + 2 ion (^{34}S isotope peak). This compound has been identified previously in coal tar [20].

A reconstructed ion chromatogram of Fraction 3 is shown in Fig. 7. Components identified in Fraction 3 include polar compounds such as

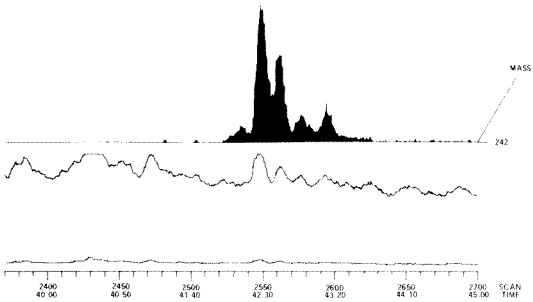

Fig. 5. Mass chromatogram (m/z 242) and reconstructed ion chromatogram of methylbenz(a)anthracene isomers.

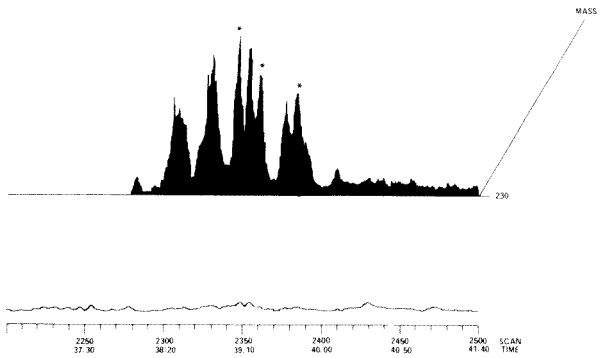

Fig. 6. Spectrochromatic map and reconstructed ion chromatogram of terphenyl isomers. Asterisks indicate terphenyl isomers.

ketones, alcohols, phenol, and several fatty acid esters. The possibility that the free fatty acids were methylated on-column during elution from the silica with dichloromethane/methanol cannot be dismissed. Aldehydes, ketones, and alcohols probably result from oxidative cleavage of higher-molecular-weight olefinic structures by bacteria. However, it is also possible that some of these materials, which have commercial usage as industrial solvents, may occur as point source pollutants from industrial activities. The fatty acids identified in this fraction probably result from metabolism by biota.

Conclusions

The purpose of a synoptic survey is to present a general, but comprehensive, overview of the environmental chemistry in the study area. The organic compounds residing on bed sediment are a complex mixture of natural products and pollutants resulting from waste discharges. In an area impacted by petrochemical industries, a predominance of materials resulting from the latter seems most likely. The deposition and concentration of these materials on bed sediment is determined by river hydrology and other general river conditions. Because of their hydrophobic nature, many of the pollutants identified are susceptible to bioaccumulation. The redistribution of some of

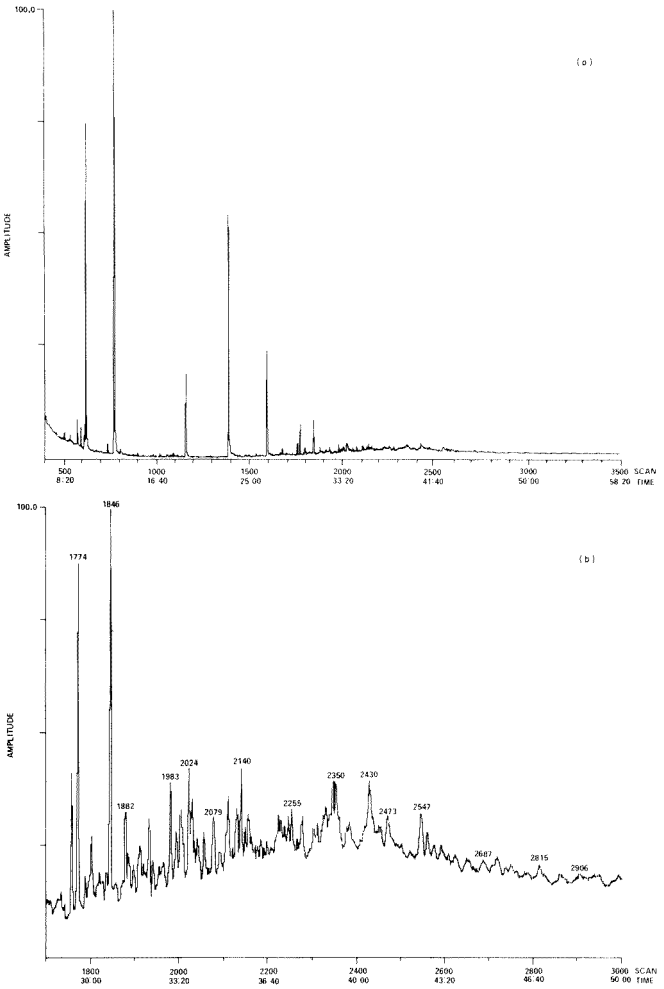

Fig. 7. (a) Reconstructed ion chromatogram of Fraction 3 from bed sediment. (b) Expanded portion of (a).

these contaminants into the water column during periods of high flow or other kinds of perturbation argues persuasively for synoptic-survey bed sediment analysis as an indicator of water-quality. Detection of trace levels of organic pollutants in a complex sample matrix is an extremely difficult task; techniques like those described are required. Additional refinements in the capillary column gas chromatographic portion of the analysis may reveal further organic pollutants of environmental significance.

The authors express their thanks to the personnel of the Louisiana District and to Frank Wells of the Texas District, U.S. Geological Survey, for their assistance and cooperation in furnishing the bed sediment sample.

REFERENCES

1 B. R. Barrett, Environ. Sci. Technol., 12 (1978) 154.
2 H. Feltz, in Contaminants and Sediments, Vol. 1, Proceedings of the Symposium on Processes Involving Contaminants in Sediments, 177th Meeting of the American Chemical Society, April, 1979. Honolulu, HI, Ann Arbor, MI, 1980, p. 271.
3 J. P. Hassett and M. A. Anderson, Environ. Sci. Technol., 13 (1979) 1526.
4 R. L. Wershaw, P. J. Burcar and M. C. Goldberg, Environ. Sci. Technol., 3 (1969) 271.
5 G. Ogner and M. Schnitzer, Geochim. Cosmochim. Acta, 34 (1970) 921.
6 M. Schnitzer and G. Ogner, Isr. J. Chem., 8 (1970) 505.
7 M. Schnitzer and S. U. Kahn, Soil Organic Matter, Elsevier, New York, 1978.
8 S. W. Karickhoff and S. D. Brown, J. Environ. Qual., 7 (1978) 246.
9 J. T. Turk and D. E. Troutman, Environ. Sci. Technol, in press.
10 J. J. Delfino, Environ. Sci. Technol., 13 (1979) 1462.
11 S. R. Heller, J. M. McGuire and W. L. Budde, Environ. Sci. Technol., 9 (1975) 210.
12 Y. L. Tan, J. Chromatogr., 176 (1979) 319.
13 W. Giger and C. Schaffner, Advances in Organic Geochemistry, Proceedings of the 7th International Meeting on Organic Geochemistry, Madrid, Spain, 1975, p. 375.
14 G. A. Jungclaus, L. M. Games and R. A. Hites, Anal. Chem., 48 (1976) 1894.
15 W. W. Youngblood and M. Blumer, Geochim. Cosmochim. Acta, 39 (1975) 1303.
16 R. A. Hites and W. G. Biemann, in T. R. P. Gibb, Jr., (Ed.), Analytical Methods in Oceanography, Symposium at the 168th Meeting of the American Chemical Society, Sept., 1974, Atlantic City, NJ, Am. Chem. Soc., Washington, DC, 1975, p. 188.
17 R. A. Hites and K. Biemann, Anal. Chem., 40 (1968) 1217.
18 R. A. Hites, J. Chromatogr. Sci., 11 (1973) 570.
19 S. Safe, N. J. Bunce, B. Chittim, O. Hutzinger and L. O. Ruzo, in L. H. Keith (Ed.), Identification and Analysis of Organic Pollutants in Water, Ann Arbor Science Publishers, Ann Arbor, MI, 1976, p. 35.
20 H. Borwitzky and G. J. Schomburg, Chromatographia, 170 (1979) 99.

Analytica Chimica Acta, 129 (1981) 69—77
Elsevier Scientific Publishing Company, Amsterdam — Printed in The Netherlands

THE DETERMINATION OF THE IONISATION CONSTANTS OF POLYMALEIC ACID AND THE STABILITY CONSTANTS OF ITS COMPLEXES WITH COPPER

T. E. EDMONDS, PU GUOGANG[a] and T. S. WEST*
The Macaulay Institute for Soil Research, Craigiebuckler, Aberdeen AB9 2QJ (Gt. Britain)
(Received 17th March 1981)

SUMMARY

The ionisation constants of unfractionated polymaleic acid, H_3A, a synthetic analogue of fulvic acid, and the stability constants of its copper complexes were determined by differential pulse polarography. The ionisation constants are: pK_1 5.16, pK_2 7.04 and pK_3 9.82 at 20° C and ionic strength 0.12 M. The stability constant of the CuHA complex, which is the predominant species at pH 5—9, lies in the range log (CuHA) = 7.15—8.7; the mean value is 8.17.

The organic matter in soil is composed of polyelectrolytes whose principal acidic functional groups are carboxyl and phenolic hydroxyl, but which also contain amino, keto and aliphatic hydroxyl groups as potential active groups. Humic colloids form stable compounds with a number of metallic ions. Recently the study of properties of metal complexes with fulvic and humic acid has received increased attention from soil chemists. Several methods have been reported for determination of the ionisation constants and the structure of humic colloids, as well as the stability constants of their metal complexes. These methods are based on the use of ion-exchange [1], titrimetry [2], potentiometric titration [3, 4], ion-selective electrodes [5, 6], and anodic stripping voltammetry [7]. The complexity of the interactions between metal ions and organic matter causes some difficulties in these studies. At least four types of interaction are possible [8]: simple neutralisation of the acid, coordination of a polar humic group with a water molecule forming part of the hydration shell around the cation, coordination in which the carboxyl group is directly coordinated with a metal ion, and chelate formation in which the cation is bound to more than one site on the ligand. In differential pulse polarography, a shift of the peak potential of the polarographic wave of the metal ion occurs upon complexation; this shift is a function of the stability of the coordination complex, or chelate. Differential pulse polarography is thus a suitable method for the determination of both

[a]On leave from Department of Chemistry, University of Science and Technology of China, Hofei, People's Republic of China.

0003—2670/81/0000—0000/$02.50

the ionisation constants of the ligand and the stability constants of its complexes [9, 10].

Because humic and fulvic acids obtained by the alkali—acid extraction of soils may be of variable composition depending on the treatment used and the nature of the soil extractant, polymaleic acid (PMA), a model compound known to be analogous to fulvic acid and soluble organic matter in soil [11], was used in these studies. The present paper describes a differential pulse polarographic method for the determination of the ionisation constants of PMA and the stability constant of its principal complex with copper. Three successive ionisation constants and the stability constant of the CuHA type of complex at 20°C and ionic strength 0.12 M are reported.

THEORY

Provided that the reduction of a metal ion, M^{n+}, and its complex ion, MX_j (charge of complex ion is omitted for clarity), to the metallic state (amalgam) at the dropping mercury electrode (DME) is reversible and diffusion-controlled, the difference between the half-wave potentials for the two processes, $\Delta E_{1/2}$, is given [12] by $\Delta E_{1/2} = 2.303\ RT(nF)^{-1} \log \beta(MX_j)[X]^j$ where [X] is the concentration of the free ligand, and $\beta(MX_j)$ is the stability constant of the complex ion, MX_j: $\beta(MX_j) = (MX_j)/[M^{n+}]\ [X]^j$.

It has been shown [13] that there is a simple relationship between the half-wave potential values ($E_{1/2}$) of d.c. polarography and the peak potential (E_p) of differential pulse polarography: $E_p = E_{1/2} - \Delta E/2$, where ΔE is the amplitude of the applied pulse in differential pulse polarography. Thus, it appears that the shift of half-wave potentials, $\Delta E_{1/2}$, between a simple aquo—metal ion and its complex ion, is equal to the shift of their peak potentials ΔE_p [10]. Then

$$\Delta E_p = \Delta E_{1/2} = 2.303\ RT(nF)^{-1} \log \beta(MX_j)[X]^j$$

$$= 2.303\ RT(nF)^{-1} \log \beta(MX_j) + 2.303j\ RT\ (nF)^{-1} \log [X] \qquad (1)$$

The shift of peak potentials ΔE_p may be measured experimentally, hence the stability constants β may be calculated if the concentration of free ligand species [X] is known. However, polymaleic acid (H_xA) is a weak organic acid, thus it is not possible to substitute the analytical concentration for the concentration of free ligand [A]. Unfortunately, there is no reliable information about the ionisation constants of polymaleic acid, which must be used to calculate the concentration of free ligand [A]. It was necessary, therefore, to determine the ionisation constants of polymaleic acid (PMA) before calculation of the stability constant.

The differential pulse polarograms of solutions containing copper(II) and PMA at various pH values were recorded (Fig. 1). The variations in ΔE_p (or E_p) as a function of the pH of the analysed solutions are shown in Fig. 2. In view of the shape of the ΔE_p (or E_p)—pH curve, it is reasonable to assume

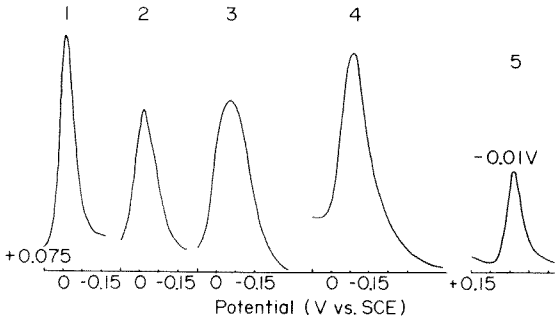

Fig. 1. The differential pulse polarographic peaks of the copper—polymaleic acid complex (1—4) and of copper ion alone (5). 2.0×10^{-4} M Cu^{2+}; 1.2 mg cm^{-3} unfractionated polymaleic acid; 0.04 M Na_2SO_4; drop time 2 s; scan rate 2 mV s^{-1}; pulse amplitude 5 mV. (1) pH 3.11, current range 5 μA; (2) pH 4.50, current range 5 μA; (3) pH 6.09, current range 2 μA; (4) pH 8.45, current range 1 μA; (5) pH 4.64, current range 10 μA.

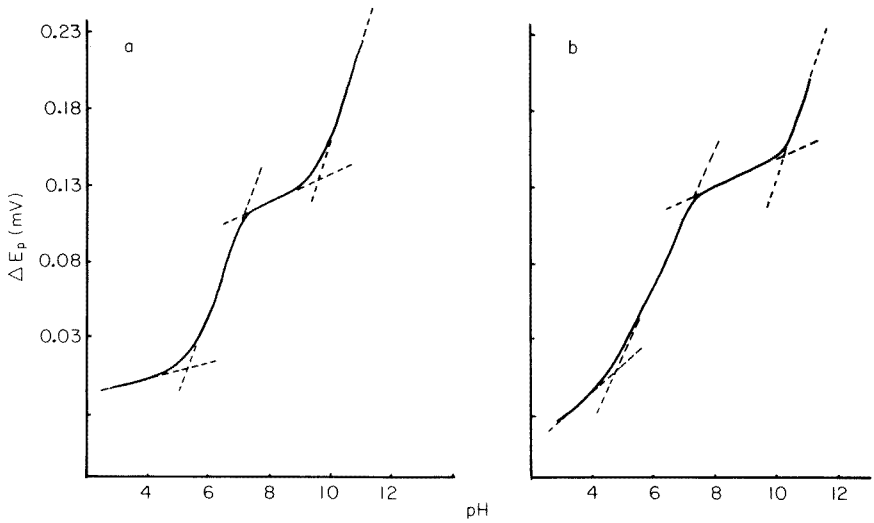

Fig. 2. The shift of peak potential as a function of pH (experimental conditions as shown in Fig. 1): (a) 1.2 mg PMA cm^{-3}; (b) 6.0 PMA cm^{-3}.

that PMA binds with three hydrogen ions, and can be considered as a tribasic acid, H_3A, with successive ionisation constants: $K_1 = [H_2A^-][H^+]/[H_3A]$; $K_2 = [HA^{2-}][H^+]/[H_2A^-]$; and $K_3 = [A^{3-}][H^+]/[HA^{2-}]$.

The total concentration of PMA species, C_A^T, may be expressed thus

$$C_A^T = [A^{3-}] + [HA^{2-}] + [H_2A^-] + [H_3A] \quad (2)$$

The concentration of each potential ligand species may be obtained from the ionisation constants in the usual way: $[A^{3-}] = C_A^T \alpha_A$; $[HA^{2-}] = C_A^T \alpha_A [H^+]/K_3$; $[H_2A^-] = C_A^T \alpha_A [H^+]^2/K_2K_3$; and $[H_3A] = C_A^T \alpha_A [H^+]^3/K_1K_2K_3$, where $\alpha_A = (K_1K_2K_3)/([H^+]^3 + K_1[H^+]^2 + K_1K_2[H^+] + K_1K_2K_3)$.

For the copper—PMA complex, substitution of these expressions for $[A^{3-}]$ to $[H_3A]$ into eqn. (1) produces

$$\Delta E_p = 2.303\, RT(nF)^{-1} \log \beta(CuA_j) + 2.303\, RT(nF)^{-1}\, j \log C_A^T + 2.303\, RT(nF)^{-1} \log \alpha_A \quad (3)$$

For certain pH ranges, the following equations may be used

$$\Delta E_p = k + 2.303\, RT(nF)^{-1} \log K_1K_2K_3 + 3\text{pH} \qquad (\text{for pH} \ll pK_1) \quad (4)$$

$$\Delta E_p = k + 2.303\, RT(nF)^{-1} \log K_2K_3 + 2\text{pH} \qquad (\text{for } pK_1 \ll \text{pH} \ll pK_2) \quad (5)$$

$$\Delta E_p = k + 2.303\, RT(nF)^{-1} \log_3 K + \text{pH} \qquad (\text{for } pK_2 \ll \text{pH} \ll pK_3) \quad (6)$$

$$\Delta E_p = k \qquad (\text{for pH} \gg pK_3) \quad (7)$$

where the constant k includes $2.303\, RT(nF)^{-1} \log \beta(CuA)$ and $2.303\, RT(nF)^{-1} \log C_A^T$ terms; $j = 1$ is assumed for eqns. (4—7). From the ΔE_p — pH curves (Fig. 2), the successive constants pK_1, pK_2, pK_3 are the pH values of the intersection points obtained by extrapolating the linear parts of the curves corresponding to eqns. (3—7), respectively.

To determine the stability constants of Cu—PMA complexes, the possible models include CuA, CuHA, CuH_2A, CuH_3A and Cu(OH)A, the corresponding stability constants being

$$\beta(CuA) = [CuA]/[Cu^{2+}][A^{3-}] \quad (8)$$

$$\beta(CuHA) = [CuHA]/[Cu^{2+}][HA^{2-}] \quad (9)$$

$$\beta(CuH_2A) = [CuH_2A]/[Cu^{2+}][H_2A^{-}] \quad (10)$$

$$\beta(CuH_3A) = [CuH_3A]/[Cu_2^{+}][H_3A] \quad (11)$$

$$\beta(Cu(OH)A) = [Cu(OH)A]/[Cu^{2+}][OH^{-}][A^{3-}] \quad (12)$$

From eqn. (1) and the expressions for $[A^{3-}]$ to $[H_3A]$ given above, the following group of equations may be obtained

$$\log \beta(CuA) = \Delta E_p/2.303\, RT(nF)^{-1} - \log C_A^T - \log \alpha_A \quad (13)$$

$$\log \beta(CuHA) = \log \beta(CuA) - \log([H^+]/K_3) \quad (14)$$

$$\log \beta(CuH_2A) = \log \beta(CuA) - \log([H^+]^2/K_2K_3) \quad (15)$$

$$\log \beta(CuH_3A) = \log \beta(CuA) - \log([H^+]^3/K_1K_2K_3) \quad (16)$$

$$\log \beta(Cu(OH)A) = \log \beta(CuA) + \log[OH^-] \quad (17)$$

Thus $\log \beta$ may be selected from the model ionisation constants determined experimentally and the pH values. For a given model, the experimentally-determined values of $\log \beta$ should remain constant over the appropriate range of pH, provided that the model is appropriate to the conditions pertaining.

EXPERIMENTAL

A Princeton Applied Research Laboratories (PAR) Model 174 Polarographic Analyzer was used. A Probion saturated calomel electrode (SCE) and a platinum electrode were used as reference electrode and counter electrode, respectively. All the potentials reported are vs. SCE. The solution to be analysed was deaerated with oxygen-free nitrogen (BOC) which was also used to maintain an inert atmosphere over the solution.

The background electrolyte was prepared from "Analar" sodium sulphate (analytical reagent grade), which was used to maintain a constant ionic strength of solution. Standard solutions of copper(II) ions were made by dissolving pure copper (99.999%) in hydrochloric acid and nitric acid, and conversion to sulphate solution by evaporation with sulphuric acid. The unfractionated polymaleic acid was synthesised as described previously [11] and dissolved in water. Its concentration was calculated from the mean molecular weight of 1240, determined by vapour pressure osmometry.

The pH values were adjusted with sodium hydroxide and sulphuric acid, being determined with a Corning pH meter 113 and an Activion glass electrode, carefully calibrated by using two standard pH buffer solutions.

Gelatin solution was used to suppress the copper wave maxima exhibited in the sodium sulphate medium. PMA is also a surface-active material, hence it could act as a maximum suppressor.

All measurements were carried out at room temperature, 20°C.

RESULTS AND DISCUSSION

A preliminary experiment was carried out to determine the stability constant of the Cu—EDTA complex; similar practical methods and calculations were employed to those used for the stability constants of the Cu—PMA complex. The log β (Cu—EDTA) value obtained was 19.2 at 20°C, I = 0.1 M and pH 4—9; this compares well with a literature value of 18.9 at 25°C [14].

The differential pulse polarographic waves of copper(II) in the presence and absence of PMA are shown in Fig. 1. The influence of pH on peak shape can be seen. The peak potential of copper(II) ions is —0.010 V in 0.04 M Na_2SO_4 in the absence of PMA. The peak potentials were measured for each experiment and were used to plot graphs from which the results were calculated.

Ionisation constants of PMA

The shift of peak potentials between the simple copper(II) ion and the copper—PMA complex as a function of pH is shown in Fig. 2. These data were used to determine the successive ionisation constants as outlined above. The results are listed in Table 1.

For humic acid, most workers usually report only one pK value in the range 4—6 [3, 7, 15, 16]. Takamatsu and Yoshida [5] reported pK_1 =

TABLE 1

The successive ionisation constants of polymaleic acid (20°C, I = 0.12 M)

C_A^T (mg cm^{-3})	6.0	3.0	1.2	1.2	Mean[a]
pK_1	4.90	4.70	5.30	5.40	5.16
pK_2	7.30	6.50	6.85	7.15	7.04
pK_3	10.20	9.60	9.45	9.55	9.82

[a]Calculated after reconversion to K values.

4.63—5.10 and pK_2 = 8.80—9.50, Borggaard [2] reported pK_1 = 2.8—3.4, pK_2 = 4.9—5.1 and pK_3 = 9.4—9.7. The differences between the reported ionisation constants could be attributed to the variable composition of the humic acids used and the inherent limitation of the methods. However, with PMA, from Fig. 2, it is clear that three intersection points are obtained by extrapolating the linear parts of the ΔE_p—pH curve. The curve above pH 10—12 may not be in exact agreement with eqn. (7) because of the possibility of the hydrolysis of PMA at high pH and the influence of copper hydroxide. The pK values reported here are the inherent ionisation constants of the ligands that form copper complexes. The influence of hydrogen ions released by non-complex-forming processes in this method has not been considered, nor have complications that could occur by copper(II) ions causing several carboxyl groups of differing pK values to dissociate at or near the same pH.

Stability constants of copper—PMA complexes

As mentioned above, there are five possible models for Cu—PMA complexes. The experimentally determined values of the ionisation constants and pH were used to calculate log β for each of the five models using the relevant eqns. (13—17). The logarithmic stability constants calculated for the five models, log β, as a function of pH are shown in Fig. 3.

Theoretically, log β should not change with pH if no new complex is formed. From Fig. 3 it may be observed that the curves for the CuHA and Cu(OH)A model are reasonably flat at pH 5—9, whereas the curves for other models are rather steep in this range. The formation of a complex including hydroxide is usually possible only in alkaline solution and is, therefore, not considered further in the context of soil. Infra-red data [17] have shown that most of the carboxylic acid groups in humic acids have dissociated by pH 7—8, though a few do not dissociate until pH 10—11. This behaviour is consistent with the ionisation constants reported here for PMA. The carboxylic acid groups are not uniformly distributed over the polymers, but have a tendency to occur in units of two or more, sufficiently close together to affect both the dissociation of different hydrogen ions and the formation of complexes with metal ions. Dissociation of phenolic hydroxyl groups in such a molecule would occur at a pH of 11 or higher; it is unlikely that they play any part in the complexation process at pH 5—9. For these reasons, it

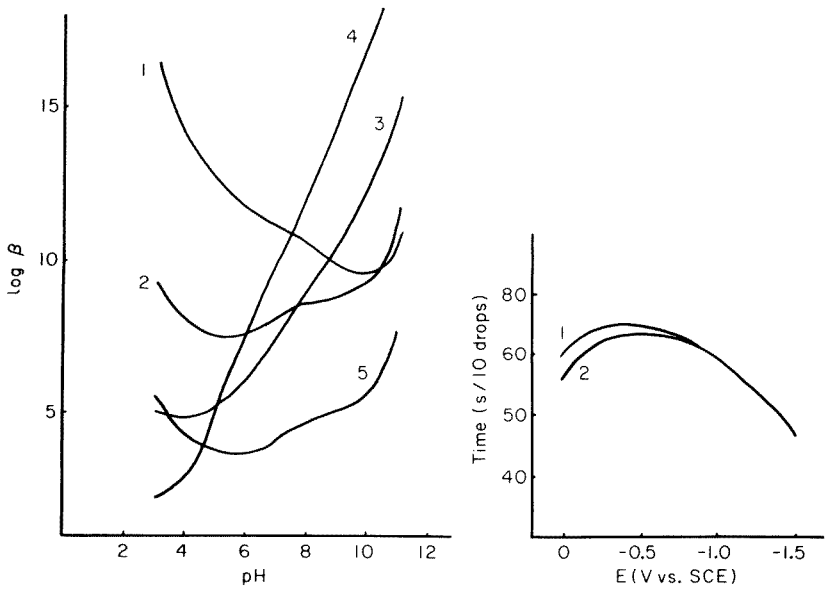

Fig. 3. Log β calculated from the hypothetical model—pH diagram. Model: (1) CuA^{-}; (2) CuHA; (3) CuH_2A^{+}; (4) CuH_3A^{2+}; (5) $Cu(OH)A^{2-}$. Experimental conditions were the same as those shown in Fig. 2(b).

Fig. 4. Electrocapillary curves of DME in 0.04 M Na_2SO_4 in (1) the absence and (2) the presence of polymaleic acid (1.2 mg cm^{-3}).

TABLE 2

The stability constants of the copper—polymaleic acid complex, CuHA, at 20°C and I = 0.12 M

C_A^T (mg cm^{-3})	log β(CuHA) at different pH values								
	5.10	5.50	6.10	6.60	7.10	7.60	8.00	8.50	9.00
6.0	7.60	7.55	7.50	7.60	8.20	8.50	8.55	8.80	8.90
3.0	6.55	6.90	6.85	7.35	7.35	7.65	7.90	8.10	8.55
1.2	6.80	6.90	6.95	7.75	8.10	8.05	8.25	8.35	8.70
1.2	7.10	6.75	7.05	7.60	7.95	8.10	8.25	8.30	8.55
Mean	7.19	7.15	7.17	7.60	8.00	8.18	8.47	8.47	8.70

is reasonable to suppose that the CuHA type of complex is formed at pH 5—9. The stability constants of the CuHA complex are shown in Table 2. The overall mean value of log β (CuHA) is 8.17 from pH 5—9.

A range of values has been reported in the literature for the stability constants of the copper complexes of fulvic and humic acids. The range is not surprising in view of the variability of these acids according to the nature of the soil organic matter from which they were obtained, and the possible

changes in their chemical composition that may occur during the separation procedure or after isolation. It is, however, interesting to compare the values obtained here for the complex of polymaleic acid which has been shown to be a good model compound for fulvic acid in several respects [11, 18—21].

Using an equilibration time of 1 h, Schnitzer and Skinner [22] reported a value of log β = 8.7 for the fulvic acid complex of copper at pH 5 and I = 0.1 M from material isolated from a podzol B-horizon. Subsequently, Schnitzer and Hansen [23], using the same source of fulvic acid but with an equilibration time of 24 h, reported log β = 4.0 and Buffle et al. [6] also recorded a value of log β = 4.0. In contrast, Mantoura and Riley [24] recorded log β = 8.42 for the copper complex of fulvic and humic acids dissolved in natural water. Courpron [25] reported values of log β = 3.23 and 7.0 for the copper complexes of fulvic and humic acids, respectively. Chmielewska [26] reported log β = 7.25—7.85 for the humic acid complex of copper in the range pH 4.7—5.8, whilst Takamatsu and Yoshida [5] recorded log β = 8.65 at pH 5 for the same complex. It is clear that the value log β = 8.17 obtained for the PMA complex of copper agrees well with the earlier results reported for the fulvic acid complex of copper and with those reported for the humic acid complex.

It may be seen from Fig. 3 that the formation of a CuH_2A complex at a pH less than 5 [log β (CuH_2A) = 4.5—5.5], and a CuA complex at pH 8—10 [log β (CuA) = 9.0—10.0] is possible, especially if the concentration of PMA is low.

Electrocapillary curves in 0.04 M Na_2SO_4 in the absence or presence of PMA are shown in Fig. 4. The surface-active behaviour of PMA could affect the reversibility of the electrode processes.

The width of the differential pulse polarographic peak increased over the range pH 3—9 (see Fig. 1), whereas the peak current decreased. These are all possible sources of experimental error.

Conclusions

Differential pulse polarography is an appropriate method for determining the successive ionisation constants of polymaleic acid, an analogue of fulvic acid, and the stability constant of its principal copper complex in the normal pH range of soil. The CuHA type of complex appears to be the prevalent species in solution at pH 5—9, i.e., the normal range for soils, and the stability constant log β (CuHA) is 8.17 at 20°C under these conditions. Values are indicated for the CuA complex which may persist at pH 8—10 and for a less stable CuH_2A complex which may form below pH 5.

The authors are grateful to the Chinese Academy of Sciences and The Royal Society for granting study leave and awarding a grant to Pu Guogang to permit this and other studies in soil electrochemistry [27]. They also thank Dr. H. A. Anderson of this Institute for providing samples of polymaleic acid and information on its characteristics and properties.

REFERENCES

1 M. S. Ardakani and F. J. Stevenson, Soil Sci. Soc. Am. Proc., 36 (1972) 884.
2 O. K. Borggaard, Acta Chem. Scand., A28 (1974) 12.
3 F. J. Stevenson, Soil Sci. Soc. Am. Proc., 40 (1976) 665.
4 F. J. Stevenson, Soil Sci., 123 (1977) 10.
5 T. Takamatsu and T. Yoshida, Soil Sci., 125 (1978) 377.
6 J. Buffle, F.-L. Greter and W. Haerdi, Anal. Chem., 49 (1977) 216.
7 T. A. O'Shea and K. H. Mancy, Anal. Chem., 48 (1976) 1603.
8 E. W. Russell, Soil Conditions and Plant Growth, 10th edn., Longman, London, 1973, 306.
9 H. M. N. H. Irving, in I. S. Longmuir (Ed.), Advances in Polarography, Pergamon, Oxford, 1960, pp. 42—67.
10 G. A. Heath and G. Hefter, J. Electroanal. Chem., 84 (1977) 295.
11 H. A. Anderson and J. D. Russell, Nature, 260 (1976) 597.
12 D. R. Crow, Polarography of Metal Complexes, Academic Press, London, 1969, 61.
13 E. P. Parry and R. A. Osteryoung, Anal. Chem., 37 (1965) 1634.
14 IUPAC Stability Constants of Metal Ion Complexes, Part B (Organic Ligands), compiled by D. D. Perrin, Pergamon, Oxford, 1979.
15 J. A. Marinsky, A. Wolf and K. Bunzl, Talanta, 27 (1980) 461.
16 F. J. Stevenson, S. A. Krastanov and M. S. Ardakani, Geoderma, 9 (1973) 129.
17 E. W. Russell, Soil Conditions and Plant Growth, 10th edn., Longman, London, 1973, 294.
18 D. J. Linehan, Plant Soil, 50 (1978) 663.
19 R. E. Malcolm and D. Vaughan, Plant Soil, 51 (1979) 117.
20 D. J. Linehan and H. Shepherd, Plant Soil, 52 (1979) 281.
21 J. M. Bracewell, G. W. Robertson and D. I. Welch, J. Anal. Appl. Pyrolysis, 2 (1980) 239.
22 M. Schnitzer and I. Skinner, Soil Sci., 102 (1966) 361; 103 (1967) 247.
23 M. Schnitzer and E. H. Hansen, Soil Sci., 109 (1970) 333.
24 R. F. C. Mantoura and J. P. Riley, Anal. Chim. Acta, 78 (1975) 193.
25 C. Courpron, Ann. Agron., 18 (1976) 623.
26 B. Chmielewska, Ann. Univ. Marie Sklodowska, 28 (1973/74) 143.
27 T. E. Edmonds, Pu Guogang and T. S. West, Anal. Chim. Acta, 120 (1980) 41.

Analytica Chimica Acta, 129 (1981) 79—86
Elsevier Scientific Publishing Company, Amsterdam — Printed in The Netherlands

EVALUATION OF DERIVATIVE NORMAL PULSE POLAROGRAPHY FOR USE IN METAL SPECIATION STUDIES

OTIS M. EVANS and KENNETH W. HANCK*
Department of Chemistry, North Carolina State University, Raleigh, NC 27650 (U.S.A.)
(Received 22nd July 1980)

SUMMARY

A simple inexpensive microcomputer-orientated approach for obtaining pseudo-derivative polarograms is demonstrated. The method, called derivative normal pulse polarography (d.n.p.p.), produces better signal-to-noise ratios, and therefore lower detection limits, than differential pulse polarography (d.p.p.). The foremost advantage of d.n.p.p. is its relative freedom from influences of homogeneous chemical kinetics which makes it an excellent method for metal speciation studies. Response curve shapes for Pb(II) between 2×10^{-4} and 8×10^{-4} M exhibit excellent agreement with theory. Titration of EDTA with 0.01 M Cu(II) and 0.01 M Cd(II) using d.n.p.p. for detection exhibited recoveries of 98.0 and 99.5%, respectively.

Derivative normal pulse polarography (d.n.p.p.) is a pseudo-derivative method in which currents sampled from successive drops are subtracted sequentially [1—3]. The technique may conveniently be implemented by using a computer to differentiate a normal pulse polarogram. Bond has demonstrated the analytical potential of the method [2, 3]. His approach requires a minicomputer and uses a rather complex, time-consuming curve-fitting algorithm to obtain the derivative. This paper describes a simpler, microcomputer-orientated approach for obtaining pseudo-derivatives from normal pulse polarograms.

One of the reasons for this interest in d.n.p.p. is its relative freedom from the complications of homogeneous chemical reactions. Differential pulse polarography (d.p.p.) is a sound analytical technique with many variations but is subject to interferences because the electrode is polarized during the entire drop life [1—8]. Normal pulse polarography (n.p.p.) is advantageous because the electrode is polarized for only a few milliseconds during the life of each drop. The limiting current of the sigmoidal curve of n.p.p. is difficult to measure at low concentration. Differentiating the n.p.p. data to obtain a peak-shaped derivative polarogram should permit the determination of low concentrations of analytes that are sensitive to interference from homogeneous chemical reactions.

One such analytical application is the determination of binding capacity or complexing power of natural water. The importance of these deter-

0003—2670/81/0000—0000/$02.50

minations has amply been demonstrated [9—14]. A popular method for making such determinations involves the use of differential pulse polarography or anodic stripping voltammetry either to locate the end-point of a micromolar complexime tric titration or to establish the fraction of a specific trace metal ion which is uncomplexed. Hanck and Dillard [11] have demonstrated that such techniques contain errors because of the lability of most metal/organic complexes. This point has been re-emphasized by Davison [15] and by Van Leeuwen [16]. This paper reports the results of complexation studies using d.n.p.p. The application of d.n.p.p. to multicomponent mixtures will be discussed in a subsequent manuscript.

EXPERIMENTAL

Reagents

Solutions were prepared in doubly-deionized water that had been passed through an activated charcoal column and filtered through a 0.2-μm membrane filter.

Solutions of Cd(II), Pb(II), Zn(II), and Tl(I) were prepared from (Fisher Scientific certified A.C.S. grade) cadmium chloride, lead nitrate, zinc nitrate, and thallium(I) nitrate. Solutions of Bi(III) were prepared from bismuth metal powder (J. T. Baker, certified A.C.S. grade) dissolved in reagent-grade nitric acid (Fisher Scientific Co.). Solutions of In(III) were prepared by dissolving the appropriate amount of high-purity metal (Alpha Inorganics) in Ultrex nitric acid. The supporting electrolytes were prepared from sodium chloride, ammonium acetate, and acetic acid (Fisher Scientific, certified A.C.S. grade) used without further purification.

All solutions were stored in polyethylene containers at 5°C and at concentrations no lower than 0.1 M.

Reagents for microcomplexime tric titrations. A standard solution of ethylenedinitrilotetraacetic acid (EDTA; Fisher Scientific) was prepared by dissolving $Na_2H_2Y \cdot 2H_2O$, oven-dried at 80°C for 3 h, in deionized water and standardizing it by titration with a known concentration of high-purity metal ion solution.

Standard solutions of metal ions were prepared at the 0.1 M level using deionized water. Copper(II) and cadmium(II) solutions were prepared by dissolving the appropriate amount of high-purity metal (Alpha Inorganics) in Ultrex nitric acid.

Acetate buffer (pH 5, 0.1 M) was prepared from reagent-grade sodium acetate and glacial acetic acid (Fisher Scientific). A 1.0 M solution of the acetate buffer was purified by controlled-potential electrolysis at a mercury pool electrode in the conventional way [17]; electrolysis time was sixteen days.

Stock and standard solutions were stored in polyethylene containers at 5°C.

Nitrogen (Air Products) used in deaerating solutions was passed through a Ridox column to remove oxygen.

Electrodes and cell

The working electrode was a dropping mercury electrode (DME; Sargent-Welch, S-29487 capillary) equipped with a PAR 172 drop timer (Princeton Applied Research Corporation). The DME and drop timer were enclosed in a Faraday cage. The reference electrode was a Corning fiber-tipped saturated calomel electrode (SCE), Catalog No. 476002. A platinum wire (12 cm of 24 gauge) served as the auxiliary electrode.

The cells were 100-ml Berzelius beakers fitted into commercially available polyethylene cell tops (Leeds and Northrup cell cover No. 067513 and ring No. 127182).

Instrumentation

A Princeton Applied Research Corporation Model 174 Polarographic Analyzer was interfaced to an Altair 8800 computer (designed around the 8-bit Intel 8080 microprocessor; manufactured by MITS, Inc., Albuquerque, NM). The microcomputer was configured with 8 K of random access memory and 1 K of programmable read only memory. An ASR-33 teletype (ComData Corporation, Skokie, IL) with paper tape reader/punch served as the system console. A Data Technology Model 3312-3½ digit panel meter with a bipolar configuration, a working input range of ±1.999 V, and an externally triggered rate of thirty conversions per second functioned as an analog-to-digital converter (ADC). Two digital-to-analog converters (DAC) were used to drive the inputs of the x-y recorder. An Analog Devices (Norwood MA) 12-bit DAC (Type DAC 1118) configured to accept binary code, and an output voltage range of 0 to +10 V was used to drive the y-axis. The x-axis was driven by a Hybrid Systems Corporation (Bedford, MA) 10-bit (Type DAC 371V-10) DAC with an output voltage range of 0 to +10 V, and configured to accept offset binary code.

The interface between the PAR 174 and the digital microcomputer is a digital data transmitter designed and built using an Analog Devices (STX 1003) serial data exchange module [14—16].

Software. All programs were written in assembly language; complete listings are available elsewhere [18]. Background currents were eliminated by subtracting a previously collected background polarogram stored in memory from the normal pulse polarogram prior to differentiation. A moving average routine was used to smooth noisy polarograms. Signal averaging was also used to improve the signal-to-noise ratio of polarograms near the detection limit.

RESULTS AND DISCUSSION

Evaluation of d.n.p.p.

The theory of derivative polarography has been presented in detail elsewhere [2, 19]. The shape of a reversible derivative polarogram is given by

$$di/dE_p = 4(di/dE)_p \exp [nF/RT\ (E - E_{1/2})]/\{1 + \exp [nF/RT\ (E - E_{1/2})]\}^2 \quad (1)$$

where $(di/dE)_p$ is the value of the derivative at the peak of the polarogram (i.e. at $E = E_{1/2}$), and is equal to $-4nFi_l/RT$ where i_l is the limiting current. Experimentally, dI/dE is approximated by $\Delta i/\Delta E$. Bond and O'Halloran [2] have shown that the approximation is excellent for $\Delta E < 5$ mV; data reported here were obtained with $\Delta E = 1$ mV. Plots of eqn. (1) for several concentrations of Pb(II) are shown in Fig. 1; comparison of experimental and theoretical slopes indicates excellent agreement (Table 1).

Three polarographic techniques (n.p.p., d.p.p., and d.n.p.p.) were applied to the reduction of Pb(II) and Zn(II). Typical polarograms of Zn(II) are presented in Fig. 2; a quantitative comparison is made in Table 2. The polarographic waveforms for Pb(II) were reversible while those for Zn(II) were somewhat unsymmetrical because of irreversibility. The slope of the Pb(II) calibration curve for each technique is larger than that of the corresponding curve for Zn(II). The difference in n.p.p. slopes is a reflection of the difference in diffusion coefficients between Pb(II) and Zn(II). The differences between the d.p.p. and d.n.p.p. slopes are due to the slow elec-

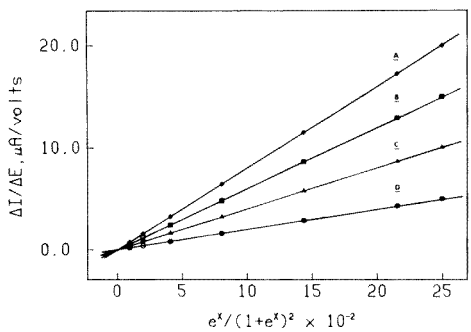

Fig. 1. Evaluation of the shape of derivative normal pulse polarograms of Pb(II) in 1 M acetic acid—ammonium acetate. (A) 8×10^{-4} M; (B) 6×10^{-4} M; (C) 4×10^{-4} M; (D) 2×10^{-4} M. $x = [(nF/RT)(E - E_{1/2})]$.

TABLE 1

Experimental evaluation of the "shape equation" for d.n.p.p.

Pb(II) concentration ($\times 10^{-4}$ M)	i_l (μA)	$(\Delta I/E)_p$ (μA/V)	Slope (exptl.)	Slope (theor.)
2	0.244	4.75	19.004 ± 0.040	18.997
4	0.488	9.49	37.994 ± 0.000	37.994
6	0.732	14.25	57.013 ± 0.004	56.991
8	0.976	19.00	75.987 ± 0.000	75.987

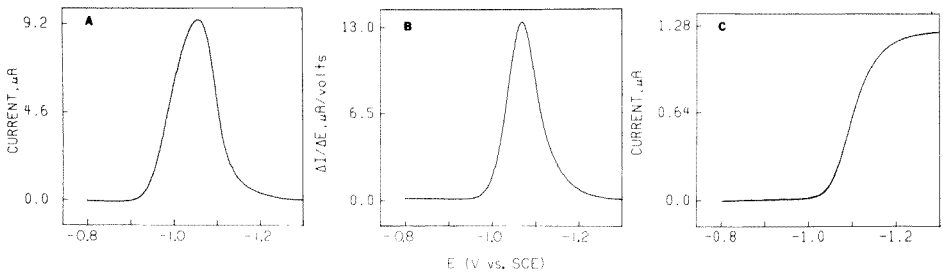

Fig. 2. Irreversible reduction of Zn(II) (2×10^{-4} M) in acetic acid—ammonium acetate. (A) Differential pulse polarogram using 100 mV modulation; (B) derivative normal pulse polarogram; (C) normal pulse polarogram.

TABLE 2

Slopes of calibration curves for Zn(II) and Pb(II)[a]

	N.p.p. (μA/mM)	D.p.p. (μA/mM)[b]	D.n.p.p. (μA/V · mM)
Zn(II)	6.54 ± 0.10	41.08 ± 0.46	63.7 ± 1.1
Pb(II)	7.21 ± 0.22	67.32 ± 0.75	128.8 ± 4.7

[a]Uncertainties are 95% confidence intervals. Concentration range: 0.10—1.00 mM.
[b]100 mV modulation.

trode kinetics of the Zn(II) reduction [20—22]. All derivative type techniques show a loss of sensitivity when the rate of electron transfer is slow; it is interesting to note that d.n.p.p. shows a smaller loss than d.p.p.

Typical calibration data for Cd(II) in 0.1 M acetic acid—ammonium acetate buffer are shown in Table 3. A composite calibration plot based on 4 separate runs with eight concentrations of Cd(II) per run and each concentration measured in triplicate had a least-squares slope of $(2.000 \pm 0.003) \times 10^6$ μA l V^{-1} mol^{-1} with a y-intercept of -0.01 ± 0.01. The detection limit for a 50-ml solution of Cd(II) was found to be 3.1×10^{-8} M. This was determined by application of the *t*-test (95% confidence level, one-tailed test, 10 degrees of freedom). Six polarographic measurements each were made on a blank solution and an arbitrarily chosen low concentration (2×10^{-7} M) of the electroactive material. The useful lower concentration is about 3×10^{-7} M. The detection limit was also determined for Cu(II) in the same supporting electrolyte. For Cu(II) the detection limit was determined to be 5×10^{-8} M.

Micromolar complexime tric titrations

Both d.p.p. and d.n.p.p. were used to quantify the titration of 4×10^{-5} M EDTA with Cu(II) in pH 5 acetate buffer. The titration procedure was the same as that used by Hanck and Dillard [11].

In pH 5 acetate buffer, two reduction peaks for the titration of EDTA with Cu(II) can be monitored: the free metal ion, Cu(II), at approximately

TABLE 3

Calibration data for Cd(II)[a] in 0.1 M acetic acid—ammonium acetate buffer

Run	Slope	Y-intercept
1	$2.00 \times 10^6 \pm 3.90 \times 10^3$	$-8.4 \times 10^{-3} \pm 2.0 \times 10^{-2}$
2	$2.00 \times 10^6 \pm 1.59 \times 10^3$	$-2.0 \times 10^{-3} \pm 8.0 \times 10^{-3}$
3	$2.00 \times 10^6 \pm 2.76 \times 10^3$	$-7.3 \times 10^{-3} \pm 1.4 \times 10^{-2}$
4	$2.00 \times 10^6 \pm 2.25 \times 10^3$	$-7.6 \times 10^{-3} \pm 1.1 \times 10^{-2}$

[a]Cd(II) concentration ranged from 1.0 to 8.0 μM.

+0.033 V vs. SCE and the metal complex ($CuEDTA^{2-}$) at approximately —0.100 V. Also present is a third peak at about +0.085 V which is due to the oxidation of Hg to $HgEDTA^{2-}$. Figure 3 shows the result of monitoring the three electrochemical reactions with d.p.p. The peak current for the oxidation of Hg to $HgEDTA^{2-}$ decreases as EDTA is consumed during the titration. The curve associated with the $CuEDTA^{2-}$ peak current which should have reached a plateau at the 100% titrated point continues to increase significantly beyond the equivalence point. The free copper line, when extrapolated to zero current, results in a low determination. Table 4 shows the results for five titrations which yield an average of 92.14% titrated.

These results indicate that d.p.p. is subject to homogeneous kinetic effects. In d.p.p., the electrode is polarized for most of the drop life because a linear ramp voltage is continuously being applied to the drop. Therefore, depletion of the free metal concentration at the electrode surface during this polarization period provides the driving force for dissociation of the metal complex. The drop time, which is typically 0.5—5.0 s, appears to be long enough for dissociation to occur.

Figure 4 shows the results of monitoring the titration with d.n.p.p. The $CuEDTA^{2-}$ reduction was not followed. Of particular interest is the free copper line which, when extrapolated to the zero current line, yields an end-point slightly less than the equivalence point. Table 4 presents the results for 8 titrations which show an average recovery of 98.08%. The results, though lower than expected, are considerably better than those obtained by d.p.p. Thus, these results indicate that d.n.p.p. is affected less by kinetic effects than d.p.p.

Meyers and Osteryoung [23] have successfully titrated Cu(II) with EDTA titrant using d.p.p. to locate the equivalence point. The present experimental conditions are nearly identical with theirs except that Cu(II) is the titrant and EDTA the analyte. It is not clear why a reversal of analyte and titrant should produce such a significant change in the accuracy of the method, but perhaps the complexes formed in the presence of excess of Cu(II) have a higher coordination number on average than those complexes formed in the presence of excess EDTA. The more highly coordinated

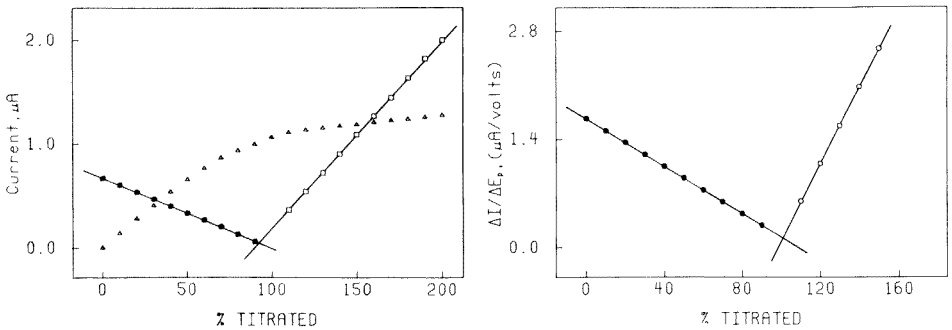

Fig. 3. Differential pulse polarographic titration of 4×10^{-5} M EDTA with Cu(II) in pH 5 acetate buffer. (□) free copper; (△) $CuEDTA^{2-}$; (●) $HgEDTA^{2-}$; (—) regression lines.

Fig. 4. Derivative normal pulse polarographic titration of 4×10^{-5} M EDTA with Cu(II) in pH 5 acetate buffer. (○) free copper; (●) $HgEDTA^{2-}$; (—) regression lines.

TABLE 4

Titrations of 2.00 μmol of EDTA with Cu(II) and Cd(II) (10^{-2} M solutions)

Differential pulse polarography		Derivative normal pulse polarography	
Titrant	% EDTA recovered[a]	Titrant	% EDTA recovered[a]
Cu(II)	92.14 ± 0.94	Cu(II)	98.09 ± 0.37
Cd(II)	96.06 ± 0.11	Cd(II)	99.47 ± 0.12

[a]Means ± standard deviation.

complexes would probably be more inert and less susceptible to low results. Presumably, if both sets of titrations were performed slowly enough to allow the complexes formed in the early stage of the titration to reach equilibrium, identical results would be obtained regardless of which species was the titrant.

The titration of EDTA with Cd(II) was also monitored with d.p.p. and d.n.p.p. The course of the titration was followed by means of the reduction of the free metal species at —0.653 V vs. SCE. Table 4 presents the results of 7 titrations monitored with d.p.p. which have an average value of 96.06% titrated. The results of the titration monitored with d.n.p.p. are also presented in Table 4. The average value of 5 titrations was 99.47% titrated. These results further verify that d.n.p.p. is less affected by chemical kinetics than d.p.p.

The standard formation constant (K_f) for Cu(II) is larger than that of Cd(II). Therefore, based on equilibrium considerations alone, the titration of Cu(II) would have been expected to have been more quantitative than Cd(II). However, the unexpected behavior may be explained by the fact that the rate of exchange between Cd(II) and EDTA may be much slower than

that between Cu(II) and EDTA. Also, it is possible that acetate ion (buffer) may form a stronger complex with Cu(II) than Cd(II) and, under the given titration conditions, the Cd(II) species may have a much larger conditional formation constant (K_f) than Cu(II).

However, it appears that d.n.p.p. should prove to be quite useful for determining the complexing capacity of water samples even when labile metal ions are used as titrants.

REFERENCES

1 P. E. Sturrock and R. J. Carter, CRC Crit. Rev. Anal. Chem., 5 (1975) 201.
2 A. M. Bond and R. J. O'Halloran, J. Electroanal. Chem., 68 (1976) 257.
3 A. M. Bond and B. S. Grabaric, Anal. Chim. Acta, 101 (1978) 309.
4 E. P. Parry and R. A. Osteryoung, Anal. Chem., 37 (1965) 1634.
5 J. H. Christie and R. A. Osteryoung, J. Electroanal. Chem., 49 (1974) 301.
6 J. H. Christie, L. L. Jackson and R. A. Osteryoung, Anal. Chem., 48 (1976) 242.
7 J. H. Christie, L. L. Jackson and R. A. Osteryoung, Anal. Chem., 48 (1976) 561.
8 J. H. Turner and R. A. Osteryoung, Anal. Chem., 50 (1978) 1496.
9 H. E. Allen, W. R. Matson and K. H. Mancy, J. Water Pollut. Control Fed., 42 (1970) 573.
10 M. E. Bender, W. R. Matson and R. A. Jordan, Environ. Sci. Technol., 4 (1970) 520.
11 K. W. Hanck and J. W. Dillard, Anal. Chim. Acta, 89 (1977) 329.
12 T. M. Florence and G. E. Batley, Talanta, 24 (1977) 151.
13 W. Davison and M. Whitfield, J. Electroanal. Chem., 75 (1977) 763.
14 T. A. O'Shea and K. H. Mancy, Anal. Chem., 48 (1976) 1603.
15 W. Davison, J. Electroanal. Chem., 87 (1978) 395.
16 H. P. Van Leeuwen, J. Electroanal. Chem., 99 (1979) 93.
17 See, e.g., J. W. Mitchell, Anal. Chem., 45 (1973) 492A.
18 O. M. Evans, Ph.D. Thesis, NC State University, 1978.
19 D. J. Fisher, W. L. Belew and M. T. Kelley, in G. J. Hills (Ed.), Polarography 1964, Macmillan, London, 1966, Vol. 1, pp. 89—134.
20 J. W. Dillard and K. W. Hanck, Anal. Chem., 48 (1976) 218.
21 R. L. Birke, Anal. Chem., 50 (1978) 1489.
22 J. W. Dillard, J. J. O'Dea and R. A. Osteryoung, Anal. Chem., 51 (1979) 115.
23 D. J. Meyers and J. Osteryoung, Anal. Chem., 46 (1974) 356.

Analytica Chimica Acta, 129 (1981) 87—100
Elsevier Scientific Publishing Company, Amsterdam — Printed in The Netherlands

ELECTROCATALYSIS OF THE REDUCTION OF NITRATE ION AT CADMIUM ELECTRODES BY ELECTRODEPOSITED COPPER

GLENN A. SHERWOOD, Jr.[a] and DENNIS C. JOHNSON*
Department of Chemistry, Iowa State University, Ames, IA 50011 (U.S.A.)
(Received 24th November 1980)

SUMMARY

The irreversible reduction of nitrate to nitrite at a cadmium electrode in slightly alkaline solution is electrocatalyzed by copper deposited on the electrode surface. Mass transport-limited currents were observed at a Cu—Cd disc electrode to rotational velocities of 1050 rad s^{-1} (10000 rev. min^{-1}). Electron micrographs revealed that the copper is plated as closely packed microspheres less than 1 μm in diameter.

Numerous colorimetric methods for the determination of nitrate ion in aqueous solution prescribe the reduction of nitrate to nitrite followed by diazotization with coupling to a suitable organic reagent and spectrophotometric measurement of the colored product. Powdered zinc was one of the first reducing agents suggested [1, 2]. Low yields were reported for reduction by zinc, both in batch and column procedures [3, 4]. Reduction of nitrate by zinc can go beyond nitrite and reproducible results are obtained only when the operating conditions are carefully controlled.

In 1960, Potzl and Reiter suggested use of cadmium metal in a column for reduction of nitrate [5]. Some loss of nitrite has been observed, but the loss apparently can be kept minimal by careful control of flow rate and pH [6]. Spongy cadmium [7, 8] and amalgamated cadmium [9] have also been used with success. Mullin and Riley [10] reported a yield of 92 ± 1% for the reduction by Hg—Cd with no reduction beyond nitrite. Addition of ammonia [11] or EDTA [12] to the solution of nitrate was observed to increase the life of a cadmium column. Perhaps this was the result of the formation of soluble coordination products of Cd(II) rather than insoluble $Cd(OH)_2$.

Reductor columns prepared from copperized cadmium give a virtually quantitative yield of nitrite [13, 14] and their use is prescribed by the United States Environmental Protection Agency as the "official" colorimetric method for nitrate [15]. Nydahl [16] compared Hg—Cd and Cu—Cd columns and concluded that the latter are superior if faster rates of reduction are desired. Otsuki [17] suggested that the cadmium be copperized again, following extensive use of the column, with a solution of 0.05 M Cu(II)

[a]Present address: E. I. DuPont de Nemours and Co. Wilmington, DE, U.S.A.

0003—2670/81/0000—0000/$02.50

in 0.1 M EDTA adjusted to pH 7. Otsuki also reported that the deposited copper has a granular form. Stainton [18] reported on the use of a copper-coated cadmium wire in a flow stream for the photometric determination of nitrate.

Davenport and Johnson [19] determined that nitrate and nitrite ions can be reduced to hydroxylamine at a polycrystalline cadmium electrode in acidic solutions, and the reactions were applied for amperometric detection in the chromatographic separation of the two ions in aqueous samples. Separation was achieved with an anion-exchange column using 0.01 M $HClO_4$ as the eluent. The nitrate and nitrite in the effluent stream were detected after mixing with a stream of sulfuric acid to produce a final concentration of 0.10 M H_2SO_4. Electrochemical activity of the detector was reported to be achieved only after a brief (90 s) anodization at 0.0 V vs. saturated calomel electrode (SCE). The anodization removed a small amount of cadmium from the surface of the polycrystalline electrode with the result that distinct crystal faces for the various crystallites were easily observed. The exposed crystal faces were concluded to be more active for the reduction of nitrate and nitrite than the smooth metal surface prepared by the customary practices of grinding and polishing. Continued use of cadmium electrodes in this laboratory has been characterized by frustration, however, in attempts to produce uniformly active electrodes made from different stocks of the polycrystalline metal. The lack of reproducibility appears related to variation in the number and arrangement of crystallites at the electrode surface.

The optimum convenience in the analytical application of cadmium electrodes would be offered by a procedure for preparing electrodes which would be independent of the crystallinity of the cadmium substrate. Bodini and Sawyer [20] proposed the electrochemical preparation of a bimetallic Cu—Cd electrode on a pyrolytic carbon substrate simultaneously with the voltammetric reduction of nitrate. A linear calibration curve was obtained for a rotated electrode over the concentration range 1 μM—1 mM NO_3^- in a solution containing 0.1 M NaH_2PO_4, 10 μM $CdCl_2$ and 50 μM $CuCl_2$. Results are described here for the reduction of nitrate at pH 8 on disk electrodes prepared from polycrystalline and single-crystal cadmium bearing thin layers of deposited copper.

EXPERIMENTAL

Reagents and chemicals

All chemicals were analytical reagents (Fisher Scientific Co.) except where noted to the contrary. Water was distilled and demineralized before use. The supporting electrolyte was 0.1 M sulfuric acid for preliminary experiments with a polycrystalline electrode; and a buffer solution at pH 8 composed of 0.10 M tris(hydroxymethyl)aminomethane (Tris) and 0.056 M hydrochloric acid was used for all work with copperized electrodes. Potassium nitrate was dried at 90°C for 4 h and stored over Drierite in a desiccator. Stock solutions

of copper(II) were prepared by dissolving copper sulfate pentahydrate. Deaeration of solutions was achieved in the electrolysis cell with dispersed nitrogen (Air Products and Chemicals, Inc., Allentown, PA).

Electrodes

Cadmium and copper disks (6—10 mm o.d.) were attached with epoxy cement to a stainless steel holder which could be attached easily to a stainless steel shaft for insertion in the chucking mechanism of the rotator (Model PIR, Pine Instrument Co., Grove City, PA).

Polycrystalline cadmium electrodes were constructed from rods prepared by melting the commercially available metal in a test tube over a Bunsen burner to release entrapped pockets of gas, and then cooled to room temperature. The cadmium disks were cut from the polycrystalline rods with their surfaces perpendicular to the axis of the test tube. A copper disk was machined from the metal as received. The cylindrical surfaces of the disk electrodes were wrapped with teflon tape so that only the end surfaces of the electrodes were exposed to test solutions during electrochemical experimentation. During use, the electrodes were immersed in the test solutions to a minimum depth (0.5—1.0 mm) just sufficient to maintain contact with the liquid.

Single crystals of cadmium (Aremco Products, NY) were encapsulated in Quick Mount, an acrylic plastic (Fulton Metallurgical Products, Pittsburgh, PA) to aid in the handling and machining of the soft metal specimen. Each encapsulated crystal was cut perpendicular to the crystal axis with a low-speed diamond saw (Model 650, South Bay Technology, El Monte, CA). The cut surface of each specimen was machined to fit the electrode holder and mounted with epoxy resin. Electrical contact between the cadmium and the stainless steel shaft was assured by a tiny protrusion of metal machined into the center of the recessed portion of the electrode holder. Each mounted specimen was then cut with the diamond saw to give a thickness for the metal disk of approximately 6 mm. The ring-disk electrode used had a glassy-carbon disk and platinum ring (Pine Instrument Co.). Unless specified to the contrary, the surfaces of all electrodes were polished with 1-μm diamond prior to each experiment by the customary procedures used in hydrodynamic voltammetry. Current—potential curves were recorded on the negative sweep of triangular scans.

The mass-transport limited current for the rotating disk electrodes was calculated by

$$I_l = 0.62\, nFAD^{2/3}\, \omega^{1/2}\, \nu^{-1/6}\, C^{b} \qquad (1)$$

where D is the diffusion coefficient ($cm^2\ s^{-1}$), ω is the angular velocity of rotation (rad s^{-1}) and ν is the kinematic viscosity of the solution ($cm^2\ s^{-1}$) [21, 22]. The remaining terms in eqn. (1) have their usual electrochemical significance.

Copperization of cadmium electrodes. Copperized cadmium-disk electrodes (Cu—Cd) were prepared either by electrodeposition at controlled potential

or at the open-circuit potential in solutions of the Tris buffer containing Cu(II). The electrode examined by electron microscopy was copperized at the open-circuit potential with manual swirling of the electrode in a solution of 0.08 M Cu(II) for approximately 10 s. The electrocatalytic effect was found to be relatively insensitive to the exact quantity of copper deposited beyond the equivalent of 10—20 monolayers and no attempt was made to control rigorously the flux of the Cu(II) to the cadmium electrode during deposition prior to the microscopic examination.

Equipment

Potential control. Potentiostatic control with measurement of electrical currents was achieved with a Model RDE3 Bipotentiostat (Pine Instrument Co.). Current—potential curves were recorded on an X-Y recorder, Model 7035B, Hewlett-Packard). Potential measurements were made with a multimeter (Model 7050, Systron Donner Corp., Sunnyvale, CA) and are reported vs. a saturated calomel reference electrode.

Microscopy. The surface of a polycrystalline cadmium electrode was examined with a scanning electron microscope (JEOL Model JSM-U3, Inc., Medford, MA) in the Energy Research Institute, Iowa State University, and the micrographs were recorded on Polaroid film. Low-power visual microscopy was done in the Department of Metallurgy, Iowa State University.

RESULTS AND DISCUSSION

Polycrystalline electrodes in acidic solutions

Electrodes made from polycrystalline cadmium exhibit irreproducible activity for the electrochemical reduction of nitrate in acidic solutions [19]. The faradaic signal (μA cm^{-2} M^{-1}) is not reproducible from one electrode to another and is usually much less than the mass transport-limited value for n = 6 [19] unless the surface of the cadmium electrode has been carefully prepared by chemical etching with nitric acid. To illustrate, the cathodic current at —0.85 V vs. SCE in 0.1 M H_2SO_4 is plotted in Fig. 1 as a function of the concentration of nitrate for three different procedures of preparing the surface of the cadmium disk electrode, each of which brings about dissolution of cadmium. Curve A corresponds to chemical etching for 2 min at the open-circuit potential in 30% hydrogen peroxide; curve B corresponds to anodization at 0.0 V vs. SCE for 2 min in the supporting electrolyte; and curve C is for chemical etching for 2 min in 2 M HNO_3 saturated with sodium nitrate. The theoretical response at 1.0 mM NO_3^- for a mass transport-limited reduction of nitrate to hydroxylamine (n = 6) is 8.6 mA. The values of the intercepts in Fig. 1 are approximately equal to the residual currents observed for current—voltage (I—E) curves obtained in the absence of nitrate. Chemical etching with hydrogen peroxide, while resulting in the dissolution of cadmium, did not produce any significant increase in electrode activity over that for an untreated electrode. The maximum increase of

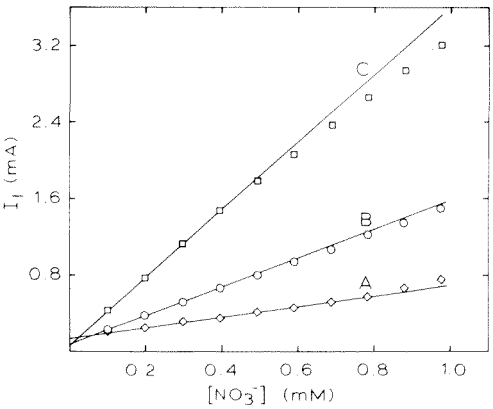

Fig. 1. Limiting current for reduction of nitrate at rotating polycrystalline Cd disk electrode in 0.10 M H_2SO_4 (E = −0.85 V vs. SCE; A_{Cd} = 0.95 cm^2; $\omega^{1/2}$ = 16.2 (rad $s^{-1})^{1/2}$). Surface treatment: (A) etching with H_2O_2; (B) anodization at 0.0 V vs. SCE, (C) etching with HNO_3.

electrode activity was produced by chemical etching with nitric acid. However, the activity for the pretreatment was still not sufficient to produce the transport-limited current.

Micrographs taken with a light microscope of the electrode surfaces which produced the data in Fig. 1 are shown in Fig. 2. The polycrystalline structure of the cadmium disk is clearly visible after chemical etching with nitric acid. Visual examination of this surface under bright light with a magnifying glass revealed that the faces of the exposed crystallites were not co-planar, and deviated from the plane of the electrode surface by 10—20°. It is concluded that the heterogeneous rate constant for reduction of nitrate is strongly dependent on the identity of the crystal plane at which the reaction occurs. Furthermore, it seems reasonable to conclude that the mechanism of the reduction of nitrate is the same for the reaction during chemical etching at the open-circuit potential and for electrochemical reduction at a potential controlled 20—200 mV more negative than the open-circuit value. Hence, the etching process occurs with the greatest rate at the preferred crystal planes and the rapid removal of cadmium parallel to these surfaces serves to

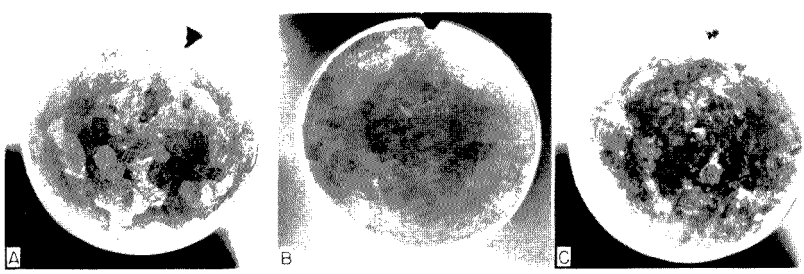

Fig. 2. Micrographs of disk electrodes producing data in Fig. 1: (A) etched with H_2O_2; (B) anodized; (C) etched with HNO_3.

increase the total area of the crystal planes which support the most rapid electrochemical reduction of nitrate under voltammetric conditions.

Copperized polycrystalline electrodes

The presence of electrodeposited copper on the surface of an electrode made from polycrystalline cadmium electrocatalyzes the voltammetric reduction of nitrate. Unfortunately, the copper also dramatically increases the cathodic background current from evolution of molecular hydrogen, and the Cu—Cd electrode is virtually useless for analytical detection in acidic media. Under weakly alkaline conditions, the background current is sufficiently low to permit quantitative measurements of nitrate; however, no signal is observed for nitrite. The current—potential curve for reduction of nitrate at a polycrystalline cadmium-disk electrode in 0.1 M Tris at pH 8 is shown in Fig. 3 (Curve B) compared to the residual curve for the absence of nitrate (Curve A). The positive limit of the triangular sweep of potential was not permitted to exceed —0.90 V vs. SCE to avoid anodic dissolution of cadmium. It should be noted that the range of accessible potentials at cadmium electrodes does not encompass the formal reduction potential estimated to be +0.12 V vs. SCE for the NO_3^-/NO_2^- couple. The current reduction of nitrate without the benefit of deposited copper is at a maximum value at a potential of —0.95 V vs. SCE and decreases as the negative potential scan continues. This decrease is concluded to be the result of an increased competition for active surface sites by adsorbed hydrogen as the rate of evolu-

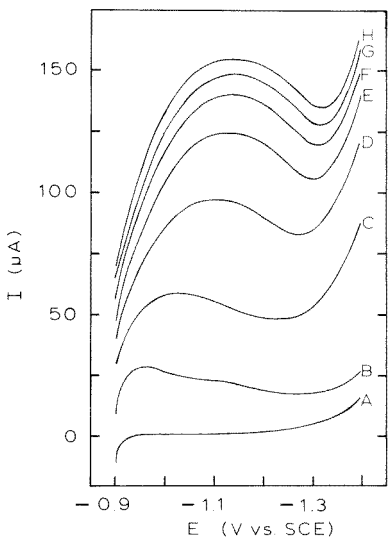

Fig. 3. Current—voltage curves for nitrate at a rotating polycrystalline Cd disk electrode in Tris buffer as a function of deposited Cu (A_{Cd} = 0.95 cm²; $\omega^{1/2}$ = 6.47 (rad $s^{-1})^{1/2}$; scan rate, —1.0 V min^{-1}). Curve A, residual; curves B—H, [NO_3^-] = 0.20 mM. Equivalent monolayers of deposited Cu at start of scan: (B) 0; (C) 0.5; (D) 1.0; (E) 1.5; (F) 2.0; (G) 2.5; (H) 3.2.

tion of molecular hydrogen increases for $E < -1.4$ V. The calculated mass transport-limited current for reduction of nitrate to nitrite ($n = 2$) under the conditions of Fig. 3 is 230 μA. This calculation was made according to eqn. (1) with $D = 1.9 \times 10^{-5}$ cm^2 s^{-1} [23] and $\nu = 8.93 \times 10^{-3}$ cm^2 s^{-1} [24].

Also shown in Fig. 3 are the I—E curves for nitrate obtained as a function of the slow accumulation of electrodeposited copper on the surface of the cadmium electrode. Copper(II) is electrodeposited at a mass transport-limited rate over the entire useful range of potential. The quantity of deposited copper corresponding to each I—E curve was estimated from the calculated limiting current for 0.8 μM Cu(II) and the total time for electrodeposition. The number of monolayers equivalent to the deposited copper was estimated assuming the packing density of pure copper and a perfectly smooth electrode surface. The deposition current was negligible on the current scale of Fig. 3 and the time necessary for accumulation of the equivalent of one monolayer of copper was approximately 21 min. Electrocatalysis of the reduction of nitrate by the copper is very evident, even for less than the equivalent of one monolayer. As the quantity of deposited copper increased (Curves D—H), the potential for the maximum cathodic current shifted from —0.95 V to approximately —1.1 V vs. SCE. Inhibition of the reduction of nitrate by the onset of hydrogen evolution was still observed at —1.3 V after several monolayers of copper had been deposited. The residual current for evolution of hydrogen on the Cu—Cd electrode for Curve H was approximately 25 μA cm^{-2} at —1.3 V, in comparison to 5 μA cm^{-2} at the unplated electrode. In other experiments with higher concentrations of Cu(II), the current for nitrate stabilized at a value within 10% of the theoretical for coverages by copper exceeding the equivalent of approximately 20 monolayers. No additional current for nitrate was obtained for quantities of copper increasing to nearly 1000 monolayers.

The electrodeposited copper was granular in appearance, as reported previously [17], and was easily removed from the cadmium surface by gentle rubbing with a soft absorbent tissue. Visual inspection of the cadmium surface following removal of copper which had been deposited under open-circuit conditions revealed that the deposition process had resulted in selective removal of cadmium and the crystallite structure of the cadmium was much more evident than that observed prior to the deposition. Initially, the selective etching of the cadmium by the deposition of copper was thought to be responsible for the electrocatalytic phenomenon. However, when copper was deposited potentiostatically at $E > 100$ mV negative of the open-circuit potential, no change in the appearance of the cadmium substrate occurred. Hence, the electrocatalysis is the result of the presence of copper on the cadmium surface rather than any variation in the morphology of the cadmium substrate.

Current—potential curves were obtained as a function of the rotational velocity (ω) for reduction of nitrate at an electrode bearing approximately 700 monolayers of copper. There was no inhibition of the reduction process

by hydrogen at −1.3 V. A plot of the limiting current (I_l) vs. $\omega^{1/2}$ measured at −1.3 V was linear for ω in the range 42—1050 rad s^{-1} (400—10000 rev. min^{-1}) with an intercept of 65 ± 4 μA which was approximately equal to the residual current observed for this electrode in the absence of nitrate. The slope, determined by the method of linear least squares, was 15.9 ± 0.2 $\mu A\ rad^{-1/2}\ s^{1/2}$. The expected slope for $n = 2$ was calculated to be 17.4 $\mu A\ rad^{-1/2}\ s^{1/2}$. These results are included in Table 1. The linearity of the I_l—$\omega^{1/2}$ plot is concluded to be indicative of an electrode reaction for nitrate which is limited by the rate of convective-diffusional mass transport. Current—potential curves for the Cu—Cd electrode in solutions of nitrite at a pH 8 revealed no evidence of electrochemical reduction of nitrite and the product of the reduction of nitrate is concluded to be nitrite.

Microstructure of deposited copper

The electrocatalytic action of electrodeposited copper was observed for accumulations of copper exceeding the equivalent of several hundred monolayers. At first thought, such a massive deposit would be deemed sufficient to cover the cadmium surface with a rather impervious plate of the metal. Voltammetric experiments with a solid copper electrode revealed little tendency for reduction of nitrate, and it was obvious that the heavily copperized surface of the Cu—Cd electrode is certainly not equivalent to solid copper in its electrochemical properties.

Based on the respective values of E° for the Cd(II)—Cd and Cu(II)—Cu couples, −0.65 and +0.09 V vs. SCE, respectively, it is predicted that cadmium should be the only metal ion produced at a Cu—Cd electrode at open-circuit potential, i.e. conditions equivalent to application of a reductor column. Yet, if the cadmium is clad with a thick copper plate, how is it possible for Cd(II) to permeate the deposited copper? Experimentation with

TABLE 1

Summary of response for reduction of nitrate ions at pH 8 ($C^b_{NO_3^-} = 1.0 \times 10^{-3}$ M; ω = 50—1050 rad s^{-1})

Electrode	Area (cm^2)	Theoretical slope ($\mu A\ rad^{-1/2}\ s^{1/2}$)	Observed slope[a] ($\mu A\ rad^{-1/2}\ s^{1/2}$)	Intercept[a] (μA)	Correlation coefficient (r)
Cu-plated polycrystalline Cd	0.95	17.4	15.9 ± 0.2	65 ± 4	0.9998
Single-crystal Cd (0001)	0.43	7.88	5.0 ± 0.1	196 ± 3	0.9993
Cu-plated Cd (0001)	0.43	7.88	7.5 ± 0.1	84 ± 2	0.9998
Single-crystal Cd ($10\bar{1}0$)	0.35	6.41	1.6 ± 0.2	26 ± 5	0.9802
Cu-plated Cd ($10\bar{1}0$)	0.35	6.41	7.3 ± 0.2	11 ± 4	0.9994

[a]Uncertainties calculated at the 90% confidence level.

a rotated ring-disk electrode was performed to determine the identity of the metal ion(s) produced during the chemical etching by nitric acid of a Cu—Cd disk electrode at the open-circuit potential. The carbon disk of the ring-disk electrode was plated with the equivalent of approximately 1200 monolayers of cadmium followed by 700 monolayers of copper. The ring-disk electrode was then rotated in a solution of 0.1 M Tris at pH 8 containing nitrate. The platinum ring of the ring-disk electrode was controlled at −1.0 V where both Cd(II) and Cu(II) are electrodeposited in the buffer solution. Sharp anodic stripping peaks are obtained at a platinum electrode in this medium for cadmium and copper at −0.7 V and −0.2 V, respectively. Following a 10-min etching period with the disk electrode at the open-circuit potential, the I—E curve was recorded for a positive scan of potential at the ring electrode. The only stripping peak observed was at −0.7 V corresponding to cadmium. The conclusion is rather obvious; the deposited copper on the cadmium electrode is highly porous with an appreciable portion of the cadmium substrate accessible to nitrate from the solution. The experiment was repeated with potentiostatic control of the Cu—Cd electrode at −1.3 V during rotation of the electrode in the solution of nitrate. No cadmium or copper was detected at the ring electrode.

Scanning electron microscopy was used to examine the surface of a Cu—Cd electrode. After the surface of the cadmium electrode had been polished, a rectangular section of the surface was observed at a magnification of 10000× for 30 min, while tuning adjustments were made on the microscopic equipment. Grooves left in the electrode surface by the diamond particles used in the last step of the polishing procedure were observed; however, no additional characteristic feature of the surface was evident. The electrode tip was removed from the microscope and copperized according to the procedure described at the open-circuit potential. The tip was reinserted into the microscope, in exactly the same position as for the initial viewing, and examined at a magnification of 3000×. At the center of the viewing scope was a dark rectangle which corresponded to the region which had been scanned previously. No change in the appearance of this rectangle had resulted from the copperization. The position of the tip was changed slightly and the surface examined at a magnification of 10000×. The resulting micrograph is shown in Fig. 4. A corner of the unplated rectangle is observed as the dark area. It is clear that the copperized portion of the electrode does not consist of a continuous film of copper. Instead, the copper is present as microspheres, 0.2—0.5 μm in diameter, in a closely packed array. The cadmium substrate is undoubtedly still accessible to the diffusion of nitrate through the interstitial spaces between the microspheres.

The section of the cadmium electrode which was not copperized was probably covered by a carbonaceous film which formed during the initial microscopic examination. Organic vapor from the oil in the vacuum pump can adsorb to the surface of the sample where the incident beam of electrons causes decomposition with adsorption of the reaction products. The presence of the adsorbed carbonaceous products prevented any deposition of copper.

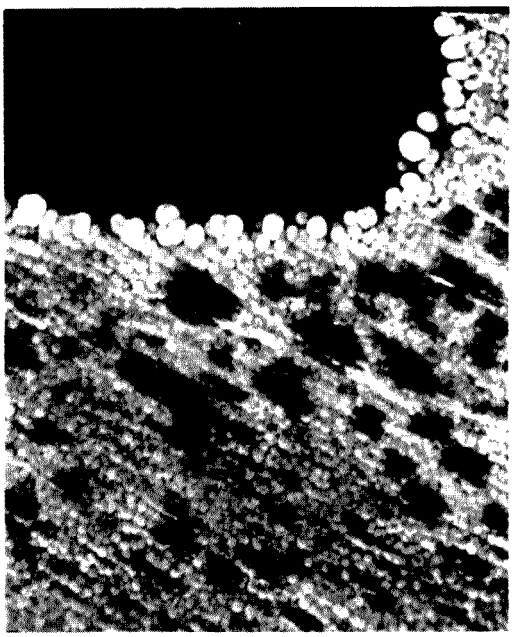

Fig. 4. Scanning electron micrograph of copperized Cd-disk electrode.

Reduction of oxygen

Dissolved oxygen is frequently a source of interference in cathodic voltammetry and the development of electroanalytical methods always includes a consideration of this source of interference. Current—potential curves were obtained for reduction of oxygen at the Cu—Cd electrode as a function of ω. The cathodic waves were fairly irreversible at high rotational velocities although a limiting-current plateau was still evident at 1050 rad s^{-1}. The plot of I_l vs. $\omega^{1/2}$ at −1.35 V was linear with an intercept equal to the residual current measured in the absence of the dissolved oxygen. It is not possible to discern separated voltammetric waves for nitrate and oxygen at the Cd or Cu—Cd electrodes because of the narrow range of accessible potentials. Hence, dissolved oxygen must be removed from the sample to obtain the most accurate voltammetric results for the determination of nitrate.

Oxygen present in samples of nitrate is also reduced when passed through a Cu—Cd reductor column. Otsuki [17] observed that copper is lost from the leading end of the column and proposed that ionic copper is a product of the reaction in the column. A more reasonable explanation, based on our results, is that Cd(II) is the only metal ion produced. However, the dissolution of the cadmium substrate under the copper microspheres allows the copper physically to be swept away by the force of the liquid stream. The loss of copper is most prominent at the leading end of a reductor column where the rate of reaction is greatest.

Single-crystal electrodes

Experiments on the activation of polycrystalline cadmium electrodes by chemical etching led to the conclusion that the heterogeneous rate constant for reduction of nitrate is strongly dependent on the identity of the crystalline plane at which the reaction occurs. Voltammetric studies were performed at two single-crystal cadmium electrodes constructed with the 0001 and $10\bar{1}1$ planes cut parallel to the disk surface. The four digits used here to designate the crystal planes are Miller—Bravais indices for hexagonal close-packed systems [25]. The residual current was very large for the 0001 electrode, perhaps resulting from evolution of hydrogen. Plots of I_l vs. $\omega^{1/2}$ were made from voltammetric data for the electrodes with and without the benefit of deposited copper. The data are summarized in Table 1. The slopes for the copperized electrodes are nearly equal to the predicted values for a mass transport-controlled reaction to produce nitrite (n = 2), and the intercepts are approximately equal to the residual currents observed in the absence of nitrate.

Current—potential curves are shown in Fig. 5 for the $10\bar{1}1$ electrode as a function of the accumulation of electrodeposited copper. The curves were obtained in an identical manner to those shown in Fig. 3. Electrocatalysis is significant even for a fraction of a monolayer of deposited copper. The inhibitory effect of hydrogen evolution on the reduction of nitrate which is observed in the absence of deposited copper is not observed for the electrocatalyzed reduction (Curve G). The limiting current of 130 μA for curve G is in good agreement with the theoretical value of 127 μA for this electrode. The electrocatalytic effectiveness of a very few layers of copper is significantly greater at the single-crystal cadmium electrode than at the polycrystalline

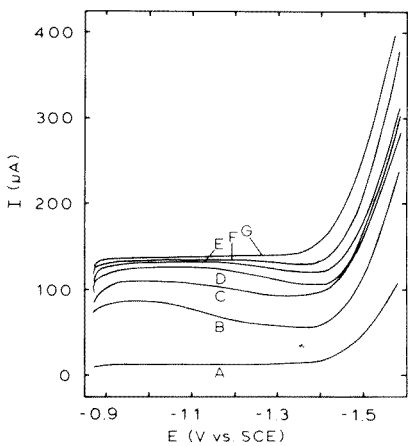

Fig. 5. Current—voltage curves for nitrate at a single-crystal Cd disk electrode ($10\bar{1}1$) in Tris buffer as a function of deposited Cu. (A_{Cd} = 0.32 cm^2; $\omega^{1/2}$ = 6.47 (rad s^{-1})$^{1/2}$; scan rate, —1.0 V min^{-1}.) Curve A, residual; curves B—H, [NO_3^-] = 0.30 mM. Equivalent monolayers of deposited Cu at start of scan: (B) 0; (C) 0.2; (D) 1.4; (E) 3.6; (F) 6.8; (G) 14.7.

electrode, as seen by comparison of curve E in Fig. 5 with curve H in Fig. 3. However, any advantage of the use of the single-crystal cadmium is more than offset by the high cost, particularly in view of the fact that mass transport-limited currents can be achieved at the polycrystalline material by the deposition of copper.

CONCLUSIONS

Trepak et al. [26] concluded, from chronoamperometric studies of the reduction of nitrate at cadmium electrodes, that the reaction proceeds by way of a pre-adsorption step. This conclusion is consistent with our interpretation of data shown in Figs. 3 and 5. The onset of the evolution of hydrogen at the cadmium electrode is apparently responsible for the significant decrease observed in the rate of nitrate reduction for the negative potential scan. Adsorption of hydrogen atoms or molecules, as a result of the onset of hydrogen evolution, would certainly interfere with the adsorption of nitrate ion required for the reduction process. The presence of electrodeposited copper on the Cu—Cd electrodes electrocatalyzes reduction of nitrate significantly and eliminates the interference by hydrogen for high coverages (>20 monolayers). It was also observed that the crystalline nature of the cadmium substrate in the Cu—Cd electrodes is not important in controlling the electrocatalytic activity when the quantity of deposited copper exceeds approximately 20 monolayers.

Electrochemical reactions which proceed by way of an adsorption step prior to electron transfer have reaction rates which are expected to be highly sensitive to the nature of the electrode surface [27]. The participation of vacant *d*-orbitals in the formation of adsorption bonds at the electrode surface has been given as a possible explanation of the large difference in the rate constant for reduction of oxygen at gold and platinum electrodes [28, 29]. Gold, $[Xe]\,5d^{10}6s^1$, has no partially filled *d* orbitals to participate in adsorptive binding with oxygen and the heterogeneous rate constant for reduction of oxygen is $10^{-8}\times$ that for Pt, $[Xe]\,5d^{9}6s^1$, which has a partially filled *d* orbital.

The case for comparing cadmium, $[Kr]\,4d^{10}5s^2$, and copper, $[Ar]\,3d^{10}4s^1$, is not so straightforward, because there are no partially filled *d* orbitals in the neutral atoms of either metal. A comparison of the inertness of the *d* electrons of the two metals can be made on the basis of their solution chemistry. The most stable cationic form of copper has a charge of +2 with the electronic configuration $[Ar]\,3d^9$. Oxidation of cadmium produces the +2 cation with no involvement of *d* electrons. It is suggested here that for copper in contact with cadmium on the Cu—Cd electrode, two electrons may be promoted to the conduction band of the electrode leaving a partially vacant *d* orbital to participate in formation of adsorption bonds with nitrate ions.

Toxic cadmium(II) is released by reductor columns prepared from cadmium or Cu—Cd during the reduction of nitrate in the conventional reduction

methods. This results in the need to collect all waste solutions for later disposal by appropriate means. It would seem desirable to eliminate the difficulties associated with production of Cd(II) in that method through utilization of a reductor column as the cathode of a coulometric, flow-through electrolysis cell (100% efficient). The electrochemical potential of the cathode would be maintained at a value which is negative of the equilibrium potential so that reduction of nitrate would proceed electrochemically with no production of Cd(II). The use of a coulometric flow-through electrode for quantitative change of the oxidation state of an electroactive species in a fluid stream has been described [30—33].

The authors are grateful to Jerry Amenson for carrying out the electron microscopy, and Harlan Baker for the light microscopy. The National Science Foundation is acknowledged for support of a portion of this research through grants GP-40646X and CHE 76-17826. Valuable discussions with Robert S. Hansen, Ames Laboratory of the United States Department of Energy, are acknowledged.

REFERENCES

1 R. H. Bray, Soil Sci., 60 (1945) 219.
2 E. Foyn, Rep. Norw. Fish. Mar. Invest., 9 (1951) 7.
3 T. J. Chow and M. S. Johnstone, Anal. Chim. Acta, 27 (1962) 441.
4 M. H. Litchfield, Analyst, 92 (1962) 132.
5 L. Potzl and R. Reiter, Z. Aerosol-Forsch. Ther., 8 (1960) 252.
6 P. G. Brewer and J. P. Riley, Deep Sea Res., 12 (1965) 765.
7 R. Fudge and R. W. Truman, J. Am. Pharm. Assoc., 11 (1973) 19.
8 M. J. Follett and P. W. Ratcliff, J. Sci. Food Agric., 14 (1963) 138.
9 A. W. Morris and J. P. Riley, Anal. Chim. Acta, 29 (1963) 272.
10 J. B. Mullin and J. P. Riley, Anal. Chim. Acta, 12 (1955) 464.
11 K. Grasshoff, Kiel. Meeresforsch., 20 (1964) 5.
12 J. D. H. Strickland and T. R. Parsons, A Manual of Seawater Analysis, Bull. Fish. Res. Board Can., 1969, No. 125.
13 E. D. Wood, F. A. J. Armstrong and F. A. Richards, J. Mar. Biol. Assoc. U.K., 47 (1967) 23.
14 R. S. Lambert and R. J. Dubois, Anal. Chem., 43 (1971) 955.
15 R. E. Crowe (Ed.), Methods for Chemical Analysis of Water and Wastes, Environ. Prot. Technol. Ser., Washington, DC, (1974) 201.
16 F. Nydahl, Talanta, 23 (1976) 349.
17 A. Otsuki, Anal. Chim. Acta, 99 (1978) 375.
18 M. P. Stainton, Anal. Chem., 46 (1974) 1616.
19 R. J. Davenport and D. C. Johnson, Anal. Chem., 45 (1973) 1979; 46 (1974) 1971.
20 M. E. Bodini and D. T. Sawyer, Anal. Chem., 49 (1977) 485.
21 V. G. Levich, Physicochemical Hydrodynamics, Prentice-Hall, Englewood Cliffs, NJ, 1962, p. 69.
22 W. J. Albery and M. L. Hitchman, Ring Disc Electrodes, Clarendon, Oxford, 1971.
23 V. M. Vdovenko, Yu. V. Gurikov and E. K. Legin, Radiokhimiya, 8 (1966) 323.
24 R. C. Weast (Ed.), Handbook of Chemistry and Physics, 52nd edn., Chemical Rubber Co., Cleveland, OH, 1972, p. D-223.
25 B. D. Cullity, Elements of X-ray Diffraction, Addison-Wesley, Reading, MA, 1967, p. 38.

26 N. M. Trepak, L. K. Il'ina, A. L. L'vov and V. N. Rodnikova, Electrokhimiya, 8 (1972) 939.
27 S. Trasatti, Chim. Ind. (Milan), 51 (1969) 1063.
28 S. Srinivasan, H. Wroblowa and J. O'M. Bockris, Adv. Catal., 17 (1967) 351.
29 M. L. B. Rao, A. Damjanovic and J. O'M. Bockris, J. Phys. Chem., 67 (1963) 2508.
30 D. C. Johnson and J. H. Larochelle, Talanta, 20 (1973) 959.
31 S. Kihara, T. Yamamoto, K. Motojima and T. Fujinaga, Talanta, 19 (1972) 329, 657.
32 S. Kihara, J. Electroanal. Chem., 45 (1973) 31, 45.
33 T. Fujinaga and S. Kihara, CRC Crit. Rev. Anal. Chem., 6 (1977) 223.

Analytica Chimica Acta, 129 (1981) 101—111
Elsevier Scientific Publishing Company, Amsterdam — Printed in The Netherlands

A CHROMATOGRAPHIC DETERMINATION OF NITRATE WITH AMPEROMETRIC DETECTION AT A COPPERIZED CADMIUM ELECTRODE

GLENN A. SHERWOOD[a] and DENNIS C. JOHNSON*
Department of Chemistry, Iowa State University, Ames, IA 50011 (U.S.A.)
(Received 24th November 1980)

SUMMARY

A copperized cadmium flow-through electrode is applied for cathodic detection of nitrate in the effluent stream of a liquid chromatograph. The nitrate is separated from dissolved oxygen in a small (10 cm) column of strong-base, anion-exchange resin (Dowex 1-X8) with 5 mM perchloric acid as the eluent. The effluent stream is buffered to pH 8 by mixing with a stream of buffer prior to detection. A large excess of chloride added to the sample dramatically improves the separation of nitrate from dissolved oxygen in the sample.

Davenport and Johnson [1] described a chromatographic separation of nitrite and nitrate on an anion-exchange column with an eluent of 0.01 M perchloric acid. The effluent stream was mixed with a stream of 0.2 M sulfuric acid before passage through a polycrystalline cadmium electrode for amperometric detection. In the acidic media, nitrate and nitrite were reduced electrochemically to hydroxylamine. Dissolved oxygen in the sample can also be detected amperometrically and was separated from the nitrate and nitrite on the chromatographic column. Difficulties in obtaining satisfactory results by this method result from the need to pretreat the cadmium electrode by anodization or, preferably, by chemical etching in dilute nitric acid to produce an active electrode surface [1, 2].

The voltammetric behavior of polycrystalline cadmium electrodes on which the equivalent of several monolayers of copper have been deposited has been described [2]. The presence of the copper also increases the rate of hydrogen evolution in acidic solutions and amperometric application is restricted to neutral or alkaline solutions. In 0.1 M tris(hydroxymethyl)-aminomethane (Tris), adjusted to pH 8 with hydrochloric acid, the reduction of nitrate to nitrite (n = 2) occurs at a copperized Cd-disk electrode at a mass transport-limited rate. Negligible reduction of nitrite is observed at pH 8. Reproducible activity of cadmium electrodes for reduction of nitrate is more easily obtained by the procedure of copperization than by chemical etching

[a]Present address: E. I. DuPont de Nemours and Co. Wilmington, DE, U.S.A.

0003—2670/81/0000—0000/$02.50

with dilute nitric acid. This paper describes the chromatographic separation of nitrate with a copperized cadmium (Cu—Cd) detector. Since detection is in a stream buffered at pH 8, nitrite cannot be determined directly.

EXPERIMENTAL

Reagents, chemicals and samples

Chemicals were Analyzed Reagents (Fisher Scientific Co.) unless specified otherwise. Standard solutions of nitrate were prepared from sodium nitrate. The buffer solution at pH 8 was 0.5 M Tris containing 0.22 M $HClO_4$. The chromatographic eluent was 5 mM $HClO_4$. All water had been distilled and demineralized.

A water sample from Saylorville Reservoir in central Iowa was obtained from the Energy Research Laboratory, Iowa State University. The sample had been acidified with concentrated sulfuric acid (2 ml l^{-1}) to prevent bacterial consumption of the nitrate. The acidic sample was neutralized by titration with 1.0 M KOH as part of the determination. The nitrate content was also determined in the Energy Research Laboratory.

Tender Quick is a commercially available substance (Morton Salt Co., Chicago) for use in the home, to preserve meat. This material contains mainly sodium chloride and approximately 0.50% each of sodium nitrate and sodium nitrite [3]. Nitrate was determined in an aqueous solution of this salt and then the sample was treated with 3% H_2O_2 to convert nitrite to nitrate. The total nitrate was then determined and the original nitrite was calculated by difference.

Ion-exchange column

The strong-base, anion-exchange resin was Dowex 1-X8 (Bio-Rad Laboratories, Richmond, CA). The resin was received in wet form with a size distribution of 200—400 mesh. The wet resin was washed with 2-propanol to remove excess of water and air-dried. The dried resin was sieved and the fraction passing through U.S. Sieve No. 325 was collected. Fines were removed from the fraction collected by flotation in 2-propanol. The 2-propanol was then washed from the resin with water and a glass column (2-mm i.d. × 10 cm) was packed by delivery of a slurry of the resin under pressure from a syringe. The resin bed was supported in the column by a small plug of glass wool.

Flow-through detector

The detector, shown in Fig. 1, was constructed in the Chemistry Shop, Iowa State University, from a design inspired by the concept of a "wall-jet" electrode as described by Yamada and Matsuda [4], and modified by Fleet and Little [5]. The body of the detector was machined from glass-filled (25%) teflon (GFT; Crown Plastic, Inc., St. Paul, MN). This material is harder than pure teflon with machining properties closer to that of Kel-F. The effluent stream entered through port A and impinged on the surface of a

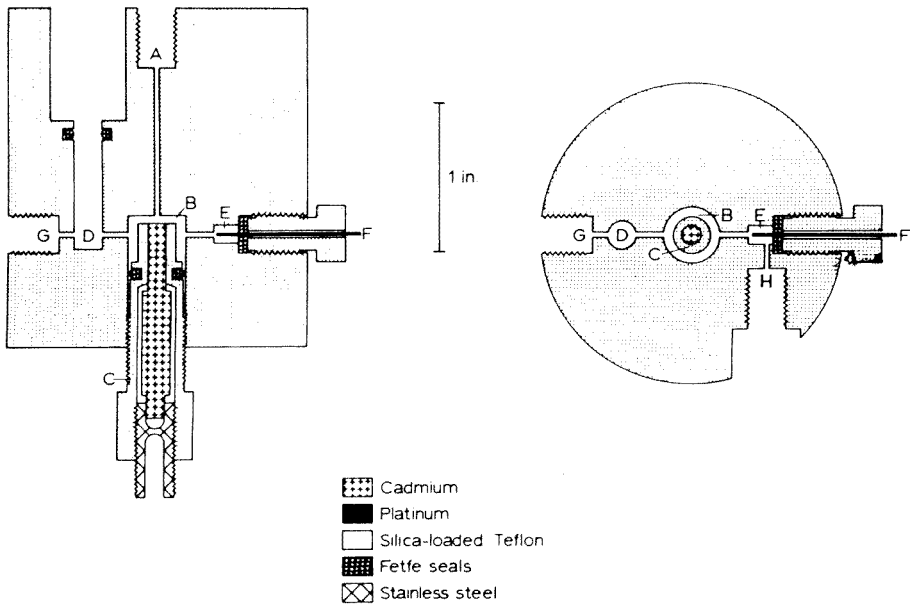

Fig. 1. Diagram of the flow-through disk detector. Vertical and horizontal cross-sections are shown. (A) Entry port for chromatographic effluent; (B) working electrode chamber; (C) retractable electrode assembly; (D) chamber for SCE reference; (E) auxiliary electrode chamber; (F) auxiliary electrode (Pt); (G) exit port from reference electrode chamber; (H) exit port from auxiliary electrode chamber.

disk electrode in compartment B. The waste fluid exited the detector via the counter electrode compartment, E, and exit port, H, and the chamber for the reference electrode, D, and exit port, G. The reference electrode was a miniature saturated calomel electrode (SCE; Beckman Instrument Co., Fullerton, CA). A FETFE O-ring around the barrel of the SCE provided a tight seal which prevented flow of solution out of the top of chamber D. FETFE is a pliable fluoroelastomer (Ace Glass, Inc., Vineland, NJ) which is inert to strong acids and corrosive oxidants.

The indicator electrode was mounted in a retractable assembly, C, which permitted adjustment of the spacing between the fluid orifice and the electrode surface, as well as removal of the electrode from the cell for visual inspection or chemical treatment. The retractable assembly consisted of a cadmium shaft press-fitted into a stainless steel banana jack and mounted in a shroud made from GFT with epoxy cement. The diameter of the exposed end of the cadmium was 3 mm. A FETFE O-ring around the retractable assembly served to prevent leakage of solution. The distance, d, between the fluid orifice and the electrode surface was estimated from the known pitch of the threads on the retractable electrode assembly and the number of turns made from a position where the electrode was in contact with the orifice and fluid flow was stopped. The variation of d with rotation of the electrode assembly was 0.8 mm per revolution.

A second electrode assembly was constructed using a Pt disk soldered to a stainless steel rod in place of the cadmium. The platinum electrode was used for characterizing the performance of the detector. A silver-wire flow-through detector was constructed identical to an earlier design [6] for amperometric detection of chloride at 0.25 V vs. SCE by the anodic reaction $Cl^- + Ag \rightarrow AgCl + e$.

Liquid chromatograph

The chromatographic system was constructed according to an earlier design [7] with components from Laboratory Data Control (Riviera Beach, FL). The solutions of eluent and buffer were deaerated in the storage tanks of the chromatograph with dispersed helium prior to experimentation. The tanks were then sealed and pressurized at $\leqslant 40$ psi. The flow rate of the eluent and buffer were regulated at 1.0 and 0.25 ml min^{-1}, respectively. The buffer was mixed with the effluent stream immediately after emergence from the column in a Kel-F tee (Laboratory Data Control) followed by passage through a short section (10 cm) of teflon tubing packed with glass wool. The sample loop of the sample injection valve had a volume of 0.309 ml. The potentiostat was a Model RDE-3 (Pine Instrument Co., Grove City, PA). Chromatographic data were recorded on a stripchart recorder (Model SR-204, Heath Schlumberger, Benton Harbor, MI). The areas of chromatographic peaks were measured with a planimeter.

Procedures

At the start of each day, the retractable electrode assembly was removed from the detector and the exposed surface of the cadmium was wiped with a tissue to remove deposited copper from previous experiments. If the surface of the cadmium was pitted, it was polished with 6-μm and 1-μm diamond polishing compound. The cadmium electrode was copperized by swirling in 0.08 M $CuSO_4$ for approximately 10 s followed by a rinse with water. The copperized electrode was reinserted into the detector and the flow of the eluent and buffer was started.

The spacing, d, between the electrode surface and the orifice in compartment B (see Fig. 1) was adjusted to the optimum value as determined by turning the retractable electrode assembly until the restriction of fluid flow was observed by a slight decrease in the flow rate of the buffer stream. A value of $d = 0.2$ mm was estimated. With continued flow of the fluid streams, the reference electrode was removed from compartment D to permit release of trapped gas bubbles and the liquid level in D was permitted to rise until that compartment was half filled. The reference electrode was reinserted into D and the resultant rush of fluid was usually sufficient to dislodge gas bubbles trapped in the channels of the detector. To ensure the removal of all gas bubbles, first one and then the other exit tube was temporarily blocked until free flow was observed from both exit tubes. Finally, the exit tubes were positioned along the wall of a collection vessel so a continuous stream

of waste solution flowed down the wall. If the waste solution was permitted to exit the tubes in intermittent drops, spikes were observed in the background signal caused by the periodic change in flow rate resulting from tiny variations in back pressure.

The potentiostat was connected to the detector and the potential of the cadmium electrode adjusted to −1.15 V vs. SCE. The background current for reduction of oxygen was permitted to decay until the concentration of oxygen in the teflon lines reached a steady value (ca. 30 min).

A stock solution containing Tender Quick (5.0 g l^{-1}) was separated chromatographically. The procedure was calibrated by standard addition with 2.00 ml of 10.0 mM KNO_3 mixed with 98.0 ml of the sample. The nitrite in the sample was determined as described above by oxidation with 10.0 ml of 3% H_2O_2 in 90.0 ml of sample. The nitrite determination was calibrated by standard addition with 2.0 ml of 10.0 mM KNO_2 and 10.0 ml of 3% H_2O_2 with 88.0 ml of sample. A second portion of the Tender Quick was dried for 4 h at 90°C prior to preparation of the solutions. The chromatographic results were compared with results obtained by the colorimetric procedure of the U.S. Environmental Protection Agency [8].

RESULTS AND DISCUSSION

Evaluation of detector

The chromatographic system was modified for the purpose of evaluating the detector with a stream of 2 mM NaI in 0.1 M H_2SO_4 pumped continuously through the detector. The platinum electrode was substituted for the cadmium electrode and was controlled at 0.70 V vs. SCE, at which reaction $2I^- \rightarrow I_2 + 2e$ occurs at a mass transport-limited rate [9]. The limiting steady-state current (I_{ss}) was determined as a function of flow rate, v_f, and electrode spacing, d, and the log–log plots of I_{ss} vs. v_f and d were linear with slopes of 0.33 and −0.75, respectively. Hence, the response of the detector is described by the empirical equation

$$I_{ss} = k\, v_f^{0.33} d^{-0.75} C_o \qquad (1)$$

where k is a proportionality constant and C_o is the analytical concentration.

The similarity of the proposed detector (Fig. 1) to designs in the literature was noted earlier. Yamada and Matsuda [4] derived and verified the theoretical response of a wall-jet detector constructed with a nozzle positioned opposite the surface of a disk electrode with fluid forced at high velocity from the nozzle in a direction parallel to the axis of the disk

$$I_{ss} = k\, n\, F D^{2/3} \nu^{-5/12} v_f^{3/4} a^{-1/2} R^{3/4} C_o \qquad (2)$$

where ν is the kinematic viscosity of the fluid ($cm^2\ s^{-1}$); a is the radius of the orifice in the nozzle (cm); R is the radius of the disk electrode (cm); and n and F have their usual electrochemical significance. No dependence of signal upon the distance between the nozzle and the electrode is predicted by eqn.

(2) and this was verified [4] for large v_f (20 ml min^{-1}), small a (0.3 mm), and d from 2 to 10 mm. There is essentially no restriction on the flow of fluid away from the disk surface of the wall-jet electrode. The present design of detector, like that of Fleet and Little [5], has the fluid emerge from an orifice in one of two parallel walls positioned at the axis of the disk electrode mounted in the opposite wall. Fluid flow in this detector is greatly restricted by the parallel walls. Although Fleet and Little refer to their detector as a "wall-jet electrode", they reported that the sensitivity of their electrode was a function of the spacing between the orifice and the disk surface, which is in contradiction to the response predicted for a wall-jet electrode by eqn. (2). Neither the proposed detector nor that of Fleet and Little acts according to the predicted response for a "wall-jet" detector.

Evaluation of separation

The primary interference in the cathodic detection of nitrate at the Cu—Cd electrode is caused by the reduction of dissolved oxygen which occurs at a mass transport-limited rate [2]. Deaeration of neutral and alkaline solutions of nitrate can be achieved with dispersed helium without loss of nitrate. The eluent and buffer solutions were deaerated in their respective storage bottles and this seemingly would have alleviated the interference. However, the teflon tubing used in construction of the liquid chromatograph is permeable to oxygen from the surrounding air and a significant background level of oxygen was always present in the effluent stream entering the detector. It was virtually impossible to match the oxygen content of the sample perfectly with that of the eluent; a positive peak for oxygen was obtained when the sample was not deaerated and a negative peak with zero retention was obtained when the sample was deaerated. For the eluent chosen, the nitrate peak was resolved from the fluctuations in the background signal caused by the mismatch of the concentrations of oxygen in the sample and the eluent stream. A typical chromatogram is shown in Fig. 2.

Change in the area of the nitrate peak caused by the presence of various anionic substances in the sample was determined for a 10:1 excess of the potentially interfering species (Table 1). Several anions gave slight interference (<10%) as a result of peak distortion which caused some overlap of peaks for oxygen and nitrate. Of the anions tested, only chlorate produced a slight cathodic signal when injected in the absence of nitrate. The net error in the nitrate peak was still negative, however, when chlorate was present at the concentration indicated.

Effect of loading samples with chloride

A beneficial effect from the presence of a large excess of chloride in aqueous samples of nitrate was discovered during experiments with Tender Quick. The chloride produced a large increase in the retention time for nitrate, T_{r,NO_3^-}, with a significant decrease in peak width. Normally, it is

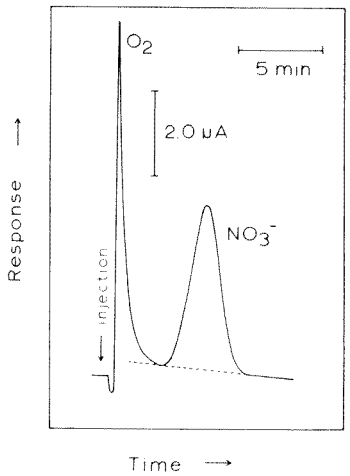

Fig. 2. Typical chromatogram for nitrate in air-saturated sample: Cd detector at −1.15 V vs. SCE; $C_{NO_3^-}$ = 0.40 mM.

TABLE 1

Detection of 0.50 mM nitrate in the presence of other anions

Compound (5.0 mM)	Relative error in peak area (%)	Compound (5.0 mM)	Relative error in peak area (%)	Compound (5.0 mM)	Relative error in peak area (%)
NaCl	+2.8[a]	$NaClO_3$	−5.6[b]	$NaHSO_4$	−2.0
NaBr	+1.4	$NaClO_4$	+0.2	$NaHSO_3$	+2.0
NaI	−3.3	$Na_2Cr_2O_7$	−4.6	$HClO_4$	+1.6
$Ca(OCl)_2$	+2.8	Na_2HPO_4	+4.0[b]		

[a]Greater retention for nitrate; peak fronting. [b]Peak broadening.

expected that peaks broaden as retention is increased. To elucidate the phenomenon, a series of solutions of 0.4 mM NO_3^-, containing variable amounts of chloride in the range 0.0–0.7 M, was analyzed using the amperometric detectors for nitrate and chloride. The chromatographic curves are shown in Figs. 3 and 4 for three representative solutions. The response for chloride present in the sample at concentrations above 0.06 M was characterized by a large spike followed by a plateau. The spike appeared at a time corresponding to the sample front, i.e. not retention, and undoubtedly corresponded to elution of chloride no adsorbed on the column. It should be noted that the quantity of chloride injected did not exceed the total capacity of the column in these experiments. Hence, it is apparent that the "dynamic" capacity of the resin for adsorption of chloride under these conditions was considerably lower than the capacity specified by the manufacturer. Following the appearance of the large spike for the unretained

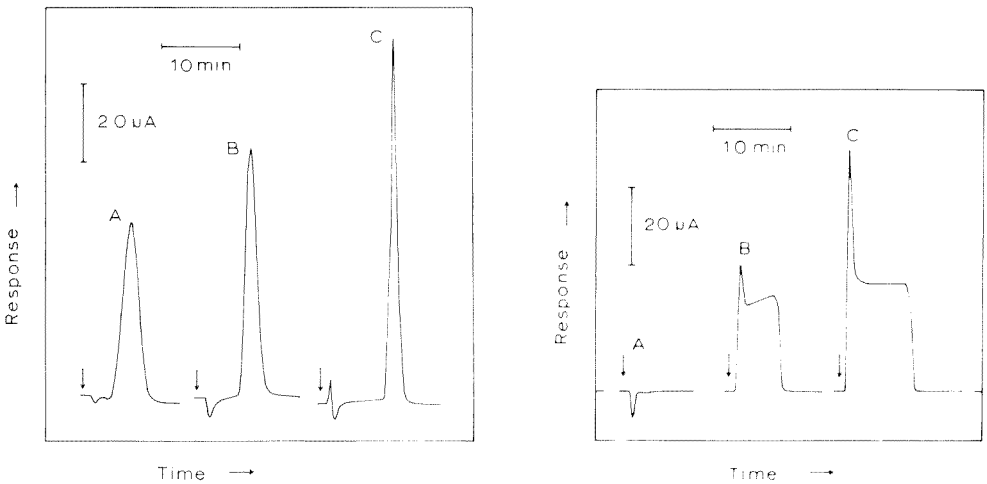

Fig. 3. Response for nitrate in chromatographic determination of nitrate in presence of chloride. (Cd detector at −1.15 V vs. SCE; $C_{NO_3^-}$ = 0.40 mM.) C_{Cl^-}: (A) 0 M, (B) 0.04 M; (C) 0.14 M. Samples deaerated prior to injection.

Fig. 4. Response for chloride in chromatographic determination of nitrate in presence of chloride. Ag detector at 0.25 V vs. SCE; other conditions as in Fig. 3.

chloride, the rate of elution of adsorbed chloride was approximately constant at the flux of perchlorate in the eluent stream entering the column. The time necessary to elute the adsorbed chloride to a current equal to one half the plateau value, $T_{1/2,Cl^-}$, was nearly equal to T_{r,NO_3^-}, for any specified value of chloride concentration, and increased with chloride concentration as shown in Fig. 5.

Gregor et al. [10] reported adsorption coefficients obtained by batch methods for a large number of anions on Dowex 2-X8, an anion-exchange resin quite similar to Dowex 1-X8. Their data show that the affinity of the

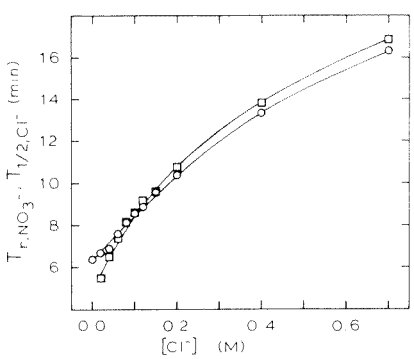

Fig.5. Retention parameters for nitrate and chloride: (○) retention time for NO_3^-, T_{r,NO_3^-}; (□) half-plateau width for Cl^-, $T_{1/2,Cl^-}$.

resin for perchlorate relative to chloride decreases dramatically as the fraction of the total capacity of the resin taken by adsorbed chloride, X_{Cl^-}, is increased. Conversely, the affinity for nitrate remains virtually unrelated to X_{Cl^-}. As a result, the order of affinities for the anions was observed to change from $ClO_4^- > NO_3^- > Cl^-$, at low X_{Cl^-}, to $NO_3^- > ClO_4^- > Cl^-$ for $X_{Cl^-} > 0.8$. These results of Gregor et al. are consistent with the present observations. For samples containing a high concentration of chloride, a major portion of the column may be converted to the chloride form following injection; however, nitrate is still retained by the resin. The elution of adsorbed chloride following injection of the sample begins at the leading end of the column with the result that perchlorate is completely removed from the mobile phase. Adsorbed nitrate is not released from any particular segment of the column until all adsorbed chloride has been exchanged in that segment and the perchlorate in the mobile phase is at a non-zero concentration. Nitrate eluted from a chloride-free segment of the column then moves ahead of the perchlorate front where it is re-adsorbed on a segment of the column with high X_{Cl^-}. Hence, the nitrate moves down the column immediately on the trailing edge of the band for chloride and ahead of the concentration front for perchlorate. This is a most interesting form of frontal elution chromatography. The presence of chloride in samples of nitrate had a decidedly beneficial effect of increasing the resolution of the nitrate peak from the peak for dissolved oxygen.

Calibration and precision

Calibration curves based on peak height and peak area were plotted on a log–log scale for standard solutions prepared with 0 M and 0.1 M potassium chloride. A linear regression analysis was carried out for each calibration curve including data for high concentrations which was obviously beyond the region of linear response; the equations of the lines are given in Table 2. All four calibration curves have linear regression coefficients greater than 0.998. The largest linear range of response was observed for measurement of peak area in the absence of chloride and the detection limit was approximately 0.1 μM NO_3^- (6.2 ppb). This compares favorably with the value of 10 μm for the detection limit reported earlier [1]. Although the linear range was less, the detection limit was more favorable by an order of magnitude in the presence of chloride. This was primarily the result of the more accurate estimation of the baseline made possible by the improved peak shape and greater resolution of nitrate from oxygen observed when chloride was present.

The precision of the analytical method based on measurement of peak area was tested for deaerated solutions of 0.010 mM and 1.10 mM nitrate with and without 0.1 M KCl. Six aliquots of each solution were processed and the results are summarized in Table 3. The relative standard deviation was acceptable (<5%) for all cases except for 0.010 mM NO_3^- without chloride. The nitrate peak was not sufficiently separated from the negative peak for oxygen unless chloride was present.

TABLE 2

Calibration of chromatographic response for nitrate
($\log I(\mu A) = a + b \log C_{NO_3^-}$; $\log Q(\mu C) = a + b \log C_{NO_3^-}$)

Plot	Range of $C_{NO_3^-}$(M)	C_{Cl^-}(M)	Parameter[a]
$\log I$ vs. $\log C$	1.0×10^{-6}—2.1×10^{-3}	0.00	a = —0.64 ± 0.02 b = 0.95 ± 0.01 r = 0.9998
$\log I$ vs. $\log C$	1.0×10^{-6}—2.1×10^{-4}	0.10	a = —0.39 ± 0.04 b = 0.94 ± 0.03 r = 0.9994
$\log Q$ vs. $\log C$	1.0×10^{-6}—4.7×10^{-3}	0.00	a = 0.39 ± 0.03 b = 0.97 ± 0.01 r = 0.9997
$\log Q$ vs. $\log C$	1.0×10^{-6}—4.8×10^{-4}	0.10	a = 0.24 ± 0.03 b = 0.96 ± 0.03 r = 0.9993

[a]Uncertainties calculated at the 90% confidence level.

TABLE 3

Precision of results

Solution	Avg. peak area (μC)	R.s.d. (%)
0.100 mM NO_3^-	177	3.7
0.090 mM NO_3^-/0.1 M Cl^-	127	2.5
0.0103 mM NO_3^-	17.0	9.1
0.0100 mM NO_3^-/0.1 M Cl^-	11.9	2.7

The sensitivity of the detector was usually observed to decrease slowly with time (2—5% h^{-1}). This decay seemed independent of the rapidity of injection of samples. As a consequence, the procedure was adopted to prepare a fresh copperized surface on the cadmium electrode at the start of each day.

Unknowns

Results for unknown samples are summarized in Table 4. The chromatographic result for the water sample is in excellent agreement with that obtained by the standard method. It must be noted here that the time saved per determination in the chromatographic procedure is very significant, as compared with the standard method. The result for nitrate in the undried Tender Quick is in excellent agreement with the value from the standard method and the value given by Morton Salt Co. The chromatographic result for nitrite is low, possibly because the peroxide did not oxidize the nitrite quantitatively. When the sample of Tender Quick was dried at 90°C as part

TABLE 4

Quantitative results for selected samples

Sample	Chromatographic results	Comparison results
Water from Saylorville Reservoir	23.6 ppm NO_3^-	22.8 ppm[a]
Tender Quick (as received)	0.54% $NaNO_3$	0.50% $NaNO_3$[b], 0.56% $NaNO_3$[a]
	0.34% $NaNO_2$	0.50% $NaNO_2$[b], 0.49% $NaNO_2$[a]
Tender Quick (dried)	0.73% $NaNO_3$	0.33 $NaNO_3$[a]
	0.76% $NaNO_2$	0.49% $NaNO_2$[a]

[a]Standard method [8]. [b]Listed on package.

of the analysis, the results by the chromatographic and standard methods were not in agreement for either nitrate or nitrite. The sample had discolored, with brown crystals observed following the drying operation, and the sample was concluded to have decomposed partially. Nitrate can be a good oxidizing agent at high temperatures and the sample does contain some sucrose which is oxidized easily.

REFERENCES

1 R. J. Davenport and D. C. Johnson, Anal. Chem., 45 (1973) 1979.
2 G. A. Sherwood, Jr. and D. C. Johnson, Anal. Chim. Acta, 129 (1981) 87.
3 J. Langler, Research Laboratories, Morton Salt Co., Woodstock, IL, June 1978.
4 J. Yamada and H. Matsuda, J. Electroanal. Chem. Interfacial Electrochem., 44 (1973) 189.
5 B. Fleet and C. F. Little, J. Chromatogr. Sci., 12 (1974) 747.
6 J. Lown, R. Koile and D. C. Johnson, Anal. Chim. Acta, 116 (1980) 33.
7 D. C. Johnson and J. H. Larochelle, Talanta, 20 (1973) 959.
8 R. E. Crowe (Ed.), Methods for Chemical Analysis of Water and Wastes, Environ. Prot. Technol. Ser., Washington, DC, 1974, p. 201.
9 D. C. Johnson, J. Electrochem. Soc., 119 (1972) 331.
10 H. P. Gregor, J. Belle and R. A. Marcus, J. Am. Chem. Soc., 77 (1955) 2713.

Analytica Chimica Acta, 129 (1981) 113—124
Elsevier Scientific Publishing Company, Amsterdam — Printed in The Netherlands

CONSTANT-CURRENT COULOMETRIC DETERMINATION OF URANIUM IN THE PURE METAL

E. MERCINY, G. PATTYN-FAUVILLE, L. SWENNEN and G. DUYCKAERTS*

Laboratories of Analytical Chemistry and Radiochemistry, University of Liège, Sart Tilman, B-4000 Liège (Belgium)

(Received 23rd March 1981)

SUMMARY

A new method is proposed for the highly precise and accurate constant-current coulometry of uranium in high-purity uranium. Precisely weighed amounts of uranium and pure iron are dissolved in 7 M sulfuric acid containing some hydrogen peroxide (40% v/v). The solution is quantitatively transferred to the coulometric cell by rinsing with 1 M H_2SO_4 saturated with cerium(III) sulfate. The first step is the quantitative electrochemical reduction to U(IV), Fe(II) and Ce(III) on a gold gauze electrode at constant current (100 mA) until evolution of hydrogen is observed. The hydrogen is then removed by flushing the solution with very pure nitrogen until the potential of a platinum gauze electrode reaches a constant value. Oxidation on the gold gauze electrode is carried out under precisely controlled constant current; after the quantitative oxidation of U(IV) to U(VI) and Fe(II) to Fe(III), and crossing the end-point, this end-point is determined very precisely potentiometrically through back-titration by successive current injections of 10 mA during 1 s. The method was tested on a NBS reference material, uranium (NBS 960).

The accurate and precise determination of uranium and plutonium in fuel elements or in a reprocessing plant is becoming an increasingly important problem owing to the expanding number of nuclear reactors: commercial transactions as well as internal accounting of a factory under the safeguards of the IAEA or of the European Communities require numerous uranium and plutonium determinations of extremely high precision and accuracy [1—4]. Therefore, it is compulsory to have at hand reference materials in order to standardize the various analytical methods.

Various methods have been proposed for determinations of uranium with a high degree of accuracy and precision: potentiometric titration [5—7], possibly with the gravimetric determination of the titrant added [8], complexiметric titration with photometric end-point detection [9, 10], polarography, and controlled-potential [11—18] or constant-current [19—27] coulometric titration, the reagent being electrogenerated within the electrolysis cell.

In the work outlined below, a modified chemical system different from those described in the literature [28—30] was investigated for the controlled-current coulometry of uranium using potentiometric end-point detection.

0003—2670/81/0000—0000/$02.50

This paper describes the basic chemical system as well as the instrument used; the validity of the procedure was tested on the NBS 960 uranium reference material.

Principle of the chemical system

In principle, uranium can be determined coulometrically either by oxidizing U(IV) to U(VI) or reducing U(VI) to U(IV). However, working at constant current requires the addition of an excess of a suitable reductant or oxidant for electrogeneration of the reactant which will oxidize the U(IV) or reduce the U(VI) quantitatively.

Table 1 gives the conditional standard potentials of various half-cells in aqueous sulfuric acid solution. Among the ions used for the coulometric reduction of U(VI), only the Ti(IV)/Ti(III) couple has given satisfactory results [19—21]; with V(III)/V(II), Eu(III)/Eu(II) or Cr(III)/Cr(II) errors arise from the reduction of protons despite some overvoltage on certain cathodes [31]. However, the U(VI)/U(IV) redox system is not completely reversible and measurement of the potential in the vicinity of the equivalence point is rather difficult; in order to overcome this difficulty, it has been suggested that titrations be done at 85°C. However, although the kinetics are then more favourable, the drawback remains that the precision in the determination of the equivalence point is rather low partly because of the relatively small difference between the standard potentials and partly because of the asymmetry of the potentiometric curve on both sides of the equivalence point.

For the coulometric oxidation of U(IV) to U(VI), the Ce(IV)/Ce(III) redox couple seems particularly promising because the difference between the standard potentials is very large; unfortunately, the oxidation of U(IV) by electrogenerated cerium(IV) is very slow at room temperature. The use of Fe(II)/Fe(III) is no more satisfactory because the difference between the standard potentials is again too small and the titration curve is asymmetric although the oxidation of U(IV) by iron(III) is very rapid.

TABLE 1

Conditional standard potentials of some half-cells in aqueous sulfuric acid solutions

Half-cell	Reduction potential (V)	Solution	Half-cell	Reduction potential (V)	Solution
Ce(IV)/Ce(III)	1.45	0.5 M H_2SO_4	H^+/H_2	0.0	
O_2/H_2O	1.229		V(III)/V(II)	−0.255	
Br_2/Br^-	1.087		Cr(III)/Cr(II)	−0.41	
Fe(III)/Fe(II)	0.67	0.5 M H_2SO_4	Eu(III)/Eu(II)	−0.43	
U(VI)/U(IV)	0.407	1 M H_2SO_4	U(IV)/U(III)	−1.06	1 M H_2SO_4
Ti(IV)/Ti(III)	0.06				

Goode et al. [25] described a procedure in which, after the chemical reduction of uranium to U(IV) by titanium(III) in nitric acid solution containing sulfamate and the addition of an excess of iron(III), the end-point corresponds to the titration of the equivalent amount of iron(II) formed with electrogenerated cerium(IV).

In the proposed procedure, a very precise known quantity of metallic iron is added to the uranium to be dissolved and, after dissolution, an excess of cerium(III) is added. After a preliminary complete electrolytic reduction to U(IV), Fe(II) and Ce(III), coulometric oxidation at a gold anode gives a two-step potentiometric titration curve: the first step corresponds to the rapid oxidation of U(IV) by electrogenerated iron(III) and the second to the oxidation of iron(II) by electrogenerated cerium(IV). The second step consists of a rapid and quantitative reaction with a symmetric potentiometric curve at both sides of the equivalence point and with a sharp end-point owing to the large difference between the standard potentials [25]. Of course, this determination of the uranium content requires a very accurate knowledge of the quantity of iron introduced into the cell; therefore, a preliminary determination of the content of the pure iron sample used is carried out by the same coulometric titration. Although the iron addition could seem to be a disadvantage of the proposed method, it appeared that its presence was favourable for the uranium dissolution which proceeds more rapidly and without any hydrogen evolution.

EXPERIMENTAL

The electronic circuits (Fig. 1)

The constant-current coulometer requires a very stable constant-current d.c. generator, a very accurate and precise timer, and a very precise potentiometric circuit for the end-point detection.

D.c. generator. Two generators are provided in the experimental set-up: the first one is relatively powerful but not very precise and can generate currents of 20, 30, 50, 70 and 100 mA; it is used for the reduction step prior to the coulometric titration (step 1). In order to avoid heating of the electronic circuit, the principle of time-proportional commutation is adopted.

The second, much more stable, gives a very precise current of the order of 20 mA or 10 mA for the back-titration; it is used during the coulometric titration (step 2): the current flows through a stable resistance consisting of a metallic film; the potential drop is compared with a reference (Zener diode at stabilized current). Although this generator delivers a very stable current, its exact magnitude is determined with a precision of 10 nA every 1000 s by means of a digital voltmeter (Solartron 7075) measuring the voltage developed across a calibrated 100-ohm resistance (Cambridge); the results are automatically recorded on a printer.

All the electric and measuring devices are placed in a thermostatted box 25.0(±0.1)°C whereas the calibrated Cambridge resistance and a Weston

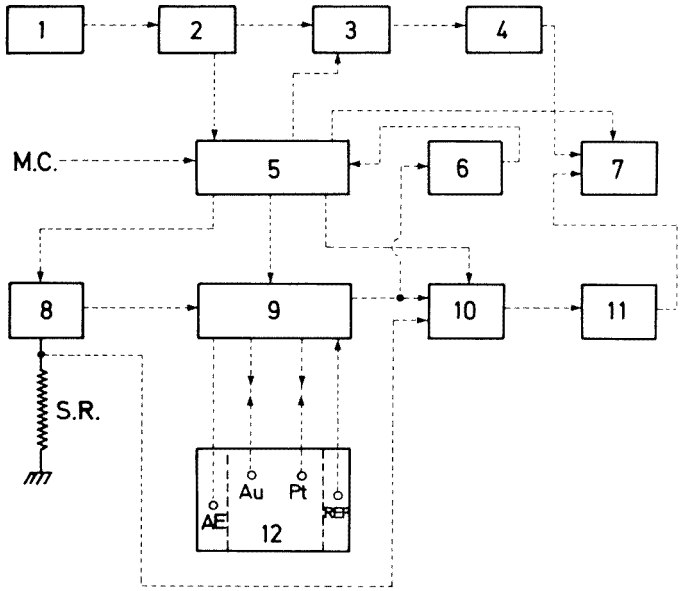

Fig. 1. Block diagram for coulometry at constant current. (1) Droitwich receiver; (2) timer; (3) switch; (4) counter; (5) programmer; (6) electrometer; (7) printer; (8) current generator; (9, 10) switches; (11) digital voltmeter; (12) titration cell; (S.R.) standard Cambridge resistance; (A.E.) auxiliary electrode; (Au) gold gauze electrode; (Pt) platinum gauze electrode; (M.C.) manual command; (REF) reference electrode.

Standard Cell (Cambridge) used for the voltmeter calibration are thermostatted at 20.40(±0.01)°C. At this temperature, the calibrated Cambridge resistance is exactly (100.0000 ± 0.0001) ohms.

In order to estimate the maximum error introduced in the determination of the electrolysis current, it must be considered (see Fig. 2) that the controlled current exhibits maximum fluctuations of 0.1 μA as well as a small drift during the oxidation period. Considering these facts, the overall error in determining the mean current value does not exceed 0.0005%.

Timer. The total time necessary for the coulometric titration at constant current is measured with a quartz crystal oscillator which can be adjusted very precisely by comparison with the Standard Droitwich broadcast frequency (200 ± 10^{-10}) kHz. The error introduced in the measurement of time is very small and negligible.

Potential measurement with the indicator electrode. The potentiometric device consists of a platinum gauze indicator electrode connected to a reference Ag/Ag_2SO_4 sat., 2 M H_2SO_4 electrode.

During the coulometric titration (oxidation of U(IV) and Fe(II)), the digital voltmeter is permanently connected to the calibrated resistance and the electrolysis current is thus measured periodically. The time necessary to approach the end-point very closely is evaluated, and then the voltmeter

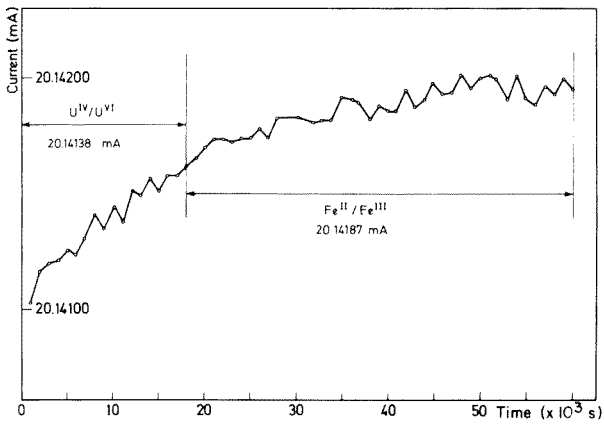

Fig. 2. Variation of the controlled-current electrolysis during the coulometric oxidation: the current is obtained through the measurement of the voltage across a Cambridge 100.000-ohm standard resistance with a digital voltmeter (Solartron).

is automatically disconnected and used for the measurement of the platinum gauze potential (step 3). During step 3, the titration is continued by injecting the same constant current (around 20 mA) during 100 s; the time between two injections can be adjusted between 1 and 15 min, depending on the reaction rate in the vicinity of the equivalence point. As soon as the titration is approximately 0.03% beyond the end-point, an analogous electrometer connected in parallel with the digital voltmeter, according to the given program, puts an end to this third step.

The fourth and last step, i.e. precise detection of the back-titration equivalence point, is carried out by reversing the flow of current through the cell. Injections of 10 mA during 1 s are made while the digital voltmeter measures and records the equilibrium potential after each injection; all the operations, i.e. commutation, current inversion, transition from one step to another, are controlled by an electronic programmer.

The cell assembly

The coulometric cell consists of three compartments: the titration cell, the reference electrode and the auxiliary electrode; all three compartments have double walls to permit thermostatting (Fig. 3).

The titration cell. The 160-ml pyrex glass cylindrical cell (23 cm^2 area, 7 cm high) is fitted with a plane teflon cap drilled to accommodate the platinum and the gold electrodes (gauzes, 50 × 60 mm), the pyrex tube ended with a sintered glass (porosity G3) for entry of nitrogen gas, and a small condenser for collection of the aerosols in the bubbling gas outlet. Finally, the platinum sheet auxiliary electrode (40 × 20 mm) is connected to the titration cell by means of wide tubing with a conical B14 joint. The cell can be heated by means of a resistance wire coil wound around the external surface. the Wilhelm electrolytic bridge sealed in the walls is connected to the reference electrode compartment.

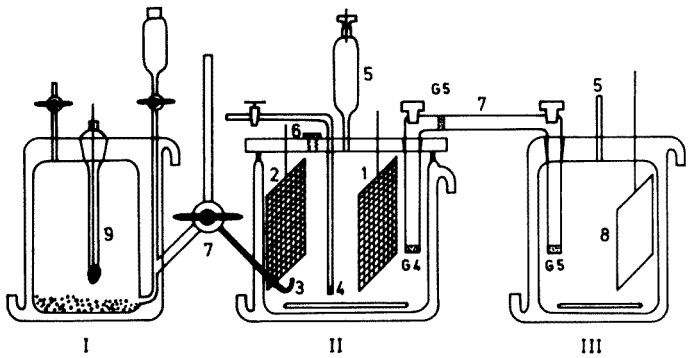

Fig. 3. Three-compartment coulometric cell: (I) reference electrode compartment; (II) coulometric cell; (III) auxiliary electrode compartment. (1) Platinum gauze electrode; (2) gold gauze working electrode; (3) "Luggin" capillary for the Wilhelm salt bridge; (4) nitrogen gas bubbling inlet through sintered glass disk; (5) condenser funnel for gas outlet; (6) valve; (7) inlets for electrolytic salt bridge between titration cell and the auxiliary electrode compartment; (8) platinum foil auxiliary electrode; (9) Ag/Ag_2SO_4 reference electrode.

The platinum auxiliary electrode. The platinum foil auxiliary electrode dips into a 2 M sulfuric acid solution contained in the double-walled flask covered with a cap having a hole for the evolution of hydrogen or oxygen produced by electrolysis and a conical hole for the introduction of the electrolytic bridge. This bridge (a U-tube, 12-mm i.d.) is filled with 2 M H_2SO_4 and is closed by sintered glass disks (G4 and G5); another sintered glass disk (G5) is inserted in the tube (see Fig. 3). The two G5 disks are specially treated by internal SiO_2 precipitation in order to reduce their porosity and thus the flow of solutions between the two compartments.

The reference electrode. The reference electrode consists of a platinum wire covered with a film of silver, obtained by thermal decomposition of silver oxide, and then coated with silver sulfate by electrolytic oxidation for 60 min at 20 mA in a solution of 2 M H_2SO_4 saturated with silver sulfate. The wire dips into a 2 M H_2SO_4 solution saturated with silver sulfate. The reference electrode is connected to the coulometric cell through a capillary bridge filled with 2 M H_2SO_4 and having in the middle a three-way teflon stopcock (Fig. 2). Owing to the high conductivity of sulfuric acid solutions, it is possible to measure the potential during the titration with the stopcock closed; this reduces considerably the leakage from one compartment to another. The solutions in the titration cell and in the auxiliary cell are homogenized by magnetic stirring.

The three compartments are maintained at a constant temperature (20.40 ± 0.01)°C by means of a Haake F3 thermostat. The whole titration equipment is located in a black box in order to prevent photochemical reactions, whether reduction of iron(III) [32] or oxidation of U(IV) [16, 33].

Flushing gas. The titration cell is continuously deaerated by bubbling pure nitrogen: after the reduction step, this removes the hydrogen produced; during the titration, it prevents any oxygen inlet.

The A28 quality nitrogen is carefully purified, first by sending it through a BASF copper catalytic bed at 150°C and then through five bubblers containing, respectively, saturated sodium sulfite solution at pH 14, 1 M NaOH, vanadium(III) solution with zinc amalgam, deionized water, and finally 2 M H_2SO_4.

Reagents. Sulfuric acid and hydrogen peroxide were of analytical grade (Merck). Cerium(III) sulfate (Merck p.a.) was purified by slow crystallization at 80°C.

Deionized water was prepared with a Millipore apparatus (Milli-Q); its resistivity was of the order of 18 Mohm. Organic constituents were removed with a charcoal filter and any dust on a cellulose filter having 0.22-μm pores.

Investigation of the method

In order to test the validity of the method, pure iron (Johnson—Matthey Specpur quality) and NBS metallic uranium reference material were used. The cylindrical iron rod (5-mm diameter, 150 mm long) was cut into small slices (2.5 mm thick) on a small lathe, under an argon atmosphere. The uranium was sliced into pieces of 0.5 g on the same lathe in a box flushed with pure argon.

Weighing of samples. All weighings of iron and uranium samples after cleaning according to NBS recommendations [34] were done with a Sartorius Electrono balance, allowing a maximum load of 1 g with a sensitivity of 1 μg. The samples are weighed by the substitution method using weights (P. Bunge, Hamburg) calibrated against certified standards by the Central Bureau of Nuclear Measurements (BCMN). The uncertainty of the weights used was ± 1 μg.

As five weights were used for each sample weighing approximately 500 mg, a maximum error of 0.002% is estimated for the two samples of iron and uranium. Furthermore, the reproducibility of the balance is of the order of 3 μg for the samples and the weights, which means an uncertainty of 0.0024% for a sample of 500 mg. The weights were corrected for air buoyancy.

Dissolution of the samples. The proposed method consisting of electrochemical reduction followed by coulometric oxidation at constant current cannot be used in the presence of chloride and nitrate ions; therefore, it is necessary to dissolve the samples in sulfuric acid.

After being cleaned and weighed, the samples of iron and uranium are introduced in the reactor (Fig. 4) containing 15—20 ml of 7 M H_2SO_4 with 6—10 ml of perhydrol. The iron dissolves at room temperature and dissolution is complete after 2—3 h. The reactor is then slowly heated around 90°C. Dissolution of uranium takes place relatively slowly (around 24 h) but without any gas evolution and at temperatures below the boiling point of the solution. This is very important, because it reduces the risk of loss through aerosols or spurting. The absence of any gas evolution and the change of color from brown to green seem to indicate that the dissolution of uranium takes place through iron(III); therefore, it is necessary, from time to time, to add a few drops of hydrogen peroxide to oxidize iron(II) in order to complete the dissolution of uranium.

Once the dissolution is complete, the side-tube of the reactor is bent, the tip is cut off, the solution is transferred quantitatively in the coulometric cell, and the reactor is rinsed carefully with 1 M H_2SO_4 saturated with cerium(III) sulfate (ca. 100 ml). These operating conditions give a 2 M H_2SO_4 solution in the coulometric cell, which means that the three compartments contain the same acid concentration, thus reducing diffusion through the bridges.

During the coulometric oxidation of U(IV) and Fe(II), hydrogen ions and cerium(III) are mainly responsible for current transport through the electrolytic bridge, reducing that of the two electroactive ions. Nevertheless, at the end of the titration step, the solution in that part of the electrolytic bridge dipping in the cell and connecting it with the auxiliary electrode, is forced through the sintered G4 disk in the sample solution by applying a small nitrogen pressure on the top.

Reduction prior to titration. The first step after transfer to the titration cell is the quantitative electrolytic reduction to U(IV), Fe(II) and Ce(III). This reduction is carried out at the gold electrode at a constant current of 100 mA. Quantitative reduction of cerium and iron causes no problem. The reduction of U(VI) to U(IV) on a platinum electrode is not quantitative because of reduction of protons. Davies et al. [18] mention that this does not happen on a specially treated gold electrode. After some time, the gold surface becomes poisoned which means a progressive increase in the time for the uranium reduction and finally incomplete reduction, which can introduce an error of the order of 0.1% in the uranium content. Treatment of the gold electrode for a few minutes in diluted aqua regia was found to restore the electrode and permit rapid quantitative reduction of uranium.

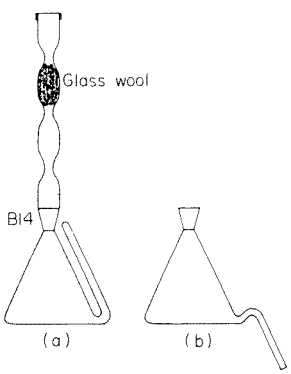

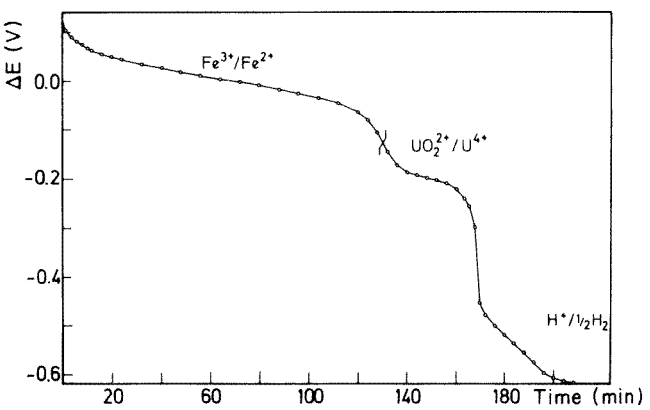

Fig. 4. Reactor for the dissolution of uranium and iron: (a) dissolution; (b) transfer of the solution to the titration cell. The flask has a capacity of 50 ml.

Fig. 5. Potentiometric curve during the reduction of iron and uranium at the gold electrode. Potentials are measured with the platinum gauze electrode with respect to the Ag/Ag_2SO_4 reference electrode.

After the completion of the uranium reaction, proton reduction is indicated by a drop of the potential to a value near —0.68 V versus the Ag/Ag_2SO_4 reference electrode (Fig. 5). The two electrolyte bridges and the gas outlet column are rinsed with 2 M H_2SO_4, and the reduction step is then continued at 100 mA for a further hour. The hydrogen produced by reduction is removed by nitrogen flushing until the potential of the platinum gauze electrode reaches a constant value (Fig. 6).

Coulometric titration through oxidation. The coulometric oxidation of U(IV) and Fe(II) is carried out at a constant current of the order of 20 mA at the gold electrode; the current is determined very accurately at intervals of 1000 s by measuring the voltage developed across the standard 100-ohm resistance using the digital voltmeter accurate to 1 μV. Figure 2 gives the measured current intensities during an experiment, showing a maximum drift of the order of 0.005%.

Knowing the weights of the iron and uranium samples and the value of the controlled-current intensity, and assuming pure metals, it is possible to preset the time for constant-current titration. In these experiments, the calculated value is of the order of 60000 s; the oxidation is continued for another 15—20 s after this point.

Provision is made within the instrument to terminate the titration automatically when the preset time has been reached; then the excess can be back-titrated by reversing the flow of current through the cell. After a waiting time of 15 min, the reduction of cerium(IV) formed is started by successive injections of 10.580 mA for 1 s, the time elapsed between two injections being 5 min. The 15-min wait between the end of the oxidation step and the beginning of the back-titration through reduction is used for rinsing the Wilhelm bridge, the electrolytic bridge and the gas outlet funnel.

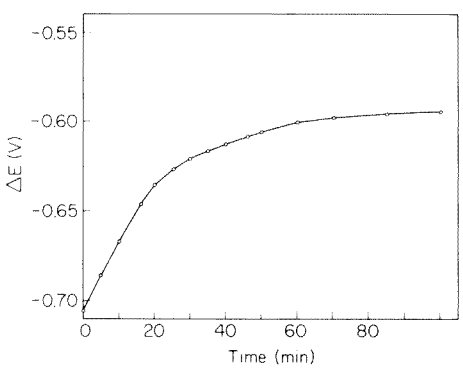

Fig. 6. Variation of the platinum gauze electrode potential on bubbling pure nitrogen during the removal of the hydrogen generated at the end of the reduction step.

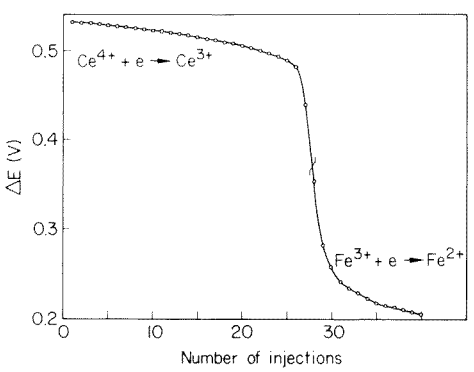

Fig. 7. Potentiometric curve corresponding to the back-titration against the number of current injections of 10.580 mA for 1 s.

The potential of the platinum indicator electrode is measured during the back-titration step after each injection. Figure 7 gives the titration curve around the end-point drawn from the recorded values. The end-point corresponds to a time of back-titration of 27.8 s at 10.580 mA, giving 0.2941 coulombs. The uncertainty of detection of the end-point, as shown in Fig. 7, does not exceed 0.2 s for a 10.580-mA current or 0.1 s for a 20.142-mA current. The titration time for uranium is approximately 18000 s, and so the error introduced is of the order of 0.005%.

The iron supplied by Johnson—Matthey was analyzed with the same apparatus. The results from 15 experiments gave an assay value of 99.992% which is accurate to within 0.001%; the oxidation required 40000 s with an error of 0.001%. As the time required for uranium is about 18000 s, this introduces a maximum error of the order of 0.003%. This error could be reduced by using a smaller amount of iron.

RESULTS AND DISCUSSION

Table 2 gives the details of a uranium assay. The reproducibility of the method was evaluated by repeating the procedure for 13 samples from NBS 960 reference material. The mean value found was 99.978% (range, 99.965—

TABLE 2

Details for a uranium assay

Constants used	
Atomic weight of iron	55.847
Atomic weight of uranium	238.029
Specific gravity of iron	7.86 g cm^{-3}
Specific gravity of uranium	19.05 g cm^{-3}
Specific gravity of weights	2.746 g cm^{-3}
Value of the Faraday	96486.7 C [34]
Assay of iron	(99.992 ± 0.001)% at 95% confidence interval
Analytical results	
Apparent weight of iron	498.875 mg
Apparent weight of uranium	439.837 mg
True (vacuum) weight of iron	498.739 mg
True (vacuum) weight of uranium	439.679 mg
Duration of oxidation	60485.00 s
Mean current during U(IV) oxidation	20.1413 mA
Mean current during Fe(II) oxidation	20.1418 mA
Calculated time for the oxidation of iron	42776.8 s
Back-titration	27.8 s at 10.580 mA equivalent to 14.6 s at 20.142 mA
Time for the oxidation of uranium	60485.0 − 42776.8 − 14.6 = 17693.6 s

$$\text{Uranium content: } \frac{20.1413 \times 17693.6 \times 238.029 \times 100}{96486.7 \times 2 \times 1000 \times 0.439679} = 99.977\%$$

99.988%) the standard deviation (s) was 0.006, and the standard deviation for the mean value was 0.0015. The NBS reference material contains 42 ppm of iron and 4 ppm of vanadium which corresponds in the titration to 99 ppm of uranium. The corrected uranium content is then: (99.968 ± 0.003)% at the 95% confidence level.

The certified value given by NBS is (99.975 ± 0.017)%; 0.017 is the uncertainty ascribed to the certified assay value for a single determination at the 95% confidence level.

It should be borne in mind that the background current should be sufficiently small in order to ensure 100% current efficiency; the delicate point occurs in the vicinity of the end-point of the iron oxidation, but it has been shown that the efficiency equals 100% for the oxidation of cerium(III) on a gold electrode [25].

Leaks in the electrical circuit must be avoided; therefore, the external part of the electrolytic bridge is insulated with PVC, rinsed and dried before each experiment.

It has already been mentioned that, in order to ensure quantitative transformation of uranium to the tetravalent state in the reduction step, the gold electrode should be adequately regenerated. A poisoned electrode gives incomplete reduction of the uranium, and this is reflected in a rapid increase of the potential of the platinum electrode during the nitrogen flushing; the value tends towards —0.4 V.

Finally, it is important to see if the precisions of the two methods are essentially the same and to establish whether or not the random deviations in the determination of total uranium by the two methods are such that they may account for the difference between the means.

The "F test" gives $F = s_1^2/s_2^2 = (0.008/0.006)^2 = 1.8$; the value from the table for 20 and 12 degrees of freedom, respectively, at the 95% confidence interval is 2.54, which indicates that there is no statistical difference between the standard deviations. The precision of the two methods being the same, the existence of a significant difference between the two means can be tested by using "t test": $t = (\bar{X}_A - \bar{X}_B)/s_{\bar{X}}$. The means of the methods ($\bar{X}_A$, $\bar{X}_B$) are 99.975 and 99.968. Now

$$s_{\bar{X}} = s\,(N_A^{-1} + N_B^{-1})^{1/2} \text{ and } s = [\sum(X_A - \bar{X}_A)^2 + \sum(X_B - \bar{X}_B)^2]/(N_A + N_B - 2)$$

The numbers of measurements (N_A, N_B) were 13 and 21, respectively, and so $t = 2.7$. In the Tables, $t = 2.8$ for a probability of 99%.

It can be concluded that the difference between the means of the results obtained by the two methods is not greater than that attributable to chance at the 99% confidence level.

The authors are very grateful to the Institut Interuniversitaire des Sciences Nucléaires for financial support and to Drs. Esbach and Le Duigou of the Central Bureau of Nuclear Measurements (BCMN) at Geel for their help, particularly with the calibration of the weights.

REFERENCES

1 Bulletin de l'AIEA, April (1978) 46.
2 Analytical Methods in the Nuclear Fuel Cycle, Proceedings series STI/PUB/291, Panel Proceedings series STI/PUB/337, IAEA, Vienna.
3 CE, CBNM, Fissile Reference Materials Z > 89. Needs in the European Communities, As-14, 1977.
4 CE, CBNM, Catalogue of fissile reference materials and other fissile materials available in the European Communities, As-13, 1977.
5 T. W. Steele, Analyst, 85 (1960) 55.
6 J. Malinowski, Talanta, 14 (1967) 263.
7 L. Pszonicki, Talanta, 13 (1966) 403.
8 T. Tamberg, Fresenius Z. Anal. Chem., 291 (1978) 214.
9 E. Lassner and R. Scharf, Fresenius Z. Anal. Chem., 164 (1958) 398.
10 Y. Le Duigou and A. Brück, Anal. Chim. Acta, 31 (1964) 394.
11 M. T. Kelley, H. C. Jones and D. J. Fisher, J. Anal. Chem., 31 (1959) 488, 956.
12 ORNL, Ionic and Process Methods 1003029-9003029 TID 7015.
13 W. D. Shults, ORNL Methods N 1219225 and 900719225 TID 7015.
14 I. J. McColm, V. M. Sinclair and R. S. Roche, Talanta, 10 (1963) 387.
15 P. Zanello, G. Raspi and A. Cinquantini, Talanta, 23 (1976) 103.
16 Y. Le Duigou, W. Leidert, Fresenius Z. Anal. Chem., 289 (1978) 279.
17 American National Standard N106, 1973.
18 W. Davies, W. Gray and K. C. McLeod, Talanta, 17 (1970) 937.
19 J. K. Taylor and S. W. Smith, Science, 124 (1956) 940.
20 J. B. Fardon and I. R. Gowan, Talanta, 19 (1972) 1312.
21 J. H. Kennedy and J. J. Lingane, Anal. Chim. Acta, 18 (1958) 240.
22 J. J. Lingane and R. T. Iwamoto, Anal. Chim. Acta, 13 (1955) 465.
23 G. Marinenko and J. K. Taylor, Round Table, Euratom Bruxelles, 42 J (1965) 141.
24 N. F. Furman, C. E. Bricker and R. V. Dilts, Anal. Chem., 25 (1953) 483.
25 G. C. Goode, J. Herrington and W. T. Jones, Anal. Chim. Acta, 37 (1967) 445.
26 W. W. Carson, Anal. Chem., 25 (1953) 466.
27 T. Tanaka, T. Yoshimori and B. Kagaku, Jpn. Analyst, 24 (1975) 614.
28 H. Sorantin, Determination of Uranium and Plutonium in Nuclear Fuels, Verlag Chemie, Weinheim, 1975, pp. 117—121.
29 F. A. Cooper and J. C. Quayle, Analyst, 91 (1966) 363.
30 G. Marinenko and J. K. Taylor, J. Res. NBS, 67 (1963) 31, 453.
31 C. A. Degueldre, PhD Thesis, Université de Liège, 1978.
32 R. Collienne, PhD Thesis, Université de Liège, 1978.
33 Y. Le Duigou and W. Leidert, Fresenius Z. Anal. Chem., 278 (1976) 29.
34 W. F. Koch, W. C. Hayle and H. Diehl, Talanta, 22 (1975) 717.

Analytica Chimica Acta, 129 (1981) 125—132
Elsevier Scientific Publishing Company, Amsterdam — Printed in The Netherlands

A DIGITAL INTEGRATOR FOR CONTROLLED-POTENTIAL COULOMETRY

THOMAS L. FRAZZINI*, MICHAEL K. HOLLAND, JON R. WEISS and CHARLES E. PIETRI

New Brunswick Laboratory, U.S. Department of Energy, 9800 South Cass Avenue, Argonne, IL 60439 (U.S.A.)

(Received 12th December 1980)

SUMMARY

Accurate electrolysis current integration is required in controlled-potential coulometry. Analog integrators have been shown to deviate from ideal response by as much as —0.1%. A digital integrator was designed to optimize the linearity of the voltage-to-frequency converter used, minimize the effects of temperature, eliminate integration errors caused by small polarity changes and signal noise, and allow interchangeability with an analog integrator in a state-of-the-art coulometer widely used throughout the nuclear field for controlled-potential coulometry. Evaluation of the digital integrator, calibrated versus the Faraday, showed bias-free determinations of plutonium with a relative standard deviation of approximately 0.02%. The integrator was designed specifically for use in the controlled-potential coulometric determination of plutonium, but many of the features incorporated can be adopted to digital integrators for other uses where accurate integration over long periods of time is required.

Accurate electrolysis current integration is required in controlled-potential coulometric determinations. Commercially-available coulometers, which use analog integrators, accumulate a charge on the integrating capacitor that is proportional to the quantity of material electrolyzed. This type of integrator deviates inherently from the ideal response by as much as —0.1% because of its inability to retain the accumulated charge quantitatively. While the causes of this non-ideal response (integrating capacitor leakage and dielectric absorption) have been quantified, and mathematical corrections and procedural modifications have been developed to reduce the systematic errors [1], a simpler solution is the use of a digital integrator. A digital integrator, consisting of a voltage-to-frequency converter to generate pulses (the sum of which is proportional to the quantity of material electrolyzed), a counter to accumulate these pulses (minimizing integrating capacitor losses), and a display which allows the value in the counter to be read, does not suffer from deviations associated with analog integrators [2]. Although digital integrators have been incorporated in commercially-available coulometers, manufacturers' specifications indicate that the accuracy of such instruments is not better than the accuracy obtained with analog integrators. A more accurate digital integrator is highly desirable.

The digital integrator [3] described here has performance characteristics that far exceed those of commercially-available integrators, both digital and analog. This digital integrator has been designed specifically for the controlled-potential coulometric determination of plutonium [4]. However, many of the techniques used in the design of this integrator can be adapted to digital integrators for other uses where accurate integration over long periods of time is required. The digital integrator was designed to obtain optimum linearity from the voltage-to-frequency converters used, to minimize the effects of temperature, to eliminate integration errors caused by changes in polarity or signal noise, and to allow interchangeability with the analog integrator used in a coulometer widely applied throughout the nuclear field for controlled-potential coulometry.

DESIGN OF THE DIGITAL INTEGRATOR

A block diagram of the digital integrator is shown in Fig. 1. The unit consists of two voltage/frequency converters with associated trim potentiometers, a 1000-Hz crystal oscillator (clock), three binary-coded decimal (BCD) counters with associated displays, a comparator circuit, a voltage reference, a power supply, and miscellaneous switches and input/output connections.

The digital integrator was designed for direct replacement of the analog integrator of a controlled-potential coulometer, the MT Model 3 instrument [5], without requiring modifications to the existing potentiostat. In order to accomplish this design, the output signal characteristics of the potentiostat were examined. The potentiostat outputs a voltage signal proportional to the current flowing through the cell during sample electrolysis. The integral of this signal over time is proportional to the quantity of material electrolyzed.

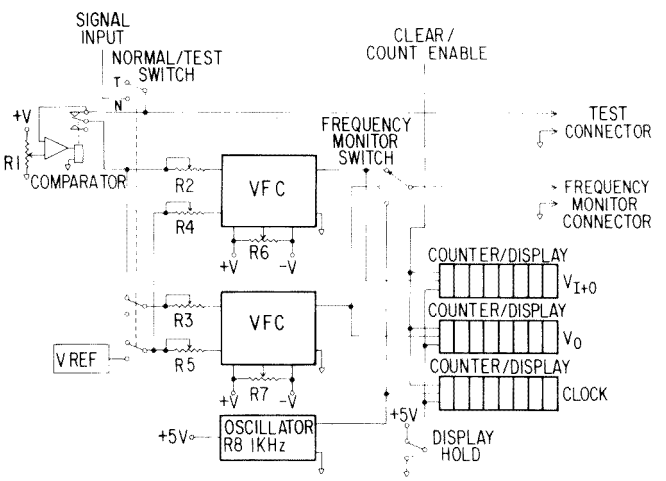

Fig. 1. Block diagram of the digital integrator. V REF is used for generating the current offset signal.

This signal is positive during sample reduction and negative during sample oxidation except for momentary reversals caused by signal noise, the sample composition, the electrolyte used, or the method of sample processing. The maximum signal output of the potentiostat during electrolysis of 6—10-mg plutonium samples is ±3.25 V (120 mA initial current through a 27-ohm load resistor). The reverse polarity excursions vary with experimental parameters. In most plutonium coulometric procedures, oxidation is the quantitative electrolytic process and current integration is not required during prereduction of the sample. During oxidation, the signal to be integrated ranges from —3.25 V to the maximum positive voltage excursion as discussed in the Performance Testing section. Since voltage/frequency converters accept signals of only one polarity, the change in polarity can be accommodated either by using sensing and logic circuits that invert signals of unacceptable polarity while reversing the direction of an up/down counter, or by applying an offset to the input signal in such a way that the resulting signal integrated by the voltage/frequency converter does not change polarity. The first method, while affording greater flexibility, requires sophisticated circuitry which increases the complexity of the digital integrator while introducing inaccuracies caused by the amplifiers used to sense and invert the signal when required. The second method requires a means of subtracting the counts arising from the offset from the total integration count so as to obtain a net value of current integration. Since a second voltage/frequency converter (which receives only the offset signal) can be used to measure accurately the counts from the offset, the second method was chosen. This selection was made because accuracy and precision were of prime concern, while extensive flexibility was not required.

The voltage/frequency converter was selected carefully for its maximum output frequency, linearity, stability, and the capability to accept a negative input signal. The Model 458L voltage/frequency converter (Analog Devices, P.O. Box 280, Norwood, MA) fits these requirements exceedingly well with its 100-kHz maximum output frequency (for a 10-V input signal) and ±0.01% nonlinearity. This converter has excellent stability and can be wired to accept either positive or negative input voltages and a positive input current as well. The current input capability was used to offset the input voltage signal without the use of an external amplifier. This feature increased the overall performance of the digital integrator because the offset and drift problems associated with amplifiers were eliminated.

The digital integrator has an adjustable offset current input which allows the normally negative voltage input to become positive. By simply increasing the current input, the voltage/frequency converter could be made to accommodate a signal up to ±5 V without additional circuitry. It must be remembered, however, that the larger the offset, the more effect changes in the offset will have on the accuracy and precision of the integration of the actual input signal. With a very large offset and very small electrolysis currents, inaccuracies in the measurement of the offset can produce significant errors

in integration. The effect of changes in the offset current was reduced by keeping the offset current as small as practical and by adding a second converter to receive only the offset current. By reducing the size of the offset current to a level which just compensates for the maximum positive excursions, a large error in the offset current results in only a small error in the overall accuracy of the integrator. The second converter integrates only the offset current signal and also compensates for variations in temperature and power supply output.

If both voltage/frequency converters were to output exactly the same frequency for the same current input, the integrated input signal value (V_i) would be equal to the counter readout value for the voltage/frequency converter that receives both the input signal and the offset current (V_{i+o}) minus the counter readout values for the converter that receives only the offset current, V_o. In practice, the two converters do not output exactly the same frequency for the same input. However, with a zero voltage input signal, V_{i+o}/V_o is the offset ratio, K_o. Thus, the offset count of both converters can change with current offset changes, but the ratio will remain substantially unchanged. The integral of the input signal is calculated as

$$V_i = V_{i+o} - K_o V_o \tag{1}$$

Further refinements of this equation and the offset ratio, K_o, are discussed in the Performance Testing section.

A clock circuit was also added to the digital integrator to facilitate the calibration of the coulometer as a system. A precision 1000-Hz crystal oscillator with an associated counter is used as a clock with a 0.001-s output.

The digital integrator also has three other features which, although they do not increase performance, protect the converters and facilitate alignment and maintenance; these features are a comparator circuit with a relay and two switches ("frequency monitor" switch and "normal/test" switch) with associated connectors. The comparator circuit is biased to activate the relay if the input signal approaches a level more positive than is compensated by the offset current. The input signal passes through the normally closed contacts of the relay before being fed to the converter. This procedure insures that the converter does not receive a positive signal greater than the offset; otherwise the converter, wired to accept a negative signal, could be damaged. The "frequency monitor" switch and connector are used to monitor the output frequency of either voltage/frequency converter or the crystal oscillator. Monitoring is done most often during alignment, although it can be done during normal operation.

In the "test" position which is used for alignment, the "normal/test" position, the switch disengages the integrator from the potentiostat, cuts out the offset current signal to the converters and ties the voltage input of each voltage/frequency converter to its associated connector. The voltage source, used in adjustments, is then connected to each converter through this connector. In the "normal" position, the signal from the potentiostat can be moni-

tored from this connector. All trim potentiometers, switches, and connectors necessary for adjustment are accessible on or through the front panel of the integrator. The digital integrator is readily incorporated into the existing coulometer (less analog integrator) through the existing wiring to the mode switch of the potentiostat which controls the "clear/count enable" function of the counters. When the potentiostat is in "standby", the counters are cleared; when in "hold" or "operate", the counters are enabled. In this way, the operation of the coulometer (as originally used with its analog integrator) is duplicated without modifications to the existing potentiostat. The front panel of the digital integrator also has a push button ("display hold") that can freeze the display while the counters continue to accumulate counts. This feature is used to allow accurate manual transcription of the data from the display.

PERFORMANCE TESTING

Instrument adjustment

The maximum positive voltage excursions during plutonium determinations were measured by monitoring the integrator input signal for both a.c. and d.c. voltage. A maximum positive voltage excursion of +75 mV was measured using the New Brunswick Laboratory controlled-potential coulometric procedure [4]. A current input of approximately 5 μA which produced 1000 counts per second and compensated for positive excursions as large as +100 mV was selected.

In preparing the digital integrator for use, the "normal/test" switch is placed in the "test" position and the initial adjustments are carried out according to the manufacturer's information sheets. This procedure minimizes the offset and full scale errors of the voltage/frequency converters by adjusting potentiometers R6 and R7 for an output frequency of 100 Hz with a 10-mV input and R2 and R3 for an output frequency of 100 kHz with a 10-V input (Fig. 1). Both converters can be adjusted concurrently since the input voltage will be fed to both of them when in the adjustment mode ("test" position). Next the "normal/test" switch is placed in the "normal" position and the potentiostat in the "standby" position, thereby insuring a zero input voltage signal to the converter. The offset current can now be adjusted using potentiometers R4 and R5 so that both converters have frequency outputs of approximately 1000 Hz. Finally, the crystal oscillator can be adjusted internally for a 1000-Hz output. The unit is now ready for calibration.

Instrument calibration

The offset ratio, K_o, is determined by first switching the potentiostat to "hold". In this mode, the counters are enabled, but the input signal is still held at zero. At the end of the desired time period, the "display hold" button on the digital integrator is pressed and the two counter/displays associated with the two voltage/frequency converters are read. The offset

ratio is calculated by dividing the value in the counter which normally receives the input voltage signal by the value in the counter which receives only the offset current. This value, K_o, is used in the calculation of both the coulometer electrical calibration factor based on the Faraday and the plutonium assay results. A 60-s time interval was found to be satisfactory for the determination of K_o.

To determine the electrical calibration factor of the coulometer, a resistor and a voltmeter are required, with the precision of the resistor and the accuracy and readability of the voltmeter significantly affecting the accuracy and precision of the calibration factor obtained. To obtain the data listed in Table 1, the coulometer was calibrated using a Julie Research 100-ohm resistor (Model NB-102A) and a Hewlett-Packard Model 3455A digital voltmeter with 6-1/2 digit readability. One side of the resistor is connected to the reference and counter electrode terminals on the potentiostat while the other side is connected to the working electrode terminal. The digital voltmeter monitors the control potential (V_c), in volts, across the resistor (R), in ohms. When the potentiostat is switched to "operate", the digital integrator receives an input voltage signal proportional to the current flowing through the resistor.

After the desired calibration interval, the "display hold" button on the digital integrator is pressed and all three counter/displays (V_{i+o}, V_o, and t) are read. The value of the integral V_i is calculated using eqn. (1). The electrical calibration factor used for plutonium, C_{Pu}, in mg Pu per count, based upon the gram equivalent weight of the plutonium being measured, is calculated from

$$C_{Pu} = V_c \times t \times (\text{g Pu eq}^{-1}) \times (1000 \text{ mg g}^{-1})/R \times V_i \times F \quad (2)$$

where t is the value in the counter associated with the crystal oscillator and F is the Faraday, 96484.56 coulombs/equivalent.

Typical data obtained during instrument calibration are shown in Table 1. These data yield C_{Pu} equal to approximately 9.1000×10^{-6} mg Pu per count for plutonium with a gram-equivalent weight of 239.08.

Although the value of K_o should be a constant, it was found actually to change slightly with time in a slow cyclic manner. Therefore, to obtain a more accurate calibration factor, it is best to determine K_o values before

TABLE 1

Typical calibration data for controlled-potential coulometer with digital integrator

Readout (V_{i+o})	Zero (V_o)	Zero factor (K_{oa})	Potential (P)	Time (t)	Calibration factor (C_{Pu})
232376	198253	0.998695	0.07008	180.171	9.09990×10^{-6}
276565	198295	0.998545	0.16012	180.170	9.09956×10^{-6}
607195	198871	0.999490	0.83021	180.667	9.09996×10^{-6}

(K_{o1}) and after (K_{o2}) the calibration data are collected, and then use the average value (K_{oa}) to calculate a corrected integrated input signal value, V'_i

$$V'_i = V_{i+o} - V_o(K_{o1} + K_{o2})/2 \quad (3)$$

$$V'_i = V_{i+o} - V_o K_{oa} \quad (4)$$

Since the value of K_o, at constant temperatures, exhibits a slight daily fluctuation, the value of the electrical calibration factor varies within 0.005% relative standard deviation (RSD). With the method of using the average value of the offset ratio, K_{oa}, and substituting V'_i for V_i in eqn. (2), calibrations with an improved precision of 0.002% RSD are routinely obtained. Variations in temperature affect the calibration factor by only 0.001%/°C.

Instrument operation

In the determination of the quantity of plutonium electrolyzed, the coulometer with digital integrator is used in a manner comparable to performing the electrical calibrations. The working, counter, and reference electrodes from the coulometry sample cell are connected to the potentiostat. The control potential dial on the potentiostat is set at a potential for plutonium reduction. The potentiostat is switched to the "operate" position and the plutonium is reduced at the desired potential. The potentiostat is then returned to the "standby" position and the control potential dial is set at a potential for plutonium oxidation. When the potentiostat is switched to the "operate" position, oxidation of the sample begins and the digital integrator receives an input voltage signal proportional to the electrolysis current flowing through the cell. At the completion of the plutonium oxidation step, the "display hold" button is pressed, and the three counter displays are read. The procedure for using the digital integrator for background current determinations (electrolysis of the supporting electrolyte only) is identical to the procedure outlined for the plutonium determinations. The integral, V'_i, in both cases is calculated using eqn. (4).

RESULTS AND DISCUSSION

Previously, the determination of 6—10 mg plutonium aliquots (prepared from NBS SRM 949e plutonium metal) using controlled-potential coulometry with an electrically calibrated analog integrator gave biased recoveries of 99.83—99.93% and a precision of 0.05—0.08% RSD [1]. Biased plutonium recovery has been customarily compensated by chemical calibration of the integrator and empirical selection of the current cut-off endpoint [6], thereby minimizing the need for ideal integrator behavior. While chemical calibration corrects for the measurement bias, the advantages of electrical calibration are lost. However, an evaluation of the digital integrator over a one-year period, using the same coulometric procedure (controlled-potential adjustment technique [4], individual blank determination, and electrical

calibration based on the Faraday), gave results superior to those obtained with an electrically calibrated analog integrator; recovery of 99.98—100.01% and precision of 0.01—0.03% RSD were obtained. All recovery values were calculated using the National Bureau of Standards certified value corrected for ^{239}Pu and ^{241}Pu decay.

The design of the digital integrator described here also incorporates features that facilitate its use in an automated system. These features, which include the "remote clear", "count enable", and "hold" functions and the multiplexed binary-coded decimal outputs of the three counters, are not required in the basic integrator design.

Although the digital integrator described here has been built for a specific application, it could be used, with minor adjustments, in other applications. For example, the offset current could be increased to allow more positive signals to be integrated as may be required in other controlled-potential coulometric plutonium methods. The load resistor could be changed to accommodate variations in electrolysis current arising from changes in sample size or cell geometry. The voltage/frequency converters could be rewired to accept positive signals with small excursions into the negative range, for applications of controlled-potential coulometry requiring integration of cathodic electrolysis currents such as in the determination of uranium. In addition, the integrator could be made to perform integration during both the reduction and oxidation cycles by the addition of a switch that changes the circuitry to allow the converters to accept either positive or negative voltage signals.

REFERENCES

1 T. L. Frazzini, M. K. Holland, J. R. Weiss and C. E. Pietri, Anal. Chem., 52 (1980) 2112.
2 J. E. Harrar, in A. J. Bard (Ed.), Electroanalytical Chemistry, M. Dekker, New York, 1975, Vol. 8, pp. 53—57.
3 T. L. Frazzini, M. K. Holland, C. E. Pietri and J. R. Weiss, U.S. Patent No. 4,244,800, January 13, 1981.
4 M. K. Holland, J. R. Weiss and C. E. Pietri, Anal. Chem., 50 (1978) 236.
5 J. E. Harrar and E. Behrin, Anal. Chem., 39 (1967) 1230.
6 1980 Annual Book of ASTM Standards, Part 45, Method ASTM C697-80, American Society for Testing and Materials, Easton, MD, 1980, pp. 258—262.

Analytica Chimica Acta, 129 (1981) 133—143
Elsevier Scientific Publishing Company, Amsterdam — Printed in The Netherlands

AN INVESTIGATION OF THE VOLTAMMETRIC CHARACTERISTICS OF THE OSAZONE OF DIHYDROXYTARTARIC ACID

C. JORDAN and G. SVEHLA

Department of Chemistry, The Queen's University, Belfast, BT9 5AG, Northern Ireland (Gt. Britain)

(Received 26th February 1981)

SUMMARY

Differential pulse polarography (d.p.p.), supplemented by other voltammetric techniques, is used to elucidate the tautomeric structures associated with buffered aqueous solutions of the osazone of dihydroxytartaric acid. In particular, d.p.p. is used to evaluate the number of electrons and protons associated with each of seven reduction processes, at pH values ranging from 2.5—11.5. The reversibility of the electrode processes is demonstrated by cyclic voltammetry and d.p.p. All the reduction processes studied are diffusion-controlled. Mechanisms for these reductions are proposed on the basis of the tautomeric equilibrium associated with the osazone in solution.

Except for the characterisation of sugars, osazones have, until recently, found little application in analytical chemistry. It is little wonder then that the voltammetric characteristics of osazones have not been studied in any detail. However, recent interest in some osazones as visual indicators over the pH range 11.5—13.5 in solutions containing high concentrations of salts, ethanol or proteins at temperatures from 0 to 80°C [1], coupled with the perhaps better known application of the osazone (the bis(phenylhydrazone)) of dihydroxytartaric acid to the detection of very low concentrations of calcium ions in aqueous solution [2], has led to a need for a better understanding of these reagents so that their analytical application can be improved. As osazones contain many potentially electroreducible groups, voltammetric methods provide an excellent technique for probing their nature.

The present study is concerned only with the voltammetric characteristics of the osazone of dihydroxytartaric acid, particularly in alkaline solution.

EXPERIMENTAL

Reagents and chemicals

The osazone of dihydroxytartaric acid (succinic acid, dioxo, 2,3-bis(phenylhydrazone)) was prepared in a four-step synthesis from tartaric acid [3, 4]. The identity and purity of the product were characterised by elemental

analysis, mass spectrometry and differential scanning calorimetry. These characteristics were checked regularly throughout the study to ensure that no deterioration of the solid had occurred. This check was necessary as all solutions of the osazone were prepared fresh from the solid osazone; preliminary investigations had shown that polarograms recorded with a given solution of the osazone varied with time. No deterioration of the solid was observed over a three-month period. Buffer—supporting electrolyte solutions were prepared from analytical-grade reagents. Analytical-grade nitrogen was used for all deaerations.

Apparatus

All polarographic measurements were made with a Tacussel PRG 5 pulse polarograph equipped with a thermostatted Tacussel CPRA DME/cell. The polarograph was coupled to a Hewlett-Packard HP 7035B X-Y recorder via specially-made adaptors. These adaptors gave an output of 50 mV cm^{-1} on the potential (X-) axis and a full scale deflection (equivalent to 125 mV) per 20 cm on the current (Y-) axis. The DME had the following characteristics: outflow velocity m = 0.63 mg s^{-1}; drop time τ = 8.7s at 0 V vs. SCE; mercury head h = 50 cm. A platinum pin auxiliary and a saturated calomel reference electrode completed the potentiostat circuit.

Cyclic voltammetric (c.v.) measurements were made on an instrument built in the Department; details have already been described [5]. An amalgamated gold pin was used as the working electrode with a platinum auxiliary and a saturated calomel reference electrode.

Ultraviolet spectra were recorded with a Pye-Unicam SP 8000 spectrophotometer at 25°C in matched 1-cm silica cells using buffered 2×10^{-5} M solutions of the osazone.

Solution preparation

Preliminary investigations with solutions of the osazone showed that the polarographic response varied with time and at a rate dependent on the pH and the temperature of the solution. Each solution reached an equilibrium condition after a couple of days at 20°C. The approach of the system to equilibrium at various pH values and over a range of temperatures is the subject of another paper [6].

As a consequence of this effect, all solutions of the osazone were prepared direct from the solid osazone and not by dilution of any stock solutions of the osazone. A series of solutions of the osazone in Prideaux buffers [7], of buffer capacity greater than 0.006 and covering the pH range 2—12, were used. All solutions were adjusted to a constant ionic strength (0.5 M) with a 2 M KCl solution. Full details of the buffer compositions and their analytical utility for polarography are given elsewhere [8].

All solutions studied contained 0.005% (w/v) of Triton X-100 to suppress maxima. Between pH 11.5 and pH 4, solutions 1×10^{-3} M in osazone were prepared; between pH 4 and pH 2.5, solutions 1×10^{-4} M in osazone were

employed. The osazone was insoluble below pH 2.5 except in strong mineral acid. On allowing these solutions to sit at 20°C for a few days to establish their equilibrium condition, a fluffy crystalline orange/yellow solid (presumably the protonated osazone) precipitated out of those solutions with pH $\leqslant$ 7.2. This solid was filtered off before the equilibrated solutions were subjected to polarography.

Polarographic procedures

Tast and differential pulse (d.p.) polarograms were recorded at a scan rate of 2 mV s^{-1} for each equilibrated solution, thermostatted at 20°C, at pH intervals of about 0.4. A controlled drop time of 2.0 s with h = 50 cm was used throughout, as was a damping setting of 3 on an 11-point scale. For d.p. polarography, a pulse amplitude (ΔE) of 50 mV (cathodic) provided the best compromise between sensitivity and resolution. Peak potentials (E_p) are related to the half-wave potential ($E_{1/2}$) by $E_p = E_{1/2} - 0.5\ \Delta E$ [9]. The number of protons (m) involved in the electrode processes can be obtained from the $E_{1/2}$ (or E_p) vs. pH plots [10], provided that the corresponding αn values are known for each process (n is the number of electrons involved in the electrode process and α is the transfer coefficient). Thus $dE_{1/2}/dpH = dE_p/dpH = -59m/\alpha n$ (mV). Values of αn at each pH value are readily estimated from the peak half-width ($W_{1/2}$). According to Barker et al. [11], $W_{1/2} \simeq 3.52\ RT/\alpha n = 89/\alpha n$ (mV, at 20°C). Thus changes in m with pH can easily be followed by d.p. polarography.

The degree of reversibility of the electrode process can be determined by d.p.p. as well as by c.v. In this special application, polarograms were first recorded with cathodic (c) going pulses, then with anodic (a) going pulses of equal amplitude (50 mV) [12, 13]. The ratio of the peak currents $(i_p)_c/(i_p)_a$ on the two scans was evaluated for each peak. If the ratio is close to unity the electrode process is behaving reversibly, while if the relationship $(i_p)_c/(i_p)_a = (3\ t_1/7\ t_m)^{1/2}$ holds, then the process is behaving in a totally irreversible way [12, 13]; t_1 is the age of the drop and t_m is given approximately by $t_m = t_2 - 0.5\ \Delta t$, where t_2 is the pulse width and Δt is the current sampling width [14]. For the polarograms obtained in this study t_1 = 1.95 s, t_2 = 48 ms and Δt = 8 ms, so the ratio equivalent to totally irreversible behaviour is 4.4. Values between 1 and 4.4 represent varying degrees of quasi-reversible behaviour.

Peak heights for the osazone were obtained by measuring the recorded peak height from the current baseline (i = 0) and subtracting from it the corresponding peak height of the supporting electrolyte alone.

RESULTS

Since interest lay in the interaction of the osazone with calcium ions, and as other oxygen-containing chelating compounds (e.g., EDTA) form strong complexes with calcium in alkaline solution, most of the polarographic

characteristics of the osazone were determined in distinctly alkaline solution (pH 11.4).

At pH 11.4, seven peaks were observed in the d.p. polarogram of a freshly prepared solution of the osazone (Fig. 1). Five of these peaks (peaks 1—5) increased in height, and the other two (peaks 6 and 7) decreased in height as time went by (until equilibrium was established). Peak 6 was resolved only up to about three quarters of the time to equilibrium. Tast polarography showed that all seven peaks correspond to reduction processes. A change in the colour of the solution from yellow (at preparation) to orange (at equilibrium) accompanies the variation in the peak currents. This is apparent from the shift of λ_{max} to longer wavelengths in the u.v. spectrum as equilibrium is established (Fig. 2).

Of the seven waves expected on the d.c. polarogram at pH 11.4, only waves 1 and 2 were sufficiently resolved as to make their wave height measurable accurately. The square-root correlation between the mercury head (h) and wave height (i) ($i \propto h^{1/2}$) found for both waves indicated diffusion-control. Evaluation of the other waves was not possible individually but the overall wave height was observed to increase with h. The electrocapillary curve for the osazone solution showed no signs of adsorption effects [15]. This, coupled with the linear correlation found between the equilibrium d.p. peak heights and the initial concentrations of the osazone solutions (Table 1), leaves little doubt that processes 3—7 are also diffusion-controlled. The effect of temperature on the equilibrium peak heights (fixed osazone concentration, pH 11.4) gave temperature coefficients [15] lower than +1.6% for all peaks except peaks 2 and 3, (+4.5% and +3.7%, respectively); this lends further support to the assignment of diffusion control to all waves/peaks.

The diffusion coefficient for wave 2 at pH 11.4 was calculated to be 3×10^{-6} cm^2 s^{-1} at 20°C, a value typical of the diffusion coefficient of most organic compounds [16].

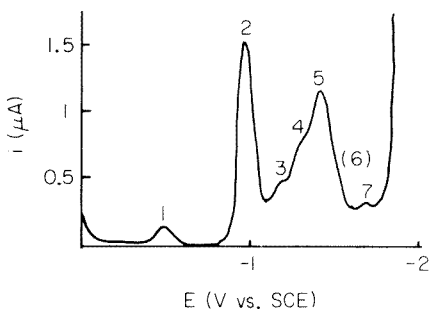

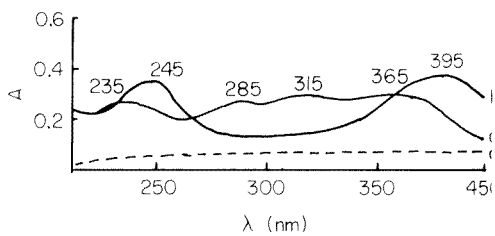

Fig. 1. A differential pulse polarogram of the osazone in a Prideaux buffer mixture at pH 11.4. ΔE = 50 mV, T = 20°C, $C_o = 1 \times 10^{-3}$ M.

Fig. 2. The u.v. spectrum of the osazone in a Prideaux buffer at pH 11.4, $C_o = 2 \times 10^{-5}$ M, T = 20°C; (a) at start, (b) at equilibrium, (c) the blank.

TABLE 1

The effect of the initial concentration (C_o) of the osazone solution on the peak height at pH 11.4 and 20°C

Initial concentration C_o ($\times 10^{-4}$ M)	Peak height i_p (μA)[a]					
	1	2[b]	3	4	5	7
9.76	0.258	1.475	0.442	0.765	1.161	0.258
7.32	0.189	1.088	0.383	0.590	0.842	0.205
4.88	0.124	0.710	0.267	0.371	0.511	0.096
2.44	0.063	0.363	0.153	0.198	0.280	0.031
0.98	0.027	0.127	0.067	0.075	0.104	0.010
0.49	0.018	0.062	0.038	0.038	0.050	—
Linear regression data:						
No. of points	6	12	6	6	6	5
Intercept, $C_o = 0$ ($\times 10^{-3}$ μA)	1.50	−17.6	31.90	−0.81	−19.46	−32.76
Slope (μA mol^{-1} dm^3)	259	1510	448	789	1184	301
Coefficient of correlation	0.9995	0.9997	0.9927	0.9995	0.9983	0.9902
Minimum determinable concentration ($\times 10^{-5}$ M)	4.3	1.6	14.1	4.1	7.3	20.4

[a]Peak current after correction for blank. [b]Results for peak 2 made in duplicate.

The effect of pH

The effect of changing the pH of the solution was found to be as complex as expected for a molecule which contains so many electroreducible groups, each of which can exist in a variety of protonated forms. The relative position, height and the number of peaks change with pH, some peaks coalescing and some "new" peaks appearing. In general, the additional peaks are assigned here to those peaks on which the new ones originally appeared as a shoulder; a capital A differentiates the additional peak from the parent. Points corresponding to peaks 3, 4, 4A and 5 were particularly difficult to assign because of peak mergers, overlapping, etc.; assignments were made on the basis of general trends observed as the pH was altered.

Plots of the peak potential (E_p) and the peak current (i_p) as a function of pH are shown in Fig. 3 for each peak observed. Breaks in the E_p vs. pH plots correspond to pK_a values of the oxidised or reduced forms of the osazone [17]. The slope of the E_p vs. pH plots allows values for $m/\alpha n$ to be calculated, as indicated under Experimental. Values for αn were obtained, as outlined above, from the peak half-width ($W_{1/2}$) for each peak, if sufficiently resolved, at each pH value studied. These values are presented in Table 2.

Both c.v. and d.p. polarography indicated that all the electrode processes were quasi-reversible in alkaline solution but tended towards total irreversibility as the pH was decreased (to about pH 3) [15].

The u.v. spectra of the equilibrated osazone solutions also showed some change with pH. Thus, while the position of the absorption with λ_{max} = 245 nm (Fig. 2) remained constant, the λ_{max} of the other absorption band increased continuously from 395 nm at pH 11.4 to 435 nm at pH 4.7.

Other work on the osazone system [6] has shown that the approach to

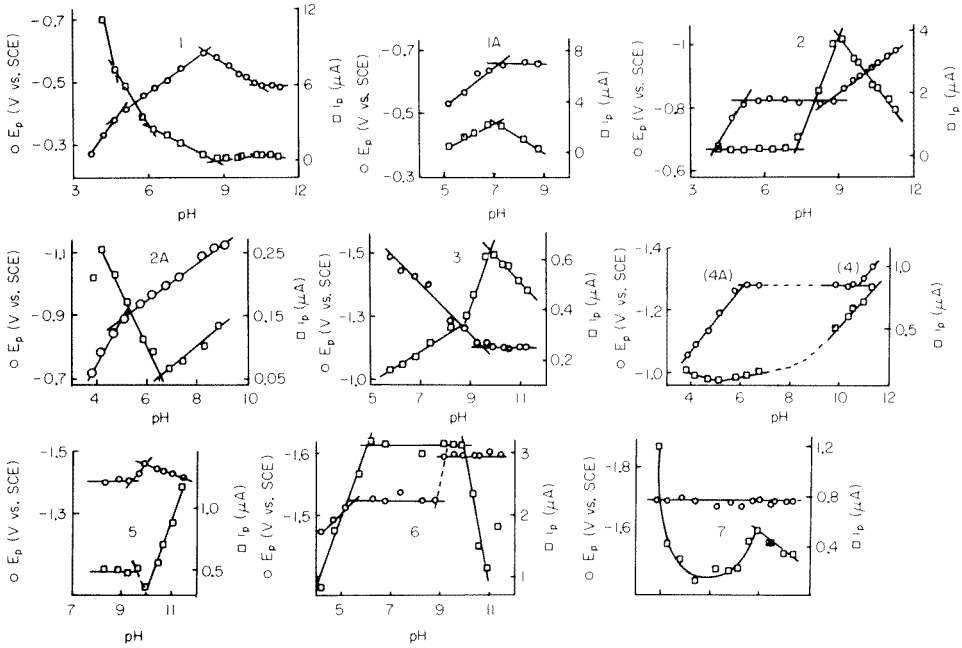

Fig. 3. The effect of pH on the peak potential and d.p. peak current for the seven peaks shown in Fig. 1. The numbers on each part of this Fig. relate to the numbered peaks in Fig. 1. In all cases, ΔE = 50 mV, T = 20°C, C_o = 1 × 10^{-3} M.

equilibrium is established by first-order rate processes in both the forward and reverse directions and that the forward process (A → B, see later) is endothermic by 22 kJ mol^{-1}; an entropy change (ΔS) of +86 J K^{-1} mol^{-1} accompanies this process (ΔG = −2.7 kJ mol^{-1} at 20°C).

DISCUSSION

In view of the first-order rate processes accompanying establishment of equilibrium, the osazone probably undergoes an isomeric change in solution. Of the possibilities considered [15], the most likely choice is a tautomeric change based on the quasi-aromatic structure of osazones first suggested by Fieser and Fieser [18] and later by Mester et al. [19] and Henseke and Binte [20].

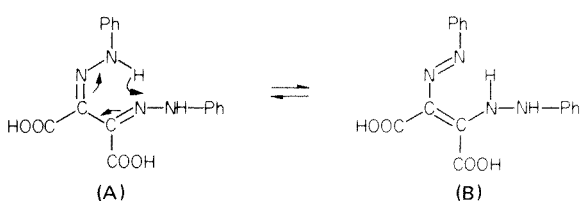

This tautomeric equilibrium not only explains the bathochromic shift in λ_{max} as A → B as the result of more extensive conjugation throughout the molecule (especially in solutions where the pH is such as to permit ionisation of the carboxyl groups) but also provides a basis from which the polarographic data can be rationalised. Molecular models of the isomeric forms above also indicate that there is less opportunity for hydrogen-bonding in the "B" form, which may explain the large positive value of ΔS as A → B. Assuming that the various electroactive groups can be reduced independently of one another, that waves 1—5 originate from the "B" form (these waves increase in size as equilibrium is established) and that waves 6 and 7 originate from the "A" form (these waves decrease in size as equilibrium is established), the following interpretations of the polarographic data shown in Figs. 1 and 3 can be made (a full descriptive interpretation has been given elsewhere [15]).

Peaks 1 and 1A

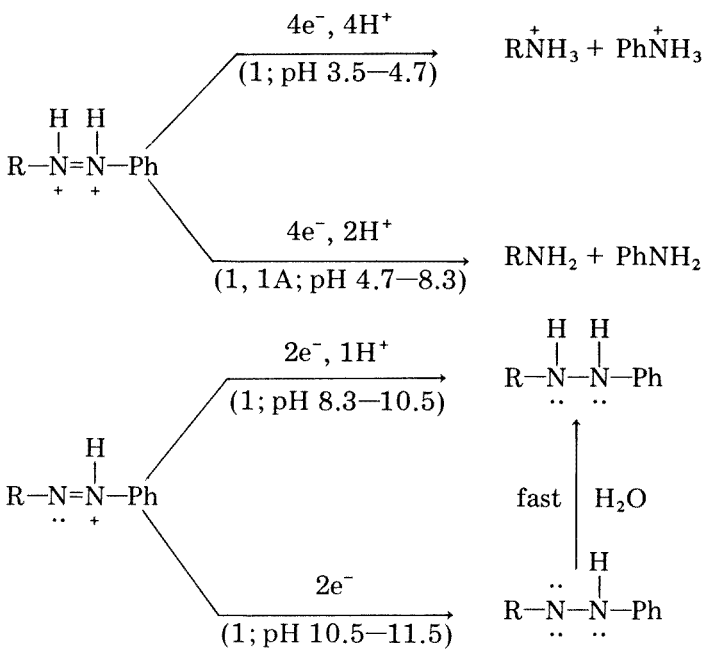

(The first numeral(s) enclosed in parentheses in the above and following schemes refers to the peak(s) involved.)

TABLE 2

Evaluation of E_p vs. pH plots

Peak		1				1A		2			2A	
pH	From:	3.5	4.8	8.3	10.5	5.0	7.3	4.0	5.2	8.6	2.9	5.1
	To:	4.8	8.3	10.5	11.5	7.3	8.8	5.2	8.6	11.5	5.1	9.2
$\frac{dE_p}{dpH}$ (mV/pH)[a]		−110	−60	+52	0	−64	0	−124	0	−60	−140	−60
$m/\alpha n$		1.86	1.02	0.88	0	1.08	0	2.10	0	1.02	2.37	1.02
αn[b]		2.2	1.1	0.89	0.85	1.11	1.11	1.1	0.95	0.90	0.74	(1.0)[c]
m		4.09	1.12	0.78	0	1.20	0	2.31	0	0.92	1.78	(1.02)
m (nearest integer)		4	1	1	0	1	0	2	0	1	2	(1)
n		4	2	2	2	2	2	2	2	2	2	(2)

[a] $dE_p/dpH = 59\ m/\alpha n$ (mV/pH). [b] Mean αn value from peak half-width. [c] Value not known but using value for peak 2.

Peaks 2 and 2A

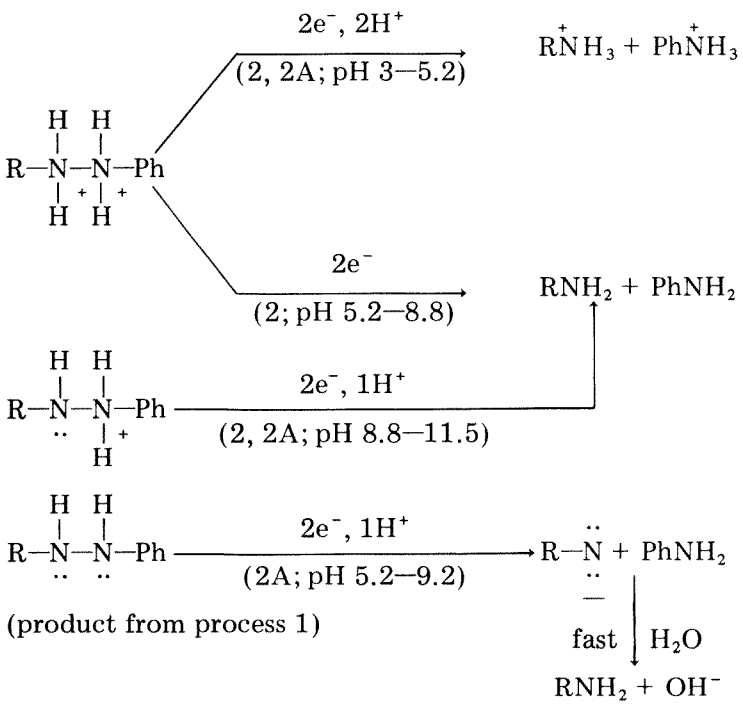

Peaks 3, 4, 4A and 5

When the osazone is complexed with calcium, these peaks exhibit a noticeable anodic shift in their peak potentials [15, 21]. Taken together with the E_p vs. pH plots, it can be concluded that these peaks are almost certainly linked to reductions of the carbon—carbon double bond linked to

3		4A	4/4A	4	5		6			7	
5.7	9.5	2.5	5.9	10.8	8.2	9.4	9.9	4	5.5	9.0	5.5
9.5	11.5	5.9	10.8	11.5	9.4	9.9	11.5	5.5	9.0	11.5	11.5
+80	0	−104	0	−100	0	−100	+30	−40	0	0	0
1.36	0	1.76	0	1.69	0	1.69	0.51	0.68	0	0	0
0.49	0.51	0.49	(0.4)	0.45	0.46	0.45	0.47	0.89	0.83	0.56	0.59
0.67	0	0.86	0	0.76	0	0.76	0.24	0.61	0	0	0
1	0	1	0	1	0	1	(0.25)	1	0	0	0
1	1	1	(1)	1	1	1	1	2	2	1	1

the carboxyl groups of the "B" form of the tautomeric equilibrium. In this respect they resemble the reductions of maleic and fumaric acid to succinic acid [16]

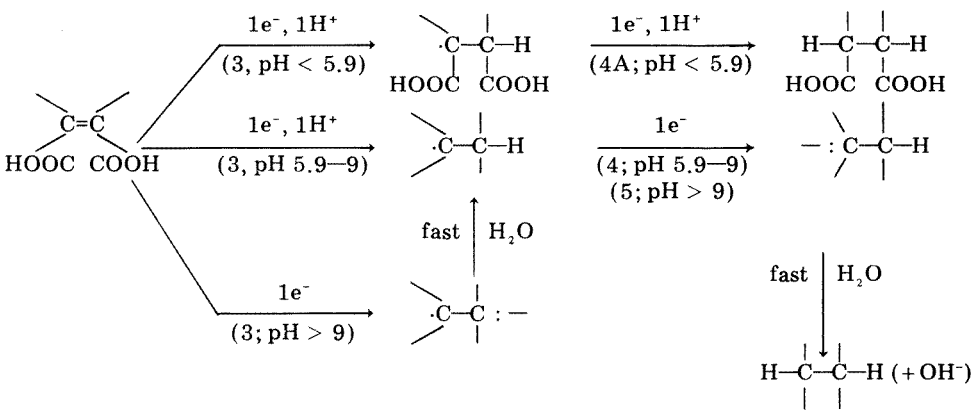

Peak 6

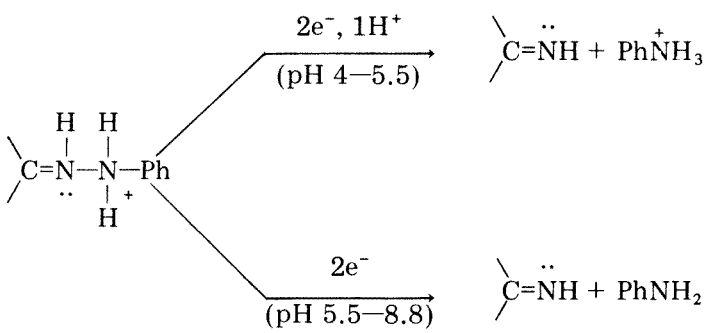

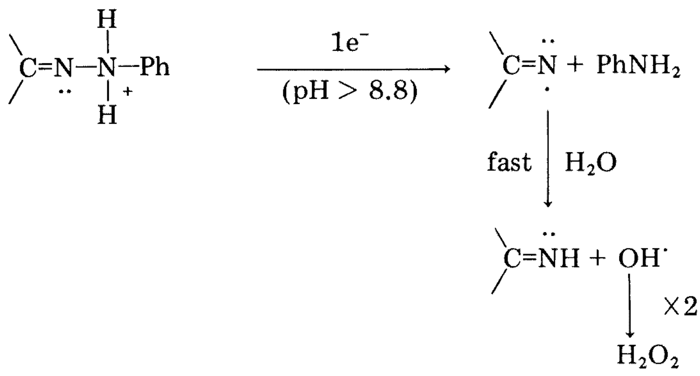

The imine, >C=NH, will probably undergo hydrolysis to >C=O under the conditions of the experiment [22].

Peak 7

The other peak corresponding to the "A" form of the tautomeric equilibrium probably arises from the reduction of a product from the processes causing peak 6, e.g., above pH 8.8,

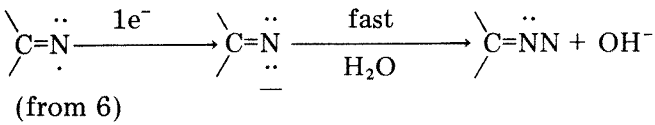

Conclusions

The reduction mechanisms proposed above, while based on all the available evidence, are still rather tentative. Comparison with the reductions of similar compounds is limited by the lack of available data. Only Jambor and Mester [23] seem ever to have looked at the polarographic characteristics of osazones and they were studying sugar osazones; few quantitative data and no reduction mechanisms were given. However, Mester et al. [19] did quote chemical, spectral (u.v. and n.m.r.) and x-ray evidence in support of an osazone structure intermediate between the "A" and "B" forms suggested here.

Evidence from the literature that the "B" form of the osazone can exist is provided in Lund's review on the electrochemistry of the C=N double bond [24]. In the examples quoted there, less than 4% of the azo—hydrazine form of the hydrazone is present at equilibrium. The high percentage (>70%) of the azo—hydrazine ("B") form present at equilibrium with the osazone of dihydroxytartaric acid is explained by the very extensive π-electron delocalisation available to this form. It is interesting to note that aniline, one of the major products of the reductions, is the dominant (base) peak in the electron-impact mass spectrum [15].

The assignments made above can only be established or rejected after a full study of simpler osazones, e.g. (Ph—NH—N=C—CH—)$_2$. Nevertheless, the present study has highlighted many of the essential features associated with the reduction processes and should serve as a useful base from which other research on osazones can evolve.

One of the authors (C.J.) gratefully acknowledges the award of a post-graduate studentship from the Department of Education for Northern Ireland.

REFERENCES

1 A. G. Asuero, Microchem. J., 24 (1979) 217.
2 F. Feigl, Spot-Tests. I. Inorganic Applications, Elsevier, Amsterdam, 1954, p. 208.
3 F. J. Welcher, Organic Analytical Reagents, Van Nostrand, New York, 1947, Vol. II, pp. 108 and 223.
4 A. Lachman, J. Am. Chem. Soc., 43 (1921) 577.
5 C. Jordan, G. Svehla and F. Glockling, Anal. Chim. Acta, 117 (1980) 193.
6 C. Jordan and G. Svehla, Anal. Chim. Acta, 129 (1981) 145.
7 E. B. R. Prideaux, Proc. R. Soc. London, 92A (1916) 463.
8 C. Jordan, Microchem. J., 25 (1980) 492.
9 E. P. Parry and R. A. Osteryoung, Anal. Chem., 37 (1965) 1634.
10 J. Heyrovsky and J. Kuta, Principles of Polarography, Academic Press, New York, 1966, pp. 161—165 and pp. 256—259.
11 G. C. Barker, R. L. Faircloth and A. W. Gardner, AERE (Harwell), C/R 1786, HMSO (1955); see also C/R 2297, HMSO (1958).
12 O. Vittori and M. Porthault, Analusis, 4 (1976) 152.
13 K. B. Oldham and E. P. Parry, Anal. Chem., 42 (1970) 229.
14 J. Osteryoung and K. Hasebe, Rev. Polarogr., Kyoto, 22 (1976) 1.
15 C. Jordan, Ph.D. Thesis, The Queen's University of Belfast, 1980.
16 L. Meites, Polarographic Techniques, 2nd edn., Interscience, New York, 1965, p. 145 and pp. 693, 696.
17 M. W. Clark, Oxidation—Reduction Potentials of Organic Systems, Baillière, Tindall and Cox, London, 1960, p. 126.
18 L. F. Fieser and M. Fieser, Organic Chemistry, D. C. Heath, Boston, 1944, p. 353.
19 L. Mester, E. Moczar and J. Parello, J. Am. Chem. Soc., 87 (1965) 596; and references therein.
20 G. Henseke and H. J. Binte, Chimia, 12 (1958) 103.
21 C. Jordan and G. Svehla, Microchem. J., 26 (1981) xx.
22 T. L. Gilchrist and C. W. Rees, Carbenes, Nitrenes and Arynes, Nelson, London, 1969, p. 94.
23 B. Jambor and L. Mester, Acta Chim. Acad. Sci. Hung., 9 (1956) 485.
24 H. Lund, in S. Paulo (Ed.), The Chemistry of the Carbon—Nitrogen Double Bond, Wiley—Interscience, Chichester, 1970 pp. 540—1; see also pp. 74—76.

Analytica Chimica Acta, 129 (1981) 145—152
Elsevier Scientific Publishing Company, Amsterdam — Printed in The Netherlands

CHARACTERISATION OF THE APPROACH TO EQUILIBRIUM OF THE OSAZONE OF DIHYDROXYTARTARIC ACID IN AQUEOUS SOLUTIONS BY DIFFERENTIAL PULSE POLAROGRAPHY

C. JORDAN and G. SVEHLA

Department of Chemistry, The Queen's University, Belfast, BT9 5AG, Northern Ireland (Gt. Britain)

(Received 26th February 1981)

SUMMARY

Differential pulse polarography is used to determine the changes in the enthalpy, entropy and Gibbs function for the forward and reverse conversions of the osazone of dihydroxytartaric acid from one tautomeric form to another at pH 11.4 in aqueous solution. This is done by determining the individual rate constants associated with these conversions at different temperatures through combining kinetic measurements with measurements on the system at equilibrium. The equilibrium constant was found to vary widely with pH and to increase with increase in temperature. The driving force for the endothermic conversion of the osazone from the hydrazone form to the azo-hydrazine form is shown to be the much greater freedom of movement (greater entropy) available to the latter form.

Earlier studies [1, 2] on the bis(phenylhydrazone) of dihydroxytartaric acid, indicated that the differential pulse polarographic response of buffered aqueous solutions of this compound, at constant temperature, varied with time. After a few days at 20°C, the peak currents recorded would reach a reproducible limiting value and remain at that value (see Fig. 1 [2]). The present paper deals with the approach of this system to equilibrium and shows how differential pulse polarography (d.p.p.) can be used to evaluate the kinetic and thermodynamic parameters associated with the equilibrium.

EXPERIMENTAL

Materials and apparatus

The osazone of dihydroxytartaric acid (succinic acid,dioxo,2,3-bis-(phenylhydrazone)) was prepared by established procedures [3, 4]. All reagents used were of analytical grade. All deaerations were made with analytical-grade nitrogen.

The pulse polarograph, cell and recorder system were the same as used earlier [2]; the DME had the same characteristics as before [2].

Procedures

All solutions of the osazone were 1×10^{-3} M in osazone, contained 0.005% (w/v) Triton X-100 to suppress maxima, had a buffer capacity greater than 0.006 and were adjusted to an ionic strength of 0.5 M with a 2 M KCl solution. Details of the buffer compositions have been described [2, 5].

All d.p. polarograms were recorded at a scan rate of 2 mV s^{-1} using a controlled drop time of 2.0 s, a mercury head of 50 cm and a damping setting of 3 on an 11-point scale. A pulse amplitude of 50 mV (cathodic) was used throughout with a pulse width of 48 ms and a sampling width of 8 ms. The temperature of each solution used was controlled to ±1°C by pumping water from a thermostatted bath through the outer jacket of the polarographic cell.

The half-life associated with the establishment of equilibrium of the osazone solutions at 20°C is more than 12 h, so the approach to equilibrium can be monitored adequately by recording d.p. polarograms of individual samples, taken from a thermostatted osazone solution, at intervals of about 30 min for the first few hours from preparation and at intervals of 2—6 h thereafter. The heights of the first two peaks recorded (peaks 1 and 2 with E_p values of —0.49 and —0.98 V vs. SCE, respectively, in Fig. 1 [2]) were used to monitor the approach to equilibrium as these peaks were the best defined and so well resolved from neighbouring peaks that there could be no contribution from the neighbours to their peak height. This procedure was used for osazone solutions at 20°C in alkaline, neutral and acid solution and in alkaline solutions at temperatures ranging from 20 to 35°C.

RESULTS AND DISCUSSION

The variation with time in the peak current for peak 2 at pH 11.4 and at 20°C is illustrated in Fig. 1A. General curve fitting to the points represented in Fig. 1A showed that the best fit was obtained by using an exponential transformation. By analogy with radioactivity, this suggests a first-order process in the forward direction. However, a reaction which proceeds towards equilibrium and in which both forward and reverse reactions are first-order will also behave like a first-order process in which the effective rate constant is the sum of the rate constants (k_1 and k_{-1}, respectively) [6].

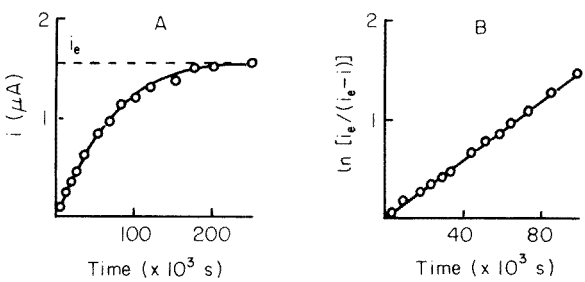

Fig. 1. (A) The approach of the peak current (i) to its equilibrium value (i_e); peak 2, pH 11.4, at 20°C. (B) A logarithmic analysis of the points shown in (A).

For the case

$$A \underset{k_{-1}}{\overset{k_1}{\rightleftharpoons}} B$$

it can be shown [6, 7] that

$$[B]_e = k_1 [A]_0/(k_1 + k_{-1}) \quad (1)$$

$$\ln [B]_e/([B]_e - [B]_t) = (k_1 + k_{-1})t \quad (2)$$

where [] represents the concentration of the enclosed isomeric form, t is the time since preparation and subscripts t, e and 0 represent the concentrations at time t, at equilibrium and at t = 0, respectively.

For the osazone solution, $(i_p)_B = \beta [B]_t$, where i_p is the d.p. peak current of a peak corresponding to the "B" form of the osazone at time t (this includes peaks 1 and 2 [2]) and β is a proportionality constant.

Thus, combining eqn. (2) with the expression for $(i_p)_B$ gives

$$\ln \{i_e/(i_e - i)\}_B = (k_1 + k_{-1})t \quad (3)$$

This equation should describe the variation of the height (i) of peak 1 or 2 with time if the equilibrium which the osazone undergoes is first-order in both directions. For such a relationship, a plot of $\ln \{i_e/(i_e - i)\}_B$ vs. t should be a straight line of slope $(k_1 + k_{-1})$. A logarithmic analysis of the results represented in Fig. 1A indicates (see Fig. 1B) that eqn. (3) correctly describes the behaviour of the osazone system. A logarithmic analysis of the i_p vs. t results at other temperatures (Table 1) and at other pH values (Table 2) indicates that the same relationship also holds under these conditions. Calculated values of the combined rate constants are included in Tables 1 and 2.

Values of the combined rate constants can also be obtained from the half-life ($t_{1/2}$) of the reaction. For the condition, $(i_p)_B = (i_e)_B/2$, we have, $\ln 2 = (k_1 + k_{-1})t_{1/2}$ or $t_{1/2} = 0.693/(k_1 + k_{-1})$. The time taken to establish equilibrium (t_e) is given by $t_e \simeq 7 \times t_{1/2}$. The results shown in Tables 1 and 2 clearly prove that the osazone undergoes a reversible change in solution which is first-order in both directions.

The individual rate constants

Logarithmic analysis of the i_p—t results gives only the combined rate constants. To obtain individual values for k_1 and k_{-1}, it is necessary to supplement the kinetic information with information about the equilibrium state. An approximate value for the equilibrium constant $K = k_1/k_{-1}$ can be obtained if a peak corresponding to the "A" form taking part in the equilibrium can be identified. For such a peak, it is easy to show [1, 7] that $(i_0)_A/(i_e)_A = 1 + K$, where i_0 and i_e are the d.p. peak currents at preparation ($t = 0$) and at equilibrium, respectively.

For the osazone, the only A-type peaks (i_p decreases with time) are peaks 6 and 7 ($E_p = -1.59$ and -1.69 V, respectively, at pH 11.4) [1, 2]. A plot of

TABLE 1

Logarithmic analysis on the approach to equilibrium data at fixed pH ($C_0 = 1 \times 10^{-3}$ M; pH 11.4)

	20°C		25°C		30°C		35°C	
	$t(\times 10^3$ s)	$\ln \frac{i_e}{i_e - i}$	$t(\times 10^3$ s)	$\ln \frac{i_e}{i_e - i}$	$t(\times 10^3$ s)	$\ln \frac{i_e}{i_e - i}$	$t(\times 10^3$ s)	$\ln \frac{i_e}{i_e - i}$
	1.325	0.0419	1.505	0.0671	1.385	0.0793	1.085	0.1008
	3.425	0.0543	3.125	0.1125	1.625	0.0936	1.925	0.1667
	9.245	0.1686	6.185	0.1858	2.105	0.1124	2.885	0.2372
	10.325	0.1633	8.105	0.2394	3.365	0.1798	4.085	0.3070
	18.425	0.2657	11.045	0.3254	4.985	0.2311	4.805	0.3632
	23.825	0.3376	15.365	0.4467	6.245	0.2942	5.525	0.4184
	28.865	0.4103	17.825	0.5079	6.485	0.3066	6.785	0.5227
	32.525	0.4598	19.985	0.5711	8.045	0.3841	7.625	0.6020
	44.46	0.6754	25.145	0.7289	9.425	0.4580	8.345	0.6605
	51.07	0.7830	28.45	0.8403	9.665	0.4696	8.945	0.7175
	58.87	0.8557	30.60	0.8790	10.805	0.5198	10.445	0.8598
	65.40	0.9605	32.83	0.9627	12.425	0.6247	11.405	0.9500
	72.67	1.0702	34.63	0.9906	13.205	0.6711	12.065	1.0258
	79.09	1.3218	35.29	1.0308	14.705	0.7197	13.085	1.1319
	99.49	1.4663	36.43	1.0423	15.665	0.7772	14.405	1.1660
			37.93	1.1057	16.805	0.8528	15.125	1.2264
			39.37	1.1620	18.065	0.9421	16.025	1.3275
					19.085	1.0144	17.165	1.4313
Intercept ($t = 0$)[a]	−0.0004		0.0088		−0.0125		−0.0208	
Slope ($=k_1 + k_{-1}$)[a]	1.51×10^{-5}		2.87×10^{-5}		5.14×10^{-5}		8.40×10^{-5}	
Coefficient of correlation[a]	0.9959		0.9995		0.9977		0.9984	
i_e (μA)	1.56		1.71		2.06		2.41	
$t_{1/2}$ ($\times 10^3$ s)	45.9		24.2		13.5		8.3	
t_e (h)	90		47		27		16	

[a] Values from a linear regression analysis of the $\ln[i_e/(i_e - i)]$ vs. t data.

i_0 vs. i_e for peaks 6 and 7 at pH 11.4 and at 20°C is shown in Fig. 2. The slopes of the lines were 8.56 for peak 6 and 3.98 for peak 7; the values of K calculated from these slopes were 7.56 and 2.98, respectively. These results were obtained by following the equilibrium of a series of solutions containing different initial concentrations of the osazone. As i_0 (and i_e for peak 6) have to be obtained by extrapolation, the values of K are subject to some error (peak 6 is not resolved after $t \approx 6\ t_{1/2}$ from start). The different values of K obtained are probably related to the different acid—base behaviour of the processes responsible for peaks 6 and 7. For consistency, it is obvious that one or other of the peaks must be chosen and it alone should be used when assessing changes in K for the system. For the equilibrium results at different temperatures, peak 7 was the peak of choice as it was best resolved (see Fig. 1 [2]); for the results at different pH values, peak 6 had to be used since peak 7 merged with the supporting electrolyte decomposition as the pH dropped. The values of K calculated on this basis are included with the corresponding values of k_1 and k_{-1} in Table 3.

While the values of K estimated by using peak 6 at different pH values do

TABLE 2

Logarithmic analysis of the approach to equilibrium data at constant temperature (C_0 = 1×10^{-3} M; T = 20°C)

	pH 11.4		pH 7.2		pH 4.8	
	$t(\times 10^3$ s)	$\ln \frac{i_e}{i_e - i}$	$t(\times 10^3$ s)	$\ln \frac{i_e}{i_e - i}$	$t(\times 10^3$ s)	$\ln \frac{i_e}{i_e - i}$
	2.280	0.0328	1.515	0.0163	1.410	0.0168
	10.800	0.1198	2.800	0.0305	5.010	0.0700
	18.720	0.1914	6.220	0.0400	8.910	0.1080
	24.600	0.2231	11.440	0.0709	12.210	0.1623
	28.380	0.2518	16.540	0.0943	15.590	0.2126
	33.18	0.2812	21.520	0.1226	21.510	0.2640
	36.48	0.3339	28.660	0.1698	26.670	0.3342
	45.30	0.4843	35.08	0.2289	34.65	0.4801
	51.90	0.5775	48.28	0.3074	36.33	0.4801
	59.58	0.6740	58.72	0.3611	48.03	0.5540
	66.18	0.7737	73.84	0.4855	61.11	0.8574
	73.26	0.9244	90.22	0.5501	73.89	1.1036
	87.96	0.9491	134.68	0.9144	89.31	1.3169
	100.32	1.0092	151.30	1.0005		
	107.16	1.1415	175.72	1.1564		
Intercept (t = 0)[a]	−0.0194		−0.0088		−0.0333	
Slope ($=k_1 + k_{-1}$)[a]	1.11×10^{-5}		6.63×10^{-6}		1.47×10^{-5}	
Coefficient of correlation[a]	0.9886		0.9990		0.9945	
i_e (μA)	0.31		1.30		5.40	
$t_{1/2}$ ($\times 10^3$ s)	62.6		104.5		47.1	
t_e (h)	122		203		92	

[a] Values from a linear regression analysis of the $\ln[i_e/(i_e - i)]$ vs. t data.

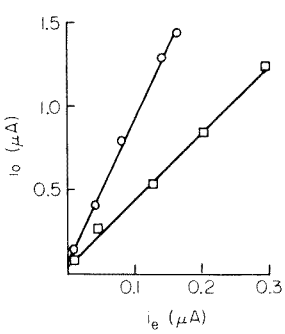

Fig. 2. Evaluation of the equilibrium constant (K) from the initial (i_0) and equilibrium (i_e) peak currents of a series of osazone solutions at pH 11.4 and at 20°C. (○) Peak 6; (□) peak 7.

TABLE 3

Values of the equilibrium and rate constants, at various temperatures and pH values, for 1×10^{-3} M solutions of the osazone

T (°C)	20	25	30	35	20	20	20
pH	11.4	11.4	11.4	11.4	11.4	7.2	4.8
K	2.98[a]	3.67[a]	3.84[a]	4.83[a]	7.6[b]	17.6[b]	7.6[b]
k_1 ($\times 10^{-5}$)	1.13	2.26	4.08	6.96	0.98	0.63	1.30
k_{-1} ($\times 10^{-6}$)	3.79	6.15	10.6	14.4	1.29	0.36	1.71

[a]Estimated using peak 7. [b]Estimated using peak 6.

not correspond to a single unchanging equilibrium but involve various acid–base equilibria [1, 2], the values of K estimated using peak 7 at a fixed pH (11.4) but at different temperatures are of considerable value. If it can be assumed that the electrode process, which does not involve protons [1, 2], remains the same regardless of temperature, the effect of changes of temperature on the values of the rate constants can be used to evaluate the change in the enthalpy (ΔH), entropy (ΔS) and Gibbs function of activation (ΔG) for the forward (A → B) and reverse (B → A) processes.

The kinetic/thermodynamic parameters

Application of statistical thermodynamics to the rates of homogeneous reactions (using activated-complex theory) gives [7]

$$k = \mathrm{K}\,(\bar{k}T/h)\exp(\Delta S^*/R)\exp(-\Delta H^*/RT) \quad (4)$$

where k is the rate constant of the process and $\bar{k}$, h and R are the Boltzmann, Planck and gas constants, respectively; T is the absolute temperature of the system and K is the transmission coefficient; asterisks indicate the activated complex state.

Assuming K equals unity [7], taking natural logarithms of both sides of eqn. (4) leads, after rearrangement, to

$$R\ln(kh/\bar{k}T) = \Delta S^* - \Delta H^*/T \quad (5)$$

A plot of $R\ln(kh/\bar{k}T)$ vs. T^{-1} should be a straight line of slope $-\Delta H^*$ and intercept ΔS^*. The Gibbs function of activation is given by $\Delta G^* = \Delta H^* - T \times \Delta S^*$.

Using the results in Table 3, plots of $R\ln(kh/\bar{k}T)$ vs. T^{-1} were made (Fig. 3) for both the forward and reverse processes. Values of ΔH^*, ΔS^* and ΔG^* at 20°C were calculated from a linear regression analysis of the points in Fig. 3 and are presented in Table 4 along with the net values of ΔH, ΔS and ΔG for the forward process (A → B).

Conclusions

The results show that while the conversion of the osazone from the "A" form to the "B" form is endothermic by 22.4 kJ mol^{-1}, a negative value for the change in the Gibbs function which must accompany the change A → B

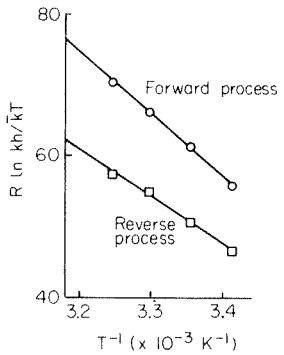

Fig. 3. The effect of temperature on the rate constants of the forward and reverse processes associated with the tautomeric equilibrium of 1×10^{-3} M osazone solutions buffered at pH 11.4.

TABLE 4

Linear regression analysis of the $R \ln kh/\bar{k}T$ vs. T^{-1} results for a 1×10^{-3} M osazone solution at pH 11.4

	Forward process $A \rightarrow X^{*a}$	Reverse process $B \rightarrow X^{*a}$	Overall process $A \rightarrow B$
Intercept	357.17	271.51	—
Slope ($\times 10^3$)	−88.278	−65.865	—
Coefficient of correlation	0.9990	0.9952	—
ΔH (kJ mol^{-1})	+88.28	+65.87	+22.41
ΔS (J K mol^{-1})	+357.2	+271.5	+85.7
ΔG (kJ mol^{-1})	−16.37	−13.69	−2.68

[a]Activated complex.

is assured by the very large increase (+85 J K^{-1} mol^{-1}) in the entropy of the system. The entropy increase must therefore be recognised as the driving force for the change of the osazone from the "A" form to the "B" form.

The latter observation supports the tautomeric equilibrium suggested by previous work on the osazone [1, 2]

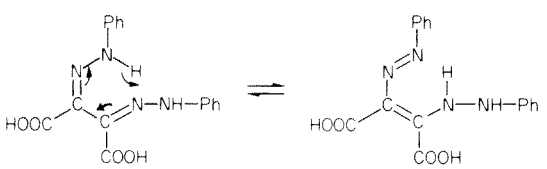

(A) (B)

since one may expect hydrogen bonding in the "B" form of the osazone to be less prevalent than in the "A" form, so that greater freedom of movement of the two phenylhydrazine residues in the "B" form is possible, particularly movement away from the quasi-aromatic ring structure.

The values of ΔH, ΔS and ΔG for this osazone system are of the same order as those associated with some keto $\rightleftharpoons$ enol isomerisations [8].

One of the authors (C.J.) gratefully acknowledges the award of a post-graduate studentship from the Department of Education for Northern Ireland.

REFERENCES

1 C. Jordan, Ph.D. Thesis, The Queen's University of Belfast, 1980.
2 C. Jordan and G. Svehla, Anal. Chim. Acta, 129 (1981) 133.
3 F. J. Welcher, Organic Analytical Reagents, Van Nostrand, New York, 1947, Vol. II, pp. 108 and 223.
4 A. Lachman, J. Am. Chem. Soc., 43 (1921) 577.
5 C. Jordan, Microchem. J., 25 (1980) 492.
6 A. A. Frost and R. G. Pearson, Kinetics and Mechanism, 2nd edn., J. Wiley, New York, 1961, p. 186.
7 P. W. Atkins, Physical Chemistry, Oxford University Press, 1978, p. 867, and pp. 906–916.
8 J. B. Conant and G. H. Carlson, J. Am. Chem. Soc., 54 (1932) 4048.

Analytica Chimica Acta, 129 (1981) 153—161
Elsevier Scientific Publishing Company, Amsterdam — Printed in The Netherlands

DETERMINATION OF ZINC, CADMIUM, LEAD AND COPPER IN SEA WATER BY MEANS OF COMPUTERIZED POTENTIOMETRIC STRIPPING ANALYSIS

DANIEL JAGNER*, MATS JOSEFSON and STIG WESTERLUND

Department of Analytical and Marine Chemistry, Chalmers University of Technology and University of Göteborg, S-412 96 Göteborg (Sweden)

(Received 24th March 1981)

SUMMARY

Water samples from the Arctic Sea were analyzed by the potentiometric stripping technique. Lead(II) and cadmium(II) were determined after pre-electrolysis for 32 min at —1.1 V vs. Ag/AgCl, the detection limits being 0.06 and 0.04 nM, respectively. Zinc(II) was determined after the addition of gallium(III) by pre-electrolysis for 16 min at —1.4 V vs. Ag/AgCl, the detection limit being 0.25 nM. Problems in the determination of copper(II) at the very low concentrations found in oceanic waters are outlined. The average zinc(II), cadmium(II) and lead(II) concentrations in eight different samples were 2.5, 0.16 and 0.10 nM as determined by potentiometric stripping analysis and 1.9, 0.16 and 0.09 nM as determined by solvent extraction/atomic absorption spectrometry. The advantages of this computerized technique for the analysis of sea water are discussed.

The high salt content of ocean water makes it an excellent matrix for electroanalytical techniques but a difficult matrix for atomic absorption techniques. Consequently, electrochemical determinations of trace elements in sea water have been investigated by several authors [1—9]. The most frequently used techniques have been anodic stripping voltammetry and differential pulse anodic stripping voltammetry but potentiometric stripping analysis [10, 11] has also been attempted [12]. The potentiometric stripping method was developed for Baltic sea-water samples containing rather high concentrations of the trace metals, zinc, cadmium, lead and copper. The detection limit, after pre-electrolysis for 1 h, was of the order of magnitude 0.1 $\mu g\ l^{-1}$ with the non-computerized instrumentation used in the investigation. The purpose of this paper is to show how computerization of a potentiometric stripping analyzer [13] not only increases the sensitivity of the technique but eliminates the necessity for deoxygenation of the sample. All samples analyzed were taken from the Arctic area and great care was taken to avoid contamination during sampling and subsequent analysis.

EXPERIMENTAL

Chemicals

Stock solutions (1 g l^{-1}) of zinc(II), cadmium(II), lead(II) and copper(II) were prepared from Merck Titrisol ampoules. The gallium(III) solution was prepared by dissolving gallium(III) nitrate in 2 M acetic acid to a total concentration of 1 g l^{-1}. The mineral acids used were either of Merck Suprapur grade or purified by sub-boiling distillation. The water used for diluting the stock standard solutions was purified in a Milli-Q (Millipore Co.) system.

Instrumentation and apparatus

A commercial instrument for potentiometric stripping analysis (Radiometer ISS820) [14] was used in combination with a laboratory-constructed microcomputer system [13]. In some experiments, the 8-bit Intel 8085 microprocessor used in the microcomputer system [13] was exchanged for a 16-bit Intel 8086 processor. This increased the sampling rate from approximately 30 kHz to 60 kHz [15].

Electrodes and electrochemical cell. A titration unit (Radiometer TTA80), equipped with a 35-ml polyethylene cell, was used as electrochemical cell. In some experiments, the sample was stirred mechanically by means of the three-edged teflon stirrer which is part of the TTA80 unit, while in some experiments the glassy-carbon working electrode was rotated at a constant rate of approximately 2400 rpm by the electric motor in the TTA80 unit. When the sample was stirred, a stationary glassy-carbon electrode with a total surface area of 8 mm^2 was used as working electrode (Radiometer F3500). The rotated glassy-carbon electrode was manufactured by pressure-fitting a 10-mm glassy-carbon rod (3.1-mm diameter) excentrically into a 120-mm teflon rod (12-mm diameter); the center of the glassy-carbon rod was placed 3 mm from the center of the teflon rod. The platinum counter electrode normally used in potentiometric stripping experiments [11] was replaced by a 100-mm glassy-carbon rod (3.1-mm diameter). The reason for this was that the glass rod, into which the platinum foil was sealed, leaked lead when immersed in acidic solutions. This leakage was small and insignificant for all kinds of samples except ocean water. The calomel electrode normally used in potentiometric stripping experiments was replaced by a double-junction silver/silver chloride electrode (Orion), the outer electrode compartment being filled with sea water. The calomel electrode was not used because the saturated potassium chloride solution contained lead(II) which leaked slowly from the electrode. Filling the calomel electrode with sea water instead of saturated potassium chloride is not recommended, owing to the high bromide concentration in sea water.

Sampling

All samples analyzed were taken from the Arctic Sea during the Swedish expedition YMER 80 in July 1980. The samples were collected with a teflon-coated GO-FLO (General Oceanic, Florida) sampler. Immediately

after sampling, the samples were acidified with nitric acid to a total concentration of 0.015 M and stored in polyethylene or teflon bottles. These bottles had been cleaned by immersing in 6 M hydrochloric acid at 60°C for one week, washed with Milli-Q-purified water and then immersed in 7.5 M nitric acid at 60°C for another week. Finally the bottles were cleaned with purified water and immersed in 0.015 M nitric acid at room temperature for one week. The samples were stored for about two months prior to the measurements. The analyses were done in a Clean Room Laboratory (U.S. Government Class 100 room).

Potentiometric stripping analysis for cadmium(II) and lead(II)

Mercury(II) nitrate was added to the acidified sea water to give a total concentration of 20 mg l^{-1}. For the extremely low concentration range, the samples were pre-electrolyzed for 32 min at −1.10 V vs. Ag/AgCl prior to the recording of the stripping curve. The cadmium and lead concentrations were evaluated by means of standard additions. If several samples were to be analyzed, however, it was not necessary to make standard additions to each sample, because sea water is an invariant matrix and the sensitivity for cadmium and lead is the same in all samples. Consequently, the first standard addition plot can be used as a calibration curve for the subsequent samples. In such cases, it is recommended that the old mercury film be removed after 2—3 h of pre-electrolysis and a new mercury film allowed to grow on the glassy-carbon surface. Although the mercury film thickness does not affect the length of the stripping plateaux, a very thick film gives less well-defined stripping plateaux.

At higher lead concentrations, i.e. concentrations above approximately 0.25 nM, pre-electrolysis times of less than 32 min can be used. In such cases, however, it was necessary to pre-coat the glassy-carbon electrode with a mercury film by means of a 2-min pre-electrolysis/stripping cycle. If the glassy-carbon electrode had been mercury pre-coated in a previous sample, the pre-electrolysis/stripping cycle for pre-coating could be omitted. Mercury films should not be used for periods longer than 3 h of pre-electrolysis.

Potentiometric stripping analysis for zinc(II)

Gallium(III) was added to the acidified sea-water sample to give a total concentration equal to about 10 μg l^{-1} and mercury(II) to a total concentration equal to 20 mg l^{-1}. The pre-electrolysis potential was adjusted to −1.4 V vs. Ag/AgCl and the sample was pre-electrolyzed for 4 min in order to coat the working electrode with the mercury film. The pre-electrolysis time was adjusted to 16 min and a pre-electrolysis/stripping cycle was made. A standard aliquot of zinc(II) was added and the pre-electrolysis/stripping cycle was repeated. The zinc(II) concentration was evaluated by means of the usual equations for standard addition.

Gallium(III) was added in order to suppress the formation of the zinc—copper intermetallic compound in the mercury film; the gallium—copper

bonding is stronger than the zinc—copper bonding [16]. It is thus necessary to have an excess of gallium in the mercury film. In such cases, a gallium stripping plateau will appear during stripping; if this plateau is absent, more gallium(III) must be added in order to obtain correct zinc(II) values. The gallium(III) concentration necessary to obtain a gallium stripping plateau varies from one sea water sample to another, probably owing to different concentrations of organic matter which may mask the gallium(III) ions. A gallium(III) concentration of 10 $\mu g\ l^{-1}$ was sufficient for all samples.

Between samples, the mercury film was wiped off and the glassy-carbon electrode rinsed with 2 M hydrochloric acid.

Potentiometric stripping analysis for copper(II)

Mercury(II) was added to the acidified sea water to a total concentration of 20 mg l^{-1} and the pre-electrolysis potential was adjusted to −0.7 V vs. Ag/AgCl. A mercury film was precoated by pre-electrolyzing for 4 min. A new pre-electrolysis/stripping cycle was started immediately after the stripping was completed. It is important that the working electrode be not left in the sample containing mercury(II) for more than 5 s without a reducing potential applied on it. After 5 s, the calomel formed on the electrode surface affected the copper signal much more than it affected the other signals. A standard aliquot of copper(II) was added and the copper(II) concentration evaluated by means of the standard addition equations.

Atomic absorption procedure for zinc(II), cadmium(II), lead(II) and copper(II)

The atomic absorption method used for trace metal determinations in sea water has been described in detail by Danielsson et al. [17]. The main features of the procedure were buffering of the acidified sea water with acetate to pH 4.5 and solvent extraction into freon using carbamates as extraction reagents. Finally, these trace metals were back-extracted into diluted nitric acid and determined by the heated graphite atomizer technique.

Determination of zinc(II), cadmium(II), lead(II) and copper(II) in the reagents

The trace metal analyte concentrations in the reagents were determined in the same way as for the sea-water samples, the sea water being replaced by Milli-Q purified water. In the potentiometric stripping techniques, the purified water was made 0.2 M in hydrochloric acid, to obtain a suitable chloride concentration.

The reagent blank concentrations of copper(II), cadmium(II) and lead(II) were found to be negligible. The reagent blank for zinc(II) corresponded to a sea-water concentration of 1.4 nM, mainly because of the zinc(II) content of the mercury(II) nitrate solution.

RESULTS AND DISCUSSION

Shape of potentiometric stripping curves in sea water

Figure 1 shows the potentiometric stripping curves for lead and cadmium recorded after pre-electrolysis for 4 min in a contaminated sea-water sample containing 4.1 nM cadmium(II) (0.46 $\mu g\ l^{-1}$) and 3.1 nM lead(II) (0.64 $\mu g\ l^{-1}$). The stripping curve recorded under the same experimental conditions after standard additions of cadmium(II) and lead(II) is also shown (curve b). Figure 2 (curve a) shows the stripping curve recorded after pre-electrolysis for 32 min for a sea-water sample containing 0.13 nM cadmium(II) and 0.32 nM lead(II); curve (b) was recorded after standard additions of 0.9 nM cadmium(II) and 0.48 nM lead(II).

Figure 3 (curve a) shows the potentiometric stripping curve for zinc recorded after pre-electrolysis for 8 min at —1.4 V vs. Ag/AgCl in an acidified sea-water sample containing 10 nM zinc(II); curve (b) was recorded under the same experimental conditions after the standard addition of 7.6 nM zinc(II).

Concentrations of zinc(II), cadmium(II) and lead(II) in Arctic Sea samples

Table 1 shows the zinc(II), cadmium(II) and lead(II) values determined by potentiometric stripping analysis and solvent extraction/atomic absorption in eight different samples drawn from different depths in the Arctic Sea area. A full report on all samples analyzed with specification of depth, position and different physicochemical parameters will be given elsewhere [18].

Considering the very low levels, the concentrations obtained by the two

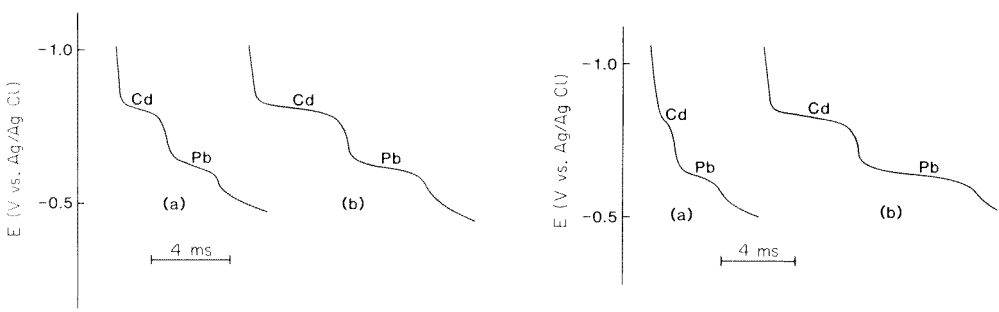

Fig. 1. Potentiometric stripping curves recorded after 4 min of pre-electrolysis at —1.10 V vs. Ag/AgCl. (a) A sea-water sample containing 4.1 nM cadmium(II) and 3.1 nM lead(II). (b) The same sample treated under the same experimental conditions after the standard addition of 4.5 nM cadmium(II) and 2.5 nM lead(II).

Fig. 2. Potentiometric stripping curves recorded after 32 min of pre-electrolysis at —1.10 V vs. Ag/AgCl. (a) A sea-water sample containing 0.13 nM cadmium(II) and 0.32 nM lead(II). (b) The same sample treated under the same experimental conditions after the addition of 0.90 nM cadmium(II) and 0.48 nM lead(II).

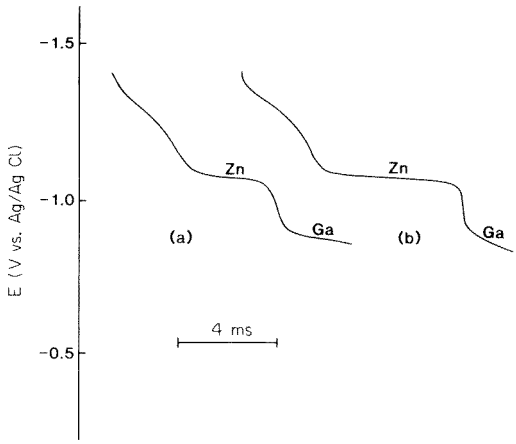

Fig. 3. Potentiometric stripping curves recorded after 8 min of pre-electrolysis at −1.40 V vs. Ag/AgCl. (a) A sea-water sample containing 10 nM zinc(II). (b) The same sample treated under the same experimental conditions after the addition of 7.2 nM zinc(II).

TABLE 1

Results obtained from eight different Arctic Sea water samples obtained by potentiometric stripping analysis (p.s.a.) and solvent extraction/atomic absorption spectrometry (a.a.s.)
(The zinc values were corrected for the reagent blank. In the determination of cadmium(II) and lead(II), some samples were pre-electrolyzed for 64 min at −1.10 V vs. Ag/AgCl.)

Sample no.	Zinc				Cadmium				Lead			
	P.s.a.		A.a.s.		P.s.a.		A.a.s.		P.s.a.		A.a.s.	
	(nM)	(ng l^{-1})	(nM)	(ng l^{-1})	(nM)	(ng l^{-1})	(nM)	(ng l^{-1})	(nM)	(ng l^{-1})	(nM)	(ng l
1	0.8	50	1.5	100	0.10	11	0.12	14	0.10	20	>0.25	>50[a]
2	2.0	130	1.2	76	0.09	10	0.13	15	0.05	10	0.06	13
3	2.6	170	1.0	64	0.13	15	0.14	16	0.05	10	0.06	13
4	1.8	120	1.0	61	0.10	11	0.14	16	0.07	14	0.08	16
5	1.5	100	1.5	95	0.18	20	0.17	19	0.07	14	0.08	16
6	1.5	100	1.5	100	0.13	15	0.16	18	0.12	25	0.11	22
7	5.2	340	3.0	200	0.18	20	0.18	20	>0.5	>100[a]	0.11	23
8	4.7	310	4.2	270	0.40	45	0.21	23	0.24	50	0.14	28

[a]See text.

different analytical techniques agree satisfactorily for cadmium and lead. Obviously sample no. 1 was contaminated with lead during the a.a.s. determination and sample no. 7 during the potentiometric stripping determination. The zinc values in Table 1 agree less satisfactorily, indicating a random source of zinc contamination.

Comments on the copper(II) determination

The concentration of copper(II) in ocean water is of the order of 2 nM or less. It has been shown previously [12] that potentiometric stripping can be used for the determination of copper(II) in coastal sea-water samples where the copper(II) concentration often exceeds 20 nM. In a normal laboratory environment, it is in fact almost impossible to prepare standard solutions containing less than 20 nM of copper(II). For this reason, potentiometric stripping for copper(II) in the very low concentration range below 10 nM had not been attempted previously. Analysis of the ocean-water samples showed that the copper stripping plateaux obtained after pre-electrolysis for 8 or 16 min at −0.7 V vs. Ag/AgCl were either non-existent or rather irreproducible. This might be due to calomel formation on the working electrode surface or to an intermetallic compound formed between copper and, for example, nickel. Obviously these aspects have to be studied in more detail. It can, however, be concluded that computerized potentiometric stripping analysis can be used for the determination of copper(II) in sea-water samples at concentrations above 20 nM; a pre-electrolysis time of 4 min is then sufficient.

Accuracy, precision and detection limits

The accuracy of the results listed in Table 1 depends on the contamination during sampling, sample pre-treatment and measurements. It is obvious from Table 1 that the results obtained for cadmium agree better than the results for lead and zinc. This is no doubt due to the well-known fact that contamination by cadmium is less likely than contamination by lead and zinc. Considering the low analyte concentrations and the presence of random contamination, however, the agreement between the potentiometric stripping results and the solvent extraction/atomic absorption results is quite satisfactory for the three elements in Table 1.

The overall precision in the computerized potentiometric stripping method was estimated by repetitive analysis of five subsamples originating from the same sample of sea water. In order to determine the precision at elevated concentrations, five sea-water subsamples were spiked with 0.25 nM of cadmium(II) and lead(II) prior to repetitive analysis. The estimated precisions are shown in Table 2. As normally happens, the relative standard deviations depend on the total concentrations of the trace metal. At concentrations above 4 nM, the relative standard deviations for cadmium and lead are better than 5%.

The detection limits in potentiometric stripping analysis are inversely proportional to the pre-electrolysis time. The detection limits for cadmium(II) and lead(II) after 32 min of pre-electrolysis can be estimated from Fig. 2 to be about 0.04 nM and 0.06 nM, respectively. The detection limit for zinc(II) after 16 min can be estimated from Fig. 3 to be approximately 0.25 nM.

The detection limit in computerized potentiometric stripping analysis is also set by the graphical display procedure. In order to obtain a measurable

TABLE 2

Estimated precisions in potentiometric stripping analyses for zinc(II), cadmium(II) and lead(II) in sea water

Element	Concentration range (nM)	Pre-electrolysis time (min)	Estimated relative standard deviation (%)
Zn	1.5—5	16	10
Cd	0.1—0.3	32	25
Cd	0.6—2.0	16	10
Pb	0.05—0.25	32	35
Pb	0.25—2	16	10

stripping plateau, the length of this plateau must be 1—2 mm. In future, the lengths of the stripping plateaux will be evaluated digitally. Preliminary experiments indicate that this will decrease the detection limit by a factor 2 to 4 compared with the graphical evaluation method.

Comparison between computerized potentiometric stripping and the anodic stripping techniques

Its high salt content and its low content of organic matter makes ocean water an ideal matrix for anodic stripping voltammetry. The major advantage of the computerized potentiometric stripping technique compared to the anodic stripping techniques is that potentiometric stripping is much less sensitive to the presence of organic matter and oxidizing agents. On that basis, the two techniques ought to show equal performance in sea-water analysis [19]. Unfortunately, most of the results reported for the trace metal concentrations in sea waters by anodic stripping techniques seem to be far too high. The most reliable values reported hitherto appear to be those of Mart [20]. From his report, differential pulse anodic stripping voltammetry, operated under optimum experimental conditions, would seem to yield a slightly higher sensitivity than computerized potentiometric stripping. From a practical point of view, however, computerized potentiometric stripping analysis has several advantages over differential pulse anodic stripping voltammetry. The fact that the samples do not have to be de-oxygenated is a major advantage; this not only decreases the total time needed for analysis but also eliminates a possible source of contamination. Furthermore, in potentiometric stripping, the working electrode is rotated at constant rate both during pre-electrolysis and stripping; this means that the "settling period" after pre-electrolysis and before recording of the stripping curve, which is necessary in anodic stripping voltammetry, is eliminated. Rotation of the working electrode during stripping also means that the potentiometric stripping technique is not sensitive to vibrations, which is of particular importance for work on-board ship. During the YMER 80 expedition, it proved possible to use the potentiometric stripping analyzer even during the

severe vibrations caused when the ice-breaker passed through ice. Another consequence of rotation of the working electrode during stripping is that the stripping curve is recorded during a few milliseconds, whereas recording a differential pulse anodic stripping voltammogram under optimum conditions takes several minutes. The above-mentioned advantages of the computerized potentiometric stripping method are particularly important when coastal sea waters are to be analyzed and extremely low concentrations are not sought.

REFERENCES

1 G. Macchi, J. Electroanal. Chem., 9 (1965) 290.
2 L. Mart, Fresenius Z. Anal. Chem., 296 (1969) 350.
3 A. Zirino and M. L. Healy, Limnol. Oceanogr., 16 (1971) 773.
4 K. Kremling, Kiel. Meeresforsch., 28 (1973) 77.
5 G. E. Batley and T. M. Florence, Mar. Chem., 4 (1976) 347.
6 W. Lund and D. Onshus, Anal. Chim. Acta, 86 (1976) 109.
7 C. Duinker and C. J. M. Kramer, Mar. Chem., 5 (1977) 208.
8 K. Kremling and H. Petersen, Meteor Forschungsergeb., Reihe A, 19 (1977) 10.
9 K. Kremling and H. Petersen, Mar. Chem., 6 (1978) 155.
10 D. Jagner and K. Årén, Anal. Chim. Acta, 100 (1978) 375.
11 D. Jagner, Anal. Chem., 50 (1978) 1924; 51 (1979) 342.
12 D. Jagner and K. Årén, Anal. Chim. Acta, 107 (1979) 29.
13 A. Granéli, D. Jagner and M. Josefson, Anal. Chem., 52 (1980) 2220.
14 A. M. Graabaek and O. J. Jensen, Ind. Res. Dev., 21 (1979) 124.
15 D. Jagner and M. Josefson, to be published.
16 T. R. Copeland, R. A. Osteryoung and R. K. Skogerboe, Anal. Chem., 46 (1974) 2093.
17 L. G. Danielsson, B. Magnusson and S. Westerlund, Anal. Chim. Acta, 98 (1978) 47.
18 L. G. Danielsson and S. Westerlund, to be published.
19 L. G. Danielsson, D. Jagner, M. Josefson and S. Westerlund, Anal. Chim. Acta, 127 (1981) 147.
20 L. Mart, Thesis, Institut für Angewandte physikalische Chemie, Kernforschungsanlage Jülich, BRD, 1979.

Analytica Chimica Acta, 129 (1981) 163—174
Elsevier Scientific Publishing Company, Amsterdam — Printed in The Netherlands

DETECTION OF TOLUENE DIISOCYANATE IN AIR WITH A COATED PIEZOELECTRIC CRYSTAL
Part 1. A Study of Coating Materials

J. F. ALDER*[a] and C. A. ISAAC[b]

Department of Chemistry, Imperial College of Science and Technology, London SW7 2AY (Gt. Britain)

(Received 10th March 1981)

SUMMARY

A method for the detection of toluene diisocyanate vapour down to its threshold limit value (0.02 ppm) is presented; the sorption of the vapour onto a piezoelectric quartz crystal coated with polyethylene glycol is utilized. The resulting change in weight of the crystal is monitored by the associated change in the oscillation frequency. An investigation into the nature of the sorption process is described, and different coatings and chemical modifications to the PEG to minimize the effect of water vapour are indicated.

The use of quartz piezoelectric crystals as mass detectors has been known for many years. In 1959, Sauerbrey [1] showed that the change in the resonant frequency resulting from the deposition of a thin uniform film of any foreign substance would be equal to that resulting from a layer of quartz of the same mass. Thus, Sauerbrey obtained the general equation $\Delta F/F = \Delta M_s F/A\rho N$, where F is the fundamental frequency, ΔF the change in frequency caused by the added mass, ΔM_s the mass of film of any substances coated on the quartz plate, A the area of the quartz plate, ρ the density of the quartz plate, and N is the frequency constant of the crystal.

This effect has been exploited by numerous workers to measure gas adsorption [2, 3], relative atmospheric humidity [4] and deposited film thickness [5], and to develop detectors in gas chromatography [6, 7] and atmospheric pollutant monitors [8—10]. In toxic gas detection, a crystal is made the frequency-determining element of an oscillating circuit and the change in frequency caused by the adsorption of the analyte gas is measured. The analyser circuitry can be made very compact and the whole unit portable. The sensitivity is good, and the theoretical detection limit is of the order of 10^{-12} g [11]. King [6] estimated that detection limits of 10^{-9} g could be realised in practice.

[a]Present address: Department of Instrumentation and Analytical Science, U.M.I.S.T., P.O. Box 88, Manchester M60 1QD, Gt. Britain.
[b]Present address: Burroughs Machines, Ltd., Astronaut House, Hounslow Road, Feltham, Middlesex TW14 9AE, Gt. Britain.

0003—2670/81/0000—0000/$02.50

One possible disadvantage of this method lies in its lack of selectivity: any gas which is adsorbed will cause a mass change and hence a response. Selectivity has to be introduced either by previous separation or by a selective physical or chemical discrimination on the crystal surface. Various chemical coatings have been used in attempts to impart chemical selectivity to the adsorption process [4]. For the detection of acidic gases, basic coatings have been employed (e.g., sulphur dioxide via triethanolamine, TEA) [12] and vice versa (e.g. ammonia with ascorbic acid) [9].

Another problem that sometimes arises is the loss of coating by evaporation (bleeding) from the crystal surface. This results in a baseline drift and loss of adsorber. Consequently the response characteristics such as sensitivity may be altered. Ideally a non-volatile coating should be used, but methods of stabilizing coatings have been tried with various degrees of success. Cheney and Homolya [8] investigated two possibilities for their sulphur dioxide detector: in the first, a solid solution of tri-isopropanolamine in TEA was used in an effort to reduce the vapour pressure of TEA, but this led to an unacceptable drop in sensitivity; the second involved spraying a thin layer of teflon over the TEA coating as teflon membranes are known to be permeable to sulphur dioxide. However, the coatings achieved were not uniform enough to stop bleeding. Another solution would be to have the coating chemically bonded to the electrode surface, e.g., by oxidation of the metal electrode or of another metal that has been electrodeposited onto the electrode, as suggested earlier [6].

It is these problems which have delayed the practical application of piezoelectric crystals as portable atmospheric gas detectors. There are situations, however, where the lack of selectivity of the detector is not a major drawback, i.e., where the presence of the contaminant gas is known and no or few other gases are present. Such a situation occurs when tanks (e.g., on board chemical-carrying ships) containing a known toxic compound are being cleaned prior to loading with another product or before the crew may enter. The only other gases present will then be atmospheric water vapour, air and the cleaning agent. In such situations, it is likely that an accurate gas analysis will not be required but only an indication of the concentration level with respect to the threshold limit value (TLV) or ceiling value [13]. The intrinsic properties of continuous and rapid response make the crystal detector almost ideal for such monitoring situations.

Toluene diisocyanate is used in large quantities in the polyurethane foam industry [14], the basic urethane polymer being formed by reaction with a polyhydric alcohol. Toluene diisocyanate is a colourless liquid (b.p. 120°C at 10 mm Hg [13], vapour pressure 0.023 mm Hg at 20°C). It is also very toxic, being a strong respiratory irritant and lachrymator, and prolonged inhalation causes symptoms resembling asthma, with sensitization of some individuals occurring on even a brief exposure. For these reasons, the detection of the vapour at low levels (TLV = 0.02 ppm, 0.14 mg m^{-3}) is important for personal protection.

The present methods employed for detection of toluene diisocyanate are as follows. Gas detection tubes are used, in which contaminated air is drawn through a glass tube containing a specific reagent, and the concentration is estimated by using colour comparison tubes. The whole analysis takes about 30 min and requires operator attention and some skill. Paper-tape devices have been employed, in which the contaminated air is aspirated through a chemically-impregnated paper tape which is moved continuously past a photometric reflectance detector in a self-contained purpose-built instrument. The intensity of the colour stain arising from reaction with toluene diisocyanate gives a signal proportional to the level of the pollutant in the atmosphere. These devices give precise and accurate results [15] and are well suited to continuous monitoring of working environments; they require little attention and minimal skill, but they are somewhat bulky and have been designed less for immediate personal protection than as a monitor for estimating exposure during a working day. Another problem is that the tapes have a shelf life of only a few weeks. A personally-portable paper-tape monitor has recently been introduced (MDA Scientific (UK) Ltd.): the small sampling head contains the tape advance and optical system and the microprocessor controller provides an output of toxic gas concentration (including organic isocyanates) in digital form every 90 s.

In the Marcali method the air sample (typically 5—20 l) is bubbled through an acidic absorbing solution. Toluene diisocyanate is hydrolysed to the diamine, subsequently diazotized, and finally coupled to *N*-1-naphthylethylenediamine, which produces a pink solution which can be compared visually with calibrated reference solutions, or the absorbance can be measured at 550 nm [16]. Analysis time is typically 30 min and the detection limit is 0.02 ppm (though this can be increased by increasing the volume sampled). The main drawback is the need for a fairly skilled operator as the results obtained are very prone to human error.

The work described in this paper is the development of a piezoelectric crystal detector for toluene diisocyanate with a view to its use as a portable monitor for personal protection, giving a continuous readout with minimal operator attention and skill. There are particular problems associated with the determination of toluene diisocyanate in air. Although toluene diisocyanate appears to be quite stable in the vapour phase, even in atmospheres of high humidity, as soon as it comes in contact with surfaces it is rapidly and firmly adsorbed, and is even chemisorbed with subsequent hydrolysis. Transfer of the air sample to the detector cell has therefore to be carried out with minimal sampling tube length and as small a ratio of wall area to gas volume as possible. It is also not practical to undertake any pre-filtering to remove water vapour without major loss of toluene diisocyanate. The generation of standard atmospheres to calibrate the equipment against other methods is also hampered by this effect.

EXPERIMENTAL

The coated piezoelectric crystals used were made part of a 10-MHz TTL oscillator, the frequency of which was measured by a Racal Model 9905 counter-timer. The last three digits of the frequency count could be fed to a chart recorder as an analog signal, or the total output fed to a home-built microprocessor based on the SC/MP II chip, which converted the data to a different format and stored it on paper tape directly. This tape could then be processed off-line on a CDC 6500 or CYBER 174 computer.

All the crystals employed were AT-cut in the range 9.7—10.1 MHz with gold electrodes in HC6/U holders (Quartz Crystal Co., New Malden, Surrey; Senator Crystals, London).

Several methods for coating the crystals were investigated: dropping the material from a microsyringe, spraying the coating through a mask, evaporation of the material under vacuum, and smearing onto the electrode with cotton swabs. In all but the vacuum-coating technique any solid samples were first dissolved in a volatile solvent, usually acetone, before application. The amount of coating was determined by the accompanying frequency change on application. This was kept within the range 1—10 kHz, as thicker coatings showed no increase in sensitivity.

Test gas mixtures in air were prepared by the diffusion cell method devised by Neilson and Booth [17] or by diluting with air a previously saturated stream of toluene diisocyanate. The test gas mixtures were analysed by the Marcali method [16] or a more recent modification [18], to give a time-averaged concentration of toluene diisocyanate. The gas stream was first passed through the detector cell and then immediately bubbled through the absorber used in the Marcali method, with the minimum amount of glassware between the inlet point and the detector cell to overcome the severe adsorption problem.

Infrared spectra were measured on a Perkin-Elmer 157 spectrometer, with a 10-cm gas cell (sodium chloride windows), the test atmospheres being generated as before.

INVESTIGATION OF CRYSTAL COATINGS

Although toluene diisocyanate is adsorbed onto the gold and quartz of an uncoated crystal, neither the sensitivity nor the reproducibility is good. As the aim of this work was to produce a monitor for personal protection, the coating would have to be useful in continuous operation for several hours, stable in storage for a period of months and unaffected by the ambient conditions. In use the coating should preferably behave reversibly to toluene diisocyanate, otherwise the response of the coating would change as its reactive sites were used up. Also, if continuous measurements are being made and the level of toluene diisocyanate decreases quickly, an artificially high result may be obtained. A certain amount of irreversibility can be tolerated

if the coating still reacts in a reproducible manner even after a number of exposures. This irreversibility may also be used to some advantage if the extent of non-recovery of baseline is proportional to the total amount of toluene diisocyanate that has passed over the crystal coating, thus acting as a form of integrator. The very reactive nature of toluene diisocyanate, not only with water, but with the crystal coating and with itself under certain circumstances, means that this permanent adsorption will be noticeable at higher concentrations of toluene diisocyanate with nearly every coating that may be used. The coating chosen was therefore a compromise between stability, bleed rate, sensitivity and reversibility. Table 1 shows the relative responses and stability of a number of compounds tested as coatings. Polyethylene glycol was chosen for further investigation as the phthalates, which gave greater responses, were found to bleed off the crystal surface at an unacceptable rate.

Polyethylene glycol with an average molecular weight of 400 (PEG 400) was found to give the most sensitive performance (Fig. 1). It was best applied by smearing the neat liquid over the whole of the gold electrode surface with a cotton swab. A freshly coated crystal was found to have a far greater response to toluene diisocyanate than an exposed coating. Figure 2 shows the change in response each time the same coated crystal was exposed to about 10 ppm of toluene diisocyanate for 5 min and then allowed to recover for 1 h in pure air passed at 50 cm^3 min^{-1}. The dashed line at 50 Hz/ppm indicates the value that corresponds to the minimum measurable response of 1 Hz at the TLV of 0.02 ppm. A fresh coating therefore gives a theoretical limit of detection just below the TLV. This degrades after about three exposures to a plateau sensitivity giving a detection limit of about twice the TLV.

In order to determine the type of reaction that occurs between toluene diisocyanate and PEG 400, i.r. spectra were obtained under various conditions (Fig. 3). Spectrum A shows pure PEG 400; the peak at 3450 cm^{-1} corresponds to free OH groups [19], that at 2900 cm^{-1} corresponds to CH_2, and the broader peak at 1485 cm^{-1} is probably a mixture of an OH deformation and an $(RO)CH_2$ deformation. These peaks are consistent with the accepted structure of PEG 400.

TABLE 1

Response of compounds tested and stability

Compound	Response[a]	Bleed rate	Compound	Response[a]	Bleed rate
Polyethylene glycol	3.8	V. slow	*o*-Phenylenediamine	1.1	Slow
Benzylamine	1.8	Medium	Resorcinol	1.9	Slow
Piperidine	0.0	Fast	Dinonyl phthalate	7.4	Medium
m-Phenetidine	1.4	Fast	Diethyl phthalate	8.7	Fast

[a]Height of the peak at 2270 cm^{-1} (NCO asymmetric stretch) when the compound under test was exposed to 10 ppm toluene diisocyanate for 30 min in an i.r. gas cell.

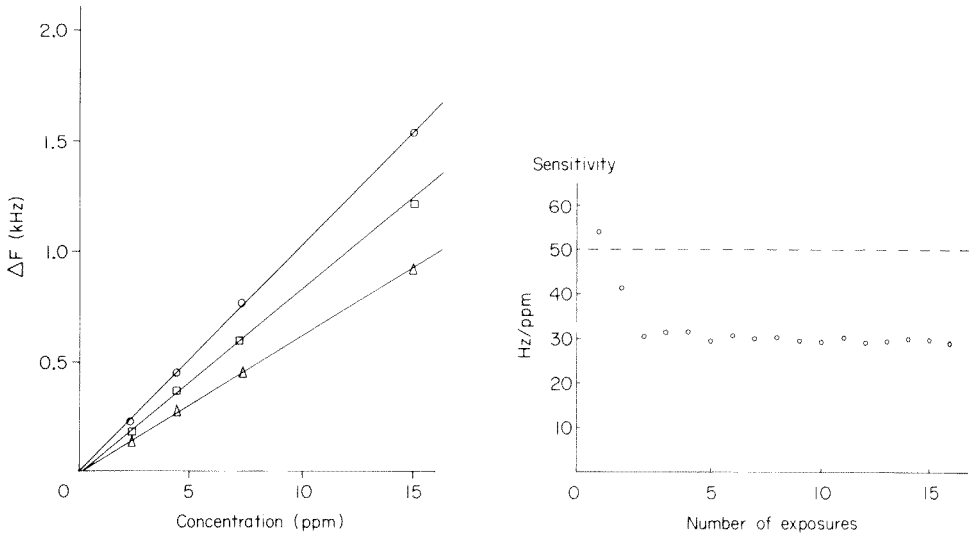

Fig. 1. Graph of concentration of toluene diisocyanate vs. frequency change for polyethylene glycol coatings of molecular weight: (○) 400; (□) 600; (△) 1000.

Fig. 2. Plot of change in response of a PEG 400-coated crystal to successive exposures of toluene diisocyanate.

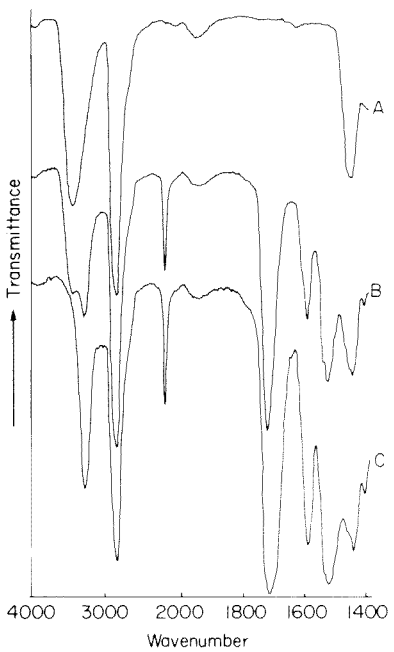

Fig. 3. Infrared spectrum of PEG 400 under different conditions. (See text for details.)

When toluene diisocyanate vapour was allowed to react with the PEG 400 surface in the gas cell, spectrum B was obtained after about 15 min. The peak at 3450 cm^{-1} was decreased in intensity and a new peak appeared at 3250 cm^{-1} which corresponds to the N—H stretch. A new peak also appeared at 2270 cm^{-1} which corresponds to the NCO asymmetric stretch and another appeared at 1725 cm^{-1} corresponding to the C=O stretch in a urethane-type structure. Peaks at 1600 cm^{-1} correspond to aromatic ring vibrations, and the one at 1530 cm^{-1} to CNH stretching.

Spectrum C shows the effect of continued exposure to toluene diisocyanate; after about 4 h all the new bands that had appeared increased in intensity and the band at 3450 cm^{-1} disappeared completely. Also, the band at 1425 cm^{-1} was narrower. All these changes point to the same reaction that occurs in the liquid bulk phase [14]

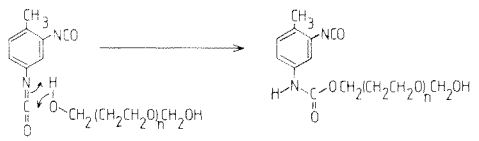

There is rapid physical adsorption, which is fairly readily reversible, followed by a fast reaction of toluene diisocyanate with the hydroxyl groups, not readily reversible at room temperature. Once these groups have reacted, the much slower reaction of toluene diisocyanate with the —NH groups formed becomes dominant, giving further substituted urethanes. This would account for both the semi-reversible nature of the reaction between toluene diisocyanate and PEG 400 and the fact that PEG 400 is more reactive than the other higher-molecular-weight polymers which have fewer hydroxyl groups per unit mass.

Neat PEG 400, if left unexposed to toluene diisocyanate on a crystal that is mounted in a vertical position, is prone to "creep" down the face of the crystal. This does not occur once the coating has been exposed to toluene diisocyanate, probably because cross-linking of the long chains in PEG 400 occurs, thus increasing its viscosity. This "creeping" can also be lessened by heating a freshly coated crystal in a horizontal position in an oven at 80°C for 1—2 h.

Incorporation of phthalates in a plastic matrix

Dioctyl and dibutyl phthalate are often incorporated as plasticizers in the polymerization of poly(vinyl chloride) (PVC). Incorporating these volatile compounds in a polymeric matrix bestows the dual advantages of an almost negligible bleed rate and the reduction of interference from water, as the plastic is intrinsically hydrophobic. A few plastic sheets were exposed to toluene diisocyanate [20] in a modified liquid i.r. cell and the changes in the spectra were observed. The greatest change was obtained with "Clingfilm", the trade name of a thin PVC sheet believed to contain alkyl phthalates. The feasibility of using this as a coating material was tested by dissolving a

sample in hot tetrahydrofuran and applying it to the faces of the sodium chloride plates in the i.r. gas cell. A strong peak appeared at 2270 cm^{-1} corresponding to the NCO asymmetric stretch. The reversibility of this adsorption was also demonstrated by passing nitrogen through the i.r. cell immediately after the toluene diisocyanate vapour and measuring the decrease in size of the NCO peak. A semiquantitative recovery of 70% was noted when this technique was used.

Chemical modification of PEG coatings

A possible improvement to the reversibility of the chemisorption of toluene diisocyanate was sought through chemical modifications of the PEG. One method of producing a reproducible coating with the modified PEG compound is to produce it in situ by first coating the crystal with PEG 400 and then passing a reactive vapour over the crystal until no more reaction occurs. To test the feasibility of this approach and to see if the irreversible reaction between toluene diisocyanate and the hydroxyl groups can be decreased, a volatile reactant was first tried. Thionyl chloride is a standard chlorinating agent in many organic reactions

$$SOCl_2 + 2ROH \rightarrow 2RCl + HCl + H_2O + SO_2$$

The other products of this reaction are volatile, therefore the resultant coating should consist of just the chlorinated product. The i.r. spectrum produced on exposure of PEG 400 to thionyl chloride (Fig. 4) supports the theory. The broad peak at 3425 cm^{-1} corresponding to terminal hydroxyl groups has disappeared completely and a new peak at 760 cm^{-1} corresponding to a C—Cl stretch is observed. The resultant coating showed a marked response to toluene diisocyanate vapour (Fig. 4) which was reversible. The

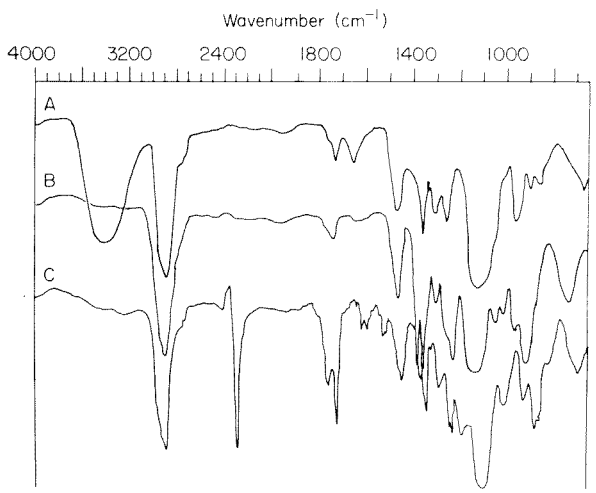

Fig. 4. The i.r. spectrum of polyethylene glycol (A) before and (B) after reaction with thionyl chloride. (C) Modified PEG after exposure to toluene diisocyanate.

replacement of the terminal hydroxyl groups should decrease the response of the coating to water because most water molecules are hydrogen-bonded to these groups.

The chemical modification of a coating in situ appears, therefore, to be feasible when the unwanted by-products are volatile. The reaction of phthaloyl chloride with an alcohol also produces gaseous hydrogen chloride: $Ar(COCl)_2 + 2ROH \rightarrow Ar(COOR)_2 + 2HCl$. The reaction of phthaloyl chloride and PEG 400 could give a coating that responds reversibly and sensitively to toluene diisocyanate with a marked decrease in interference from water. This modification and the response to water vapour are currently being studied.

Studies on water interference

A convenient method of producing an atmosphere of known humidity is to dissolve an excess of different inorganic salts in water. The change in frequency of a PEG 400-coated crystal was observed for the range of humidities shown in Table 2. This was achieved by using a B34 ground-glass cone with sealed-in tungsten rods to allow the crystal to be placed in a humidostat containing the salt solution whilst monitoring the frequency. A dynamic method of creating known atmospheres was devised, to reflect more accurately the conditions in which a monitor would be used. The frequency change obtained by recycling air in a closed system consisting of the detector cell, a gas scrubber filled with one of the salt solutions and a pump, was observed (Fig. 5). The change was compared with results obtained from a dynamic system in which the carrier gas passed through a scrubber containing a salt solution and the detector cell and was subsequently passed to waste.

The results obtained were almost identical in both instances (Fig. 5). They show quite clearly that the sorption of water on PEG 400 occurs in two stages. Below 43% relative humidity, the weight gained approximates to a Langmuir isotherm suggesting the formation of a monolayer which covers the surface of both coating and crystal. Above 43%, the slope increases more rapidly, suggesting multilayer sorption and the formation of regions of

TABLE 2

Relative humidity above saturated solutions of some salts

Salt	Temperature (°C)	Relative humidity (%)	Ref.
$LiCl \cdot H_2O$	25	11	[21]
$CaCl_2 \cdot 6H_2O$	24.5	31	[22]
$K_2CO_3 \cdot 2H_2O$	24.5	43	[22]
$Ca(NO_3)_2 \cdot 4H_2O$	24.5	51	[22]
$NH_4Cl + KNO_3$	25	71	[22]
$(NH_4)_2SO_4$	25	81	[22]

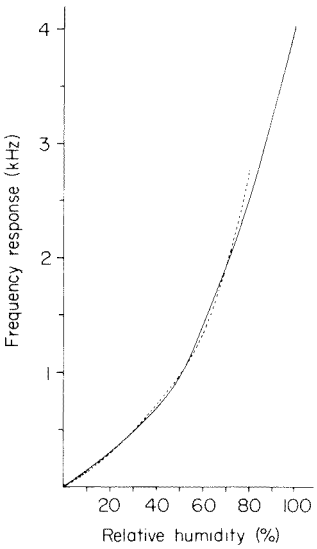

Fig. 5. Response of a polyethylene glycol-coated crystal to a water vapour flow of 1000 cm^3 min^{-1}: (—) closed system; (----) open system.

condensed water vapour and greater penetration of the polymer matrix. The times taken to reach equilibrium at these humidities were much longer (at least 1.5 h), which suggests that a different rate-determining step was involved for sorption. Most of the water is likely to be held in place on the coating by hydrogen bonding to the terminal hydroxyl groups of the PEG. Hydrogen bonding to the ether linkages in PEG is probably less significant in terms of bond strength, although, because of their greater number by a factor of 9 : 2, it probably contributes to the sorption process.

The reproducibility of the response to water vapour was investigated by exposing the coated crystal to an atmosphere of 11% relative humidity generated on four different days. The average frequency change for a flow rate of 300 cm^3 min^{-1} was 94.4 Hz and the standard deviation was 9.7 Hz. Once a monolayer of water had been sorbed, the frequency change does not appear to vary greatly, suggesting that the monolayer may be retained unless more drastic measures are used to remove it.

Silicone coatings

A water repellent (Repelcote; Hopkin and Williams) which consists of a solution of dimethyldichlorosilane in trichlorethane was tested as a coating material. It is normally applied to glass surfaces, the —SiOH groups in the glass being changed to $-SiOSi(CH_3)_2$. The solution was applied to the cleaned surface of the gold electrodes and subsequently hydrolysed by passing water-saturated air over the crystal for 1 h. Bleeding does not occur from glass surfaces because the molecules are bound to the glass, but on the gold surface a frequency drift of 2 Hz min^{-1} was observed at a flow rate of

150 cm^{-3} min^{-1}. When exposed to toluene diisocyanate (10 ppm) and water (90% relative humidity) (Figs. 6 and 7), the response to water was observed to drop about 9-fold compared with PEG 400. Unfortunately the response to toluene diisocyanate decreased about 4-fold. The use of neat Repelcote as a coating material was not considered further at the time because of the low sensitivity. It may, however, be useful to silanize a reactive coating in situ thereby increasing the reversibility of any toluene diisocyanate adsorption and minimizing the effect of water vapour.

Conclusions

PEG 400 has proved to be very useful in studying the nature of toluene diisocyanate adsorption onto the coated crystals and is a useful adsorbing medium for the determination of toluene diisocyanate in dry atmospheres. It has the advantage of a very low bleed rate, good sensitivity and long-term stability. The adsorption process is partly physical, partly chemisorption. The kinetics of the chemical reaction are slow and it is possible to desorb the major part of the toluene diisocyanate before chemical reaction occurs. Coating lifetime is reasonable, provided that the concentration of toluene diisocyanate measured is low, but sensitivity decreases after major exposures and falls below a useful level. The i.r. studies of the chemisorption/adsorption process of toluene diisocyanate have provided valuable information and indicated the problems associated with the determination of this reactive, water-sensitive compound. The effect of water vapour on PEG is considerable, as would be expected, and this substrate would not be useful as an adsorbent for practical applications where changes in humidity are to be expected. It does, however, provide a useful base material with reactive sites which can be modified chemically to impart a degree of specificity towards toluene diisocyanate and against water.

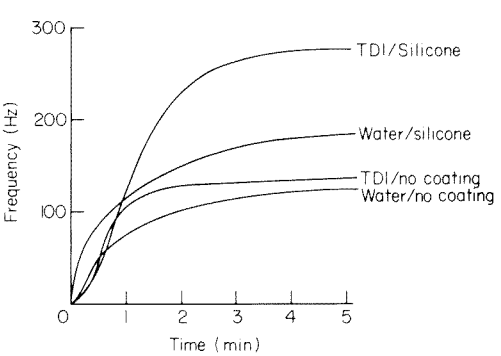

Fig. 6. Comparison of the adsorption of toluene diisocyanate (TDI) and water on silicone-coated and uncoated crystals.

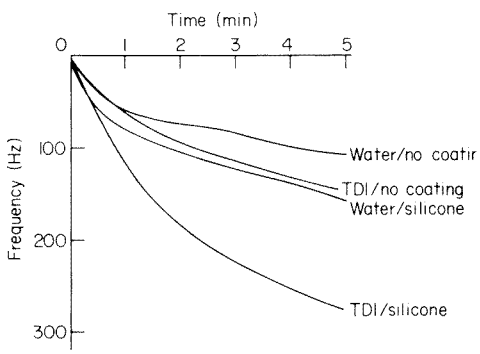

Fig. 7. Comparison of the rates of desorption from silicone-coated and uncoated crystals.

The immobilization of phthaloyl chloride on the PEG coating seems an attractive approach, combining the stability of PEG with the apparent selective adsorption of toluene diisocyanate associated with phthalates.

This work was supported by an S.R.C. CASE award in collaboration with Panocean Anco Limited. The authors are grateful to the Central Research Fund, University of London, for an equipment grant.

REFERENCES

1 G. Z. Sauerbrey, Z Phys., 155 (1959) 206.
2 R. V. Bucur, Rev. Roum. Phys., 19 (1974) 779.
3 L. J. Slutsky and W. H. Wade, J. Chem. Phys., 36 (1962) 2688.
4 J. Hlavay and G. G. Guilbault, Anal. Chem., 49 (1977) 1890.
5 A. W. Werner, Bell System Tech. J., 39 (1960) 1193.
6 W. H. King, Jr., Anal. Chem., 36 (1964) 1735.
7 F. W. Karasek, P. Guy, H. H. Hill and J. M. Tierney, J. Chromatogr., 124 (1976) 179.
8 J. L. Cheney and J. B. Homolya, Sci. Tot. Environ., 5 (1976) 69.
9 L. M. Webber and G. G. Guilbault, Anal. Chem., 48 (1976) 2244.
10 E. P. Scheide and G. G. Guilbault, Anal. Chem., 44 (1972) 1764.
11 A. W. Warner and C. D. Stockbridge, The Measurement of Mass using Quartz Crystal Resonators, Symposium on Vacuum Microbalance Techniques, Los Angeles, 1962.
12 J. L. Cheney and J. B. Homolya, Anal. Lett., 8 (1976) 175.
13 K. Verschueren, Handbook of Environmental Data on Organic Chemicals, Van Nostrand-Reinhold, New York, 1977.
14 K. C. Frisch and J. H. Saunders, Plastic Foams, Part I, M. Dekker, New York, 1972, p. 109.
15 B. A. Denenberg and R. Kriesel, Chemically Impregnated Paper Tapes as a Detection Method in Continuous Personal and Area Monitors, American Industrial Hygiene Conference, Minneapolis, MN, 1975.
16 K. Marcali, Anal. Chem., 29 (1957) 552.
17 A. Neilson and K. S. Booth, Am. Ind. Hyg. Assoc. J., 36 (1975) 169.
18 K. E. Grim and A. L. Linch, Am. Ind. Hyg. Assoc. Qtr., 25 (1964) 285.
19 N. B. Colthup, L. H. Daly and S. E. Wiberley, Introduction to Infrared and Raman Spectroscopy, Academic Press, New York, 1964.
20 C. Fox, Internal Report, Imperial College, 1979.
21 A. Findlay, Practical Physical Chemistry, 9th edn., Longman, London, 1973.
22 R. C. Weast (Ed.), Handbook of Chemistry and Physics, 52nd edn., Chemical Rubber Co., Cleveland, OH, 1971, E40.

Analytica Chimica Acta, 129 (1981) 175—188
Elsevier Scientific Publishing Company, Amsterdam — Printed in The Netherlands

DETECTION OF TOLUENE DIISOCYANATE IN AIR WITH A COATED PIEZOELECTRIC CRYSTAL
Part 2. Development of an Instrumental Method For Personal Monitoring

J. F. ALDER[a] and C. A. ISAAC[b]

Department of Chemistry, Imperial College of Science and Technology, London (Gt. Britain)

(Received 10th March 1981)

SUMMARY

Gases in the atmosphere are monitored with chemically-coated quartz piezoelectric crystals; the method is demonstrated in the use of polyethylene glycol for toluene diisocyanate determination. A microprocessor is used to control the gas sample flow through the detector head as well as the data acquisition. A computer-based procedure for data treatment permits signal integration and background drift correction, resulting in a theoretical detection limit of about 0.006 ppm. The design of a basic portable instrument for piezoelectric crystal monitoring of toxic gas is described with a view to future modification and microprocessor control.

In previous work [1], polyethylene glycol of average molecular weight 400 (PEG 400) was chosen as a model for the study of the adsorption of toluene diisocyanate on a coated piezoelectric crystal. It was recognised that this was not an ideal substrate but it had the attractive features of imparting high sensitivity to the crystal detector whilst having a low bleed rate with resultant baseline stability. The reactive nature of toluene diisocyanate means that chemisorption will occur, to a degree, on any adsorbing medium. Indeed, this diisocyanate self-polymerises on surfaces and is also readily hydrolysed when on a surface in the presence of water vapour.

For personal monitoring, a crystal lifetime of 4—6 h would be acceptable. As the threshold limit value (TLV) and ceiling value for toluene diisocyanate is 0.02 ppm and its saturated vapour pressure is 0.023 mm Hg at 20°C (about 12—15 ppm), the crystal is unlikely to be seriously overloaded, apart from exceptional circumstances, during this working period. The low levels which need to be determined, however, require good sensitivity and baseline stability with high selectivity for toluene diisocyanate and against water vapour; this last criterion is unattainable with PEG. In order to develop the

Present addresses: [a]Department of Instrumentation and Analytical Science, U.M.I.S.T., P.O. Box 88, Manchester M60 1QD, Gt. Britain.
[b]Burroughs Machines Ltd., Astronaut House, Hounslow Road, Feltham, Middlesex TW14 9AE, Gt. Britain.

0003—2670/81/0000—0000/$02.50

instrumentation and investigate the adsorption/desorption processes, however, PEG was retained as it is a well-defined material and the reaction with toluene diisocyanate was reasonably well understood.

The monitor envisaged would have a remote sensing head, which could be used to "sniff" into restricted areas or be attached to the operator's clothing or breathing equipment, and joined to the pump and data handling packs on a belt by a cable and aspiration tube. The readout would be a digital display with a fail-safe audible alarm set to the TLV response which could be remote from, or built into the main pack. These features were borne in mind during the development stage.

DESIGN OF THE INSTRUMENT

Sensing head

The distance between entry port and crystal was kept to a minimum to avoid loss of toluene diisocyanate on the walls and the crystal chamber was protected from draughts and particulate matter by a fine copper gauze across the inlet. The head (Fig. 1) was machined from teflon, the internal

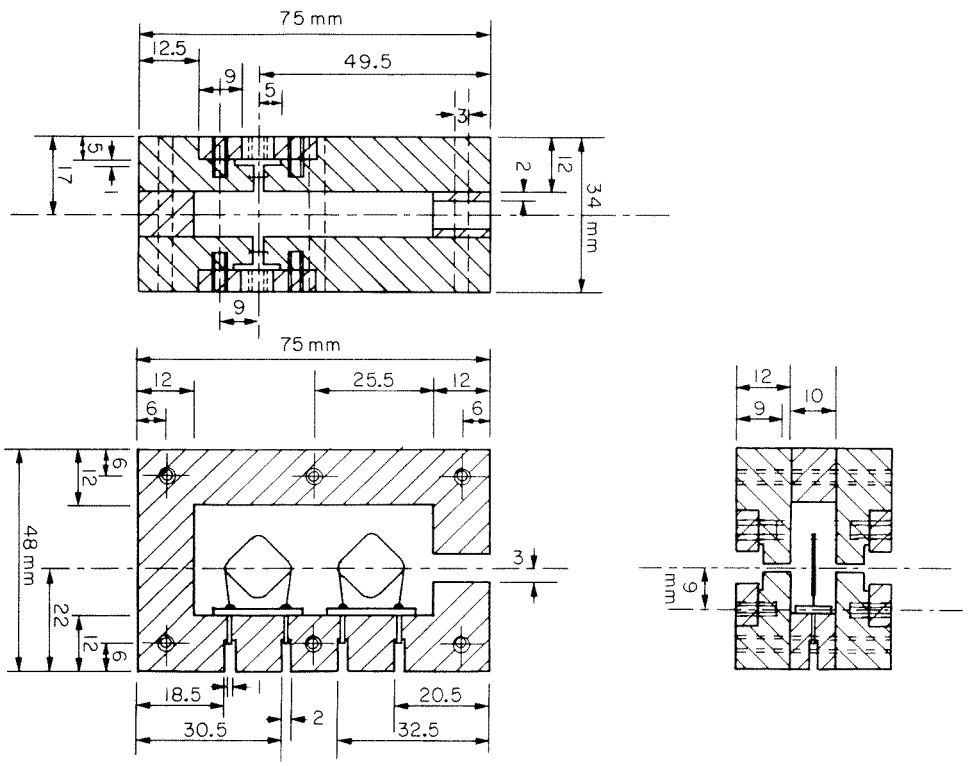

Fig. 1. Scale diagram of the sensor head (dimensions in mm).

volume being kept as small as practical to allow a fast response time. A second, uncoated, reference crystal, matched to have similar temperature characteristics to the analyser crystal, was incorporated in the cell. The matching was achieved using a programmable gas chromatography oven and the dry crystal temperature coefficient measured around ambient temperature; quite reasonable pairing could be achieved in this way.

The two crystals were made parts of oscillator circuits using TTL components. The outputs were mixed in an exclusive OR gate, the mixer output shaped in a Schmitt trigger and the low-frequency component passed to a line driver to transmit it down the cable to the main data-processing device. The oscillator/mixer/line driver circuit was built onto a small printed circuit board bolted on the base of the crystal housing, and the whole surrounded by an aluminium screening box.

In order to maintain the integrity of the signal from the detector head, the line driver—receiver system employed two data lines and a ground line with a differential detection system to minimise the effects of spurious signals which may be picked up on the cable, and thus limit the amount of noise on the signal.

Data acquisition

For the laboratory development work, the signal from the detector head was routed to a Racal 9905 frequency counter/timer, with which the frequency could be read to ±0.01 Hz with a 100-s gating period; normally a 10-s gate was used which allowed the frequency to be measured to within ±0.1 Hz. The eight digits, representing the number of counts during the gate period, were fed to an SC/MP II microprocessor (Science of Cambridge, Ltd.) which acted as an interface to a Data Dynamics 1133 paper-tape punch. The frequency data recorded on the paper tape were processed later on the Imperial College CDC 6500 or Cyber 174 computers using the statistical analysis package called "Minitab" [2]. The microprocessor also controlled the flow switching valve described below.

Flow control

The slow complicated reaction of toluene diisocyanate with PEG 400 results in the mass adsorbed on the crystal not reaching an equilibrium value but continually increasing on exposure to a constant level of the diisocyanate. Although this phenomenon can be exploited analytically to give a time-averaged total exposure, it is generally not a useful characteristic. At higher concentrations (10 ppm) the initial rapid increase in mass levels reaches a steady rate after 1 min and recovers in about 3.5 min to a steady state after switching from contaminated to clean air. The adsorption and desorption times are influenced by the sorption and evaporation of toluene diisocyanate on and from the surface of the glassware between the bubbler cell and the reference cell. Where the sensor head, described above, is used in an open atmosphere, the rates of change are much better defined.

The slow attainment of equilibrium detracts considerably from the analytical utility of the method if absolute frequency change is the measured parameter. In order to overcome this problem a switched flow system, operated by the microprocessor, was adopted (Fig. 2). The tap controlling the flow of air through the bubbler or diffusion cell was turned at predetermined times, using a reversible motor, to permit either contaminated air or clean air to pass over the crystal. In this way the adsorption/desorption cycle was repeated regularly and the crystal, being alternately cleaned, did not experience overloading on exposure to toluene diisocyanate. As a result, maximum benefit could be obtained from the initial rapid rise in mass caused by the adsorbed toluene diisocyanate, which was then quickly desorbed to minimise irreversible chemisorption. This resulted in good sensitivity with a prolonged crystal-coating lifetime. The microprocessor controlled the valve-turning mechanism and initiated the transfer of the frequency data from the frequency meter to punched tape. In this way information on the frequency change during the clean/contaminated air cycle was stored each time the frequency reading was updated (see below).

Calibration

The Marcali method [3, 4] was used as the reference method as described in the previous paper [1], using the calibration apparatus shown in Fig. 3. A modification permitting the use of a reference crystal and including a bubbler rather than the diffusion cell of Neilson and Booth [5] is shown in Fig. 4. This permitted more concentrated atmospheres of toluene diisocyanate to be generated and higher flow rates to be employed.

The main differences between the method employed and the standard published technique were in the sampling and the subsequent measurements. When sampling, the bubblers were incorporated into the sealed gas-flow system immediately after the detector cell containing the crystal; the flow rate used for sampling was therefore identical for the detector cell and the

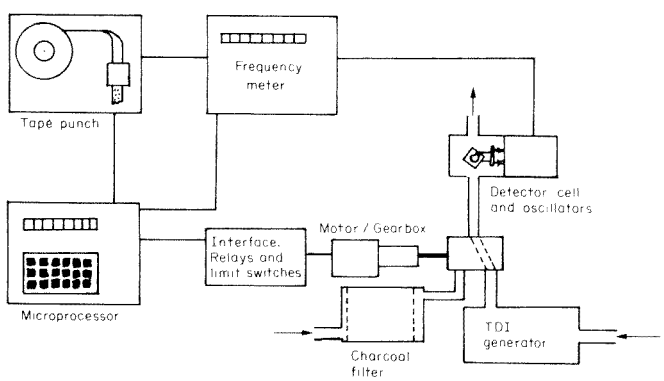

Fig. 2. Schematic diagram of microprocessor-controlled flow switching and data acquisition for toluene diisocyanate (TDI).

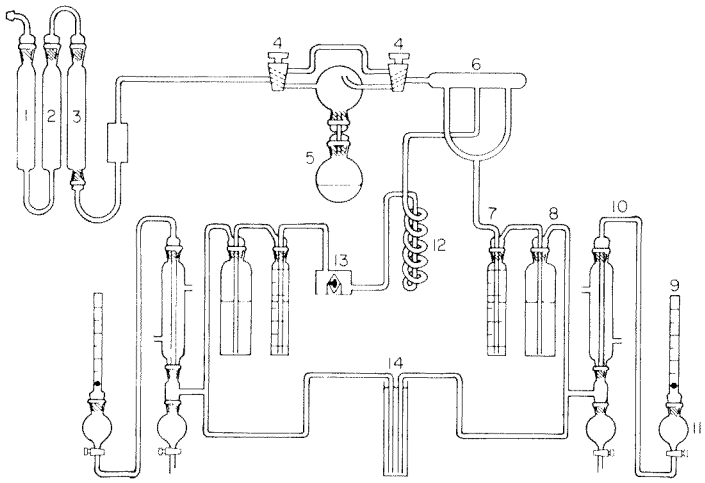

Fig. 3. All-glass calibration apparatus. Carrier gas (air or nitrogen) is dried by passing through scrubbers containing molecular sieve type 4A (1), activated charcoal (2) and silica gel (3) then filtered (Whatman Mini-filter, 5-μm) and passed via teflon double-oblique taps (4) to the diffusion cell (5). The lower flask of this toluene diisocyanate cell is maintained at a known temperature in a water bath and the rate of diffusion through the connecting tube dictates the concentration in the gas stream. The mixture is passed into a glass manifold (6) and split; one stream passes into the reference scrubber (7) containing the reagent solution for the Marcali method determination [3] and is then scrubbed clean with water/ethanol/ 0.880 s.g. ammonia (50: 40: 10) in a Dreschel bottle (8). The gas flow rate is monitored in a rotameter (10) protected by a condenser (9) and drying bulb (11) containing silica gel. The rest of the gas is passed through a glass coil (12) immersed in a bath to maintain the temperature and then over the crystal in the cell (13). The gas leaving the crystal cell is then passed through the Marcali reagents [3] and scrubbed, etc., as in the other arm. A constant pressure head (14) is maintained.

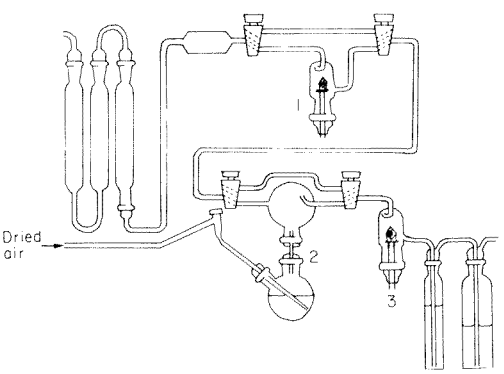

Fig. 4. Part of the glass apparatus containing a reference cell. This adaptation permits the generation of higher concentrations of toluene diisocyanate (TDI). Air, dried as in Fig. 3, is passed over a reference crystal (1) and is mixed in the upper chamber of the TDI bubbler (2) with TDI-saturated dry air and passed over the detector crystal (3). The gas is then passed into a bubbler containing the reagent solution for the Marcali method and scrubbed clean prior to flow rate measurement (see Fig. 3).

Marcali bubbler. Because of the interconnection of the bubbler, the flow rate through the detector cell was limited to 150 cm^3 min^{-1} as higher values caused bubbler efficiency to drop below 90%. When the glove box was used, however, the bubbler had air drawn through it at a rate of 150 cm^3 min^{-1} by a water pump while the detector head was attached to a pump which could either draw or pump air at flow rates up to 1000 cm^3 min^{-1}. The other change made to improve the reproducibility of the spectrophotometric technique involved the use of an ultrasonic bath to remove the nitrogen dioxide produced when sulphamic acid is added to destroy any excess of nitrous acid present. If any gases are not removed prior to the absorption measurement, bubbles usually are formed which cling to the sides of the cell, causing an erroneous absorption reading. The limit of detection of this method is largely determined by the volume of air sampled; the smallest quantity of toluene diisocyanate that can reliably be detected in the bubbler solution is 100 ng.

The crystal detector appeared to follow the gas phase concentration profile with time, although this cannot be proved as the spectrophotometric method provided only time-averaged concentration values; this lack of time resolution makes the study of response speed difficult. The only alternative method for use in calibration is the paper tape monitor which has a continuous response. A commercial instrument was obtained and used for a short period of time. The instrumental range (0.00—0.025 ppm) proved unsuitable for calibration purposes as the adjustment of concentration inside the glove box within this limited range could not be achieved.

A large part of the calibration and testing work involving the sensing head and portable prototype instrument was carried out in a glove chamber of about 1-m^3 capacity. The toluene diisocyanate was generated by passing laboratory air, which had previously been dried by passing it over silica gel, through the bubbler shown in Fig. 4. This mixture could be diluted with air from a cylinder to vary the concentration as required (Fig. 5). The laboratory air was pumped using an air compressor and any of the unused air-line connecting ports in the glove box were connected to an extractor fan, the air inside the box being replaced at about 500 cm^3 min^{-1}. This was a good method of creating controlled concentrations of toluene diisocyanate inside the glove box, as the crystal detector head either samples air from inside the box at rates of up to 1 dm^3 min^{-1} or reverses this flow so that clean air passes over the crystals into the box at similar rates; this variation in flow would upset the concentration in a static atmosphere. In addition, a range of different concentrations was difficult to produce with a static method because of the almost irreversible adsorption of toluene diisocyanate on the sides of the glove box, especially at low concentrations. With both methods, in order to lower the concentration inside the box, clean air had to be aspirated for a period of days before the last traces of toluene diisocyanate were desorbed. Consequently the atmosphere in the box was changed continuously, starting with low concentrations. With air flows over the range 1.0—3.0 dm^3 min^{-1}, concentrations of 0.02—0.2 ppm toluene diisocyanate were attainable in the chamber.

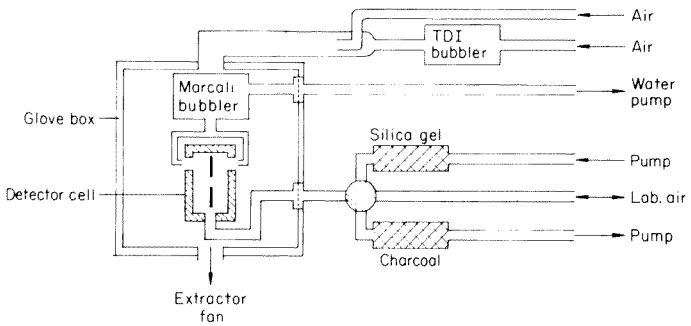

Fig. 5. Glove box calibration apparatus. Dry air is passed through a TDI bubbler (as in Fig. 4) and mixed with dry air before entering the glove box. The glove box air is sampled immediately adjacent to the entrance ports of the detector head and drawn through a bubbler containing the Marcali reagents. Either laboratory air is dried on a silica gel column and passed over the detector crystal (on the desorb cycle), or glove box air is sucked over the crystals in the detector head (on the adsorb cycle). The air in the glove box is continuously extracted to maintain a reasonably stable atmosphere.

DATA INTERPRETATION WITH THE COMPUTER

The adsorption/desorption cycle adopted overcomes some major problems. The frequency change on exposure to a constant concentration of toluene diisocyanate never reaches a plateau as, once adsorbed, toluene diisocyanate is able to adsorb onto itself. Consequently the time at which the frequency change is determined is critical, together with the extent of exposure that the crystal coating has already had. Further, only a coating that has not had prolonged exposure to high concentrations of toluene diisocyanate has a signal:noise ratio giving a theoretical detection limit of the same order as the TLV (0.02 ppm) [1].

Flow switching prevents overloading of the crystal on prolonged exposure and increases the reproducibility of the frequency changes obtained. Sensitivity is increased by integrating the signal obtained over each adsorption/desorption cycle. Integration of the frequency signal followed by subtraction of the integrated baseline reduces both the random frequency noise of the system and the noise from digitization of an analog signal. The main problem associated with integration of the frequency change is to allow for changes that occur in the baseline value and to make certain that the value chosen is valid, especially if the method is to form the basis of an automatic continuous monitor that needs neither a skilled operator nor interpretation of results. Changes in baseline often occur when high concentrations of toluene diisocyanate are sampled, thereby encouraging the irreversible chemisorption of toluene diisocyanate on the PEG 400 substrate. If any particulate matter such as dust lands on the surface of the crystal during a measurement, it could upset all the subsequent readings unless the change in baseline is taken into account. Figure 6 shows the drift in baseline that can occur when toluene diisocyanate at a high concentration (10 ppm) is sampled at a high flow rate (300 cm^3 min^{-1}).

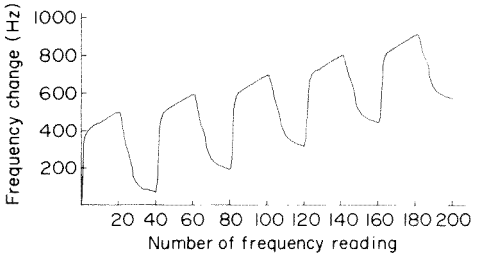

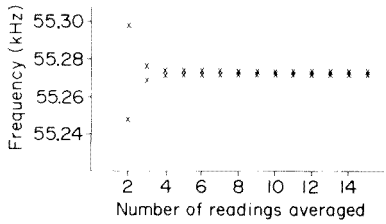

Fig. 6. Adsorption/desorption profile for 5 consecutive runs with 10 ppm toluene diisocyanate.

Fig. 7. Variation of the 99% confidence interval with the number of readings averaged.

Integration is carried out by first passing pure air over the detector crystal coated with PEG 400 and the uncoated reference crystal. A typical baseline frequency profile shows no appreciable drift; one such profile shows a standard deviation of ±0.005 on its mean value of 70.272 kHz over 200 readings. Therefore, on integration the value obtained should be approximately zero. Figure 7 shows the variation of the 99% confidence interval with the number of readings used to calculate the average value for the baseline. The confidence interval is given by $\bar{x} \pm tsN^{-1/2}$ where $\bar{x}$ is the mean of the N data points, s is their standard deviation and t is the value obtained from the t-table (corresponding to 99% confidence and $(N - 1)$ degrees of freedom). The confidence interval decreases rapidly from an initially high value (about 50 Hz) to a low value by the time 10 readings have been averaged and this limits to 0.52 Hz after 17 readings have been averaged. Thus 10 readings seem to be sufficient to give confidence in the value chosen as the baseline, though this of course does not mean that the baseline will be drift-free, so a check is initially made by averaging a second group of 10 readings and comparing this new value to the one obtained previously. Provided that they are within ±10 Hz of each other the sampling of analyte can commence; if not, pure air is passed over the crystals until the drift is reduced below this limit. As soon as sampling has begun integration of the signal is started and continued for 40 readings, which also include the flushing part of the "run". A "run" consists of 20 readings taken one every 10 s (the gate period of the frequency meter) whilst sampling, and another 20 readings taken whilst passing pure air over the crystals. The last 3 readings of each run are also averaged to provide the new baseline value for the next run of 40 readings. Figure 8 shows this for one run in the middle of a series. The drift area is calculated by multiplying by 20 the difference between the baseline value of the previous run and that of the next run. The drift area is subtracted from the value of the integrated signal above the baseline.

Table 1 shows the mean integrated values obtained by this method for 5 runs in which no toluene diisocyanate was present in the analyte airstream. The values are not zero as would be expected; this is due to the pressure fluctuations that occur when the valve is turned, which give rise to a fairly

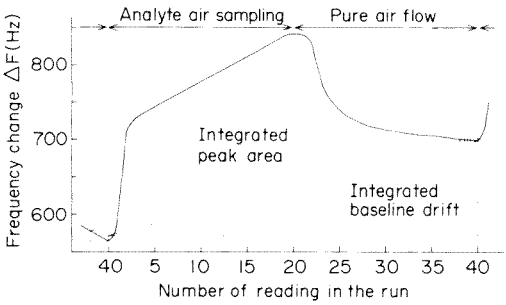

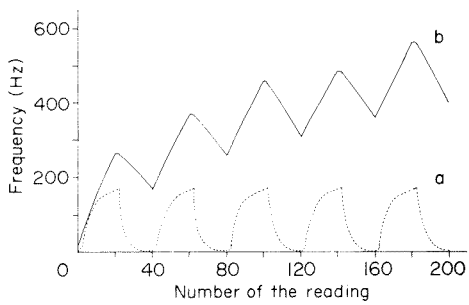

Fig. 8. Graph of one adsorption/desorption cycle in the middle of a series.

Fig. 9. Response of a Clingfilm-coated crystal to (a) water and (b) toluene diisocyanate.

reproducible frequency change which, when integrated as above, produces a negative value. In this example, the mean and standard deviation of the baseline frequency over the 200 readings is 55272 ± 0.52 Hz which indicates the noise value possible with properly matched crystals. Table 1 also gives the integrated values for the 5 runs shown in Fig. 6 and the integrated values for another typical series of runs. These results show that for a concentration of 12 ppm the integrated signal is 1.5 kHz. With noise of 0.7 Hz, which is twice the standard deviation of the integrated signal when no toluene diisocyanate is present, the theoretical detection limit is 0.006 ppm which is well below the TLV of 0.02 ppm toluene diisocyanate.

Dependence of response on flow rate

The variation of response with flow rate was studied using the glove box and the adsorption/desorption method of sampling. Table 2 shows the results. Increasing the flow rate increases the absolute frequency change. This would be expected as at higher flow rates more toluene diisocyanate comes into contact with the crystal coating. A limit might be expected when the molecules are not resident in the cell long enough to react with the coating but this levelling off was not observed at any of the flow rates used. Absolute frequency changes for desorption have a much smaller standard

TABLE 1

Integrated responses for toluene diisocyanate (TDI)

TDI conc. (ppm)	Flow rate (cm^3 min^{-1})	Integrated signal (Hz s)[a]	Baseline drift (Hz s)[a]
0	300	−2.18 ± 0.7	−0.5 ± 0.3
10	300	504.3 ± 49.1	304.6 ± 34.9
12	350	1526 ± 76	1451 ± 98

[a]Mean and standard deviation of 5 results.

TABLE 2

Effect of flow rate on crystal response to about 1 ppm toluene diisocyanate in air

Flow rate ($cm^3\ min^{-1}$)	ΔF Absorption (Hz)[a]	ΔF Desorption (Hz)[a]
100	−69 ± 2.5	60 ± 1.1
150	−87 ± 3.4	77 ± 1.5
200	−132 ± 2.9	120 ± 0.8
250	−150 ± 6.3	135 ± 1.8
300	−166 ± 6.8	152 ± 1.7

[a]Mean of 6 results ± standard deviation.

deviation for a given flow rate, as the desorption is almost logarithmic in profile and its value is smaller than that for adsorption.

Response of a Clingfilm-coated crystal

It was observed in earlier work [1] that Clingfilm (the trade name of a PVC film) exhibited reversible adsorption characteristics with toluene diisocyanate. Clingfilm dissolved in tetrahydrofuran was spotted onto the gold electrode and its response to toluene diisocyanate was measured. Air saturated with toluene diisocyanate (about 15 ppm) were passed over the crystal in the sensor head described previously. The response obtained (Fig. 9) is about the same as for water vapour, the latter being totally reversible. This is a significant improvement over PEG 400 and points the way to further possible improvements.

PROTOTYPE PORTABLE MONITOR DESIGN

The work described above showed that correct sampling and data interpretation could give adequate sensitivity for toluene diisocyanate in dry air using PEG 400 as a coating material. It is doubtful whether PEG would be a useful coating in practical applications because of its water response although, as has been indicated, modification of the coating and the use of other materials may alleviate this problem.

No matter what crystal coating is employed or which toxic gas is being determined, the design criteria for a portable piezoelectric crystal-based monitor are much the same. Indeed, one could say that toluene diisocyanate, with its low TLV, water sensitivity, self-reactivity and low vapour pressure represents the worst possible combination of properties in a species to be determined. With this in mind a device was planned which could equally well determine toluene diisocyanate, when a better coating can be found, or other gases for which suitable coatings already exist.

Apart from the air sampling pump and power supply, the instrument is comprised entirely of data processing and information display components.

The processing circuitry receives only a frequency count; any chemistry or selectivity has to be imparted by the crystal coating itself, although the data themselves can be so manipulated and presented as to require no further interpretation.

The measuring circuit used in the semi-automatic monitor used phase-locked loop (PLL) chips to impart high stability and wide dynamic range. The PLL circuit employed has a resolution of 1 Hz and a range of 500 Hz to 65 kHz with a stability of greater than 0.1 Hz. The frequency synthesizing circuit was adapted from one designed by P. R. Fielden in this department incorporating two PLL chips to provide the backing-off signal (Fig. 1D). The rest of the electronics display the backed-off frequency on a large, easily read display, located on the top-face of the control box worn on the belt. The display circuit also contains a register in which a number can be preloaded. The preloaded number is continuously compared to the value on the display and a signal is generated if the preloaded number has been exceeded. The preloaded value is used as the threshold value above which the alarm is activated. A fail-safe device detects the mixer output arriving at the belt pack; if the mixer output fails, an alarm LED switches on.

In operation, the user starts the pump blowing clean air over the crystals by reversing a manually operated valve (Fig. 11). The crystals are then given enough time for any adsorbed water to be removed; this can vary from less than 1 min up to about 10 min. After the crystal stabilisation period is over, a reset switch is activated, and the frequency of the heterodyne output from the detector head is averaged over 10 s. The average value is fed through to a latch which provides the signal for the PLL circuit to lock with. Until lock is achieved, the display remains unlit; once locked, the display is enabled and a LED is turned on to signify that measurement of subsequent frequency change can be monitored. The display is driven by a counter/timer chip which counts the mixed frequency of the PLL circuit and the detector head heterodyne frequency. Initially the display should show an almost zero value because the PLL output should match the heterodyne output exactly.

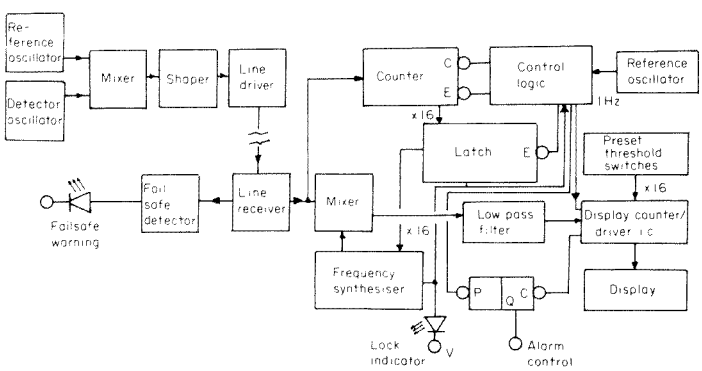

Fig. 10. Block diagram of the portable monitor electronics C, E, P and Q have their usual meanings (clear, enable, preset and output).

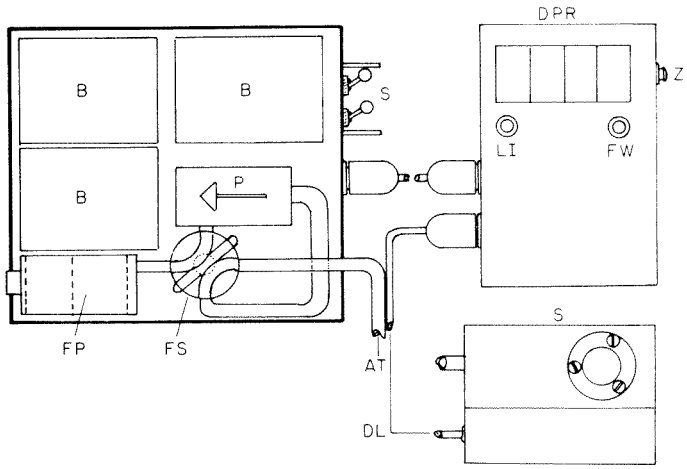

Fig. 11. Schematic diagram of the portable monitor: B, battery; FP, filter pack (molecular sieve, charcoal); FS, flow switching tap; P, pump; S, power switches; AT, aspiration tube; DL, data lines; DPR, data processing and readout; LI, lock indicator; FW, fail-safe warning; Z, zero button; S, sensing head.

Subsequently the flow control valve is reversed to sample the contaminated air. If toluene diisocyanate is present, the heterodyne frequency will change but the PLL output which is still controlled by the original latched heterodyne frequency remains the same; therefore the displayed value will increase directly with the change in heterodyne frequency.

To overcome the continual adsorption of toluene diisocyanate, which precludes the use of absolute frequency change as the measure of concentration, a timer was incorporated. This is initiated as soon as the air is sampled and automatically terminates the count after 250 s, thus the backed-off frequency change is integrated over this length of time. The display continually displays the current value as it is integrating, to give a visual indication of concentration level almost instantly. At the end of the measurement period, the value is retained on the display and sampling can be terminated or repeated again.

The main drawback of this instrument is the lack of flexibility in the method of signal processing. The best method of achieving flexibility, retaining the inherent low noise of digital circuits and providing more automatic control, is to employ a microprocessor. Logic decisions based on incoming data are better dealt with automatically to reduce operator errors. Typical tasks in this area are confirming that the value chosen as the backing-off frequency is within acceptable error limits; checking that the baseline drift is acceptable; ensuring that the PLL is locked continuously and not jittering; and investigation of the location of any fault conditions.

The mathematical data manipulations that can be undertaken are also increased. This is almost essential in this case if any improvement in reproducibility is required. The rate of adsorption on coatings has been found to

be quite variable, reflected in the fairly high variation in integrated signal obtained for consecutive adsorption/desorption sample cycles. Adsorption of toluene diisocyanate depends on both the concentration present and the extent of exposure the sensor has had during the current measurement cycle. This latter is reflected in the relatively large standard deviations obtained for consecutive cycles in the adsorption/desorption method of measurement. The integrated values usually obtained for 5 consecutive runs decrease in proportion to the concentration being measured. To a first approximation this is linear, and the standard deviations obtained for the points, with respect to the best line through them, is improved by about a third.

Sampling pump unit

The pump used was a double-acting diaphragm type capable of aspirating about 1 dm^3 min^{-1} through the system. It was installed in a die-cast box along with three 8.5 V, 1.2-Ah nickel—cadmium batteries which served to supply the pump, oscillator and data processing circuits. Although no attempt was made to ensure intrinsic safety, the boxes used were all sealed, with locking connectors. Flow stabilisation was achieved using a simple capillary restrictor to give pump rates of 50—1000 cm^3 min^{-1}.

Performance of the prototype device was quite acceptable in laboratory conditions. The simple data manipulation could not achieve the sensitivity obtained using the main computer statistical package, but the portable monitor, incorporating the sensing head, manual flow switching and PLL/synthesiser back-off system was able to detect the vapour from pools of liquid toluene diisocyanate on the bench. When left in the open laboratory, the reading on the display stayed quite steady and the movement associated with walking did not have any significant influence.

Conclusions

This work has shown that with microprocessor-aided control of the air sampling and correct manipulation of the data using the computing ability of a microcomputer on board the instrument, a small portable piece of equipment for coated piezoelectric crystal gas detection can be realized.

At present the displayed value is an integrated frequency reading; this yields a valid indication of the concentration present, but a true concentration output would be preferable. Adoption of a dedicated microprocessor for data handling and control into the present prototype will permit this transformation although a more sophisticated compensation for changes in ambient conditions will be necessary. The monitoring of temperature and humidity, using additional sensors and subsequent correction of the output for any changes, is well within the capabilities of these devices.

There is little doubt that the limiting factor at present is a truly selective coating for toluene diisocyanate; the modified PEG and sensitive polymer film having hydrophobic properties offer the best response at present. For other organic vapours, less difficult to handle, a solution may be easier to achieve.

This work was supported by an SRC/CASE Award in collaboration with Panocean Anco Limited. The authors are grateful to the Central Research Fund, University of London, for an equipment grant and to David Owen, Safety Manager, Panocean Anco, for many helpful discussions.

REFERENCES

1 J. F. Alder and C. A. Isaac, Anal. Chim. Acta, 129 (1981) 163.
2 T. A. Ryan, B. L. Joiner and B. F. Ryan, The Minitab Student Handbook, Duxbury, North Scituate, MA, 1978.
3 K. Marcali, Anal. Chem., 29 (1957) 552.
4 B. Dimitriades, Health Lab. Sci., 12 (1975) 278.
5 A. Neilson and K. S. Booth, Am. Ind. Hyg. Assoc. J., 36 (1975) 169.

Analytica Chimica Acta, 129 (1981) 189—194
Elsevier Scientific Publishing Company, Amsterdam — Printed in The Netherlands

EXTRACTION DE L'ACIDE OXALIQUE PAR FORMATION DE PAIRES D'IONS ET APPLICATION AU DOSAGE DE L'ACIDE OXALIQUE URINAIRE

Y. PEGON*

Département de Chimie Analytique Chimie Générale et Minérale et Bromatologie, Faculté de Pharmacie, 8, Avenue Rockefeller, 69373 Lyon Cédex 2 (France)

J. J. VALLON

Laboratoire de Biochimie, Toxicologie et Analyse des Traces, Hôpital Edouard Herriot, Place d'Arsonval, 69374 Lyon Cédex 2 (France)

(Reçu le 2 avril 1981)

SUMMARY

(Extraction of oxalic acid by ion-pair formation with application to the determination of oxalic acid in urine)

The yield of ion-pair extraction of oxalic acid by trioctylamine and triisooctylamine in chloroform depends on the pH of the aqueous phase. The optimum pH is 2.7, proving that hydrogenoxalate ion is the extractable form. Extraction yield depends on the acid used for pH adjustment and dissolution of the calcium oxalate formed in complex medium. The best results are obtained with hydrochloric and sulfuric acids and with trioctylamine extraction. This extraction was applied to oxalic acid determination by colorimetry and gas chromatography in urines from twenty healthy patients. Mean excretion was found to be 0.30 mmol/24 h. Extraction yields lie between 94 and 106%.

RESUME

Le rendement d'extraction de l'acide oxalique sous forme de paires d'ions par la trioctylamine et la triisooctylamine en solution dans le chloroforme dépend du pH de la phase aqueuse. Il est maximum à pH 2,7 ce qui montre que l'ion hydrogénooxalate est la forme extractible. Le rendement d'extraction dépend également de l'acide que l'on emploie pour amener le pH de la solution à 2,7 et pour redissoudre l'oxalate de calcium formé en milieu complexe. Les meilleurs résultats sont obtenus avec l'acide chlorhydrique et l'acide sulfurique en réalisant l'extraction par la trioctylamine. Cette extraction a été utilisée pour le dosage de l'acide oxalique urinaire par colorimètrie et par chromatographie en phase gazeuse dans les urines de 20 sujets normaux. Les quantités éliminées sont en moyenne de 0,30 mmol/24 h. Les rendements d'extraction sont compris entre 94 et 106%.

L'extraction de l'acide oxalique par formation de paires d'ions avec des trialkylamines, trioctylamine (TOA), triisooctylamine (TIOA) et méthyldioctylamine, a fait l'objet de plusieurs publications [1—4] portant sur la structure de ces paires d'ions et leur coefficient de distribution dans différents solvants. Aucune étude n'a été faite sur l'influence de la composition de la

phase aqueuse sur le rendement d'extraction, ni sur les possibilités d'utilisation de ces paires d'ions pour l'extraction quantitative de l'acide oxalique à partir des milieux complexes comme l'urine.

Le dosage de l'acide oxalique urinaire peut-être réalisé par colorimétrie [5—9], fluorimétrie [10], chromatographie en phase gazeuse [11—14], absorption atomique [15], h.p.l.c. [16] ou par voie enzymatique avec l'oxalate oxydase [17, 18], ou l'oxalate décarboxylase [19, 20]. Le dosage est précédé d'une étape de séparation par résine échangeuse d'ions, par extraction avec un solvant, ou, le plus souvent, par précipitation de l'oxalate de calcium. Aucun de ces modes de séparation ne présente à la fois une praticabilité et un rendement satisfaisants. C'est pourquoi nous avons étudié l'influence du pH de la phase aqueuse, de la nature de l'acide utilisé pour fixer ce pH et de la trialkylamine sur l'extraction de l'acide oxalique. Puis nous avons utilisé cette extraction pour le dosage de l'acide oxalique urinaire par colorimétrie et par chromatographie en phase gazeuse (c.p.g.).

PARTIE EXPERIMENTALE

Réactifs et appareillage

Tous les produits utilisés sont de qualité pour analyse sauf la trioctylamine (Merck) et la triisooctylamine (Riedel de Haën).

Les dosages par colorimétrie sont effectués sur un spectrophotomètre Unicam SP 8 100. Les séparations par c.p.g. sont faites sur un appareil Packard modèle 427 équipé d'un détecteur à ionisation de flamme et d'une colonne de verre de 3 m contenant FFAP 9% sur Supelcoport (100—120 mesh). La température de l'injecteur et du détecteur est de 250°C. La température du four est programmée pour monter de 2°C min^{-1} de 90 à 140°C.

Etude du rendement d'extraction en fonction du pH

On ajoute à 10 ml d'une solution aqueuse d'acide oxalique 0,1 mmol l^{-1}, 10 ml de chloroforme et 2 ml d'alkylamine: TOA ou TIOA. Le pH de la phase aqueuse est amené à pH 1 avec de l'acide chlorhydrique 1 M pour que la concentration en chlorure de la solution soit constante; puis le pH est ajusté à la valeur désirée avec de la soude 0,2 M. Les différentes opérations sont faites en agitant le mélange avec un barreau magnétique entre chaque ajout de réactifs. Les deux phases sont transférées dans une ampoule et agitées 15 min; le pH de la phase aqueuse est vérifié, ajusté si nécessaire et le mélange est agité de nouveau 15 min. L'acide oxalique restant dans la phase aqueuse est dosé par colorimétrie.

Recherche de l'alkylamine et de l'agent d'acidification donnant le meilleur rendement d'extraction

On introduit dans 10 ml d'une solution aqueuse d'acide oxalique 0,1 mmol l^{-1}, une quantité d'acide (HCl, H_2SO_4, $HClO_4$, CCl_3COOH) égale au double de la capacité d'extraction de l'alkylamine utilisée (4,1 mmol pour 2 ml de

TOA et 4 mmol pour 2 ml de TIOA). On ajoute 10 ml de chloroforme et 2 ml d'alkylamine. On ajuste le pH à 2,7 et on réalise l'extraction selon la technique décrite dans le paragraphe précédent. Les différentes espèces sont dosées dans la phase aqueuse et dans la phase organique.

Mode opératoire

Dosage de l'acide oxalique urinaire. Avant extraction, chaque urine est amenée à pH 1 pour dissoudre l'oxalate de calcium. On prélève ensuite 10 ml d'urine auquels on ajoute 10 ml de chloroforme et 2 ml de TOA. On amène le pH de la phase aqueuse à 2,7 en agitant le mélange avec un barreau magnétique entre chaque ajout de réactif. Le mélange est transféré dans une ampoule et agité 15 min avec un agitateur mécanique. On centrifuge. On reprend 8 ml de la phase organique à laquelle on ajoute 10 ml d'une solution concentrée d'ammoniac. On agite 15 min pour réextraire l'acide oxalique. On centrifuge et on dose l'acide oxalique dans la phase aqueuse par colorimétrie.

Chaque urine a été extraite et dosée avant et après un ajout correspondant à une concentration en acide oxalique de 0,1 mmol l^{-1}.

Colorimétrie. Nous avons modifié la méthode de dosage colorimétrique de l'acide oxalique proposée par Pernet et Pernet [5] pour en augmenter la praticabilité: à 2 ml de la solution à doser, on ajoute 1 ml de HCl 1 M, quelques grains de zinc et on agite 15 min. On filtre et on reprend 2 ml de filtrat auquel on ajoute 0,2 ml d'une solution à 1% dans l'eau de chlorhydrate de phénylhydrazine. On porte ce mélange 2 min à 100°C. Après refroidissement, on ajoute 1,8 ml d'acide chlorhydrique concentrée et 0,2 ml d'eau oxygénée à 10 volumes. On laisse à l'obscurité 8 min et on photomètre à 520 nm contre un blanc préparé de la même façon, hormis l'addition d'eau oxygénée.

Chromatographie en phase gazeuse. Une portion (2 ml) de la solution ammoniacale obtenue après extraction est évaporée à 110°C après acidification par l'acide chlorhydrique concentré. Le résidu est repris par 1 ml d'éthanol, 0,1 ml de HCl 11 M et 0,2 ml d'une solution d'acide maléique à 0,2 g l^{-1} dans l'éthanol (étalon interne). La solution est laissée 1 h à 110°C en tube bouché. On injecte 4 μl. Les temps de rétention sont de 13 min pour l'ester de l'acide oxalique et de 21 min pour l'ester de l'acide maléique.

RESULTATS ET DISCUSSION

Etude du rendement d'extraction en fonction du pH

L'acide oxalique H_2A ne peut être extrait de sa solution aqueuse sous forme de paires d'ions qu'à un pH où il est ionisé. D'autre part, le pH optimum d'extraction dépend des coefficients d'extraction des paires d'ions qu'il est possible de former à partir de A^{2-} et HA^-. C'est pourquoi nous avons étudié le pourcentage d'acide oxalique extrait en fonction du pH de la solution aqueuse. La concentration en chlorure des solutions utilisées est maintenue constante car elle peut modifier le rendement d'extraction.

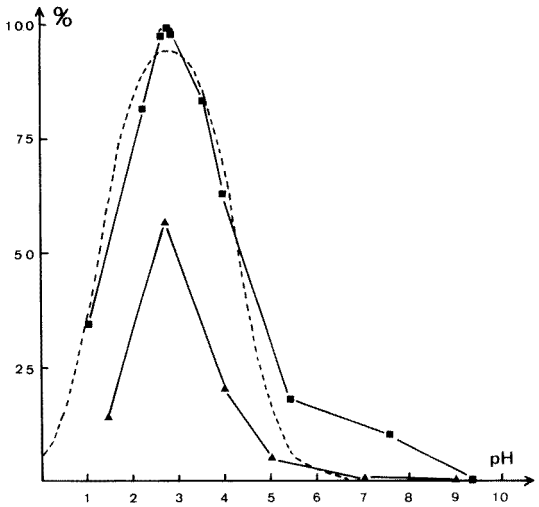

Fig. 1. Rendement d'extraction de l'acide oxalique par TOA (■) et par TIOA (▲) en fonction du pH. (----) Cette courbe représente le pourcentage d'acide oxalique sous forme d'hydrogénooxalate en fonction du pH.

Les résultats sont donnés sur la Fig. 1. Avec les deux alkylamines, le pH optimum d'extraction est de 2,7. Ce pH est celui où la concentration de la solution aqueuse en ions HA^- est maximum. Ceci confirme que les formules des paires d'ions sont HA^- $TOAH^+$ et HA^- $TIOAH^+$ [1, 3, 4]. Lorsque la solution aqueuse est basique, ces paires d'ions ne peuvent plus se former; il est donc possible de réextraire par une solution alcaline la totalité de l'acide oxalique se trouvant en milieu organique sous forme de paires d'ions pour le doser par colorimétrie.

Recherche de l'alkylamine et de l'agent d'acidification donnant le meilleur rendement d'extraction

L'extraction de l'acide oxalique devant avoir lieu à pH 2,7, il est nécessaire d'ajuster le pH de la phase aqueuse en ajoutant un acide fort H_nB. Cet acide donne en solution un anion $H_mB^{(n-m)-}$ qui est extrait sous forme de paires d'ions par la solution organique d'alkylamine au fur et à mesure que l'on abaisse le pH de la solution. A pH 2,7, environ 90% de la capacité d'extraction de l'alkylamine sont ainsi utilisés. De plus en milieu complexe, en présence d'ions Ca^{2+}, l'oxalate précipite sous forme d'oxalate de calcium. Pour redissoudre ce précipité, il faut amener le pH du milieu à 1 avec un acide fort [21]. Pour ces deux raisons, au moment de l'extraction, il y a un excès d'ions $H_mB^{(n-m)-}$ par rapport à la capacité d'extraction de l'alkylamine.

Afin de déterminer quel est l'acide fort dont l'utilisation permet le meilleur rendement d'extraction de l'acide oxalique, nous avons calculé la constante apparente d'échange K_e pour les ions oxalate HA^- et les ions $H_mB^{(n-m)-}$. Cette constante apparente est la constante d'équilibre de la réaction

$(H_mB^{(n-m)-})_o + (n - m)\ HA^- \rightleftharpoons H_mB^{(n-m)-} + (n - m)\ (HA^-)_o$, l'indice o désignant les espèces en phase organique. Nous avons d'abord dosé les ions correspondant aux différents acides H_nB étudiés, avant et après extraction à pH 2,7 par une solution d'alkylamine dans le chloroforme. Les résultats montrent que chaque molécule d'alkylamine fixe un ion B^- pour les mono-acides (HCl, $HClO_4$, CCl_3COOH), un ion $H_2PO_4^-$ pour H_3PO_4 et qu'il faut deux molécules d'alkylamine pour fixer un ion SO_4^{2-}. Afin de pouvoir comparer entre elles les valeurs de K_e, nous avons exprimé les concentrations en équivalents H^+ par litre, ce qui permet d'avoir quel que soit l'acide la même expression pour K_e. Ce mode d'expression est justifié par le fait que la quantité d'acide fort exprimé en équivalent H^+ qu'il faut introduire dans une solution de composition donnée pour l'amener à un pH fixé ne dépend pas de l'acide. Comme le montre le Tableau 1, les constantes apparentes d'échange les plus favorables sont obtenues avec la trioctylamine en utilisant comme acide: HCl ou H_2SO_4. L'étude n'a pu être faite avec l'acide nitrique car les ions NO_3^- à concentration élevée interfèrent avec la réaction colorée de dosage.

Application à l'acide oxalique urinaire

L'intérêt de l'extraction de l'acide oxalique par formation de paires d'ions pour son dosage dans les milieux complexes, est mis en évidence par la mesure de la quantité d'acide oxalique urinaire éliminée par 24 h chez 20 sujets normaux. Le rendement d'extraction déterminé sur 20 urines en utilisant l'acide chlorhydrique comme agent d'acidification est compris entre 3,7 et 94% avec une moyenne de 32,9%. Ceci est dû au fait que l'oxalate de calcium précipite pendant l'extraction. Pour éviter ce phénomène, il faut ajuster les pH avec une solution d'acide sulfurique. Les résultats et les rendements

TABLEAU 1

Constantes apparentes d'échange de l'ion hydrogénooxalate pour l'extraction par les alkylamines à pH 2,7

Alkylamine	Cl^-	SO_4^{2-}	$H_2PO_4^-$	CCl_3COO^-	ClO_4^-
TOA	15,2	12,8	3,5	0,58	0,55
TIOA	2,16	4,1	1,26	0,1	0,09

TABLEAU 2

Quantité d'acide oxalique éliminée par 24 h dans les urines et rendement d'extraction déterminés sur les urines de 20 sujets normaux

	Moyenne	Écart type	Valeurs extrêmes
Mmol/24 h	0,30	0,11	0,11—0,49
Rendement extraction (%)	98,7	3,8	94—106

d'extraction obtenus ainsi sont donnés dans le Tableau 2. Les valeurs trouvées sont très proches de celles qui ont été publiées précédemment [7, 12, 13, 17, 19, 20].

Les concentrations en acide oxalique des solutions ammoniacales résultant de l'extraction des urines ont également été déterminées par c.p.g. Les valeurs obtenues par colorimétrie et par c.p.g. ont été comparées par régression linéaire. Les coefficients de la régression sont: a = 1,009; b = —0,005; r = 0,99. Ceci montre que la méthode colorimétrique est très spécifique.

L'extraction par formation de paires d'ions est une technique facile à mettre en oeuvre pour réaliser l'étape de séparation nécessaire au dosage de l'acide oxalique dans les milieux complexes comme l'urine. Le rendement obtenu est supérieur à celui de la précipitation ou à celui de l'extraction par différents solvants.

Nous remercions Mlle. C. Bichon pour sa collaboration technique.

BIBLIOGRAPHIE

1 V. S. Smelov et A. V. Strakhova, Radiokhim., 5 (1963) 509.
2 A. A. Pushkov, V. S. Shmidt et V. N. Shesterikov, Tr. Mosk. Khim. Tekhnol. Inst., 43 (1963) 12.
3 A. A. Lipovskii et M. G. Kuzina, Radiokhim., 10 (1968) 175.
4 A. S. Vieux, N. Rutagengwa, J. B. Rulinda et A. Balikungeri, Anal. Chim. Acta, 68 (1974) 415.
5 J. L. Pernet et A. Pernet, Ann. Biol. Clin., 20 (1962) 737.
6 A. Hodgkinson et P.M. Zarembski, Analyst, 86 (1961) 16.
7 A. Hodgkinson et A. Williams, Clin. Chim. Acta, 36 (1972) 127.
8 H. Baadenhrijsen et A. P. Jansen, Clin. Chim. Acta, 62 (1975) 315.
9 R. H. B. Sample, M. E. Farber et M. R. Glick, Clin. Chem., 26 (1980) 1105.
10 P. M. Zarembski et A. Hodgkinson, Biochem. J., 96 (1965) 717.
11 G. Charransol et P. Desgrez, J. Chromatogr., 48 (1970) 530.
12 C. J. Farrington et A. H. Chalmers, Clin. Chem., 25 (1979) 1993.
13 M. A. Gelot, G. Lavoué, F. Belleville et P. Nabet, Clin. Chim. Acta, 106 (1980) 279.
14 K. Y. Pork et J. Gregory, Clin. Chem., 26 (1980) 1170.
15 C. Koehl et J. Abecassis, Clin. Chem., 70 (1976) 71.
16 W. J. Mayer, J. P. McCarthy et M. S. Greenberg, J. Chromatogr. Sci., 17 (1979) 656.
17 G. Kohlbecker, L. Richter et M. Butz, J. Clin. Chem. Clin. Biochem., 17 (1979) 309.
18 M. F. Laker, A. F. Hofmann et B. J. D. Meeuse, Clin. Chem., 26 (1980) 827.
19 P. C. Hallson et G. A. Rose, Clin. Chim. Acta, 55 (1974) 29.
20 J. Yriberri et S. Posen, Clin. Chem., 26 (1980) 881.
21 A. Hodgkinson, Clin. Chim. Acta, 109 (1981) 239.

Analytica Chimica Acta, 129 (1981) 195—203
Elsevier Scientific Publishing Company, Amsterdam — Printed in The Netherlands

FLUORIMETRIC DETERMINATION OF GALLIUM WITH LUMOGALLION BY FLOW INJECTION ANALYSIS BASED ON SOLVENT EXTRACTION

TOTARO IMASAKA, TAKESHI HARADA and NOBUHIKO ISHIBASHI*

Department of Applied Chemistry, Faculty of Engineering, Kyushu University, Hakozaki, Fukuoka 812 (Japan)

(Received 16th March 1981)

SUMMARY

Gallium in the concentration range 4×10^{-6}—8.7×10^{-5} M is determined fluorimetrically with lumogallion by an extraction—flow injection procedure. Sensitivity and selectivity are improved compared to those obtained earlier with an entirely aqueous system. The transient phenomena occurring in extraction in a narrow teflon tube are examined by a laser excitation technique, in which the concentration profile of the gallium—lumogallion complex is measured directly without phase separation. The results show that mixing between segments plays an important role in dispersion of the sample in the extraction coil. Two extraction processes with different rates were observed in the transient signals during extraction.

In environmental, clinical and material science, large numbers of samples often have to be analyzed in short periods. Flow injection analysis, which is based on the use of a continuous flow stream, has proved reliable for repetitive determinations of many inorganic and organic species. This technique is useful in routine work, and a large literature is now available on analytical applications and fundamental theories [1].

In many practical assays, pretreatment such as solvent extraction may be necessary to increase sensitivity and selectivity. Such procedures are tedious and time-consuming when done batch-wise; batch methods also involve risks of contamination. However, ultramicro solvent extraction can be achieved in flow injection procedures: an aqueous carrier stream containing a sample and an organic solvent are mixed by a segmentor, the extraction proceeds downstream, and the extracted sample can be measured with or without phase separation [2—11]. This experimental technique is very versatile, for only a small volume of the sample is necessary and the analytical procedure is quite rapid and simple. Therefore, flow injection analysis based on solvent extraction has the potential to open up a new field of practical assays.

Solvent extraction in a teflon tube and phase separation may be very complicated, because they are controlled by numerous parameters. Several phase separators have been reported, e.g., a chamber type [7], a T-piece type [2], and a membrane type [5, 9]. Recently, the performances of the

0003—2670/81/0000—0000/$02.50

separators have been compared [6], and it has been concluded that the membrane type gives much narrower peak width and larger peak height than the T-piece type. The optimum extraction coil length and flow rates have been discussed by some research workers, and dispersion in the extraction coil is usually considered to be negligible [2, 5, 11]. However, no information is available with respect to extraction processes in the extraction coil.

In the study described here, the sensitivity and selectivity of the flow injection determination of gallium with lumogallion [4-chloro-6-(2,4-dihydroxyphenylazo)-1-hydroxybenzene-2-sulfonic acid] were improved by using a solvent extraction system. Furthermore, a laser excitation technique was introduced to examine the extraction phenomena in the narrow teflon tube by direct observation of fluorescence from the segmented stream.

EXPERIMENTAL

Apparatus for determination of gallium

A schematic diagram of the flow injection system is shown in Fig. 1. The aqueous and organic solutions were pumped by a two-channel peristaltic pump fitted with silicone pump tubes. A 10-μl sample aliquot was injected manually by means of a rotary valve (Kusano Kagaku). Tubings for the mixing and extraction coils were of teflon. The optimum parameters finally established for the manifold were as follows: lumogallion flow rate, 1.5 ml min^{-1}; isoamyl alcohol flow rate, 1.5 ml min^{-1}; mixing coil, 35 cm long, 1.0 mm i.d.; extraction coil, 50 cm long, 1.0 mm i.d.

A stream of lumogallion solution including a sodium acetate—hydrochloric acid buffer was mixed with a stream of isoamyl alcohol. The stream of alternative aqueous and organic segments was separated by a membrane device shown in Fig. 2. The body is made of Daifron, and the groove dimensions are 12 mm long by 4 mm wide by 4 mm deep. The teflon (PTFE) porous membrane used was permeable to isoamyl alcohol but impermeable to the aqueous solution (0.8-μm pore size; Sumitomo Electric Ind. Ltd, FP080). The fluorescence intensity of the organic phase including the gallium—lumogallion complex was measured by a conventional spectrofluorimeter (Kyowa KLF-3080) equipped with a 10-μl flow-through cell. The excitation wavelength used was 490 nm, and the fluorescence was monitored at above 520 nm by using a V-O 52 color filter.

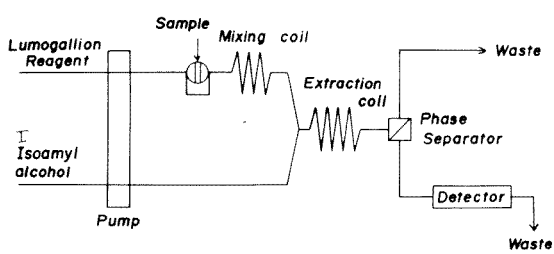

Fig. 1. Diagram of the solvent extraction—flow injection system.

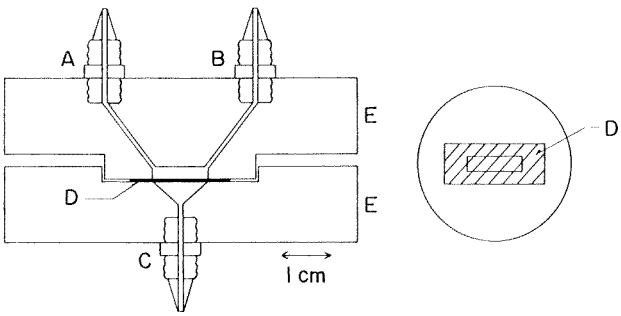

Fig. 2. Construction of membrane phase separator. (A) Joint for inlet of segmented stream; (B) joint for outlet of aqueous phase; (C) joint for outlet of organic phase; (D) PTFE membrane; (E) Daiflon body.

Apparatus for measurement of transient phenomena in the extraction

Solvent extraction based on flow injection could be achieved without any phase separation, when a small volume of an aqueous sample was injected rapidly as small droplets of water into a continuously flowing stream of an organic solvent [11]. It is difficult to measure transient phenomena in flowing segments when a conventional flow cell made of glass is used, because it is important to keep the cell surface free from water. A teflon tube is semitransparent, so that it should be possible to use the teflon tube as a cell for the fluorescence measurement. However, when the measurement is carried out in a conventional spectrofluorimeter, severe scattering from the tube surface will affect the fluorescence detection.

The laser excitation technique provides a number of advantages in this instance. The laser beam can be so tightly focused that light scattering from the surface of the teflon tube can be completely removed by introducing the light perpendicular to the tube surface. Furthermore, the tightly focused laser source provides good resolution of position and time. The excitation source used in this study was the 488-nm line of a CW argon ion laser (NEC-GLG-3200). Fluorescence from the sample in the extraction coil was collected by a lens onto the entrance slit of a double monochromator (CT-40D). Fluorescence was detected by a photomultiplier, and the signal was amplified by a picoammeter (Keithley 417). This signal was converted to a pulse train, the frequency of which corresponded to the signal voltage, and was recorded by a multichannel analyzer (IT-5300). The time resolution of the system was 2 ms.

The sample preparation and the experimental procedure were similar to the previous report [12].

RESULTS AND DISCUSSION

Effect of pH on fluorescence intensity

A set of standard gallium solutions was injected to find the optimum pH of the carrier solution. The results are shown in Fig. 3. The fluorescence

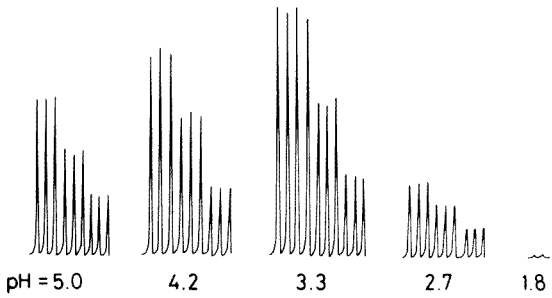

Fig. 3. Effect of pH on the flow injection determination of gallium with lumogallion. Gallium concentrations, 0.5×10^{-4} M, 1.0×10^{-4} M, 1.5×10^{-4} M; flow rates, 1.3 ml min^{-1}; carrier solutions, 2×10^{-4} M lumogallion; extraction coil, 200 cm long, 1.0 mm i.d.

intensity of the extracted gallium—lumogallion complex was at a maximum at pH 3.3, and the calibration graph was linear over the range indicated.

Effects of reaction coil length and extraction coil length

In order to obtain optimum conditions for the determination, the reaction coil length and inner diameter (i.d.) of the tube were studied. Dispersion increases with increasing coil length, and this leads to decrease in peak height; yet excessively short reaction coils give poor mixing and inadequate residence times. Various reaction coils were examined; Fig. 4 shows some condensed results. Tubing 35-cm long and of 1.0 mm i.d. provided the best results under these conditions; poor linearities were observed for shorter tubes and smaller internal diameters, probably because the residence times were insufficient.

The results in Fig. 5. show the influences of the extraction coil length and internal diameter on peak height. The profiles show a maximum. If dispersion is negligible because of the segmented flow, the peak height should increase with increasing coil length and reach a constant value. The present results imply that mixing can occur between the segments separated by the aqueous phase. This tendency has been also observed in the fluorimetric determination of zinc with 5-sulfo-8-quinolinol and tetradecyldimethylbenzylammonium chloride (Zephiramine) [13] and of sodium dodecyl sulfate with acriflavin by a flow injection method based on solvent extraction [14]. The use of small i.d. teflon tubing increased the peak height, but the results were much less reproducible. Accordingly, an extraction coil 50 cm long (1.0 mm i.d.) was used in further work. The sensitivity of the solvent extraction system is 2.6 times better than that of the aqueous phase system under these conditions.

Calibration graphs for gallium

Samples containing 2.2×10^{-5}—8.7×10^{-5} M gallium were injected into the carrier stream, and the fluorescence intensity of the extracted gallium—lumogallion complex was measured. The calibration graph obtained was

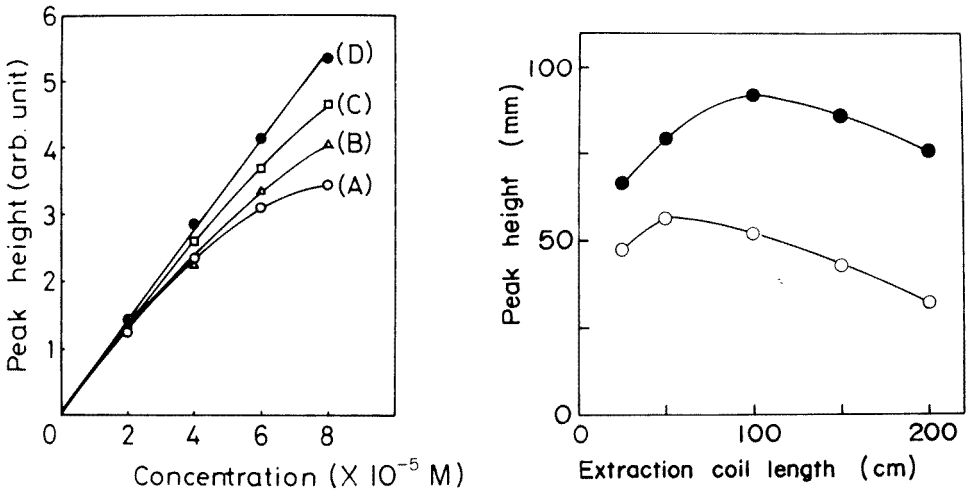

Fig. 4. Effect of reaction coil length (cm) and inner diameter (mm) on the determination of gallium. (A) 15 cm, 0.5 mm; (B) 30 cm, 0.5 mm; (C) 45 cm, 0.5 mm; (D) 35 cm, 1.0 mm. Flow rates, 1.5 ml min^{-1}; carrier solution, 2 × 10^{-4} M lumogallion; pH 3.3; extraction coil, 50 cm long, 1.0 mm i.d.

Fig. 5. Effect of extraction coil length on the determination of gallium: (•) 0.5 mm i.d.; (○) 1.0 mm i.d. Flow rates, 1.3 ml min^{-1}; reaction coil 25 cm long, 1.0 mm i.d.; carrier solution, 2 × 10^{-4} M lumogallion; sample, 0.54 × 10^{-4} M gallium solution.

linear and quite reproducible. Figure 6 shows the analytical curve at yet lower concentrations, when samples of 4 × 10^{-6}—1.6 × 10^{-5} M gallium were injected. The results were reproducible so that the determination of gallium was possible at concentrations of about 10^{-6} M, because of the high sensitivity of the fluorimetric method. However, some deviation from linearity was observed. This sigmoidal type of analytical curve has sometimes been observed in other solvent extraction—flow injection methods combined with sensitive fluorimetric determinations [13, 14].

Effect of diverse ions

The effects of Mg(II), Co(II), Zn(II), Ni(II) and Fe(II) were examined by measuring the fluorescence peak heights for mixed solutions of gallium and the diverse ion. These ions scarcely affected the determination of gallium; Al(III), Fe(III) and Cu(II) were reported to cause large errors [12]. The results obtained for these ions and chromium(VI) by the extraction modification are listed in Table 1 along with the results obtained earlier by the flow injection method without extraction but with fluorescence enhancement by polyethylene glycol monolauryl ether [12]. The negative errors caused by these metals are definitely reduced by using the solvent extraction system. Interference can be reduced further by using a more concentrated lumogallion solution. Moreover, masking with ascorbic acid and thiourea were very effective for Fe(III) and Cu(II) ions, respectively; ten-fold molar

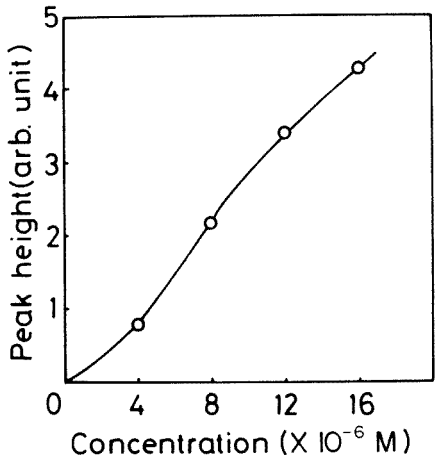

Fig. 6. Analytical curve for low concentrations of gallium. Flow rates, 1.0 ml min^{-1}; reaction coil, 110 cm long, 1.0 mm i.d.; carrier solution, 1.5×10^{-4} M lumogallion; sample volume, 100 μl.

amounts of these ions did not interfere when the masking reagents were added at 1×10^{-2} M concentrations.

Transient phenomena in extraction

The solvent extraction process in the narrow teflon tube is really quite complicated. If extraction were possible only at the boundary of the organic and aqueous phases and if mixing in the segment were not efficient, then it would be expected that the concentration of the extracted sample would be different depending on the position of the segment. Furthermore, if the segmented flow were exactly "segmented", no inter-segment mixing could take place. However, the experimental results in Fig. 5 suggest that mixing occurs even between organic segments separated by an aqueous phase. The concentration profiles of the gallium—lumogallion complex in the extraction tube were therefore examined by laser fluorimetry. The observed transient phenomena during extraction are shown in Fig. 7. This figure

TABLE 1

Effect of diverse ions on the determination of 1.0×10^{-4} M gallium[a]

Metal ion added[b]	Recovery (%)	
	With 2×10^{-4} M lumogallion	With 6×10^{-4} M lumogallion
Al(III)	106 (109)[c]	111
Fe(III)	60 (17)	66
Cu(II)	30 (4)	57
Cr(VI)	12	10

[a]Length of reaction tube, 100 cm; length of extraction tube, 50 cm. [b]Molar ratio; [M]:[Ga] = 100:1. [c]Data from ref. [12] are given in parentheses.

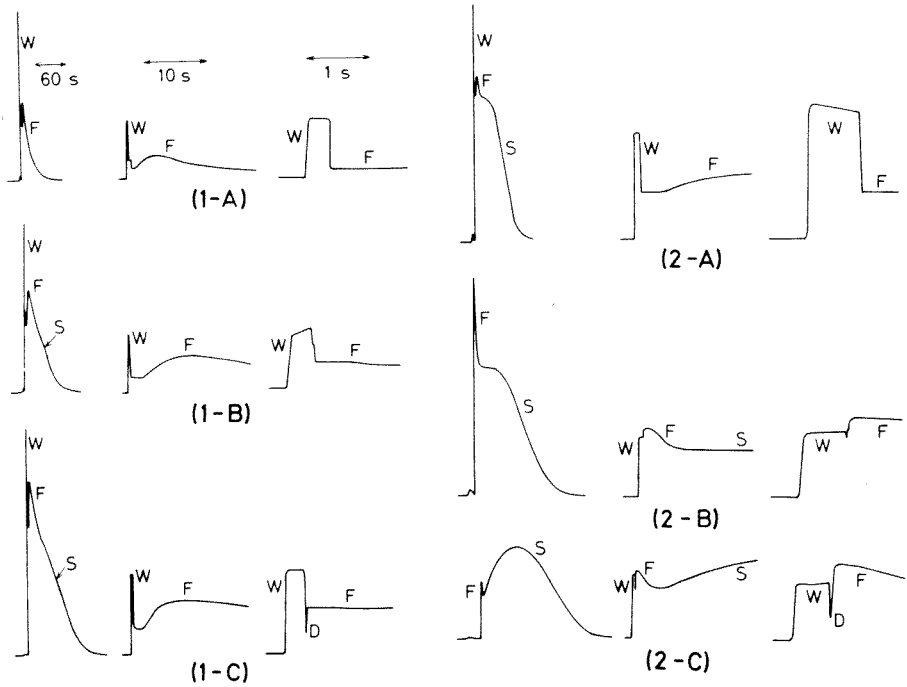

Fig. 7. Transient phenomena in the extraction of the gallium—lumogallion complex. An aqueous sample (10 μl) containing 1×10^{-4} M of gallium and 2×10^{-4} M of lumogallion was injected into an isoamyl alcohol stream. The abscissa relates to time and the ordinate to fluorescence intensity. Flow rates: (1) 1.3 ml min^{-1}; (2) 0.6 ml min^{-1}. Coil length: (A) 20 cm; (B) 55 cm; (C) 90 cm. W, water phase; F, fast component; S, slow component; D, dip. In each set of three curves, the left-hand one was measured by the chart recorder and the other two were measured with the multichannel analyzer.

provides interesting information about the extraction process in flow injection analysis. First, the intensity ratio of the organic phase to that of the aqueous phase increases with increasing coil length and decreasing flow rate. This not unexpected result confirms that extraction indeed occurs in the range examined. Secondly, the fluorescence intensity of the organic phase preceding the injected aqueous phase is very weak or negligibly small; the extracted complex is observed only downstream from the aqueous phase. Accordingly, it cannot be assumed that extraction takes place only at the boundary between the organic phase and the aqueous phase containing the sample when the segments of extracted substance are separated by the aqueous phase.

Thirdly, two extraction processes, a fast process and a slow process, are observed in Fig. 7. As shown in Fig. 7 (1-A, left), the fluorescence intensity in the organic phase increases quickly to a maximum and then decreases gradually. The semilogarithmic plot of the transient decay signal was linear, so that this decay might be ascribed to dispersion of the complex in the tube.

Just after the aqueous phase, as shown in Fig. 7 (1-A, middle), it takes a time of about 4 s to reach the maximum, so that this corresponds to a very fast extraction process. There is a slower component in the extraction system; this appears as a shoulder only when the extraction coil is long, as in Fig. 7 (1-C, left), but it is much more obvious at the lower flow rate, as shown in Fig. 7 (2-A, B, C). A dip appears between the organic and aqueous phases when a long coil is used (Fig. 7, 1, 2-C, right). This dip was reproducible at a flow rate of 1.1 ml min^{-1} with an extraction coil length of 90 cm. The extraction rate is therefore considered to be not so fast that extraction of the complex from the aqueous phase may be almost complete.

In further tests, an air bubble or an aqueous segment was inserted after the organic phase following the injected aqueous solution. Also, the aqueous sample was injected into a flow consisting of alternate segments of the aqueous and organic phase. However, the dispersion could not be removed. These results show that inter-segment mixing takes place in the extraction coil.

From all these results, it appears that the model which must be considered involves the aqueous segment running through a sheath of organic solvent on the inner surface of the teflon tube. If this is true, extraction takes place instantly and the concentration of the extract decays gradually owing to dispersion. This may be the fast process shown in Fig. 7. Some part of the complex is considered to be strongly adsorbed on the surface of the teflon tube, and it takes time to release the complex; this desorption is the probable cause of the slow process.

For the best use of flow injection analysis, the experimental conditions of the extraction system must be optimized carefully. To achieve complete extraction, the residence time in the extraction coil must be quite lengthy, but an increase in the length of the extraction coil increases the dispersion of the extract in the tube, while a decrease in the flow rate decreases the sample injection rate. Thus the residence time requires careful adjustment. Adsorption seems to play an important role in the mixing and dispersion processes in the extraction system discussed here. It should be stressed that if the residence time is identical, dispersion is much less for the fast process than for the slow process, as shown in Fig. 7. Therefore, it appears that a high flow rate and a long extraction coil should be used because this reduces the contribution of the slow process. This adjustment of the experimental conditions would improve the sensitivity and the sample injection rate, though it would increase the amount of solvent needed and would also require a separator which could be operated at a higher flow rate than the one described in this paper.

The authors thank Hirotaka Kurogi for helpful discussions during this study. This research was supported by a Grant-in-Aid for Environmental Science (Grant No. 303046) from the Ministry of Education of Japan.

REFERENCES

1 J. Růžička and E. H. Hansen, Anal. Chim. Acta, 114 (1980) 19.
2 B. Karlberg and S. Thelander, Anal. Chim. Acta, 98 (1978) 1.
3 B. Karlberg, P. A. Johansson and S. Thelander, Anal. Chim. Acta, 104 (1979) 21.
4 B. Karlberg and S. Thelander, Anal. Chim. Acta, 114 (1980) 129.
5 P. A. Johansson, B. Karlberg and S. Thelander, Anal. Chim. Acta, 114 (1980) 215.
6 L. Nord and B. Karlberg, Anal. Chim. Acta, 118 (1980) 285.
7 H. Bergamin F°, J. X. Medeiros, B. F. Reis and E. A. G. Zagatto, Anal. Chim. Acta, 101 (1978) 9.
8 J. Kawase, A. Nakae and M. Yamanaka, Anal. Chem., 51 (1979) 1640.
9 J. Kawase, Anal. Chem., 52 (1980) 2124.
10 O. Klinghoffer, J. Růžička and E. H. Hansen, Talanta, 27 (1980) 169.
11 K. Kina, K. Shiraishi and N. Ishibashi, Talanta, 25 (1978) 295.
12 N. Ishibashi, K. Kina and Y. Goto, Anal. Chim. Acta, 114 (1980) 325.
13 M. Ichishima and N. Ishibashi, 1980, unpublished work.
14 H. Kurogi and N. Ishibashi, 1981, unpublished work.

Analytica Chimica Acta, 129 (1981) 205—211
Elsevier Scientific Publishing Company, Amsterdam — Printed in The Netherlands

DETERMINATION OF MANGANESE IN SERUM AND URINE BY ELECTROTHERMAL ATOMIC ABSORPTION SPECTROMETRY

D. J. HALLS* and G. S. FELL
Department of Biochemistry, Glasgow Royal Infirmary, Glasgow G4 0SF (Gt. Britain)
(Received 18th March 1981)

SUMMARY

Manganese is determined in serum and urine by graphite-furnace atomic absorption spectrometry after dilution (1 + 1) with distilled water. Simple aqueous standards are used for calibration. Background absorption from the matrix is decreased by attention to the heating programme, sample dilution and gas flow-rate during atomisation. Remaining background absorption is removed by a deuterium-arc background correction system. To obtain accurate results, great care is needed in collecting samples to avoid contamination. Blood is collected through a plastic cannula, because stainless steel needles introduce considerable contamination. The mean normal concentration of manganese in serum was found to be 0.58 $\mu g\ l^{-1}$ (n = 9) which is in agreement with other literature values. For urine, the mean normal concentration found was 0.7 $\mu g\ l^{-1}$ (n = 16). Patients on total parenteral nutrition with manganese supplements show elevated serum and urine manganese concentrations.

Manganese is considered to be an essential trace element. This is well-proven from studies on animals, but convincing proof of its essentiality in man has not yet been obtained [1]. However, it is recommended for inclusion in trace element supplements for patients on intravenous feeding [2, 3], although the amount of manganese actually required is not known. As part of a continuing programme of assessing trace element requirements for patients on intravenous feeding, methods have been developed here for measuring manganese in serum and urine.

As manganese is excreted mainly in faeces, the concentration of manganese in urine is normally quite low, around 1 $\mu g\ l^{-1}$. Serum levels are of the same order. There are two main problems in measurement by any method. The first is in making measurements at such low levels without interference from the matrix; the second is in avoiding contamination in the collection and treatment of samples. Disagreement over values for normal levels of manganese in serum [4] shows that there are still many problems involved in this measurement.

Techniques which have been used for measurements of manganese in serum include graphite-furnace atomic absorption spectrometry (a.a.s.) [5—12], catalytic reaction-rate spectrophotometry [13] and neutron activation analysis [14—17]. Methods involving furnace a.a.s. have given, to date,

higher values for normal levels than the most careful work based on neutron activation analysis and catalysis. For urine, the larger amount of sample available allows the use of solvent extraction procedures to concentrate the sample for analysis by flame a.a.s. [18, 19] or furnace a.a.s. [20]. Direct determination by furnace a.a.s. has also been described [19]. The aim in the work described here was to develop simple direct methods for determination of manganese in serum and urine using graphite furnace a.a.s., and to elaborate practical sample collection procedures which minimise contamination.

EXPERIMENTAL

Instrumentation and reagents

A Perkin-Elmer 272 atomic absorption spectrometer was used with an HGA 500 graphite furnace, AS1 auto-sampler and Model 56 recorder.

Acids used were of Aristar grade (BDH Chemicals Ltd.). Water used to prepare standards and dilute samples was first deionised and then distilled.

Collection of samples

Blood was collected through a plastic cannula (Venflon, Viggo AB, Sweden). The first 10 ml, at least, was discarded or used for other tests. A further 10 ml was taken into a syringe and transferred to an acid-washed plastic centrifuge tube. After the blood had clotted, the tube was centrifuged. The serum was transferred to an acid-washed sample tube.

Urine samples obtained from healthy laboratory workers were voided directly into acid-washed 25-ml Sterilin Universal containers, and 0.5 ml of concentrated sulphuric acid was added to acidify the urine. Samples from patients were 24-h collections in acid-washed polythene containers containing glacial acetic acid (1 ml for preterm infants; 5 ml for adults).

Precautions against contamination

All glassware, pipettes, micropipette tips, autosampler cups and sample tubes were cleaned with 20% (v/v) nitric acid and thoroughly rinsed with distilled water before use.

Analytical procedures

Serum. Dilute the serum samples (1 + 1) with distilled water directly into acid-washed autosampler cups. Mix on a vibromixer. Analyse against standards of 0, 1, 2 and 3 μg Mn l^{-1} in 0.1 M nitric acid using the instrumental conditions in Table 1.

Urine. Dilute urine samples (1 + 1) with distilled water as for serum. Analyse against standards of 0, 2, 5 and 10 μg Mn l^{-1} in 0.1 M nitric acid using the instrumental conditions in Table 1. This calibration range should cover the higher levels of manganese in urine found in samples from patients on total parenteral nutrition with manganese supplements. For normal levels of manganese in urine, lower standards are preferable (0, 1, 2 and 3 μg l^{-1}) as for serum.

TABLE 1

Instrument settings for the determination of manganese in serum and urine Wavelength 279.5 nm; slit width 0.7 nm; injection volume 20 μl; background correction ON

Furnace programme step	Serum			Urine		
	Temp. (°C)	Ramp (s)	Hold (s)	Temp. (°C)	Ramp (s)	Hold (s)
Dry	110	7	13	100	7	13
Ash	1100	7	23	1100	7	23
Atomise	2700	2	10	2700	2	10
Clean	2700	2	5	2700	2	5
Gas flow during atomisation	10 ml min^{-1}			30 ml min^{-1}		

RESULTS AND DISCUSSION

Removal of background absorption

It is important that the background absorption from the matrix should be removed completely. A deuterium arc background correction system can be used successfully provided additional steps are first taken, if necessary, to reduce the background to an acceptable level. The background absorption was found to decrease with increasing ashing temperature. The maximum ashing temperature which could be used without loss of manganese was 1100°C; this temperature is used in the methods for serum and urine. Dilution of the sample also will decrease the background. For serum, the sample is diluted (1 + 1) with water for this reason and also because undiluted serum tends to dry unevenly in the furnace.

The problem of background is more significant in the analysis of urine samples. Dilution (1 + 1) decreased the background, but it was also found necessary to use an increased gas flow during atomisation. An increase in gas flow during atomisation from 10 to 30 ml min^{-1} decreased the background by over 50%, but only decreased the manganese peak height by 27%. Many urine samples could probably be analysed accurately without dilution, but the higher background makes greater demands on the background correction system. The effect of dilution on recoveries (Table 2) illustrates the benefit to be obtained from the dilution step. Although the mean recovery is not very different, the range of recoveries is much greater with undiluted urine.

TABLE 2

Effect of dilution on recovery of manganese in urine

	n	Range	Mean recovery (%)	Coeff. of variation (%)
Undiluted urine	9	83—122	104	11.9
Urine diluted (1 + 1)	12	88—111	102	7.4

Determination of manganese in serum

A large part of the matrix is removed in the ashing stage. The remainder appears to have a minimal effect on the signal from manganese. Thus simple aqueous standards can be used for calibration and good recoveries are obtained, as shown in Table 3. Other data on the performance of the method are also given in Table 3.

One of the most important considerations for accurate results is the procedure for sample collection. Versieck et al. [21] have demonstrated that stainless steel needles can introduce considerable contamination when used to collect biological samples. For their studies [22] they collected blood samples using plastic cannulae; Damsgaard et al. [14] used platinum needles. In the present studies, Venflon plastic cannulae were used. These are inserted with an inner stainless steel needle which is then withdrawn leaving the cannula in place. Since contact with the needle may have contaminated the inside surface of the cannula, it was important to determine how much blood should be passed through the cannula to wash out the contamination. The serum manganese concentration was measured in 10-ml aliquots of blood taken consecutively through the cannula. The results showed that the first 10 ml is contaminated (it contained 0.90 μg Mn l^{-1}) and should be discarded or used for other biochemical tests. The subsequent 10-ml aliquots all contained 0.60 μg Mn l^{-1}.

The mean value obtained from analyses of the sera of nine normal subjects was 0.58 μg l^{-1} which is close to values obtained by other workers using care in sample collection [14, 15, 17], as is shown in Table 4. When blood samples were collected in the normal way through a stainless steel needle and using untreated plastic sample tubes, a higher mean value for normal sera of 1.3 μg l^{-1} was obtained. As can be seen from Table 4, this value is similar to other values obtained by graphite-furnace a.a.s.

Determination of manganese in urine

For urine also, the matrix effect appears to be minimal as is shown by good recovery of added manganese (Table 3). Thus standardisation can be

TABLE 3

Precision, recovery and normal concentrations obtained using the methods outlined

		Serum	Urine
Coeff. of variation (within batch)			
at 0.6 μg l^{-1}		7.5%	—
at 4.6 μg l^{-1}		3.7%	—
at 11.6 μg l^{-1}		—	2.4%
Recovery		95 ± 2%	102 ± 8%
Normal concentration (μg l^{-1}):	mean	0.58[a]	0.7[b]
	range	0.36—0.96	0.1—1.3

[a] $n = 9$. [b] $n = 16$.

TABLE 4

Comparison of measured values of the normal concentration of manganese in serum

Authors	Technique[a]	Mean concn. ($\mu g\ l^{-1}$)	Range ($\mu g\ l^{-1}$)	Ref.
Ross and Gonzalez	G.f.a.a.s.	21.8	8.5—40.5	9
Bek. et al.	G.f.a.a.s.	13.4	8—17.5	11
Kanabrocki et al.	N.a.a.	13	11—14	16
Muzzarelli and Rocchetti	G.f.a.a.s.	9	5—16	5
Grafflage et al.	G.f.a.a.s.	1.94	—	6
Pleban and Pearson	G.f.a.a.s.	1.82	0.94—2.92	7
D'Amico and Klawans	G.f.a.a.s.	1.02	0.74—1.25	8
Fernandez et al.	Catalysis	0.63	0.36—0.90	13
Cotzias et al.	N.a.a.	0.59	—	17
Versieck et al.	N.a.a.	0.57	0.38—1.04	15
Damsgaard et al.	N.a.a.	0.54	0.36—0.78	14
This work	G.f.a.a.s.	0.58	0.36—0.96	—

[a]G.f.a.a.s., graphite furnace atomic absorption spectrometry; [b]N.a.a., neutron activation analysis.

made with simple aqueous standards. Table 3 summarises the performance of the method. Analysis of random urine samples from 16 healthy laboratory workers gave a mean concentration of 0.7 μg Mn l^{-1} which is close to that obtained by Watanabe et al. [19] and Buchet et al. [20], but lower than that obtained by Van Ormer and Purdy [18] (Table 5). The advantage of the present method over earlier methods is that no prior solvent extraction is necessary.

Contamination in collection of samples is again a serious problem. Acid-washed containers should be distributed for urine collection, but the main problem originates from the kind of urine bottle given to patients who are confined to bed. Disposable urine bottles made of compressed fibre cause extreme contamination by manganese and other trace elements (especially zinc) [23]. The contamination is so severe that it is possible to use manganese values obtained by the less-sensitive flame a.a.s. as a screening procedure to

TABLE 5

Comparison of measured values of the normal concentration of manganese in urine

Authors	Technique[a]	Mean concn. ($\mu g\ l^{-1}$)	Range ($\mu g\ l^{-1}$)	Ref.
Van Ormer and Purdy	Solv. Ext./f.a.a.s.	3.0[b]	2.0—4.2[b]	18
Buchet et al.	Solv. Ext./g.f.a.a.s.	0.65	($\pm$0.53)[c]	20
Watanabe et al.	Solv. Ext./f.a.a.s.	0.53	0.08—2.67	19
This work	G.f.a.a.s.	0.7	0.1—1.5	—

[a]F.a.a.s., flame atomic absorption spectrometry; g.f.a.a.s., graphite furnace atomic absorption spectrometry; Solv. Ext., solvent extraction. [b]5 urine samples from the same subject. [c]Standard deviation of results. Range not quoted.

identify urines which have been collected in such bottles. The best kind of bottle was found to be one made of plastic, which can be cleaned thoroughly prior to use and which introduces no significant contamination for a range of trace elements.

Manganese levels in patients on total parenteral nutrition

Complete intravenous feeding (total parenteral nutrition, TPN) should include all essential nutrients including trace elements. The only trace element additive marketed to date for adult patients (Addamel, Vitrum AB, Stockholm) includes manganese (2.2 mg/day). Use of this additive in a TPN regimen results in elevated serum and urinary manganese levels, as can be seen in Table 6. Adult patients on TPN given an additive mixture containing less manganese (0.83 mg/day) also show elevated manganese levels in serum and urine. Whether these increased levels are a result of over-supply of manganese or are caused by other components of the TPN regimen is being investigated. The additive prepared for neonates and infants (Ped-El, Vitrum AB, Stockholm) also appears to cause elevated manganese levels in serum and urine as is shown in Table 6 for premature infants. At the recommended dose, Ped-El supplies 55 μg manganese/kg body weight/day.

Conclusions

With care taken in collecting specimens, the simple procedures outlined above make it possible to obtain values for normal levels in serum which are similar to the value quoted by Versieck and Cornelis [4] as the consensus among experienced investigators. These values were obtained by neutron-activation analysis [14, 15, 17] and catalytic reaction-rate spectrophotometry [13]. Results obtained previously by atomic absorption spectrometry have always given higher results. Thus this paper illustrates that there is no

TABLE 6

Concentrations of manganese in serum and urine of some patients on total parenteral nutrition receiving manganese supplements

Patient	Mean serum concn. ($\mu g\ l^{-1}$)	Mean urine concn. ($\mu g\ l^{-1}$)	Patient	Mean serum concn. ($\mu g\ l^{-1}$)	Mean urine concn. ($\mu g\ l^{-1}$)
Adults receiving Addamel			Normal adults on oral diet	0.6	0.7
P.P.	2.4	7.8			
E.C.	16.3	13.1			
J.T.	2.6	3.0	Premature infants receiving Ped-El		
			B.W.	8.2	5.4
Adults receiving a supplement			B.B.	11.2	12.7
containing 0.83 mg Mn/day			B.D.	7.5	6.6
P.P.	2.5	10.7			
R.M.	1.3	3.6			
W.O.	1.1	1.6			

systematic difference between the techniques; improvement in quality of results has been obtained mainly through attention to the collection procedure. Graphite-furnace a.a.s. provides results more quickly than neutron activation analysis and is more suitable for the clinical laboratory. The introduction of these a.a.s. methods should help in achieving a greater appreciation of the role of manganese in nutrition and disease, the literature for which is somewhat clouded by suspect analytical data.

The authors are grateful to Dr. A. Shenkin for providing samples and for his support for this work; to Mrs. P. Dunbar and Mrs. S. Nigdikar for technical assistance; to Professor F. Cockburn and Dr. S. M. Jorge of the Royal Hospital for Sick Children, Yorkhill, Glasgow, for providing samples from premature babies and to Vitrum AB, Stockholm, Sweden, for financial support, in particular, a fellowship for D. J. H.

REFERENCES

1 R. M. Leach, Jr., Metabolism and Function of Manganese, in A. S. Prasad and D. Oberleas (Eds.), Trace Elements in Human Health and Disease, Vol. II, Academic Press, New York, 1976, p. 235.
2 Expert Panel for Nutrition Advisory Group of the American Medical Association, J. Am. Med. Assoc., 241 (1979) 2051.
3 A. Shenkin and A. Wretlind, World Rev. Nutr. Diet., 28 (1978) 1.
4 J. Versieck and R. Cornelis, Anal. Chim. Acta, 116 (1980) 217.
5 R. A. A. Muzzarelli and R. Rocchetti, Talanta, 22 (1975) 683.
6 V. B. Grafflage, G. Buttgereit, W. Kubler and H. M. Mertens, Z. Klin. Chem. Klin. Biochem., 12 (1974) 287.
7 P. A. Pleban and K. H. Pearson, Clin. Chem., 25 (1979) 1915.
8 D. J. D'Amico and H. L. Klawans, Anal. Chem., 48 (1976) 1469.
9 R. T. Ross and J. G. Gonzalez, Bull. Environ. Contam. Toxicol., 12 (1974) 470.
10 F. Alt and H. Massman, Fresenius, Z. Anal. Chem., 279 (1976) 100.
11 F. Bek, J. Janouskova and B. Moldan, At. Absorpt. Newsl., 13 (1974) 47.
12 H. Hoffman, Klin. Wochenschr., 58 (1980) 157.
13 A. A. Fernandez, C. Sobel and S. L. Jacobs, Anal. Chem., 35 (1963) 1721.
14 E. Damsgaard, K. Heydorn, N. A. Larsen and B. Nielson, Simultaneous Determination of Arsenic, Manganese and Selenium in Human Serum by Neutron Activation Analysis, Risø Report No. 271, 1973.
15 J. Versieck, F. Barbier, A. Speecke and J. Hoste, Acta Endocrinol. (Copenhagen), 76 (1974) 783.
16 E. L. Kanabrocki, L. F. Case, L. Graham, T. Fields, E. B. Miller, Y. T. Oester and E. Kaplan, J. Nucl. Med., 8 (1967) 166.
17 G. C. Cotzias, S. T. Miller and J. Edwards, J. Lab. Clin. Med., 67 (1966) 836.
18 D. G. Van Ormer and W. C. Purdy, Anal. Chim. Acta, 64 (1973) 93.
19 T. Watanabe, R. Tokunuga, R. Iwahana, M. Tati and M. Ikeda, Brit. J. Ind. Med., 35 (1978) 73.
20 J. P. Buchet, R. Lauwerys and H. Roels, Clin. Chim. Acta, 73 (1976) 481.
21 J. Versieck, A. Speecke, J. Hoste and F. Barbier, Clin. Chem., 19 (1973) 472.
22 J. Versieck, F. Barbier, A. Speecke and J. Hoste, Clin. Chem., 20 (1974) 1141.
23 G. S. Fell, A. Shenkin and D. J. Halls, in P. Bratter and P. Schramel (Eds.). Trace Element Analytical Chemistry in Medicine and Biology, W. De Gruyter, Berlin, 1980, p. 217.

Analytica Chimica Acta, 129 (1981) 213—220
Elsevier Scientific Publishing Company, Amsterdam — Printed in The Netherlands

DOSAGE DE LA SILICE DES SILICATES, APRES DISTILLATION, PAR GRAVIMETRIE DU MOLYBDOSILICATE DE QUINOLEINE

V. HERNANDIS[a], J. LOUVRIER et I. A. VOINOVITCH*

Laboratoire Central des Ponts et Chaussées, Service de Chimie, 58, Boulevard Lefèbvre, 75732 Paris Cedex 15 (France)

(Reçu le 29 décembre, 1980)

SUMMARY

(The determination of silica in silicates by distillation and gravimetry as quinoline 12-molybdosilicate)

Quantitative distillation of silica as hexafluorosilicic acid is followed by gravimetric determination of the silicate as quinoline 12-molybdosilicate. Precise results are obtained even when the samples contain phosphorus and fluorine. Compared to classical insolubilization procedures with strong acids, the proposed method is quicker and more sensitive, being applicable down to ca. 1 mg SiO_2. Its application is limited to silicates decomposed by hot sulphuric acid—hydrofluoric acid mixtures. The accuracy of the procedure is confirmed by the results for numerous reference standards.

RESUME

On a pu montrer la possibilité du couplage distillation quantitative de la silice sous forme d'acide hexafluorosilicique et dosage gravimétrique par la quinoléine du complexe molybdosilicique. Des résultats précis sont obtenus, même lorsque les échantillons analysés renferment du phosphore et du fluor. Par rapport aux insolubilisations classiques de la silice par les acides forts, la méthode proposée est plus rapide et plus sensible, car son seuil de dosage est de l'ordre du milligramme de SiO_2. Son domaine d'application est limité toutefois aux silicates décomposables par le mélange acide sulfo—fluorhydrique à chaud.

L'expérience montre que le dosage gravimétrique de la silice après insolubilisation par un acide fort donne généralement des résultats par défaut, même en utilisant des coagulants tels que le polyox ou la gélatine. De ce fait, pour obtenir un résultat exact, il est nécessaire d'effectuer, de plus, la détermination par colorimétrie de la silice non insolubilisée [1—4]. L'expérience montre également que la précipitation de la silice sous forme de K_2SiF_6, en raison de sa solubilité non négligeable, ne peut être retenue pour des analyses précises. Par contre, on sait que la quinoléine permet de précipiter quantitativement le complexe stoéchiométrique formé entre l'ion silicium et le molybdate d'ammonium [5—7]. On obtient ainsi directement la valeur exacte de SiO_2, à condition que le milieu ne contienne ni phosphore, ni

[a]Facultat de Ciencias, Departamento Quimica Analitica, Universidad Alicante, Espagne.

arsenic qui forment également avec ce réactif des complexes précipitant par la quinoléine. Donc, si l'on peut séparer quantitativement la silice, on pourra dans tous les cas la doser avec précision par la quinoléine.

Or, Bosch Arino et al. [8] a mis au point une méthode de distillation quantitative de l'acide hexafluorosilicique libéré par décomposition des silicates par le mélange sulfo—fluorhydrique. Cette séparation fournit d'une part une solution fluorhydrique de silicium sous forme de H_2SiF_6 et d'autre part un résidu contenant tous les autres constituants de l'échantillon sous forme de sulfates. Il est évident que dans le distillat on pourra doser le silicium sans aucune interférence par une méthode qui soit compatible avec la présence de HF en excès, c'est-à-dire par précipitation de K_2SiF_6 [9—11] ou par formation du complexe molybdosilicique. D'autre part, les éléments contenus dans le résidu pourront être ensuite dosés en absence du silicium souvent gênant [12]. C'est pourquoi nous avons estimé que la combinaison de la distillation de la silice et de sa précipitation sous forme de molybdosilicate de quinoléine constituerait une méthode de dosage à la fois juste, assez rapide et exempte d'interférences.

Etude des conditions de précipitation

Le dosage de la silice par précipitation par la quinoléine du complexe molybdosilicique est effectué habituellement sur des attaques réalisées à l'aide des hydroxydes alcalins, des acides chlorhydrique ou nitrique et des borates alcalins. Afin d'effectuer ce dosage après séparation de la silice par distillation fluorohydrique, nous avons étudié divers paramètres.

Lorsqu'on opère en milieu fluorhydrique, il est nécessaire de libérer le silicium de son complexe fluorosilicique. Ceci se fait généralement par addition d'acide borique qui fixe en même temps l'excès d'acide fluorhydrique sous forme d'acide tétrafluoroborique. Dans tous les cas, nous avons employé 100 ml de solutions à 5% d'heptamolybdate d'ammonium pour la formation du complexe et 100 ml de solution à 2% de quinoléine pour sa précipitation [7].

Influence du pH. On a d'abord utilisé l'acide borique dans le rapport constant de 4 mol de H_3BO_3 par mol de HF, en ajoutant le molybdate immédiatement après la décompléxation. On a travaillé sur une solution de silice pure (99,8% SiO_2) en milieu fluorhydrique. Le pH est ajusté par addition de solutions diluées de HCl ou de NH_3. On constate que pour les pH 1,5; 2,5 et 3,5 les valeurs de SiO_2 trouvées sont, respectivement, de 98,14; 99,66 et 99,78%. Au dessus de pH 3,5 on observe une décroissance des valeurs.

Influence du temps. Pour des valeurs de pH comprises entre 2,5 et 3,5 et pour un rapport molaire H_3BO_3/HF égal à 4, on obtient 99,82% de SiO_2 lors d'une précipitation immédiate, 99,11% après un jour, et 72,65% après 4 jours.

Influence du rapport H_3BO_3/HF. On a travaillé à pH 2,6—2,7, en précipitant par la quinoléine immédiatement après la décomplexation et la forma-

tion du complexe molybdosilicique. On a fait varier le rapport H_3BO_3/HF en augmentant la quantité de H_3BO_3 employée pour une quantité fixe de HF. On constate que pour une variation de ce rapport de 4 à 8 le pourcentage de SiO_2 obtenu passe de 99,55 à 99,76.

De tous ces résultats on peut tirer les conclusions suivantes. Le pH optimal pour la formation de l'acide molybdosilicique est compris entre 2,5 et 3,5. La formation du complexe et sa précipitation doivent être effectuées immédiatement après avoir décomplexé le silicium (ou tout au moins dans un délai ne dépassant pas 4 h), c'est-à-dire avant polymérisation de l'acide silicique, cette polymérisation le rendant moins réactif vis-à-vis du molybdate. La quantité d'acide borique a peu d'influence si elle est en grand excès par rapport à la quantité d'acide fluorhydrique.

L'acide borique peut être remplacé par d'autres agents capables de complexer l'acide fluorhydrique, par exemple les sels d'aluminium. Dans des essais avec du chlorure d'aluminium, on a pu constater que la polymérisation de l'acide silicique est beaucoup plus rapide qu'en présence d'acide borique, mais que malgré tout on peut obtenir de bons résultats avec les mêmes conditions que pour l'acide borique: pH compris entre 2,5 et 3,0 car au delà du pH 3,0 il y a risque de précipitation de $(OH)_3Al$; rapport moles $AlCl_3$/mole HF compris entre 3 et 4; précipitation immédiate après la décomplexation. Il est, de plus, préférable d'ajouter la solution de molybdate avant celle de chlorure d'aluminium.

PARTIE EXPERIMENTALE

Appareillage et matériel utilisés

La distillation est effectuée dans un appareil en PTFE (téflon) comportant un vase de réaction d'une capacité de 40 ml [11] que l'on introduit dans un chauffe-ballon (Fig. 1).

Tous les réactifs sont de qualité pure pour analyse.

Mélange acide. Mélanger 40 ml de H_2SO_4 (d = 1,84) à 20 ml de HNO_3 (d = 1,40). Après refroidissement, ajouter ce mélange à 80 ml de HF (d = 1,13). Conserver dans un flacon en plastique.

Solution de molybdate d'ammonium. Dissoudre 20 g de $(NH_4)_6Mo_7O_{24}\cdot 4H_2O$ dans 375 ml d'eau et ajouter, sans attendre sa dissolution complète, 25 ml de HCl dilué (1 + 9).

Solution de quinoléine à 2%. Mélanger 20 ml de quinoléine et 50 ml de HCl dilué au demi et amener à 1 l.

Solution de lavage. Mélanger 5 ml de HCl (d = 1,19) avec 10 ml de solution de quinoléine à 2% et amener à 1 l.

Technique opératoire

Distillation. On pèse 200—400 mg de l'échantillon (contenant 5—200 mg de SiO_2) dans le vase de distillation. On ajoute 7 ml du mélange acide en agitant doucement pour former une suspension.

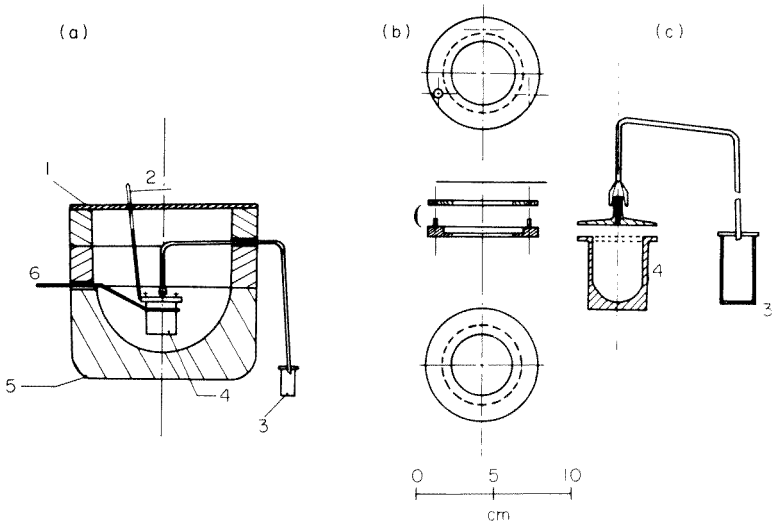

Fig. 1. Le système de distillation. (a) Vue d'ensemble: (1) couvercle amiante; (2) thermomètre; (3) éprouvette; (4) vase; (5) chauffe-ballon; (6) cylindres amiantes. (b) Vue de dessus et de dessous avec l'ensemble serrage (couvercle et vase). (c) Détail montrant le couvercle du vase.

On introduit le système de distillation dans le chauffe-ballon et on règle sa température intérieure à 120°C à l'aide d'un thermomètre à contact. On maintient cette température pendant 30—40 min pour l'attaque de la prise d'essai. Puis, on porte la température à 220—230°C pendant 40 min. C'est pendant cette seconde péroide que se fait la distillation de l'acide fluorosilicique que l'on recueille dans une éprouvette en plastique renfermant 20 ml d'eau distillée. On arrête le chauffage et on lave l'intérieur du tuyau avec deux ou trois petites portions d'eau qu'on ajoute au distillat contenu dans l'éprouvette.

On transvase le distillat dans un bécher en plastique et on ajoute 100 ml de solution de H_3BO_3 à 4%. Cette solution est introduite dans une fiole jaugée et le volume est complété à 250 ml avec de l'eau distillée. Immédiatement après, on prélève les aliquotes nécessaires (50 ml en général) pour effectuer les précipitations.

Le résidu, après refroidissement du vase, est transféré, à l'aide d'un jet d'eau, dans un bécher de 250 ml avec les eaux de lavage du vase et du couvercle. On dilue à 50 ou 100 ml et l'on chauffe jusqu'à ébullition douce, avec agitation, pendant quelques minutes, pour que le résidu se dissolve et si nécessaire, on ajoute 10 ml de HCl dilué (1 + 3). On laisse refroidir et on amène au volume convenable (100 ou 250 ml). Cette solution sert aux dosages de tous les éléments sauf les sulfates, les fluorures et bien entendu le silicium.

Gravimétrie. On prélève 50 ml de la solution du distillat (qui doivent contenir de 1—40 mg de SiO_2) et on les introduit dans un bécher en plastique

(600 ml). On y ajoute 100 ml de la solution de H_3BO_3 à 4% et 100 ml de la solution de molybdate d'ammonium. Le pH de la solution doit être de 2,5 à 3,5. S'il n'en est pas ainsi, il faut l'ajuster avec NH_3 ou HCl dilués. On couvre le bécher et on le place dans un bain d'eau thermostaté à 60°C pendant 30 min, pour que le complexe molybdosilicique se forme quantitativement. On ajoute ensuite, dans l'ordre: 50 ml de HCl concentré (afin d'empêcher la précipitation du molybdate de quinoléine) et 100 ml de la solution de quinoléine. La précipitation est instantanée. On maintient le bécher à 80°C pendant 10 min, puis après refroidissement, on filtre sur creuset en verre fritté de porosité 4, préalablement taré, et on entraîne les dernières particules du précipité avec de petites portions de solution de lavage. Enfin, on lave le précipité 2 ou 3 fois avec la solution de lavage et on sèche à l'étuve à 150°C pendant 1 h. On laisse refroidir le creuset et on le pèse. Le précipité a pour formule $(C_9H_7N)_4SiO_4H_4(MoO_3)_{12}$ (facteur, 0,02566).

La technique opératoire décrite ci-dessus a été testée sur un ciment Portland artificiel (CPA), un ciment contenant 80% de laitier de haut fourneau et 20% de clinker (CLK), une brique réfractaire, un feldspath sodique et un basalte.

RESULTATS ET DISCUSSION

Pour le ciment CPA (BCS 372, valeur certifiée SiO_2 = 21,30%), le dosage de la silice a été effectué par deux opérateurs. Le premier analyste a fait 12 attaques avec distillation et sur chaque distillation il n'a fait qu'un dosage. Dans ce cas, la moyenne est de 21,34% et l'écart-type de 0,16. Le deuxième analyste a fait 8 distillations et sur chaque distillat il a fait 3 dosages. La moyenne des valeurs moyennes des 3 dosages réalisés sur chacune des 8 distillations est de 21,40% avec un écart type de 0,11. De ces résultats on peut déduire qu'il n'y a pas de différences significatives ni en ce qui concerne l'exactitude, puisque les deux analystes donnent des valeurs moyennes qui sont en bon accord avec la valeur certifiée, ni en ce qui concerne la reproductibilité car les deux écarts types sont très voisins.

Ensuite, des dosages ont été réalisés sur 4 échantillons étalons ayant des teneurs croissantes en SiO_2. Sur chaque échantillon 8 distillations ont été faites et sur chaque distillation un seul dosage a été effectué. Les résultats (Tableau 1) sont satisfaisants dans leur ensemble et en particulier pour le basalte BR—CRPG, qui contient 1,04% de P_2O_5. D'autre part, sur 3 échantillons BCS on a effectué également le dosage de SiO_2 par absorptiométrie dans le jaune après distillation (Tableau 2). Si les résultats moyens sont très voisins des valeurs certifiées pour les deux méthodes, par contre, la reproductibilité de la gravimétrie est dans tous les cas supérieure à celle de la colorimétrie.

Ces résultats confirment ceux obtenus par Michalska [13] qui, dans un travail appuyé sur un calcul statistique approfondi, a comparé sur plusieurs ciments la méthode normalisée polonaise (par insolubilisation) à celle par

TABLEAU 1

Dosage de la silice dans 4 silicates étalons

Echantillon	Valeur certifiée (%)	Moyenne trouvée (%)	s ($n = 8$)
Ciment CLK (CERILH, 78-79)[a]	28,28	28,44	0,20
Basalte BR (CRPG)[b]	38,20	38,19	0,11
Brique réfractaire (BCS 315)[c]	51,20	51,11	0,27
Feldspath sodique (BCS 375)	67,10	67,16	0,31

[a]Centre d'Etudes et de Recherches des Industries des Liants Hydrauliques, Paris. [b]Centre de Recherches Pétrographique et Géochimique, Nancy. [c]British Chemicals Standards, Londres.

précipitation du complexe molybdo-silicique par la quinoléine, suivie du dosage volumétrique en retour du précipité redissout. Cet auteur a constaté que cette dernière méthode donne des résultats plus précis et plus reproductibles que ceux fournis par insolubilisation.

Pour mettre en évidence l'effet du phosphore sur le dosage gravimétrique de la silice par la quinoléine, on a déterminé la teneur en silice du basalte BR (qui renferme 1,04% de P_2O_5) après fusion au tétraborate de lithium. Par dosage direct à la quinoléine, on trouve 39,12% de SiO_2 pour une valeur certifiée de 38,20%, c'est-à-dire que l'on obtient une valeur qui correspond sensiblement à la teneur vraie de SiO_2 augmentée de celle du P_2O_5 contenue dans cette roche. On a aussi appliqué la technique par distillation pour l'analyse de 3 échantillons adressés par le CRPG en 1979 à 122 laboratoires en vue de définir la composition de ces 3 nouveaux étalons. Sur chacun de ces échantillons deux distillations et un seul dosage de SiO_2 par distillation ont été réalisés. Le CRPG vient de publier le traitement statistique de l'ensemble des résultats. Dans le Tableau 3 sont regroupés nos résultats et les valeurs moyennes de SiO_2 obtenues par les méthodes chimiques pour l'ensemble des laboratoires ainsi que les écarts types pour les méthodes chimiques, les spectrométries d'absorption atomique et de fluorescence-x et les valeurs retenues par le CRPG comme valeurs de référence.

TABLEAU 2

Comparaison des écarts types correspondant aux résultats obtenus par colorimétrie et par gravimétrie à la quinoléine

Echantillon	Colorimétrie		Gravimétrie		Valeur certifiée (%)
	Moyenne (%)	Ecart type	Moyenne (%)	Ecart type	
Ciment Portland CPA (BCS)	21,1	0,4	21,34	0,16	21,30
Brique réfractaire (BCS)	51,4	0,5	51,11	0,27	51,20
Feldspath sodique (BCS)	67,1	0,5	67,16	0,31	67,10

TABLEAU 3

Echantillons du CRPG, 1979
(Dosage de la silice)

Echantillon	Nos valeurs			Moyenne chimie	Ecarts types, σ			Valeur retenue
	V_1	V_2	Moyenne		Chimie	A.a.s.	F.-x.	
Anorthosite AN-G	46,38	46,47	46,43	46,35	0,50	0,91	0,74	46,3
Basalte BE-N	38,51	38,37	38,44	38,41	0,56	0,79	0,68	38,2
Granite MA-N	65,93	66,37	66,15	66,51	0,68	1,05	0,85	66,6

On constate que nos valeurs, obtenues avec deux dosages seulement, sont en bon accord avec les moyennes des valeurs chimique [14]. Ceci confirme que l'association de la distillation de la silice suivie de son dosage par gravimétrie du complexe molybdosilicique par la quinoléine s'avère tout à fait justifiée. Cette technique pourrait également s'appliquer aux dosages de la silice dans les verres, les aciers, les alliages, etc., contenant notamment du phosphore et de l'arsenic.

Conclusions

Ce travail avait pour objet d'examiner la possibilité du couplage: distillation quantitative de la silice et dosage par gravimétrie par la quinoléine du complexe molybdosilicique. Les essais effectués ont montré que ce couplage est valable et que la méthode proposée conduit à des résultats précis, même lorsque les échantillons analysés renferment des éléments interférents et notamment du fluor et du phosphore.

Par rapport aux méthodes d'insolubilisation par les acides suivies de l'absorptiométrie de la silice non insolubilisée, la méthode proposée est nettement plus rapide et elle est aussi précise tout en étant plus sensible car son seuil de dosage est de l'ordre du milligramme de SiO_2. Par conséquent, elle peut être conseillée comme méthode de référence pour le dosage de la silice des silicates. Toutefois, son domaine d'application est limité aux silicates décomposables par le mélange sulfo—fluorhydrique à chaud.

V. Hernandis remercie la Fondation Angel Garcia Rogel pour la bourse qu'elle lui a accordée et la Direction du Laboratoire Central des Ponts et Chaussées pour son aimable accueil.

BIBLIOGRAPHIE

1 L. Burglen et P. Longuet, Rev. Mater. Constr. Trav. Publics, 606 (1966) 207.
2 I. A. Voinovitch, J. Debras-Guedon et J. Louvrier, L'Analyse des Silicates, Hermann, Paris, 1962.
3 H. Bennett et R. A. Reed, Chemical Methods of Silicate Analysis, Academic Press, Londres, 1971.
4 Comité Européen de Normalisation, 4ème Avant-projet CEN/139 F (Analyses chimiques des ciments), Bruxelles, 1979.

5 H. N. Wilson, Analyst, 76 (1951) 65.
6 M. Armand et J. Berthoux, Anal. Chim. Acta, 8 (1953) 510.
7 I. A. Voinovitch, R. Barbaras, G. Cohort, G. Koelbel, G. Legrand et J. Louvrier, Chim. Anal. (Paris), 50 (1968) 334.
8 F. Bosch Arino, F. Bosch Reig et V. Hernandis, Quim. Anal., 30 (1976) 82.
9 I. Sajo, Acta Chim. Acad. Sci. Hung., 6 (1955) 233.
10 J. Louvrier et I. A. Voinovitch, Ind. Ceram., 510 (1959) 1.
11 F. Bosch Reig, V. Hernandis et M. L. Martin, Bol. Soc. Esp. Ceram. Vidrio, 18 (1979) 93.
12 I. A. Voinovitch, M. Druon, J. Louvrier, M. Bouzanne, M. Sors, G. Friant et J. M. Liagre, Spectrochim. Acta, Part B, 35B (11/12) (1980) 807.
13 Z. Michalska, Cem.-Wapno-Gips, 5 (1969) 135.
14 K. Govindaraju, Geostand. Newsl., 4 (1980) 49.

Analytica Chimica Acta, 129 (1981) 221—229
Elsevier Scientific Publishing Company, Amsterdam — Printed in The Netherlands

SUBSTOICHIOMETRIC ISOTOPE DILUTION ANALYSIS FOR URANIUM BY SYNERGIC EXTRACTION

NOBUO SUZUKI*, KAZUMASA YOSHIDA and HISANORI IMURA
Department of Chemistry, Faculty of Science, Tohoku University, Sendai, 980 (Japan)
(Received 19th January 1981)

SUMMARY

Substoichiometric extraction of uranyl ion in a synergic system of a chelating reagent and a neutral ligand is described. The system is based on a substoichiometric amount of 2-thenoyltrifluoroacetone (TTA) and an excess of tributylphosphate (TBP); this is compared with a system involving a substoichiometric amount of trioctylphosphine oxide and an excess of TTA. The reproducibility of the substoichiometric extraction is 0.46 or 0.62%, respectively. The former method is superior because extraction of uranyl ion with TBP alone is negligible. The method is applicable to > ca. 10 μg of uranium.

Uranium is closely involved in energy problems and is one of the most important elements of current geochemical interest. Accurate information about quantities of uranium has always been required because of the need for strict control of uranium stocks. Various methods for the determination of uranium (isotope dilution mass spectrometry (i.d.m.s.), amperometry, potentiometry, coulometry, gravimetry, spectrophotometry and fluorimetry) have been reviewed critically [1]. It was pointed out that i.d.m.s. is the most precise and accurate method available for the determination of small amounts of uranium in the presence of appreciable amounts of impurities. The merits of the method are that the determination does not require calibration standards, and that the separation and recovery need not be quantitative. There are disadvantages, however, such as the high cost of the equipment and the time taken for each determination.

Radioisotope dilution combined with substoichiometry, substoichiometric isotope dilution analysis [2, 3], has some advantages in that the analytical procedure is easy and the equipment simple, in contrast to i.d.m.s. A substoichiometric determination of uranium has already been reported [4], in which uranium was extracted with an excess of 2-thenoyltrifluoroacetone and then back-extracted with a substoichiometric amount of arsenazo-III, but different calibration curves for various ranges of U(VI) had to be prepared, and the α-counting technique for ^{233}U used as a tracer seemed to be troublesome.

Extraction constants for uranyl ion with the usual chelating extractants such as β-diketones, dithiocarbamates and 8-quinolinol are too small for

substoichiometric extractions with these reagents to be viable. However, the extraction constants can be enhanced by several orders of magnitude by adduct formation of the uranyl chelates with uncharged molecules. Previously substoichiometric extractions with synergic effects have been used for copper(II), zinc, europium [5] and manganese(II) [6]. In these studies, an excess of the chelating agent and a substoichiometric amount of the neutral ligand were used. As two reagents are used in the extraction, two substoichiometric combinations must be examined: the system with an excess of chelating reagent and a substoichiometric amount of the neutral ligand, and vice versa.

In the present paper, both systems for the substoichiometric extraction of uranium(VI) are described in detail, with 2-thenoyltrifluoroacetone (TTA) as chelating agent and trioctylphosphine oxide (TOPO) or tributylphosphate (TBP) as the neutral ligand. Uranium-237 was used as the radiotracer, as it seemed to be the most useful uranium nuclide for this purpose.

EXPERIMENTAL

Reagents and apparatus

Unless otherwise stated, the reagents used were of guaranteed grade.

A standard uranium(VI) solution (9.41×10^{-3} M) was prepared by dissolving triuranium octaoxide (99.97%) in 7 M nitric acid.

Uranium-237 ($t_{1/2}$ = 6.75 d) was prepared by photon irradiation with maximum bremsstrahlung energy of 30—60 MeV in the Tohoku University electron linear accelerator. The tracer was purified by TBP extraction from the nitric acid solution, as described previously [7].

2-Thenoyltrifluoroacetone (TTA) was purified by sublimation in vacuo. TOPO (Dojin Chem. Lab.) was used without further purification. The TBP—cyclohexane solution was purified by washing it successively, several times, with 1% sodium hydroxide and redistilled water.

A 50 × 50 mm NaI(Tl) well-type scintillation detector connected to a single-channel analyser (Nippon Atomic Industry Group Ltd.) was used for radioactivity counting. Phases were agitated by an Iwaki KM Shaker, and a Hitachi—Horiba pH meter M-7 was used for pH measurement.

Substoichiometric extraction

A 2-ml portion of 10^{-5}—10^{-3} M uranium(VI) solution labelled with ^{237}U, and 8 ml of an aqueous solution adjusted to the desired pH, were placed in a 50-ml centrifuge tube having a ground-glass stopper. A cyclohexane solution (10 ml) containing the substoichiometric amount of TTA (or TOPO) and excess of TBP (or TTA) for the amount of uranium(VI) carrier in the aqueous phase was added, and the contents were shaken for 10—120 min. The γ-activity of a 3-ml portion of the organic phase obtained was measured over a suitable period of time, so that the counting error was less than 0.5%.

Recommended procedure

A known amount (M_s) of uranium(VI) labelled with ^{237}U was added to a sample solution containing uranium(VI) (M) and other ions. Uranium(VI) was extracted from 6 M nitric acid into 25% TBP in toluene, washed with 6 M and 2.5 M nitric acid, and stripped with water several times. The aqueous solution was washed with pure toluene and adjusted to pH 6—7 (about 30 ml) with 0.1 M sodium hydroxide. A 10-ml portion of the aqueous solution was shaken for 2 h with 10 ml of a 2.0×10^{-5} M TTA—0.18 M TBP solution in cyclohexane. A 3-ml portion of the organic phase was pipetted and the γ-activity (a) measured. This substoichiometric extraction was also applied to the ^{237}U(VI) spike solution and the γ-activity (a_s) was measured. The unknown amount of uranium in the sample was calculated from the equation, $M = M_s[a_s/a - 1]$ [2, 3].

THEORY

The extraction of a cation, M^{n+}, with a chelating agent, HL, can be expressed by $M^{n+} + nHL_o \rightleftharpoons ML_{n,o} + nH^+$, where the subscript o denotes organic phase. The extraction constant is $K_{ex} = [ML_n]_o [H^+]^n / [M^{n+}] [HL]_o^n$.

The synergic extractions in the presence of a neutral ligand A, and the extraction constant, $K_{ex,s}$, are expressed by $M^{n+} + nHL_o + mA_o \rightleftharpoons ML_n A_{m,o} + nH^+$, the extraction constant being $K_{ex,s} = [ML_nA_m]_o [H^+]^n / [M^{n+}] \times [HL]_o^n [A]_o^m$.

Substoichiometric extraction with the neutral ligand in the presence of the chelating agent

As the concentration of the organic reagents in the expression for $K_{ex,s}$ must be the equilibrium concentrations, the following points should be considered. In the present investigation, the concentrations of neutral ligands in the aqueous phase are negligible because their distribution coefficients, P_A, are large, e.g., $P_{TBP} = 10^{2.9}$ (cyclohexane) [8] and $P_{TOPO} = 10^{4.38}$ (cyclohexane) [9]. However, the concentration of the chelating agent in the aqueous phase must be taken into account because its distribution coefficient is rather small ($P_{TTA} = 10^{0.56}$ for cyclohexane) [10]. Furthermore, the concentration of the anions of the ligand, L^-, can be made negligible by carefully selecting the experimental conditions. When the amount of L^- in the aqueous phase is negligible, $[L^-] V \leqslant 0.01 C_{HL} V_o$, where C_{HL} is the initial concentration of the chelating agent, and V_o and V are the volumes of the organic and aqueous phases, respectively. From this equation

$$pH \leqslant pK_a + \log (1 + P_{HL}) + \log V_o/V - 2 \qquad (1)$$

where pK_a and P_{HL} are the acidity constant and the distribution coefficient of the chelating agent, respectively. When the pH of the aqueous phase fulfils the above criterion, the following equations may be derived.

When $100x$% of the neutral ligand initially added is used to form the com-

plex $ML_n A_m$, the pH of the aqueous phase can readily be calculated from the expression for $K_{ex,s}$

$$pH = n^{-1} \log (xC_A/m) - n^{-1} \log (C_M - xC_A V_o/mV) - \log [P_{HL} C_{HL}/(1 + P_{HL})] - n^{-1} \log (1 - x)C_A - n^{-1} \log K_{ex,s} \quad (2)$$

where C_M and C_A are the initial concentrations of the metal ion and the neutral ligand, respectively. The extraction of M^{n+} with the excess of chelating agent takes place simultaneously. The magnitude of this effect can similarly be estimated from the expression for K_{ex}. From these equations, the relationship between the pH and the fraction of uranium extracted into the organic phase can be estimated by substituting the experimental values used. In Fig. 1, the solid line is the theoretical extraction curve computed by employing the following constants; $n = 2$, $m = 1$, $pK_a = 6.46$ [11], $P_{TTA} = 3.63$ [10], $\log K_{ex} = -2.86$ [7], and $\log K_{ex,s}$ (TOPO) = 6.66 [12].

Substoichiometric extraction with the chelating agent in the presence of an excess of the neutral ligand

When $100x\%$ of the chelating agent initially added is used to form the extractable complex, $ML_n A_m$, the pH of the aqueous phase can be readily calculated from the expression for $K_{ex.s}$

$$pH = n^{-1} \log (xC_{HL}/n) - n^{-1} \log (C_M - xC_{HL} V_o/nV) - \log [(1 - x) P_{HL} C_{HL}/(1 + P_{HL})] - n^{-1} \log C_A - n^{-1} \log K_{ex,s} \quad (3)$$

The theoretical curve computed by employing $\log K_{ex,s}$ (TBP) = 3.95 [13] is the solid line shown in Fig. 4 (see below).

RESULTS AND DISCUSSION

Extraction with a substoichiometric amount of TOPO in the presence of an excess of TTA

Effect of pH. The pH region where a constant quantity of U(VI) may be extracted is shown in Fig. 1. The equilibrium for the substoichiometric extraction is readily attained by shaking for over 2 min. Quantitative extraction with a substoichiometric amount of TOPO is achieved at pH 2.6–3.8. The experimental results agree well with theoretical prediction below pH 3 but a large deviation is observed above pH 3; this may be ascribed to hydrolysis and/or polynuclear complex formation of uranium. It was also observed in preliminary experiments that the plateau pH region becomes narrower with increasing amount of carrier uranium. For example, when the mole ratio of uranium to TOPO increases from 2 (in Fig. 1) to 17, the plateau width decreases from pH 1.2 to only 0.3. This is attributed to increased extraction of the uranyl–TTA chelate not involving TOPO into the organic phase.

Effect of concentration of TTA. Figure 2 shows the dependence of the

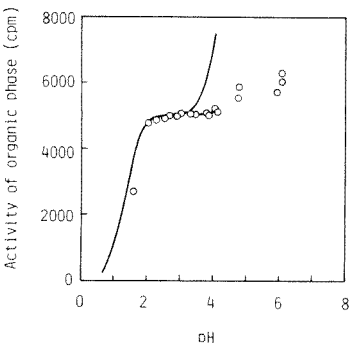

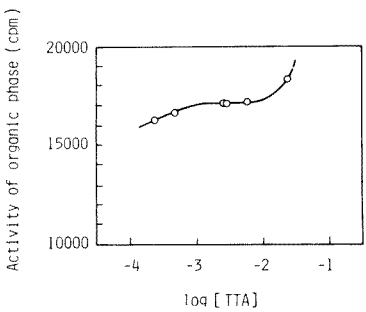

Fig. 1. Effect of pH on the substoichiometric extraction of 1.2×10^{-4} M UO_2^{2+} with 6.1×10^{-5} M TOPO and 3.0×10^{-3} M TTA; shaking time, 10—20 min. Solid line is the theoretical curve (see text).

Fig. 2. Effect of TTA concentration on the substoichiometric extraction of 1.2×10^{-4} M UO_2^{2+} with a constant amount of TOPO (6.1×10^{-5} M); pH 2.8, shaking time, 15 min.

extracted fraction of uranium(VI) with the substoichiometric amount of TOPO on the concentration of TTA. The experimental values are in fair agreement with the theoretical results derived from eqn. (2), i.e., $C_{HA} = 1.2 \times 10^{-3}$ M, when more than 99% of the TOPO added is used to form the adduct, and $C_{HA} = 5.5 \times 10^{-3}$ M when extraction with excess of TTA alone is less than 1%. If TBP is used instead of TOPO, C_{HA} must be 2.8×10^{-2} M for reaction of 99% of the TBP. Consequently, substoichiometric extraction with TBP in the presence of an excess of TTA may never be successful.

Reproducibility of the substoichiometric extraction. A substoichiometric extraction with 4.6×10^{-5} M TOPO in the presence of 2.3×10^{-3} M TTA was applied to a series of solutions containing different quantities of uranium(VI) labelled with ^{237}U. As shown in Fig. 3(a), the radioactivity of the organic phase increases with increase in the amount of labelled uranium up to the point corresponding to a UO_2^{2+}: TOPO ratio of 1:1. Beyond this point, i.e., under substoichiometric conditions, a constant amount of uranium(VI) is extracted. The reproducibility of this substoichiometric extraction is seen in Table 1; this method is clearly precise for submilligram amounts of uranium.

Extraction with a substoichiometric amount of TTA in the presence of an excess of TBP

Effect of pH. As shown in Fig. 4, a constant amount of uranium(VI) is extracted with a substoichiometric amount of TTA at pH 5.1—7.0. The extraction curve obtained is highly consistent with the theoretical results. The plateau pH region did not vary with the amount of carrier uranium(VI), so that this extraction system is superior to that described above. The depression of the extraction at higher pH values may be ascribed to the

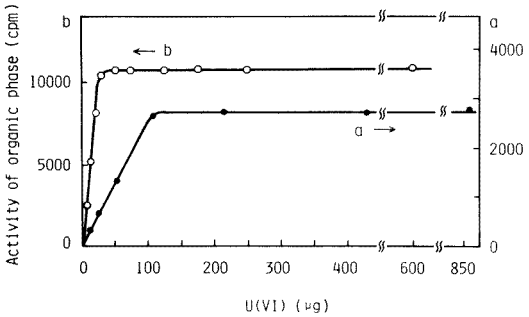

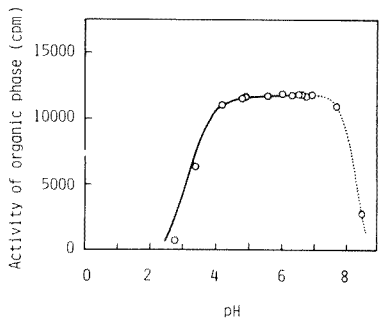

Fig. 3. Reproducibility of the substoichiometric extraction. (a) 4.6 × 10^{-5} M TOPO, 2.3 × 10^{-3} M TTA; pH 2.5—3.6, shaking time, 10 min. (b) 2.0 × 10^{-5} M TTA, 0.18 M TBP; pH 5.8—6.4, shaking time, 2 h.

Fig. 4. Effect of pH on the substoichiometric extraction of 2.6 × 10^{-5} M UO_2^{2+} with 2.0 × 10^{-5} M TTA and 0.18 M TBP; shaking time, 2 h. Solid line is the theoretical curve (see text).

TABLE 1

Precision of the substoichiometric extraction

Substoichiometry with respect to neutral ligand[a]		Substoichiometry with respect to chelating agent[b]	
U(VI) taken (μg/10 ml)	Activity of organic phase (cpm)	U(VI) taken (μg/10 ml)	Activity of organic phase (cpm)
238	4814	48	10707
286	4845	72	10702
476	4787	120	10694
571	4843	168	10723
714	4854	240	10725
952	4871	599	10828
	Mean = 4836 ± 30 cpm		Mean = 10730 ± 50 cpm
	R.s.d. = 0.62%		R.s.d. = 0.46%

[a] 4.5 × 10^{-5} M TOPO, 2.3 × 10^{-3} M TTA, pH 2.7—3.1, shaking time, 10 min.
[b] 2.0 × 10^{-5} M TTA, 0.18 M TBP, pH 6.1—6.4, shaking time, 2 h.

polymerization of UO_2^{2+} in the aqueous phase.

The dependence of the substoichiometric extraction of U(VI) on shaking time was investigated. The counting rates of ^{237}U in the organic phase after shaking for 5, 30, 60, 120 and 180 min were 12440, 12822, 12977, 13104 and 12 946 cpm, respectively. The equilibrium was found to be achieved by shaking for $\geqslant$ 60 min. Thus the extraction in this TTA—TBP system was

slower than that found with TOPO in the presence of an excess of TTA. Inasmuch as complex formation of UO_2^{2+} with TTA in the aqueous phase seems to be the rate-determining step in the present system, the equilibrium in the substoichiometric extraction system with excess of TTA will be faster than that with an excess of the TBP.

Effect of concentration of TBP. Figure 5 shows the dependence of the extraction on the concentration of TBP. The radioactivity of ^{237}U in the organic phase gradually increases with increase in the concentration of TBP and becomes constant at 0.1—0.2 M TBP. Under these conditions, TTA initially added quantitatively, reacts with UO_2^{2+} to form the adduct. The decrease in the radioactivity at higher concentrations of TBP may be due to an antagonistic effect caused by interaction of TTA with excess of TBP. The experimental results obtained cannot be compared directly with the theoretical values because the pH value used, pH 6.6, is much higher than that (pH 5.1) given by eqn. (1). However, if more than 99% of TTA forms the extractable complex, $UO_2(TTA)_2TBP$, at pH 5.1, the concentration of TBP necessary is readily computed, i.e., more than 0.18 M. If TOPO is employed in place of TBP, a threshold concentration of TOPO of 3.47×10^{-4} M is obtained. However, decreased extraction because of the antagonistic effect may also appear at lower concentrations of the neutral ligand.

Reproducibility of the substoichiometric extraction. A substoichiometric extraction with 2.0×10^{-5} M TTA in the presence of 0.18 M TBP was applied to a series of solutions containing various quantities of uranium(VI) labelled with ^{237}U. As shown in Fig. 3(b), the radioactivity of the organic phase increases with increasing quantities of labelled uranium up to the point corresponding to a UO_2^{2+}:TTA ratio of 1:2. Under the substoichiometric conditions, it is clear that a constant amount of uranium(VI) is extracted into the cyclohexane. The reproducibility of the separation is shown in Table 1 to be very satisfactory. This method should be applicable to the determination of 10—100 μg of uranium. The extraction with a substoichiometric amount of TTA seems to be superior, though slower, than the TOPO—TTA

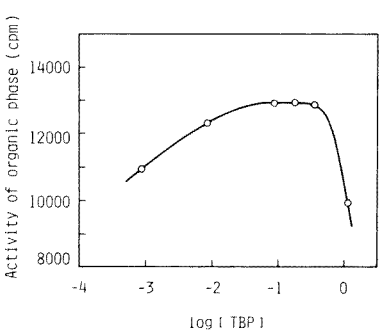

Fig. 5. Effect of TBP concentration on the substoichiometric extraction of 2.6×10^{-5} M UO_2^{2+} with a constant amount of TTA (2.0×10^{-5} M); pH 6.6, shaking time, 2 h.

TABLE 2

Determination of uranium(VI) in a synthetic mixture by the TTA—TBP system

U(VI) taken (μg)	Other ions added (mg)	Labelled U(VI) spike (μg)	Activity from spike solution (cpm)	Activity from test solution (cpm)	U(VI) found (μg)[a]
113.0	H_3PO_4 480; Ca 350; Al 10; Fe 10; Mg 1; Ti 0.5; Mn 0.5; Cu 0.1; Zn 0.1; Zr 0.1; Th 0.1	114.4	25732	12917	113.5
				12897	113.9
				12922	113.4

[a]Mean value ± σ = 113.6 ± 0.3 μg, r.s.d. = 0.23%; deviation from amount of U(VI) taken is +0.5%.

method, probably because extraction with only the TBP is negligible under the given conditions.

Determination of uranium in a synthetic mixture

The accuracy and precision of the substoichiometry were evaluated by determining uranium(VI) in a synthetic mixture containing a known amount of uranium(VI) and large amounts of diverse ions together with phosphoric acid. In a preliminary investigation of the influence of diverse ions on the substoichiometric TTA—TBP separation, it was found that several ions such as Al(III), Fe(III), Zn(II) and Zr(IV) interfered because of the competitive complex formation of these metal ions. Phosphate interfered strongly because it forms a strong complex with uranyl ions. Thus the uranium(VI) was separated from these diverse ions in a preliminary extraction from 6 M nitric acid into 25% TBP in toluene, and back-extracted as in the recommended procedure. The recovery of uranium(VI) by this procedure was 80—85%. Because a substoichiometric process is used, the quantitative recovery of uranium is not necessary.

The results obtained by the present method involving pre-separation are summarized in Table 2. The precision (0.23%) is very satisfactory, as is the accuracy. Thus the method is applicable to the determination of uranium in complex samples.

REFERENCES

1 M. V. Ramanadah, P. R. Natarajan and P. Venkatamana, Radiochim. Acta, 22 (1975) 199.
2 K. Kudo and N. Suzuki, J. Radioanal. Chem., 26 (1975) 327.
3 J. Růžička and J. Stary, Substoichiometry in Radiochemical Analysis, Pergamon, Oxford, 1968, p. 42.
4 S. M. Grashchenko and E. V. Sobotovich, Radiokhimiya, 9 (1967) 412.
5 J. W. Mitchell and R. Ganges, Anal. Chem., 46 (1974) 503.
6 J. W. Mitchell and R. Ganges, Talanta, 21 (1974) 735.
7 K. Akiba, N. Suzuki, H. Asano and T. Kanno, J. Radioanal. Chem., 7 (1971) 203.
8 K. Alcock, S. S. Grimley, T. V. Healy, J. Kennedy and H. A. C. McKay, Trans. Faraday Soc., 52 (1956) 39.

9 K. Akiba and T. Kanno, Res. Rep. Lab. Nucl. Sci., Tohoku Univ., 9 (1976) 272.
10 K. Akiba, N. Suzuki and T. Kanno, Bull. Chem. Soc. Jpn., 42 (1969) 2537.
11 J. Stâry and H. Freiser, Equilibrium Constant of Liquid—Liquid Distribution Reactions: Part IV, Chelating Extractants, Pergamon, Oxford, 1978, p. 137.
12 K. Akiba, J. Radioanal. Chem., 36 (1977) 153.
13 K. Akiba and N. Suzuki, Bull. Chem. Soc. Jpn., 44 (1971) 1043.

Analytica Chimica Acta, 129 (1981) 231—236
Elsevier Scientific Publishing Company, Amsterdam — Printed in The Netherlands

Short Communication

A FLUORISTATIC METHOD FOR THE DETERMINATION OF ALKALINE PHOSPHATASE, SORBITOL DEHYDROGENASE, PEROXIDASE AND PSEUDOCHOLINESTERASE

SIEGBERT PANTEL

Lehrstuhl für Analytische Chemie, Chemisches Laboratorium der Universität, Freiburg i.Br. (W. Germany)

(Received 25th January 1981)

Summary. Instrumentation for fluoristatic procedures and several applications are described. The simple device is used to determine alkaline phosphatase (7—150 mU), sorbitol dehydrogenase (1—10 mU) and peroxidase (0.5—5 mU) with fluorescent substrates and pseudocholinesterase (10—100 mU) with a non-fluorescent substrate and erythrosine as fluorescence quencher. The method is of special interest for the determination of enzymes with low substrate concentrations.

The applicability of "stat" methods in analytical chemistry for the determination of catalysts, activators and inhibitors has been reported quite recently [1—3]. The main advantage of these open-system methods lies in the fact that well-defined, low concentrations of substrate or product can be kept constant for a much longer time than in closed systems. This is of special interest in enzymatic analysis, as has been pointed out earlier [1]. Fluorimetry can be up to several orders of magnitude more sensitive than absorption spectrophotometry [4]. It seemed therefore to be of interest to study the use of fluorescence for regulating the addition of a suitable reagent in a stat method.

With the fluoristatic technique described here, it is possible to determine inorganic catalysts and enzymes which react with a fluorescent substrate to form non-fluorescent products. This is done by controlled addition of the fluorescent substrate solution at a speed such that the fluorescence remains constant during the reaction time observed. The added volume per time unit is a measure of the catalyst concentration, the activity of the enzyme being given in units analogous to international units (1 I.U. = catalytic activity which transforms 1 μmol of substrate per minute under the reaction conditions used). The technique can also be used to follow reactions that produce fluorescent products from non-fluorescent substrates. In this case, the increasing fluorescence is quenched by controlled addition of a suitable substance [5, 6] at a speed such that again the fluorescence remains constant during the measuring time. This mode of working is not that of a conventional stat method; the substrate or product concentration is not kept constant during the reaction time, but a physical property of the product is

0003—2670/81/0000—0000/$02.50

diminished to a preset level. This method has the advantage that non-fluorescent substrates can be used for the determination of enzymes, and the disadvantage that the addition curves for the quenching substance are not linear over a long period of time, because the quenching effect is not linear with the added volume of the quenching solution.

Some examples are given below for the determination of enzymes by means of fluorescent substrate. An example of the determination of an enzyme with a non-fluorescent substrate producing a fluorescent reaction product is also described.

Instrumentation

The apparatus used (Fig. 1) consists of the Combi-Titrator 3 D (Metrohm, Herisau, Switzerland) [7] and the fluorescence unit of the MPI-System (McKee—Pedersen, Danville, USA).

Procedure with a fluorescent substrate. Into the quartz cuvette (18 mm inner diameter) of the measuring compartment M (Fig. 1) are pippetted 2 ml of buffer solution and water up to 7.5 ml. The well-stirred solution is thermostatted (circulating thermostat) for 5 min to 25.0 ± 0.1°C and the millivoltmeter is set to zero with the aid of the mV source (U). Now a definite volume of the appropriate titrant, equivalent to the substrate concentration to be kept constant in the enzyme reaction, is added to the cuvette from the 1-ml burette of the Microdosigraph. For this titrant concentration, the millivoltmeter is set to 60 mV (most sensitive switching region; preset working potential) by means of the variable feed-back resistor R_f. After the instrument has been set thus, the enzyme activity can be determined as described below.

Enzyme and substrate solutions were stored at 0°C in the dark. Unless otherwise stated, enzymes and reagents were obtained from Boehringer, Mannheim.

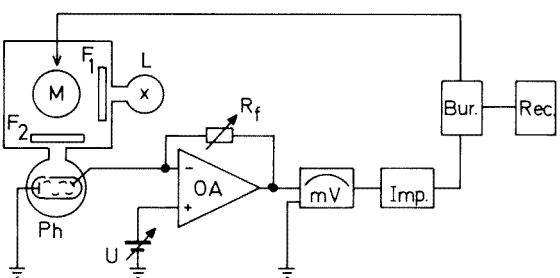

Fig. 1. Schematic representation of the measuring/regulating circuit. M, Sample/filter holder MP-1017 with magnetic stirrer MP-1024; OA, Operational amplifier MP-1006; U, millivolt source MP-1008; ±0—2 V; Ph, photomultiplier MP-1021; L, mercury lamp Hanau St. 41/220 V (Quarzlampen GmbH-Hanau, FRG) with stabilized voltage supply; mV, mV-meter E510 (Metrohm); Imp, impulsomat E473 (Metrohm); Bur./Rec, microdosimat (1-ml burette) with recorder attached (Metrohm); F_1, F_2, optical interference filters.

Determination of alkaline phosphatase with 1-naphthylphosphate

Alkaline phosphatase catalyzes the hydrolysis of 1-naphthylphosphate to form 1-naphthol [8]. Both the substrate and the product are fluorescent, but under suitable conditions (F_1 = 313 nm, F_2 = 365 nm; Fig. 1), the substrate can be measured selectively.

Procedure. To the quartz cuvette are added 2 ml of sodium hydroxide—glycine buffer solution (pH 9.8, 0.2 M) and 0.05—1 ml of a solution of alkaline phosphatase (EC 3.1.3.1, 0.15 U ml^{-1}) for preparing a calibration graph or a definite amount of the sample solution within the specified range. After dilution with water to 7.5 ml, this solution is thermostatted for 5 min. The millivoltmeter is set to zero and the titrant addition is started; an aqueous solution of monosodium-1-naphthylphosphate monohydrate (0.25 mg ml^{-1}) (EGA, Steinheim) is used. The working potential (60 mV; R_f = 9 kohm) is chosen so as to maintain a constant substrate concentration of 25 μM 1-naphthylphosphate in the solution. A typical recorder plot is given in Fig. 2.

The calibration graph (tan α versus enzyme concentration) is slightly and smoothly curved towards the tan α axis, but passes through the origin of the coordinates. Table 1 gives some results for the determination of alkaline phosphatase.

Determination of sorbitol dehydrogenase with reduced β-nicotinamide adenine dinucleotide (NADH)

Sorbitol dehydrogenase (SDH) catalyzes the reduction of D-fructose with NADH [1, 9, 10], which is fluorescent (F_1 = 365 nm, F_2 = 458 nm). The resulting NAD^+ does not fluoresce under these conditions.

Procedure. To the quartz cuvette are added 1 ml of sodium phosphate buffer solution (pH 6.1, 0.3 M), 2 ml of D-fructose solution (10 mg ml^{-1}) and 0.1—1 ml of a solution of SDH (EC 1.1.1.14, 10 mU ml^{-1}) for preparing a calibration graph or an appropriate amount of the sample solution. After dilution with water to 7.5 ml, this solution is thermostatted for 5 min, the millivoltmeter is set to zero and addition of the titrant (0.1 mg of β-$NADHNa_2$ per ml of water) is started. The working potential (60 mV;

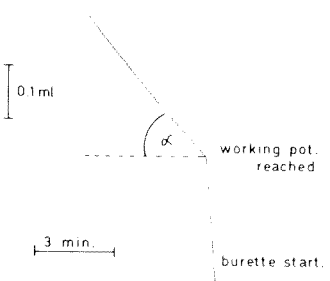

Fig. 2. Recorder graph for the determination of 90 mU of alkaline phosphatase in 7.5 ml with 1-naphthylphosphate.

TABLE 1

Determination of various enzymes by the proposed methods

Alkaline phosphatase (mU/7.5 ml[a])										
Given	13.8	38.5	49.2	69.2	73.8	95.4	100.0	120.0	147.7	147.7
Found	14.0	40.1	46.8	72.1	73.5	93.5	101.5	122.9	146.9	146.9
Sorbitol dehydrogenase (mU/7.5 ml[b])										
Given	1.40	2.78	3.24	3.54	4.40	5.60	5.64	7.71	8.39	10.52
Found	1.35	2.78	3.30	3.46	4.33	5.49	5.72	7.79	8.39	10.54
Horse-radish peroxidase (mU/7.5 ml[c])										
Given	0.52	1.02	1.56	2.08	2.60	3.12	3.64	4.16	4.68	5.20
Found	0.62	1.09	1.51	2.11	2.55	3.10	3.70	4.20	4.68	5.10
Pseudocholinesterase (mU/8.0 ml[d])										
Given	9.8	19.6	29.4	39.2	49.0	58.8	68.6	78.4	88.2	107.8
Found	8.8	18.6	29.6	40.2	49.0	58.8	68.4	76.4	87.2	108.0

[a] 1 U ≈ 40 *p*-nitrophenylphosphate units (Boehringer). [b] 1 U ≈ 20 fructose/NADH units (Boehringer). [c] 1 U ≈ 500 guaiacol units (Boehringer). [d] 1 U ≈ 1000 butyrylcholine units (Sigma).

R_f = 100 kohm) is chosen so as to maintain a constant concentration of 4 μM NADH.

The plot of tan α (ordinate) versus enzyme concentration is linear over the range specified and cuts the ordinate at tan α = 0.05. Table 1 gives some results for the determination of SDH.

Determination of horse-radish peroxidase with scopoletine

Horse-radish peroxidase catalyzes the oxidation of fluorescent scopoletine (6-methoxy-7-hydroxycoumarin) to form non-fluorescent oxidation products [11, 12] (F_1 = 365 nm, F_2 = 458 nm).

Procedure. To the quartz cuvette are added 2 ml of sodium acetate buffer solution (pH 4.3, 0.2 M), 2 ml of aqueous hydrogen peroxide solution (0.5 mg ml^{-1}) and 0.2—2 ml of a solution of horse-radish peroxidase (EC 1.11.1.7, 2.6 mU ml^{-1}) for preparing a calibration graph or a suitable amount of the sample solution. After dilution with water to 7.5 ml, thermostatting for 5 min and adjustment to 0 mV, addition of the titrant (0.01 mg of scopoletine per ml of water; SERVA, Heidelberg) is started. The working potential (60 mV; R_f = 10 kohm) is chosen so as to maintain a constant concentration of 1.3 μM scopoletine.

In this case, the plot of tan α versus enzyme concentration is sigmoidal (Fig. 3). Some results for the determination of horse-radish peroxidase are given in Table 1.

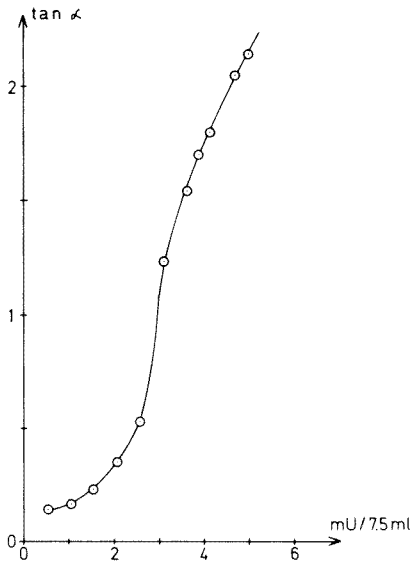

Fig. 3. Calibration graph for the determination of horse-radish peroxidase with scopoletine.

Measurements via a fluorescence quenching substance

Pseudocholinesterase can be determined with non-fluorescent 1-naphthylacetate, fluorescent 1-naphthol being formed [13]. It was shown that this fluorescence can be quenched by erythrosine, added stepwise from the automatic burette (F_1 = 365 nm; F_2 = 458 nm).

Procedure. To the quartz cuvette are added 1 ml of sodium phosphate buffer solution (pH 8.0, 0.4 M) and 0.1—1 ml of a solution of butyrylcholinesterase (EC 3.1.1.8, 100 mU ml^{-1}; Sigma, München) for preparing a calibration graph or a definite amount of the sample solution. After dilution with water to 7.5 ml, and thermostatting for 5 min, 0.5 ml of 1-naphthylacetate (1 mg ml^{-1} in methyl cellosolve; Serva) is added, the millivoltmeter is zeroed and addition of the titrant (0.6 mg of erythrosine per ml of water) is started. The working potential (40 mV; R_f = 134 kohm) is chosen so as to maintain a constant fluorescence corresponding to about 42 μM 1-naphthol, the original concentration of 1-naphthylacetate being 0.33 mM.

The plot of tan α (ordinate) versus enzyme concentration is linear and cuts the ordinate at tan α = 0.36. Some results for the determination of pseudocholinesterase are given in Table 1.

In a similar way, lipase from porcine pancreas can be determined with fluorescein diacetate as a non-fluorescent substrate [14] and erythrosine as a quencher for the fluorescence of the resulting fluorescein in phosphate buffer solution of pH 7.5. The resulting "titration" curves, however, bend quickly, thus showing that the system is rapidly deactivated.

REFERENCES

1 S. Pantel and H. Weisz, Anal. Chim. Acta, 109 (1979) 351.
2 B. Tan and J. K. Grime, Anal. Lett., 12 B (1979) 1551.
3 J. K. Grime and K. R. Lockhart, Anal. Chim. Acta, 106 (1979) 251.
4 G. G. Guilbault, Practical Flourescence; Theory, Methods and Techniques, M. Dekker, New York, 1973, p. 277.
5 Th. Förster, Z. Elektrochem., 53 (1949) 93.
6 H. Landolt and R. Börnstein, Numerical Data and Functional Relationships in Science and Technology, New Series, Vol. 3, Springer-Verlag, 1967, p. 296.
7 S. Pantel and H. Weisz, Anal. Chim. Acta, 74 (1975) 275.
8 D. W. Moss, Clin. Chim. Acta, 5 (1960) 283; Biochem. J., 76 (1960) 32P.
9 H. U. Bergmeyer, Methoden der enzymatischen Analyse, 3. Aufl., Verlag Chemie, Weinheim, 1974, Vol. 1, p. 601.
10 E. L. Wehry (Ed.), Modern Fluorescence Spectroscopy, Vol. II, Heyden, London, 1976, p. 57.
11 W. A. Andreae, Nature, 175 (1955) 859.
12 H. Perschke and E. Broda, Nature, 190 (1961) 257.
13 G. G. Guilbault and D. N. Kramer, Anal. Chem., 37 (1965) 1675.
14 G. G. Guilbault and D. N. Kramer, Anal. Chem., 36 (1964) 409.

Analytica Chimica Acta, 129 (1981) 237—241
Elsevier Scientific Publishing Company, Amsterdam — Printed in The Netherlands

Short Communication

ION FLOTATION—SPECTROPHOTOMETRIC DETERMINATION OF TRACES OF CHROMIUM(VI)

MAMORU AOYAMA*, TOSHIYUKI HOBO and SHIGETAKA SUZUKI

Department of Industrial Chemistry, Faculty of Technology, Tokyo Metropolitan University, Fukasawa, Setagaya-ku, Tokyo (Japan)

(Received 10th February 1981)

Summary. Ion flotation is used to concentrate chromium(VI) in the range 3—70 $\mu g\ l^{-1}$ from 1-l samples. The chromium(III)—diphenylcarbazone complex formed by reaction with diphenylcarbazide is floated efficiently with sodium lauryl sulfate, and the subsided foam is measured spectrophotometrically after simple dilution. Continuous flotation methods at solution flow rates of 2, 3 and 4 $l\ h^{-1}$ are discussed.

Much attention has recently been given to environmental pollution by chromium ions, with particular respect to their speciation. Chromium(VI) probably exists at $\mu g\ l^{-1}$ levels (or lower) in unpolluted natural waters, and must therefore be concentrated prior to any known technique of determination. Ion exchange [1], liquid—liquid extraction [2] and coprecipitation [3] have been used for preconcentration, but techniques can be time-consuming or troublesome for large volumes of samples. A simple concentration of chromium(VI) based on the foam separation in the presence of a cationic surfactant, cetylethyldimethylammonium bromide, has been proposed [4]; this method allowed concentration of $\mu g\ l^{-1}$ levels of chromium(VI) from aqueous solutions with a limit of determination of 3 $\mu g\ l^{-1}$ and a concentration ratio of 120. Unfortunately, comparatively large amounts of sulfate, such as are present in natural waters, interfered with this determination. Possible procedures involving conversion of chromium(VI) to a cationic form and collection with an anionic surfactant were therefore considered.

Chromium(VI) readily forms the chromium—diphenylcarbazone (DPCO) complex, $Cr(DPCO)^{2+}$, on reaction with diphenylcarbazide (DPCI) [5]. It was thought therefore that $Cr(DPCO)^{2+}$ should form an ion-associate with an anionic surfactant such as sodium lauryl sulfate (SLS) which could be separated easily by foam separation. The present communication is concerned with an investigation of the usefulness of DPCI as a selective collector for chromium. Optimum conditions are described for the flotation of chromium(VI) in batch and continuous experiments. The proposed method is rapid, and applicable to the determination of chromium(VI) at $\mu g\ l^{-1}$ levels.

Experimental

Apparatus. A schematic diagram of the foam separation system is illustrated in Fig. 1. The foam separator (A) consists of three parts; a lid, a separation tube (70 mm i.d. and 570 mm high) and a base. Between the separation tube and the base, a polyethylene filter (pore size 30 μm) is installed for bubble generation; the base is connected to the nitrogen cylinder (D) via a float-type flow meter. The separation tube has two side-arms through which sample, DPCI solution and SLS solution can be introduced. Another side-arm near the bottom serves to drain the waste water. The lid has a narrow tube that leads the foam into a foam collector (B) containing a little n-butanol, which collapses the foam coming out of separator.

The absorbances of subsided foam solutions were measured with a Yanagimoto UO-101 derivative spectrophotometer in 1-cm cells.

Chemicals. A chromium(VI) stock solution (1 mg ml^{-1}) was prepared by dissolving 2.829 g of potassium dichromate in 1 l of water. Working standards (10 μg ml^{-1}) were freshly prepared by dilution just before use. Diphenylcarbazide solutions (1% w/v DPCI) were also prepared freshly by dissolving 1.000 g of diphenylcarbazide in 100 ml of aqueous 50% (v/v) acetone solution. Sodium lauryl sulfate solutions (1% w/v SLS) were prepared in pure water. All chemicals used were of analytical grade except SLS. Water used was purified by distillation and ion exchange.

Procedure for batch flotation. To a 1-l sample containing 3—70 μg of chromium(VI), enough sulfuric acid was added to make the acidity 0.1 M. After addition of 5 ml of 1% DPCI solution and shaking for 5 min, the solution was transferred to the separation tube. Nitrogen was passed at a flow rate of 105 ml min^{-1} into the tube through the polyethylene filter, and the 1% SLS solution was pumped into the tube at a flow rate of 0.54 ml min^{-1}. The foam coming out of the separation tube was collected for 20 min in the foam collector which contained 0.5 ml of n-butanol. The subsided

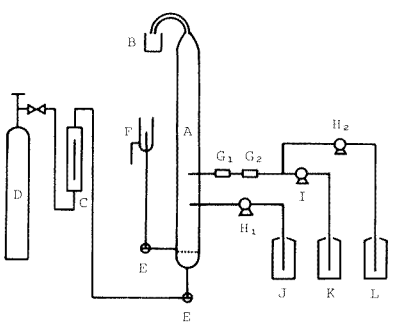

Fig. 1. Schematic diagram of foam separation system. A, Foam separator; B, foam collector (containing 0.5 ml of n-butanol); C, flow meter; D, nitrogen cylinder; E, three-way cock; F, effluent drain; G_1, G_2, mixing chambers; H_1, H_2, plunger pumps; I, diaphragm pump; J, surfactant solution (1% SLS) reservoir; K, sample reservoir; L, 1% DPCI solution reservoir.

foam solution was transferred to a 50-ml volumetric flask and diluted to the mark with water. The absorbance was measured at 540 nm, using water as reference.

Procedure for continuous flotation. Water (1 l) previously acidified to 0.1 M with sulfuric acid, was placed in the separation tube, nitrogen was passed into the tube at about 105 ml min^{-1}, and the 1% SLS solution was pumped at an appropriate rate. The sample, previously acidified to 0.1 M with sulfuric acid, and the 1% DPCI solution were continuously supplied to the separation tube at rates of 2, 3 or 4 l h^{-1}, and 0.230 ml min^{-1}, respectively. The sample and DPCI solutions were mixed in the mixing chambers (Fig. 1, G_1, G_2) before entering the tube. The foam subsided in the collector was intermittently transferred to flasks and diluted to 50-ml with water, and the absorbances were measured as described above.

Results and discussion

Batch flotation. The acidity of the sample solution affects the formation of $Cr(DPCO)^{2+}$ as well as its flotation. The complex is best formed in acidic solution. A study of the effect of the sulfuric acid concentration in the range 0.005—0.25 M for 1-l samples containing 50 μg of chromium(VI) showed that recoveries were satisfactory from samples 0.005—0.125 M in sulfuric acid. At higher acidities the color was not stable, and 0.1 M was chosen for all further work.

As the ion flotation depends on the liquid—gas interfaces, the effect of the SLS supply rate on the chromium(VI) recovery was investigated. Quantitative recoveries were obtained at flow rates in the range 0.54—0.7 ml min^{-1} of the 1% SLS solution; recoveries decreased by about 5% at a flow rate of 0.3 ml min^{-1}. Thus a flow rate of 0.54 ml min^{-1} was selected for the 1-l samples. An investigation of the amount of 1% DPCI solution required for complete flotation of chromium(VI) showed that recoveries were very poor with only 0.5 ml of 1% DPCI solution in the 1-l sample, almost quantitative with 1—3 ml, and quantitative with 4—7 ml; 5 ml of the 1% DPCI solution was used in further work.

The nitrogen flow rate and separation time are obviously important. Flow rates of 60—90 ml min^{-1} gave low recoveries of 50 μg of chromium(VI) for the conditions recommended in the procedure, whereas recoveries were quantitative for flow rates in the range 100—150 ml min^{-1}. For convenience, 105 ml min^{-1} was used thereafter. Flotation of chromium(VI) was found to be complete after 18 min. The calibration graph obtained under the recommended conditions (see Experimental) was linear over the range 3—70 μg l^{-1} of chromium(VI). The relative standard deviation for 10 separate runs of a solution containing 50 μg Cr(VI) l^{-1} was 1.2%.

The effects of diverse ions on the flotation of Cr(VI) were investigated, with the results shown in Table 1. As can be seen, few ions interfered. Only copper(II) and iron(III) in 10-fold amounts, and vanadium(V) in 20-fold amounts caused fading of the color. Even in those cases, however, Cr(VI) could be measured by a standard addition method.

TABLE 1

Effect of diverse ions[a] on the determination of 50 μg of chromium(VI)

Ion	Amount added (mg)	Cr(VI) found (μg)	Error (%)	Ion	Amount added (mg)	Cr(VI) found (μg)	Error (%)
Fe^{3+}	0.1	48.3	−3.4	Bi^{3+}	5.0	49.0	−2.0
	0.5	45.7	−8.6	Na^{+}	50.0	50.0	0
Cu^{2+}	0.1	47.8	−4.4	Mg^{2+}	50.0	50.0	0
	0.5	44.0	−12.0	Ca^{2+}	50.0	48.7	−2.6
V(V)	0.5	48.3	−3.4	K^{+}	50.0	50.0	0
	1.0	45.7	−8.6	NH_4^{+}	50.0	49.6	−0.8
Mo(VI)	5.0	48.0	−4.0	PO_4^{3-}	50.0	49.5	−1.0
Hg^{+}	5.0	47.4	−5.2	ClO_4^{-}	50.0	49.8	−0.4
Cr^{3+}	5.0	49.5	−1.0	I^{-}	50.0	49.5	−1.0
Ni^{2+}	5.0	49.6	−0.8	CO_3^{2-}	50.0	50.0	0
Cd^{2+}	5.0	50.4	+0.8	$C_2O_4^{2-}$	50.0	48.4	−3.2
Mn^{2+}	5.0	50.8	+1.6	CH_3COO^{-}	50.0	50.0	0
Co^{2+}	5.0	50.9	+1.8	NO_3^{-}	50.0	50.0	0
Zn^{2+}	5.0	49.1	−1.8	Br^{-}	50.0	49.2	−1.6
Ag^{+}	5.0	50.4	+0.9	BO_3^{3-}	50.0	49.1	−1.8
Pb^{2+}	5.0	50.0	0				

[a]Cations were added as their chloride, sulfate or nitrate salt; anions were added as their ammonium, sodium or potassium salts; borate was added as boric acid.

Continuous flotation. Further experiments were done on continuous flotation. This involved the steady-state ion flotation of chromium(VI) from the aqueous sample fed continuously by a pump to the separation tube, which was identical with that used in batch flotation. Initially, sample solution feed rates of 2 l h^{-1} were used. The optimum flotation conditions, sought on the basis of the batch experiments, were found to be: 0.1 M H_2SO_4 in the sample solution, 105 ml N_2 min^{-1}, 0.23 ml min^{-1} of the 1% DPCI solution, and 0.39 ml min^{-1} of the 1% SLS solution.

As shown in Fig. 2, steady-state flotation was achieved at 1 h after flotation was started. Continuous flotations were also attempted at sample solution feed rates of 3 and 4 l h^{-1}. The optimum conditions were same as those in the case of 2 l h^{-1} except for the SLS solution supply rate. For flow rates of 3 and 4 l h^{-1}, the 1% SLS solution was best supplied continuously into the separation tube at flow rates of 0.425 and 0.460 ml min^{-1}, respectively. Satisfactory results were obtained for each run. Recoveries and calibration curves were similar to those obtained by batch flotation.

It should be noted that, in the continuous flotation of chromium(VI), the mean concentration of Cr(VI) in the sample is measured. If this system were connected with a continuous photometric detector, a good pollution monitor system would be realized.

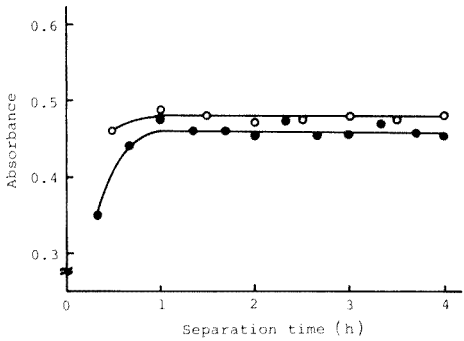

Fig. 2. Variation of absorbance with time for 50 μg Cr(VI) l^{-1} in 0.1 M H_2SO_4 solution. Sample feed rate: (○) 2 l h^{-1}; (●) 3 l h^{-1}. DPCI supply rate: 0.230 ml min^{-1}. SLS supply rate: (○) 0.390 ml min^{-1}; (●) 0.425 ml min^{-1}. N_2 flow rate: 105 ml min^{-1}.

REFERENCES

1 K. Yoshimura and S. Ohashi, Talanta, 25 (1978) 103.
2 S. Inoue, T. Yotsuyanagi, M. Sasaki and K. Aomura, Bunseki Kagaku, 27 (1978) 142.
3 M. Hiraide, Y. Yoshida and A. Mizuike, Anal. Chim. Acta, 81 (1976) 185.
4 M. Aoyama, T. Hobo and S. Suzuki, Bunseki Kagaku, 30 (1981) 224.
5 G. J. Willems, N. M. Blaton, O. M. Peeters and C. J. Deranter, Anal. Chim. Acta, 88 (1977) 345.

Analytica Chimica Acta, 129 (1981) 243—246
Elsevier Scientific Publishing Company, Amsterdam — Printed in The Netherlands

Short Communication

DETERMINATION OF TRIS(NONYLPHENYL) PHOSPHITE AND NONYLPHENOL IN BUTADIENE-STYRENE COPOLYMERS BY HIGH-PERFORMANCE LIQUID CHROMATOGRAPHY

J. F. SCHABRON* and D. Z. BRADFIELD
Phillips Petroleum Company, Research Center, Bartlesville, OK 74004 (U.S.A.)
(Received 24th October 1980)

Summary. A polar stationary phase high-performance liquid chromatography method was developed to determine the additives, tris(nonylphenyl) phosphite (TNPP) and the hydrolysis product, nonylphenol, in butadiene-styrene copolymers. Polymers were dissolved in cyclohexane, separated on a μPorasil stationary phase with a heptane/dichloromethane mobile phase gradient, and detected by ultraviolet absorption at 280 nm. Typical relative standard deviations were 1.2% for TNPP and 2.0% for nonylphenol. Response was linear in the ranges 0—52 μg for TNPP and 0—29 μg of nonylphenol.

Selective methods are required to determine additives in polymers for both quality assurance and lot certification. Some methods for determining the additive, tris(nonylphenyl) phosphite (TNPP) are based on determination of phosphorus [1—3], separation by thin-layer chromatography [4], hydrolysis of TNPP followed by detection of the nonylphenol produced [1] or the phenolate ion in alkaline solution [5], and separation by molecular exclusion chromatography [3].

In the present work, a polar stationary phase high-performance liquid chromatographic (h.p.l.c.) system with μPorasil used previously [6] for the determination of 2,6-di-tert-butyl-4-methylphenol (BHT), Irganox 1076, Irganox 1010, and other additives in polyolefin extracts was applied for the determination of TNPP and nonylphenol in solutions of butadiene—styrene (BDS) copolymers.

Experimental

High-performance liquid chromatography. The liquid chromatograph used was a Waters Model 204 liquid chromatograph (Waters Associates, Milford, MA) equipped with two Model 6000-A pumps, a Model 660 solvent programmer, and a U6K injector.

The column used (3.9 mm i.d. × 30 cm) was packed with 10-μm porous silica (μPorasil). The effluent was monitored with a Waters Model 450 variable-wavelength detector set at 280 nm and a 10-mV strip chart recorder.

Reagents. Three samples of heptane were distilled in glass: heptane (Burdick and Jackson, Muskegon, MI), spectro-grade (Phillips Chemicals,

Borger, TX), and h.p.l.c. grade (Fisher Scientific). Dichloromethane was from Burdick and Jackson. These solvents were all filtered through Millipore F-H 0.5-μm filters prior to use. Cyclohexane was spectro-grade (Phillips Chemicals). Tris(nonylphenyl) phosphite (Weston TNPP; Borge-Warner Chemicals, Morgantown, WV) and nonylphenol (Pfaltz and Bauer, Stamford, CT) were used as received.

Procedure. A 25-ml portion of cyclohexane was pipetted into a 4-oz. widemouth bottle containing about 1 g of BDS pellets. The bottle was capped and placed on a shaker (Eberbach No. 5850) at 20-40 excursions per minute until dissolution was complete (about 1 h).

The solvent programmer was set at Program 6 (linear), to give from 100% heptane to 100% dichloromethane in 5 min. The detector was set at a sensitivity of 0.2 absorbance and the recorder chart speed was 1 cm min^{-1}. The heptane to methylene chloride gradient was run initially without a sample injection having been made. After about 12 min, the reset button on the programmer was pushed. After about 5 min, a peak (identified herein as the "reset" peak) appeared on the chart; this represents the heptane beginning to emerge from the column (Fig. 1). Sample and standard injections were all made at the point at which the reset peak dropped to the baseline. Duplicate injections (25 μl) of the sample solutions of TNPP and nonylphenol standard solutions (0.2—0.5 mg ml^{-1}) were made. The mobile phase gradient was started at the point of injection. The peak heights for TNPP and nonylphenol at retention volumes of about 8.6 ml and 17.3 ml, respectively, were measured to the nearest 0.5 mm. The positions of the peaks are shown in Fig. 1, along with the peaks for BHT and BDS polymer. A blank injection

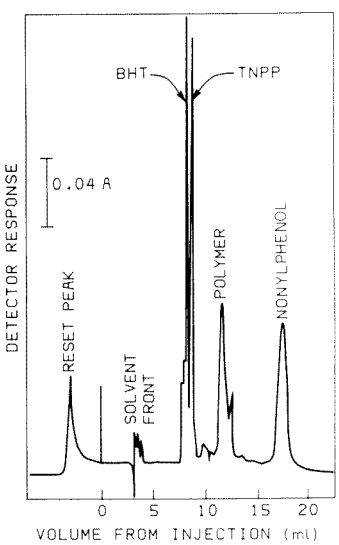

Fig. 1. Liquid chromatogram of additives in BDS copolymer on μPorasil with a heptane/dichloromethane mobile phase gradient. Sample, 984 μg of BDS; wavelength 280 nm.

of cyclohexane was made also to show from what point on the baseline peak-height measurements should be made.

Results and discussion

All concentrations are reported as weight percent.

Linearity of response. Studies with four sets of duplicate standards including zero showed linear response for peak height vs. amount injected up to 51.8 μg of TNPP and up to 29.1 μg of nonylphenol. Linear regression equations were $y = (6.74 \pm 0.08)\,x - 3.5 \pm 2$; $S_{yx} = 3.8$; $r = 0.9997$ for TNPP, and $y = (10.4 \pm 0.1)\,x - 0.3 \pm 2$; $S_{yx} = 2.9$; $r = 0.9997$ for nonylphenol where uncertainties are ± one standard deviation. The regression lines were used only to evaluate linearity. Sample peak heights were compared with the peak heights for duplicate standard injections made the same day.

Spiking studies. Spiking experiments were done by dissolving about 1 g of BDS pellets in cyclohexane containing known amounts of TNPP and nonylphenol. For duplicate sample runs at levels corresponding to 1.08% TNPP and 0.60% nonylphenol in the polymer sample, the average recoveries were 97% for TNPP and 92% for nonylphenol. For duplicate sample runs at levels corresponding to 0.50% TNPP and 0.26% nonylphenol, the average recoveries were 102% for TNPP and 94% for nonylphenol. Some spiking studies with nonylphenol alone were also done. For duplicate sample runs at levels of 0.22% and 0.43%, the average recoveries were 96% and 98%, respectively. Other spiking experiments were done with TNPP alone. For duplicate sample runs at levels corresponding to 0.49% and 0.10%, the average recoveries were 97% and 98%, respectively. The presence of BHT (Fig. 1) in some of the samples did not affect the accuracy of the TNPP determinations.

Sample size variation. Sample amounts of about 0.5, 1. and 2 g of BDS processed in duplicate gave results of 0.61—0.68% TNPP and 0.50—0.52% nonylphenol. Determination of TNPP alone in another BDS sample processed in duplicate (1 g) and singly (0.508 g and 2.01 g) gave results of 1.03% to 1.08% TNPP. All the above results indicated the absence of significant additive error.

Precision. Six replicate determinations were done for a BDS sample containing TNPP. The results were $\bar{x} = 1.04 \pm 0.0047\%$ (95% confidence) with $s = 0.0045\%$. For another BDS sample, containing both TNPP and nonylphenol, the results of six replicate determinations were $\bar{x} = 0.63 \pm 0.0079\%$ with $s = 0.0075\%$ for TNPP and $\bar{x} = 0.51 \pm 0.0105\%$ with $s = 0.0103\%$ for nonylphenol. The results from four replicate determinations with another BDS copolymer sample containing TNPP were $\bar{x} = 1.04 \pm 0.011\%$ with $s = 0.0087\%$. Three other BDS samples, each containing both TNPP and nonylphenol, were processed in duplicate. The pooled standard deviation was 0.020% for TNPP with average results ranging from 0.71% to 0.90%. For nonylphenol, the pooled standard deviation was 0.0032% with average results ranging from 0.36% to 0.50% for the three samples. All the above results show good repeatability for the method.

Standard purity. The occurrence of one large and two smaller adjacent peaks for TNPP and a somewhat broadened peak for nonylphenol in the chromatogram of a standard mixture suggested the presence of several isomeric structures for TNPP and nonylphenol. This was confirmed by mass spectrometry for a fraction corresponding to about 1 mg of TNPP collected following separations by h.p.l.c.

TNPP peak height variation. Several experiments showed that the TNPP peak height is dependent on the point of injection relative to the "reset peak", and that the dependence is quantitatively different for each of several different batches of heptane with and without small amounts of dichloromethane added. Peak heights for BHT [6] and nonylphenol were not affected. The phenomenon probably resulted from a specific interaction between TNPP and species present in the mobile phase [7], as any change on the stationary phase would have affected BHT peak heights as well, because it elutes near TNPP (Fig. 1). These dependencies do not detract significantly from the usefulness of the analytical method described above if injections are always made at the same point relative to the "reset peak" and if the same batch of heptane is used for standards and samples.

The authors thank Gil J. Greenwood for the mass spectrometric work with TNPP.

REFERENCES

1 R. W. Wise and P. H. Campbell, in Snell-Hilton Encyclopedia of Industrial Chemical Analysis, Vol. 6, Interscience, New York, 1968, pp. 117—120.
2 T. R. Crompton, Europ. Polym. J., 4 (1968) 473.
3 M. J. Shepherd and J. Gilbert, J. Chromatogr., 178 (1979) 435.
4 British Standards Institute, BS 2782; Part 4, Method 434A, Feb. 1975.
5 H. J. Brandt, Anal. Chem., 33 (1961) 1390.
6 J. F. Schabron and L. E. Fenska, Anal. Chem., 52 (1980) 1411.
7 L. R. Snyder, Principles of Adsorption Chromatography, M. Dekker, New York, 1968, pp. 216—225.

Analytica Chimica Acta, 129 (1981) 247—252
Elsevier Scientific Publishing Company, Amsterdam — Printed in The Netherlands

Short Communication

THERMODYNAMICS OF THE SECOND-STAGE DISSOCIATION OF *N*-(2-ACETAMIDO)IMINODIACETIC ACID IN WATER FROM 5 to 55°C

RABINDRA N. ROY*, JAMES J. GIBBONS, JORGE L. PADRON and RICHARD G. CASEBOLT

Department of Chemistry, Drury College, Springfield, MO 65802 (U.S.A.)

(Received 24th November 1980)

Summary. The thermodynamic second dissociation constants of the protonated form of *N*-(2-acetamido)iminodiacetic acid were determined at 12 temperatures from 5—55°C by measurement of the electromotive force using a cell without liquid junction, with hydrogen and silver—silver bromide electrodes. At 25°C, pK_2 is 6.844. The standard changes in Gibbs energy, enthalpy, entropy and heat capacity were derived from the change of the pK_2 values with temperature. At 25°C, ΔG^0 = 9335 cal mol^{-1}, ΔH^0 = 2928 cal mol^{-1}, ΔS^0 = −21.5 cal K^{-1} mol^{-1}, and ΔC_p^0 = −34 cal K^{-1} mol^{-1}. The results are interpreted and compared with those of structurally related compounds.

There is considerable interest in the control of pH in the biochemically important pH range 6—8 [1—4]. Buffer substances recommended by Good et al. [5] have been shown to be useful for pH measurement and control in this range [6—8]. These compounds are either *N*-substituted aminoethanesulfonic acids (MES, TES, HEPES, etc.), or derivatives of glycine (Tricine, Bicine, etc.).

As a prerequisite for the determination of conventional pa_H values in cells without liquid junction, as well as the pH values of buffer solutions in isotonic saline medium (ionic strength I = 0.16) in cells with liquid junction, attention has recently been drawn to *N*-(2-acetamido)iminodiacetic acid (ADA, I)

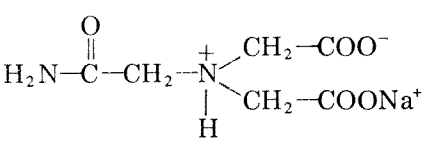

(I)

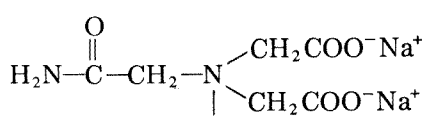

(II)

This ampholyte with a pK_2 value of 6.844 at 25°C is highly suitable for the control of pH between 5.7 and 7.7. As an extension of earlier studies of the thermodynamics of the dissociation of protonated weak bases [3, 9, 10], the pK_2 values and associated thermodynamic quantities of ADA at 12 temperatures from 5 to 55°C (including 37°C) were determined as described below.

0003—2670/81/0000—0000/$02.50

Experimental

Research-grade *N*-(2-acetamido)iminodiacetic acid (U.S. Biochemical Co.) was used. A CO_2-free solution of sodium hydroxide was prepared and standardized against multiple samples of primary-standard potassium hydrogenphthalate under CO_2-free conditions. This solution was added to ADA to form the monosodium and disodium salt solutions which were then used to prepare all the buffer solutions. Reagent-grade potassium bromide was recrystallized twice from conductivity water; it was heated at 200°C for 4 h and stored over Drierite.

In order to determine the standard potential of the Ag—AgBr electrode, reagent-grade hydrobromic acid solution was purified by distillation and bromide was determined gravimetrically as AgBr. Measurements of test cells using hydrogen and silver—silver bromide electrodes in a 0.01 mol kg^{-1} hydrobromic acid solution yielded results that were in agreement with the standard e.m.f. of the cell, as determined by Harned et al. [11] (average deviation of 0.04 mV), and those of Hetzer et al. [12] (average deviation of 0.08 mV). In the present study, the former data [11] were used for later calculations.

All six cell solutions were prepared individually by weight from ADA, KBr, the standard NaOH solution, and the CO_2-free distilled water in amounts giving approximately equimolal concentrations of NaADA, Na_2ADA, and KBr. Buoyancy corrections were applied to all weighings. Hydrogen was bubbled through each solution to remove dissolved air. The cells were filled as usual with the buffer solutions after air was excluded.

The preparation of the hydrogen electrodes [13] and the silver—silver bromide electrodes (thermal type) [14], the design of the all-glass cells [15], and other experimental details were as described previously [2, 10].

The initial e.m.f. measurements were made at 25°C. After the equilibrium values of the cells had been recorded, the e.m.f. measurements were repeated at intervals of 5°C from 25 to 5, back to 25, and then on to 55°C (including 37°C). The initial and the middle e.m.f. data at 25°C differed by not more than 0.06 mV on average, demonstrating the excellent reproducibility and stability of the cells.

Results and discussion

The dissociation constant was determined by the measurement of the e.m.f. of hydrogen—silver bromide cells without liquid junction of the type

$$Pt;\ H_2(g,\ 1\ atm)|ADA^z(m_1),\ ADA^{2-}(m_2),\ KBr(m_3)|AgBr;\ Ag \qquad (A)$$

where m is the molality. The e.m.f. was measured from 5 to 55°C at 5° intervals. Here the zwitterion of ADA is represented as ADA^z (I) and the disodium salt as ADA (II) and the second ionization step (i.e. removal of the proton from the substituted ammonium group of the derivative of glycine) is indicated by the equilibrium $ADA^z \overset{K_2}{\rightleftharpoons} H^+ + ADA^{2-}$, where K_2 is the thermodynamic equilibrium constant.

The pH of the buffer solutions of ADA and its sodium salt is so close to

TABLE 1

Experimental and calculated[a] values of pK_2 for ADA and Pipes

Temperature (°C)	ADA			Pipes[b]		
	pK_2(exp.)	s.d.	pK_2(calc.)	pK_2(exp.)	s.d.	pK_2(calc.)
5	7.011	0.004	7.015	7.277	0.009	7.272
10	6.968	0.004	6.966	7.238	0.008	7.241
15	6.924	0.004	6.921	7.207	0.008	7.209
20	6.884	0.004	6.880	7.171	0.010	7.176
25	6.844	0.004	6.842	7.141	0.006	7.141
30	6.796	0.007	6.808	7.109	0.010	7.106
35	6.780	0.004	6.777	7.073	0.010	7.071
37	6.763	0.004	6.760	7.053	0.009	7.050
40	6.749	0.004	6.748	7.035	0.010	7.034
45	6.723	0.003	6.723	6.997	0.010	6.997
50	6.704	0.005	6.700	6.959	0.011	6.959
55	6.678	0.006	6.680	6.918	0.011	6.920

[a]From eqn. (2). [b]Corrected values in contrast with those given earlier [3]. These corrections were necessary because of the error involved in the earlier calculation of the ionic strength.

neutrality that the correction for hydrolysis is negligible. In all instances, the stoichiometric molalities (m) of the acid, its sodium salt, and potassium bromide were nearly identical.

The e.m.f. of cell A is related to the "apparent" second dissociation constant, K_2', of ADA by

$$pK_2' = pK_2 - \log(\gamma_{ADA^z}\,\gamma_{Br^-}/\gamma_{ADA^{2-}}) = (E - E^0)F/(RT \ln 10)$$
$$+ \log(m_1 m_3/m_2) + 2AI^{1/2}/(1 + Ba_0 I^{1/2}) \quad (1)$$

where γ_{ADA^z} and $\gamma_{ADA^{2-}}$ indicate the activity coefficients of the monosodium salt of ADA and its disodium salt, respectively, and E^0 is the standard electrode potential of the silver—silver bromide electrode [11] and a_0 = 4.87 Å, so that Ba_0 = 1.6. As explained in earlier studies [2, 9, 10], the pK_2' is expected to be directly proportional to the ionic strength, I, which is given for cell A by $I = m_1 + 3m_2 + m_3$. The values of pK_2 listed in Table 1 were obtained by linear regression analysis using the equation $pK_2' = pK_2 - \beta I$, where the intercept at $I = 0$ yields the values of pK_2.

The calculated values of pK_2 (on the molal scale) entered in the third column of Table 1, were computed from

$$pK_2 = A/T + B + CT = 1740.2/T - 2.6842 + 0.01238T \quad (2)$$

where T is the thermodynamic temperature in K. The standard deviation for the fit was 0.004 for all eleven temperatures (excluding 37°C), but if the somewhat deviant point at 30°C was excluded, the standard deviation became 0.003. The constants in eqn. (2) were computed by fitting the experimental values of pK_2 at each temperature by the method of least squares to an equation of the form suggested by Harned and Robinson [16].

TABLE 2

Thermodynamic quantities (molal scale) for the dissociation (pK_2) of ADA and Pipes in water

Temp. (°C)	ADA ΔG^0 (cal mol^{-1})	s.d.	Pipes[a] ΔG^0 (cal mol^{-1})	s.d.	ADA ΔH^0 (cal mol^{-1})	s.d.	Pipes[a] ΔH^0 (cal mol^{-1})	s.d.
5	8928	5	9255	14	3581	141	2173	380
15	9125	3	9504	8	3260	91	2486	245
25	9335	3	9472	8	2928	48	2811	129
35	9555	3	9969	8	2585	51	3145	137
45	9787	3	10185	8	2230	99	3493	267
55	10030	5	10390	14	1864	157	3581	423

Temp. (°C)	ADA ΔS^0 (cal K^{-1} mol^{-1})	s.d.	Pipes[a] ΔS^0 (cal K^{-1} mol^{-1}	s.d.	ADA ΔC_p^0 (cal K^{-1} mol^{-1})	s.d.	Pipes[a] ΔC_p^0 (cal K^{-1} mol^{-1})	s.d.
5	−19.2	0.5	−25.5	1.3	−32	5	31	14
15	−20.4	0.3	−24.4	0.8	−33	5	32	15
25	−21.5	0.2	−23.2	0.4	−34	6	33	15
35	−22.6	0.2	−22.1	0.4	−35	6	34	16
45	−23.8	0.3	−21.0	0.8	−36	6	35	16
55	−24.9	0.5	−19.9	1.3	−37	6	36	17

[a]Recalculated from the equation $pK_2 = -461.24/T + 12.296 - 0.012100T$ for the reasons cited in the footnote in Table 1.

Thermodynamic functions. The standard thermodynamic quantities for the dissociation process $ADA^z \overset{K_2}{\rightleftharpoons} H^+ + ADA^{2-}$ were calculated by an application of the usual thermodynamic formulae to the constants of eqn. (2). The values from 5 to 55°C at 10° intervals for the standard changes of Gibbs free energy (ΔG^0), enthalpy (ΔH^0), entropy (ΔS^0) and heat capacity (ΔC_p^0) are given in Table 2. Also included are the standard deviations, which were estimated from the standard deviation of pK_2 by the method of propagation of error described by Please [17].

The values for pK_2 and the thermodynamic quantities for the dissociation of protonated ADA are compared in Table 3 with the corresponding values for zwitterionic species of related structure. This type of comparison was made at 25°C for the parent compound taurine and the derivatives of taurine, as well as the parent compound glycine and *N*-substituted glycines (such as ADA).

It can be seen from Table 3 that the values of pK_2 decrease uniformly from the parent compound taurine to *N*-substituted taurine (Pipes), and also from the parent compound glycine to its derivative (ADA). This enhancement in acidic strength for ADA is probably attributable to the inductive effects of the oxygen atoms form both COO^- groups, and $-\overset{O}{\overset{\|}{C}}-$, and the nitrogen atoms in $-NH_2$, as well as the steric effects of the three bulky substituent groups attached to the central nitrogen atom from which the deprotonation occurs.

TABLE 3

Thermodynamic quantities (molal scale) at 25°C for the dissociation of a series of structurally related compounds in water

Compound	pK_2	ΔH^0 (cal mol^{-1})	ΔS^0 (cal K^{-1} mol^{-1})	ΔC_p^0 (cal K^{-1} mol^{-1})	Ref.
$\bar{O}_3S-CH_2-CH_2-\overset{+}{N}H_3$ (taurine)	9.061	10000	−7.9	−8	20
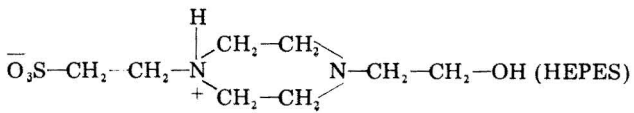	7.565	4870	−18.3	11	7
$\bar{O}_3S-CH_2-CH_2-\overset{+}{N}H_2-C(CH_2OH)_3$ (TES)	7.550	7680	−8.8	−4	7
$\bar{O}_3S-CH_2-CH_2-\overset{+}{N}H(C_2H_4OH)_2$ (BES)	7.187	5780	−13.5	−1	10
	7.187	5830	−13.3	0	7
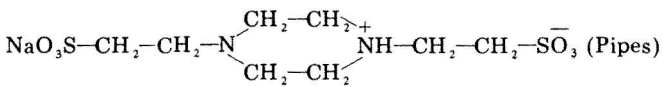	7.141	2811	−23.2	33	3
$H_3\overset{+}{N}-CH_2-COO^-$ (glycine)	9.780	10550	−9.4	−12	21
$(HO-CH_2-CH_2)_2=\overset{+}{N}H-CH_2-COO^-$ (Bicine)	8.333	6279	−17.1	1	18
$(HO-CH_2)_3\equiv C\overset{+}{N}H_2-CH_2-COO^-$ (Tricine)	8.135	7520	−12.0	−12	9
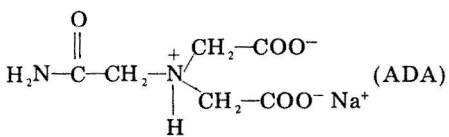 (ADA)	6.844	2928	−21.5	−34	This work

With the exception of Tricine, the values of ΔH^0 decrease from glycine to ADA for the isoelectric dissociation process, as expected. The values of both ΔS^0 and ΔC_p^0 for ADA are expected to be negative because electrostatic interactions with charged species (such as ADA^z, ADA^{2-} and H^+) will lead to orientations of solvent molecules (water) close to these ions, and consequently the order (negative entropy) is increased. For Bicine [*N*,*N*-bis-(2-hydroxyethyl)glycine], the value of ΔS^0 is reasonably close to that of ADA, but the difference in magnitude of ΔC_p^0 between ADA and Bicine is -35 cal K^{-1} mol^{-1}, which may be attributed to both the charge type [18] and the changes in water structure caused by nonelectrostatic effects [19]. The explanations of these complex interactions are still far from quantitative.

The pK_2 of ADA at 25°C is 6.844, and ADA is therefore of particular use as a secondary standard for pH measurements in clinical chemistry. More work is in progress to determine the pH of buffers composed of ADA, the sodium salt of ADA, and NaCl matching the ionic strength (I = 0.16) of blood serum, based on the e.m.f. of cells with and without liquid junction.

The authors thank Mr. Qui Duc Ta, Mr. David Bliss, Mr. Brad Baker and Mr. Mark Taylor for some preliminary work. They also acknowledge the National Institutes of Health for partial support (Grant NIH 1 R01 GM 26809-02 BMT).

REFERENCES

1 R. G. Bates, R. N. Roy and R. A. Robinson, Anal. Chem., 45 (1973) 1663.
2 R. N. Roy, E. E. Swensson, G. LaCross, Jr. and C. W. Krueger, Anal. Chem., 47 (1975) 1407.
3 R. N. Roy, J. J. Gibbons, J. L. Padron and J. Moeller, Anal. Chem., 52 (1980) 2409.
4 R. N. Roy, J. J. Gibbons, J. L. Padron, K. Buechter and S. Faszholz, Clin. Chem, 26 (1980) 1919.
5 N. E. Good, G. D. Winget, W. Winter, T. N. Connolly, S. Izawa and R. M. M. Singh, Biochemistry, 5 (1966) 467.
6 M. Sankar and R. G. Bates, Anal. Chem., 50 (1978) 1922.
7 C. A. Vega and R. G. Bates, Anal. Chem., 48 (1976) 1293.
8 R. G. Bates, C. A. Vega and D. R. White, Jr., Anal. Chem., 50 (1978) 1295.
9 R. N. Roy, R. A. Robinson and R. G. Bates, J. Am. Chem. Soc., 95 (1973) 8231.
10 R. N. Roy, J. J. Gibbons, C. Krueger and G. LaCross, Jr., J. Chem. Thermodyn., 9 (1977) 325.
11 H. S. Harned, A. S. Keston and J. G. Donelson, J. Am. Chem., Soc., 58 (1936) 989.
12 H. B. Hetzer, R. A. Robinson and R. G. Bates, J. Phys. Chem., 66 (1962) 1423.
13 R. G. Bates, Determination of pH, J. Wiley, 2nd edn., Ch. 10, 1973.
14 R. Gary, R. G. Bates and R. A. Robinson, J. Phys. Chem., 68 (1964) 1187.
15 R. N. Roy, R. A. Robinson and R. G. Bates, J. Chem. Thermodyn., 5 (1973) 559.
16 H. S. Harned and R. A. Robinson, Trans. Faraday Soc., 36 (1940) 9373.
17 N. W. Please, Biochem. J., 56 (1954) 196.
18 H. S. Harned and B. B. Owen, The Physical Chemistry of Electrolytic Solutions, 3rd edn., Reinhold, New York, 1958, Ch. 15.
19 S. P. Datta, A. K. Grzybowski and R. G. Bates, J. Phys. Chem., 68 (1964) 275.
20 E. J. King, J. Am. Chem. Soc., 75 (1953) 2204.
21 E. J. King, J. Am. Chem. Soc., 67 (1945) 2178.

Analytica Chimica Acta, 129 (1981) 253—257
Elsevier Scientific Publishing Company, Amsterdam — Printed in The Netherlands

Short Communication

EVALUATION OF PULSED-STIRRING VOLTAMMETRY

JOSEPH WANG

Department of Chemistry, New Mexico State University, Las Cruces, NM 88003 (U.S.A.)

(Received 24th February 1981)

Summary. The technique of pulsed-stirring voltammetry at a stationary electrode, in which a current difference is measured between two degrees of stirring is described. The response of this technique is characterized with respect to concentration dependence, reproducibility, response time, modulation frequency, detection limit, and other variables. Ascorbic acid, epinephrine, hexacyanoferrate(II), and dopamine were used as test systems. Calibration plots of current vs. concentration are linear. For ascorbic acid, the sensitivity is near 30 nA μM^{-1}. For hexacyanoferrate(II), the detection limit is near 0.24 μM. detection limit is near 0.24 μM.

Increasing effort is being directed toward the development of reliable and simple analytical techniques employing solid electrodes. Hydrodynamic modulation voltammetry (h.m.v.) using forced convective solid electrodes is a method which has gained increasing attention in recent years. The principles, applications, and recent developments of h.m.v. have been reviewed recently [1]. The technique is based upon pulsing the flux of electroactive material at the electrode surface between two rates and measuring the corresponding current difference that is free from most background interferences. Various procedures for pulsing solutions hydrodynamically have been described; these include varying the speed of a rotated disk electrode [2, 3] or modulating the flow rate of solution passing through or past a stationary electrode [4, 5]. While a considerable amount of progress has been made in developing reliable h.m.v. procedures, the technique has not yet become widely used. One of the problems is that rotating disk electrode (RDE) assemblies with programming circuitry for changing the rotation speed are not available commercially. Some of the difficulties which arise in setting up a "home-made" RDE have been noted [6].

This communication presents an alternative method for h.m.v., called pulsed-stirring voltammetry, in which a current difference is measured between different stirring rates. The angular motion of a stirred solution has long been used to transport electroactive material to electrode surfaces [7]. Some characteristics of a procedure that involves modulation of the stirring rate of a sample solution near the surface of a stationary disk electrode, by means of simple magnetic stirring, are described below.

Experimental

Apparatus. A 200-ml (6.5-cm-diameter, 7.5-cm high) pyrex glass cell with a 4-hole plexiglas cover was employed. A 0.75-cm diameter glassy carbon disk (Model DDI, Pine Instruments Co., Grove City, PA) served as the working electrode. The cell was joined to a reference electrode (Ag/AgCl, Model RE-1, Bioanalytical Systems, West Lafayette, IN) and a counter electrode (a Pt coil immersed in 0.1 M phosphate buffer) via salt bridges through two holes in its cover. The working electrode was mounted on a rotating disk assembly (Model PIR, Pine Instruments Co.), allowing direct comparison of the pulsed-stirring experiments with those of so-called stopped-rotation voltammetry [8]. The cell was placed on a magnetic stirrer (Sargent-Welch, model 76490) and a 3.5-cm long magnetic stirring bar (Sargent-Welch, 5-76507-40-R) was placed in the center of the cell bottom, exactly 2.5 cm below the center of the glassy carbon disk. The working electrode was initially polished with 0.1-μm alumina slurry until a mirror-like finish was obtained. The three electrodes were connected to a Princeton Applied Research Model 364 Polarographic Analyzer, the output of which was displayed on a Houston Omniscribe strip-chart recorder. The arbitrary scale of the stirrer controller was calibrated with a digital tachometer (Model 8211, Cole-Parmer Inc.). The stirring settings 1, 3, 5, 7, and 9 yield stirrer speeds of 180, 265, 425, 660, and 1020 rpm, respectively, with an error of about 3% caused by difficulties in reproducing the same setting.

Procedure. A 200-ml aliquot of the buffer was pipetted into the cell and the electrode was pretreated by cycling the applied potential between +1.1 V and −1.1 V for 10 min, allowing 2 min at each potential. Following this, measurements were made on blank sample solutions and data were corrected for background. Pulsed-stirring experiments were done by switching manually between low and high stirring speeds 15 s to 3 min after the working potential was applied. All data reported are based upon the arbitrary scale of the controller. Stopped-stirring voltammograms were developed pointwise by making 100-mV changes in applied potential and waiting about 30 s before applying the stirring pulse.

Reagents. Deionized water was used to prepare all solutions. The supporting electrolyte was 0.10 M phosphate buffer (pH 7.4), prepared from a 1:4 mixture of KH_2PO_4 and K_2HPO_4. Millimolar stock solutions of $K_4Fe(CN)_6 \cdot 3H_2O$, ascorbic acid (analytical grade, Baker Chemical Co.), epinephrine, and dopamine (reagent grade, Sigma Chemical Co.) were prepared each day. Aliquots of the stock solution were added to the supporting electrolyte to give the desired concentrations.

Results and discussion

Characteristics of pulsed-stirring currents. Mass-transport processes in stirred solutions are difficult to evaluate because of the complex dependence of the transport on cell geometry and the mode of stirring [9]. An approximate theoretical analysis of the limiting current of a stationary electrode

with a stirred solution has been formulated recently [10]. In practice, however, quantitative applications of hydrodynamic voltammetry usually rely on calibration with suitable standards so that an established theoretical treatment is not essential.

Figure 1 presents characteristics of pulsed-stirring reponses for epinephrine with different cycling times and stirring rates. The times required to reach steady state in the stopped-stirring mode are about 7 s (on) and 25 s (off) (Fig. 1, A). The response times for the pulsed-stirring mode are about 4 s (high) and 3 s (low) (Fig. 1, D). The measurement cycle time in the stopped-stirring mode can be shortened by making measurements before steady state is achieved (Fig. 1, B and C). This may be the best compromise between sensitivity and speed because decreasing the on—off periods slightly decreases the sensitivity but significantly reduces the length of the measurement cycle; it is noteworthy that the 44% and 78% reductions in the cycling period (curves B and C vs. A) result in current reductions of only 9% and 33%, respectively. The relatively rapid stopped-stirring approach (5 s on, 5 s off) yields a current difference larger than that of the steady-state pulsed-stirring approach as illustrated by curves C and D. The precision of the stopped-stirring operation is better than that of the pulsed-stirring. Of the stirrer settings examined for the stopped-stirring mode, a setting of 7 gave the best analytical results; higher settings produced turbulent motion and bubbles, with significantly increased noise levels and without increased depolarizer response. The dependence of the current on ascorbic acid concentration was examined in the steady-state (15 on, 35 off) and non-steady-state (10 on, 10 off) versions of the stopped-stirring mode (with other conditions as in Fig. 1 except that the applied potential was +0.9 V). For ascorbic acid between 2.5 and 15μM, regression equations were $I_{ss} = (318 \pm 6)C + 139 \pm 61$ nA with $S_{yx} = 65$ nA for steady-state and $I_{nss} = (281 \pm 6)C + 87 \pm 56$ nA with $S_{yx} = 60$ nA for nonsteady-state. These data confirm good linearity for the measurements.

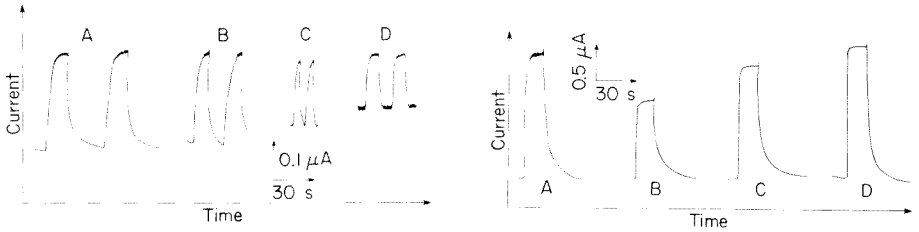

Fig. 1. Pulsed-stirring response for the oxidation of 7 μM epinephrine. Stirrer settings: (A—C) 7 (on) and 0 (off); (D) 7 (high) and 3 (low). Cycling times: (A) 15 s (on) and 30 s (off); (B) 10 s (on) and 15 s (off); (C) 5 s (on) and 5 s (off); (D) 10 s (on) and 10 s (off). Applied potential +0.5 V; supporting electrolyte, 0.1 M phosphate buffer pH 7.4.

Fig. 2. Stopped-stirring (A) and stopped-rotation (B—D) response for 10 μM $K_4Fe(CN)_6$. Cycling times: 15 (on) and 30 (off) s. Stirrer setting (on): (A) 7. Rotation speed (on): (B) 400; (C) 900; (D) 1600 rpm. Applied potential +0.6 V; supporting electrolyte, 0.1 M phosphate buffer.

Figure 2 compares the stopped-stirring (A) and stopped-rotation (B—D) [8] currents obtained for the oxidation of 10 μM potassium nexacyanoferrate(II). Stopped-rotation volammetry is the most sensitive modulated approach with rotating disk electrodes because it involves 100% modulation [8]. The stopped-stirring response (A) yields 38% and 11% larger currents than those of the stopped rotation between 400 and 0 rpm (B), and between 900 and 0 rpm (C), respectively. Stopped-rotation voltammetry between 1600 and 0 rpm (D) yields a slightly larger (5%) current difference than that obtained by the stopped-stirring procedure. While the sensitivity of the stopped-stirring procedure is similar to that of stopped-rotation voltammetry, the limit of detection with modulated rotating disk electrodes is lower because of its lower noise level (about 10 nA compared to about 45 nA for the stopped-stirring procedure).

Current—potential curves. The attainment of reproducible current—potential data for low concentrations of electroactive species at solid electrodes is difficult using conventional potential scanning techniques. Techniques described herein can overcome this limitation as was demonstrated with modulated rotating and flow-through electrodes [2, 3, 5]. Figure 3 shows a stopped-stirring current—potential curve for the oxidation of 7 μM epinephrine, together with the corresponding background current (dotted line). The rapidly rising wave and plateau are well-defined. The background current is very low, indicating good correction for nonconvective currents and the absence of electroactive contaminants. The stopped-stirring half-wave potential is +0.085 V.

Precision and detectability. The precision of results was estimated by 12 successive stopped-stirring measurements of 3.75 μM dopamine (conditions: stirrer setting 7 for 15 s and 0 for 40 s; 0.9 V applied potential; 0.1 M phosphate buffer pH 7.4). The mean current found was 198.7 nA with a range of

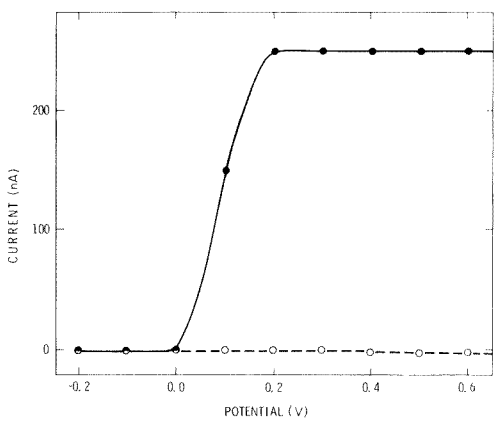

Fig. 3. Hydrodynamic voltammogram for 7 μM epinephrine. Stopped-stirring conditions: 15 s (on, 7); 30 s (off). Supporting electrolyte, 0.1 M phosphate buffer. (○) Background; (●) sample.

197.0—200.5 nA and a standard deviation of 1.3 nA. For the manual operation described here, the stopped-stirring mode yields more reproducible measurements than those achieved by the pulsed-stirring mode because the two convection rates can be more precisely controlled (on—off vs. level changes), and the noise level for the off setting is reduced.

A 1.9 μM solutions of potassium hexacyanoferrate(II) in 0.1 M phosphate buffer gave a current amplitude of 320 nA with a noise level of 40 nA, corresponding to a limit of detection near 0.24 μM (conditions as in Fig. 2A).

No attempt was made to study the effect of different cell dimensions on the signal-to-noise ratio. Different stirring apparatus and/or different stirring modes such as a rotating stirrer coaxial to a stationary electrode [10] may yield lower noise levels.

The support of the Research Center of the College of Arts and Sciences (NMSU) through its Minigrant Program is gratefully acknowledged.

REFERENCES

1 J. Wang, Talanta, in press.
2 B. Miller and S. Bruckenstein, Anal. Chem., 46 (1974) 2026.
3 W. J. Blaedel and R. C. Engstrom, Anal. Chem., 50 (1978) 476.
4 W. J. Blaedel and D. Iverson, Anal. Chem., 49 (1977) 1563.
5 W. J. Blaedel and J. Wang, Anal. Chem., 53 (1981) 78.
6 S. Hamada, M. Itoh and H. Matsuda, J. Electroanal. Chem., 91 (1978) 107.
7 P. Delahay, New Instrumental Methods in Electrochemistry, Interscience, New York, 1954, p. 221.
8 J. Wang, Anal. Chem., August (1981) in press.
9 R. N. Adams, Electrochemistry at Solid Electrodes, M. Dekker, New York, 1969, p. 67.
10 B. V. Ratna Kumar and S. Sathyanarayana, J. Electroanal. Chem., 112 (1980) 207.

Analytica Chimica Acta, 129 (1981) 259—261
Elsevier Scientific Publishing Company, Amsterdam — Printed in The Netherlands

Short Communication

FLAME EMISSION INHIBITION TITRATION PROCEDURE FOR THE DETERMINATION OF TRACES OF TITANIUM

M. TADDIA

G. Ciamician Chemical Institute, University of Bologna, I-40126 Bologna (Italy)

(Received 4th March 1981)

Summary. Calcium atomization inhibition titration followed by release with lanthanum is applied to the determination of titanium (0.05—1 μg ml^{-1}). The detection limit is 15 ng ml^{-1}. The effect of some interfering ions that form involatile calcium compounds is examined.

Conventional atomic absorption methods for the determination of titanium, involve the use of a nitrous oxide—acetylene flame. Although higher sensitivity is the main consideration in using this flame, its cost and the precautions necessary call for more convenient procedures. Recent developments in titrimetry have extended the application of flame emission inhibition effects for the determination of a number of cations and anions [1, 2]. Liu and Huber [2] have reported the determination of aluminum by atomic emission spectrometry with calcium atomization inhibition titration and subsequent lanthanum release. As titanium proved to interfere strongly, this suggested the possibility of using the same technique for its determination.

Experimental

Apparatus. Emission measurements were made with a Perkin-Elmer 372A atomic absorption spectrometer with flame emission capability. The flow rates of air and hydrogen were adjusted to obtain the maximum depressive effect of titanium on the calcium signal. The wavelength used was 422.7 nm and the nominal bandpass 2 nm.

Reagents. A titanium standard solution (1000 μg ml^{-1}; titanium tetrachloride in hydrochloric acid; Merck) was used to prepare 0.05—1 μg ml^{-1} solutions daily. To prevent hydrolysis, all standards were made 0.2 M in hydrochloric acid. Titrant solutions of calcium (20 μg ml^{-1}) and lanthanum (1000 μg ml^{-1}) were prepared from the chloride and nitrate, respectively.

Procedure. The sample solution (100 ml), 0.2 M in hydrochloric acid, was titrated with calcium to reach the appropriate calcium emission signal (I_0). Lanthanum was then added until a new constant emission reading was obtained. The signal enhancement (ΔI) caused by the lanthanum releasing effect was determined. A blank solution was also measured. Titrant flow

rates were 3.0 ml min^{-1} for calcium and 4.0 ml min^{-1} for lanthanum. The aspiration rate was 4.8 ml min^{-1}.

Results and discussion

The titanium inhibition effect on calcium atomic absorption in the acetylene—air flame is well documented [3]. The cooler hydrogen—air flame was expected to emphasize this effect. Figure 1 shows the interference curve; with rising concentration of the interfering ion, the depression of the signal approaches saturation. A decrease of about 97% on the calcium emission was observed for a titanium/calcium molar ratio of 6:1. Such severe inhibition can be ascribed to the formation of calcium metatitanate [4], which decreases the concentration of calcium atoms in the flame. On this basis the atomization inhibition titration method was developed.

Titrations were carried out on solutions containing 0.05—1 μg Ti ml^{-1}. Values of I_0 between 0.100 and 0.140 were found to give reproducible values of ΔI. The lanthanum titrant concentration must be carefully controlled. The magnitude of ΔI was found to increase with increasing lanthanum concentration and then to become constant in the range 1000—2000 μg La ml^{-1}. This suggests that the releasing action is progressive. A calibration graph of ΔI vs. titanium concentration was constructed. It was curved at higher titanium concentrations (Fig. 2), but the curve is sufficiently reproducible to be useful analytically. Ten repetitive determinations on 0.05

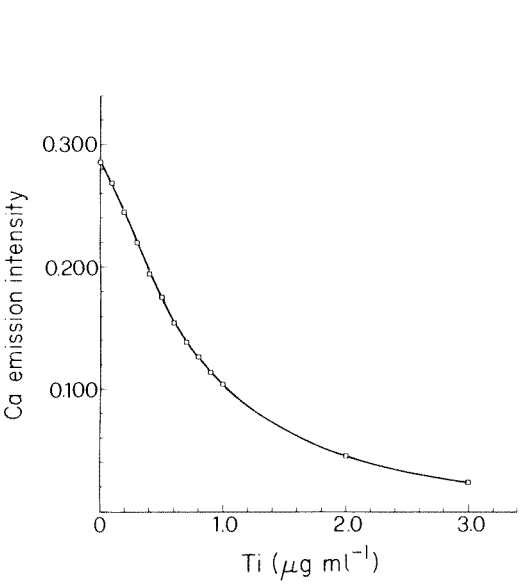

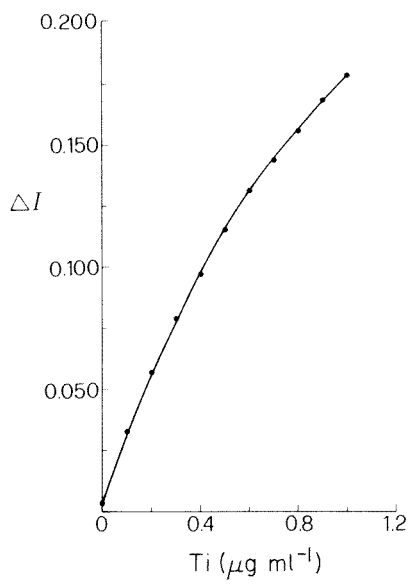

Fig. 1. Effect of titanium on the emission of calcium in the hydrogen—air flame (1 μg Ca ml^{-1}, 0.2 M HCl).

Fig. 2. Calibration graph for titanium. For conditions, see text.

TABLE 1

Effect of various ions on titanium determination (0.2 μg ml^{-1})

Ion	Source	Concentration[a] (μg ml^{-1})	ΔI[b] (arbitrary units)	Ion	Source	Concentration[a] (μg ml^{-1})	ΔI[b] (arbitrary units)
$H_2PO_4^-$	KH_2PO_4	0.1	91	VO^{2+}	V_2O_5	0.5	83
		0.5	232			1.0	106
SiO_3^{2-}	Na_2SiO_3	0.1	96	Cr^{3+}	$CrCl_3$	10.0	64
		0.5	161	$Mo_7O_{24}^{6-}$	$(NH_4)_6Mo_7O_{24}$	10.0	53
SO_4^{2+}	Na_2SO_4	0.2	92	Mn^{2+}	$MnCl_2$	10.0	62
		0.5	119	Ni^{2+}	$NiCl_2$	10.0	57
WO_4^{2-}	Na_2WO_4	0.5	110	Co^{2+}	$CoCl_2$	10.0	58
		1.0	125	Cu^{2+}	$Cu(NO_3)_2$	10.0	56
Al^{3+}	$Al(ClO_4)_3$	1.0	68	Fe^{3+}	$FeCl_3$	10.0	63
		10.0	177				

[a]As the element. [b]With no interference present, $\Delta I = 58$.

μg Ti ml^{-1} samples gave a relative standard deviation of 5.6%. Accuracy was tested by analyzing synthetic samples containing known amounts (0.05—1 μg ml^{-1}) of titanium. Recovery was always better than 97%. The detection limit (3σ) was found to be 15 ng ml^{-1}.

The effect of foreign ions on the titanium determination was investigated. The results are shown in Table 1. Phosphate, sulfate, silicate, tungstate, vanadium and aluminum interfere strongly. This was expected from their ability to compete with titanium in the formation of refractories with calcium. The titration curve for a mixture of titanium and interfering ion does not show any characteristic point to permit a selective determination. This is usually the main limitation of the atomization inhibition titrations. However, by taking into consideration that both flame and electrothermal atomic absorption methods for titanium suffer from a number of interferences [5], the method described here may in some cases provide a useful alternative.

REFERENCES

1 J. R. Sand, J. H. Liu and C. O. Huber, Anal. Chim. Acta, 87 (1976) 79.
2 J. H. Liu and C. O. Huber, Anal. Chem., 50 (1978) 1253.
3 W. A. Magill and G. Svehla, Fresenius Z. Anal. Chem., 268 (1974) 177.
4 N. S. Poluéktov and R. A. Vitkun, Ukr. Khim. Zh., 26 (1960) 648.
5 M. Studnicki, Anal. Chem., 52 (1980) 1762.

Analytica Chimica Acta, 129 (1981) 263—267
Elsevier Scientific Publishing Company, Amsterdam — Printed in The Netherlands

Short Communication

DETERMINATION OF TRACE METALS IN ALUMINIUM OXIDE BY ELECTROTHERMAL ATOMIC ABSORPTION SPECTROMETRY WITH DIRECT INJECTION OF AQUEOUS SUSPENSIONS

ZDENĚK SLOVÁK* and BOHUMIL DOČEKAL

Research Institute of Pure Chemicals, Lachema, CS-621 33 Brno (Czechoslovakia)

(Received 3rd March 1981)

Summary. Trace amounts (10^{-5}—10^{-6}% w/w) of Ca, Cr, Cu, Fe, Na and Pb in aluminium oxide can be determined by graphite-furnace a.a.s. with injection of stirred sample suspensions into the tube. Calibration is possible either with Al_2O_3 standards for peak height and peak area measurements, or with standard solutions containing no aluminium for peak area measurements (except for copper). The analytical signals do not depend on the quantity of applied sample (0.02—1 mg Al_2O_3). Relative standard deviations are 2—6%.

Recently it has been shown that direct sampling and injection of solids in the form of simple aqueous suspensions for graphite-furnace atomic absorption spectrometry (a.a.s.) is possible [1]. This technique was applied to the determination of some elements (Hg, As, etc.) bound on selective organic sorbents [2, 3]. The sensitivity and reproducibility were similar to those obtainable with traditional manual sampling of solutions by means of micropipettes. In the present communication, the range of materials amenable to this technique is extended to inorganic powders, especially for the quality control of barely soluble chemicals of high purity.

The dissolution of aluminium oxide, especially its α-modification, and its subsequent analysis by a.a.s. is possible only after fusion or treatment of the sample with acids in an autoclave. The high levels of blanks make determination of low concentrations of certain elements, such as sodium, calcium and iron impossible. For this reason fine aluminium oxide powder was a very suitable subject to show that the proposed sampling and injection technique is applicable to inorganic powders.

Experimental

Instrumentation and materials. The atomic absorption spectrometer was a Perkin-Elmer 420 with a model 56 recorder and an HGA-74 graphite furnace. Standard graphite tubes were used, and 10, 20 and 50-μl Eppendorf pipettes were used for injection of aqueous suspensions and solutions.

Aluminium oxide (γ-and α-Al_2O_3) with particle size <20 μm was used. Its quality was tested by d.c. arc emission spectrography. It contained $<1 \times 10^{-4}$% Fe, Cr, Cu and Pb. Standard powders containing 1×10^{-3}%

and 1×10^{-2}% of Ca, Cr, Cu, Fe and Pb were prepared from an aluminium oxide sample of highest purity, which was mixed with a standard solution of the nitrates of the above metals, followed by evaporation and ignition at 600—700°C. Emission spectrography (and later, a.a.s.) showed that no losses took place during ignition up to 800°C, compared with standards dried at 110°C only.

Procedure. The quality of the water (or acid) used should first be established. A known volume (50 ml) of doubly distilled water or 0.01 M hydrochloric acid was placed in a teflon beaker and stirred with a magnetic stirrer. A 50-μl sample was removed by means of an Eppendorf pipette and placed in the HGA-74 furnace. The peak height for each element to be determined should have an absorbance $\leqslant 0.001$ (0.005 for sodium).

A weighed quantity of sample ($\geqslant 2$ g for 50 ml of suspension) was added to the liquid in the beaker and, during continuous magnetic stirring, known portions of the suspension (10, 20 or 50 μl) were sampled and injected as usual into the furnace. For calibration, aluminium oxide standards with known concentrations of impourities were applied. It is also possible to inject various volumes of a single standard suspension. The operating parameters for the HGA-74 and spectrometer are given in Table 1. All measurements were done with appropriate hollow-cathode lamps with automatic background correction.

Discussion and results

Figure 1 shows spectra of the non-selective absorption by the aluminium oxide matrix and their relationship to the chosen wavelengths for the determinations. The spectra were measured by means of a number of lines of a Ag—Ni—Cr—Cu multi-element hollow-cathode lamp. No selective atomic absorption could be observed at these lines using the automatic background corrector. The possibility of high-performance background correction is the limiting factor for the quantity of sample which can be applied, especially

TABLE 1

Operating parameters
(Data from Perkin-Elmer manuals were not verified)

	Ca	Cr	Cu	Fe	Na	Pb
Wavelength (nm)	422.7	357.9	324.7	372.0	589.5	283.3
Slit width (nm)	2.0	0.7	0.7	0.2	0.7	0.7
Char[a] (°C;s)	700;15	700;10	700;10	500;10	700;10	300;15
Atomize (°C;s)	2700;15	2700;15	2700;15	2700;10	2500;10	1850;10
Clean (°C;s)	—	—	—	—	2700;6	2700;6
Inert gas	N_2	Ar	Ar	N_2	Ar	N_2, Ar
Gas flow (ml min^{-1})	50	50	50	50	350	50

[a]Drying was at 100°C for 30 s.

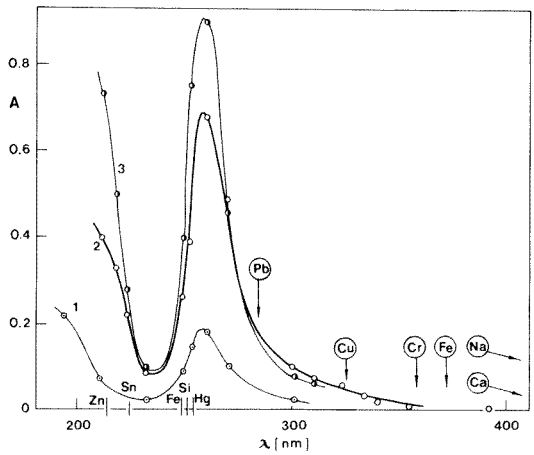

Fig. 1. Spectra of non-selective absorption. (1) 40 μg Al_2O_3, 350 ml N_2 min^{-1}; (2) 40 μg Al_2O_3, 50 ml N_2 min^{-1}; (3) 200 μg Al_2O_3, 350 ml N_2 min^{-1}.

in the determinations of lead (and Zn, Sn, Fe, Si, Hg at their main resonance lines marked in Fig. 1). For this reason, the less sensitive 372.0-nm line was selected for the determination of iron.

Apart from the background absorption caused by molecular absorption, and stray light reflected by solid particles, the maximum amount of applied sample is limited by the evaporation of the large amount of matrix in the atomization device during or after the atomization step. The recommended maximum sample weight of 1 mg of aluminium oxide injected into the furnace corresponds to 50 μl of a 2% (w/v) sample solution. The sensitivity of the proposed determination would be therefore at least as high as by applying a sample solution after dissolution. The detection limits, which depend on the fluctuations of the blanks, are significantly better when a suspension is used, because the "blank" of the proposed procedure comes solely from pure water, and is confirmed to be sufficiently small in the water—beaker—stirrer system immediately before the aluminium oxide sample is added. This possibility of complete elimination of blanks is unique in the analysis of barely soluble samples by a.a.s., and enables determinations of common elements such as Na, Ca, Mg and Fe to be achieved in ordinary analytical laboratories without any need for special equipment or high-purity chemicals.

For practical analysis, calibration with aluminium oxide standards is recommended. The quantity of oxide injected into the furnace has no significant influence on the analytical signals (in the range 0.02—1 mg of Al_2O_3 per injection). Therefore it is possible to use diluted suspensions of standards with relatively high known concentrations (e.g. 1×10^{-2}%) of added impurities, which can be checked separately after dissolution in an autoclave. Furthermore, it is possible to apply various portions of a single suspension for the calibration. The main analytical characteristics of the proposed procedure are summarized in Table 2.

TABLE 2

Analytical characteristics of the proposed procedure (peak height measurements)

	Ca	Cr	Cu	Fe	Na	Pb
Blank Abs.	0.005	0.002	0.002	0.005	0.01—0.03	0.002
S.d.[a]	0.002	0.001	0.001	0.002	0.01	0.001
Sensitivity[b] (ng)	0.015	0.015	0.052	0.13	0.012	0.066
Detection limit[c] (ng)	0.020	0.010	0.035	0.18	0.082	0.045
Max. sample injected (mg)	1	1	1	1	1	0.1
Detection limit in real sample ($\times 10^{-4}$%)	0.02	0.01	0.04	0.2	0.08	0.5
C.v. (%)[d]	1.5	2	2	5	6	5

[a]Standard deviation of 6 measurements. [b]Weight giving an absorbance of 0.0044. [c]Giving 3 standard deviations of the blank signal. [d]Coefficient of variation from 6 measurements on real samples giving a peak height absorbance of about 0.2.

TABLE 3

Slopes of calibration curves (absorbance ng^{-1})

	Al_2O_3 suspension		Al solution		Standard solution without Al	
	Height	Area	Height	Area	Height	Area
Ca	0.289	3.67	0.285	3.71	0.284	3.67
Cr	0.291	3.31	0.197	3.15	0.200	3.15
Cu	0.084	1.18	0.068	0.92	0.067	0.93
Fe	0.034	0.28	0.025	0.29	0.025	0.28
Pb	0.066	0.35	0.061	0.39	0.054	0.35

TABLE 4

Difference (%) in sensitivity with respect to a solution containing no aluminium (%)

	Al_2O_3 suspension		Al solution	
	Height	Area	Height	Area
Ca	+1.8	0	+0.4	+1
Cr	+46	+5	—1.5	0
Cu	+25	+27	+1.5	—1
Fe	+36	0	0	+4
Pb	+22	0	+13	+11

For studying possible chemical interferences, peak height and peak area sensitivities for injection of aluminium oxide suspensions were compared with those of aluminium salt solutions and standard solutions of nitrates of the determined metals in 0.01 M hydrochloric acid (Table 3). The amount of aluminium in any form injected into the tube was always 0.2 mg. Alu-

minium nitrate of special purity (for the determination of Cr, Cu, Fe and Pb) or a solution of aluminium oxide after autoclaving with hydrochloric acid (for Ca) were used in this comparison. It was not possible to make analogous measurements for sodium because of high blanks. Higher peak height sensitivities were observed for all elements determined when injected as suspensions, but peak area measurements were relatively similar. Table 4 shows that this phenomenon cannot be explained only in terms of chemical interferences: no influence of the presence of aluminium in the tube, if sampled as a solution, was observed in determinations of Ca, Cr, Cu or Fe. This problem does not only affect the analysis of aluminium oxide and for this reason it will be discussed in more detail in a later paper [4]. Thus, for calibration, if peak height measurements are to be made, aluminium oxide standards must be used. However, for peak area measurements, a standard solution containing no aluminium can be used for all the elements studied except copper (Table 3).

REFERENCES

1 Z. Slovák, Anal. Chim. Acta, 110 (1979) 301.
2 Z. Slovák and H. Dočekalová, Anal. Chim. Acta, 115 (1980) 111.
3 Z. Slovák and B. Dočekal, Anal. Chim. Acta, 117 (1980) 293.
4 Z. Slovák and B. Dočekal, Anal. Chim. Acta, 130 (1981) 000.

Analytica Chimica Acta, 129 (1981) 269—272
Elsevier Scientific Publishing Company, Amsterdam — Printed in The Netherlands

Short Communication

THE EFFECT OF ETHYLENEDIAMINE VS. GLYCIDOXY SIDE-CHAINS ON THE REACTIVITY OF ORGANOSILANES TOWARD SILICA SURFACES

RICHARD J. KVITEK, MARK W. WATSON, JOHN F. EVANS* and PETER W. CARR*
Department of Chemistry, University of Minnesota, Minneapolis, MN 55455 (U.S.A.)
(Received 5th March 1981)

Summary. Factors affecting the coverage of two organosilanes, N-2-aminoethyl-3-aminopropyltrimethoxysilane (1) and 3-glycidoxypropyltrimethoxysilane (2), bonded to silica have been investigated. The coverage of 1 is much higher than that of 2 for surfaces modified under identical reaction conditions. This is attributed to the rapid adsorption of 1 via specific interaction between the ethylenediamine group and the silanol groups of the silica surface. The difference in coverage is not simply due to pH differences. The nature of the side-chains of such silanes and the nature of the surface to be modified must be considered in the development of a derivatization scheme.

In view of the use of N-2-aminoethyl-3-aminopropyltrimethoxysilane [$(CH_3O)_3Si—(CH_2)_3—NH—(CH_2)_2—NH_2$, 1] in the preparation of chemically modified electrodes [1, 2], chromatographic supports [3, 4] and materials for use in preconcentration of trace analytes [5, 6], a brief study of the relative reactivity of 1 and a related compound 3-glycidoxypropyltrimethoxysilane [$(CH_3O)_3Si—(CH_2)_3—O—CH_2—\underset{\diagdown\,O\,\diagup}{CH}—CH_2$, 2] towards silica surfaces was undertaken.

Compound 2 was chosen for comparison to 1 for several reasons. Both molecules are very similar in terms of physical size and molecular weight. The reactive portion of each is the same and both are water-soluble. Furthermore, compound 2 can be assayed after attachment by the reaction of periodate with the bound diol arising from hydrolysis of the oxirane ring [7].

Experimental

Chemicals. All chemicals were reagent grade or equivalent. The silica used was 230—400 mesh Fractosil 500 (Merck) with an average pore diameter of 42 nm. In all calculations, the manufacturer's estimates of a surface area of 50 $m^2\ g^{-1}$ and a pore volume of 0.8 $cm^3\ g^{-1}$ were assumed. The silanes were obtained from Petrarch Systems, Inc. (Levittown, PA). Compound 1 was vacuum-distilled and stored under vacuum in glass ampoules. Upon receipt, 2 was stored under nitrogen in sealed glass ampoules.

Procedure. The reaction scheme used here has been reported to yield a

0003—2670/81/0000—0000/$02.50

uniform monolayer of bound silane when 3-aminopropyltrimethoxysilane was reacted with controlled pore glass [8, 9]. Prior to derivatization, the silica was pretreated by soaking overnight in concentrated nitric acid at room temperature, followed by thorough rinsing with deionized water and drying at 110°C. In this work, 5 g of silica was suspended in 50 ml of deionized water, and placed in an ultrasonic bath under reduced pressure until outgassing ceased. The silane (1 ml) was added to 10.0 ml of water and dissolved by stirring. The silica slurry and silane solution were then combined and allowed to react for 1 min with vigorous stirring. After reaction, the supernatant liquid was rapidly removed by filtration through a fritted glass funnel. The derivatized material was then dried and "cured" by heating for 24 h at 50°C and atmospheric pressure, followed by 24 h at 110°C and 2.6×10^2 Pa.

Samples reacted with **1** were passed through a 200-mesh sieve to break up aggregates and then total nitrogen was determined. Those samples reacted with **2** did not require sieving and were analyzed for total carbon and assayed titrimetrically by the periodate oxidation method [7]. The titration procedure was modified by the use of a 35% (v/v) solution of perchloric acid in water to insure the complete hydrolysis of the oxirane ring to a diol.

Results and discussion

As shown in Table 1, the derivatization reactions under conditions in which the silane concentrations were the same, gave markedly different degrees of coverage. It was suspected that this discrepancy might result from a difference in the pH of the reaction solution, because of the presence of amine functionalities in **1**, which are absent in **2**. The pH of the unbuffered solution of **1** (1:60 silane:water) was found to be in the range 10—11 whereas the pH of the unbuffered solution of **2** was 3—4. To assess any effect that this might have on the coupling chemistry, a borate buffer solution was substituted for the water used in the coupling reaction such that the reaction was carried out at pH 9 in both cases. These results (Table 1) show that, although increasing the pH of the reaction mixture did increase the coverage of **2** (by a factor of approximately 1.5), the coverage obtained was still much less than that found for **1**. It is evident that the loading of **1** in buffer is much greater than that of **2** under the same conditions.

TABLE 1

Amount of silane bound to silica gel

Reaction solution	Silane coverage (μmol m^{-2})		
	Silane 1	Silane 2	
	N determination	C determination	Diol determination
Unbuffered	4.2 ± 0.1	1.1 ± 0.1	1.1 ± 0.2
Buffered	4.0 ± 0.1	1.8 ± 0.1	1.3 ± 0.2

The possibility that the difference in coverage could be due to strong adsorption of **1** was evaluated by substituting an equimolar solution of ethylenediamine for the silane in the coupling procedure. The ethylenediamine which was not adsorbed was collected and quantified by thermometric titration with copper(II). The amount of ethylenediamine retained by the silica corresponded to 3.0 (±0.2) μmol m^{-2}. The maximum amount of ethylenediamine which could be trapped in the pores of the silica is calculated to be 1.2 μmol m^{-2}, assuming the concentration of ethylenediamine in the pore volume to be equal to that in the bulk solution. It was found that upon wetting and filtration, the weight of a silica sample increases by an amount equal to the weight of water corresponding to the pore volume of the sample. By using the concentration of ethylenediamine in the original sample and the pore volume of the sample, an estimate can be made of the amount of ethylenediamine trapped in the pore volume. The difference (1.8 μmol m^{-2}) is attributed to the quantity of ethylenediamine adsorbed on the silica surface. Furthermore, increasing the contact time of the ethylenediamine solution with the silica did not affect the quantity of ethylenediamine retained, indicating the adsorption process for **1** could reach equilibrium during the time frame of the coupling reaction (1 min).

It is concluded that the adsorption of the ethylenediamine-like portion of **1** on the silica surface has a much greater effect on the degree of coverage of **1** vs. **2** than does the pH of the reaction mixture. The difference between the coverages of **1** (1.6 μmol m^{-2}, after correction for the amount possibly adsorbed) and **2** (0.92 μmol m^{-2}) obtained by reaction at pH 9 suggests that there is an additional factor beyond adsorption involved in the relatively high reactivity of **1** towards silica. The presence of amines in reaction mixtures of silica and alkoxysilanes activates the surface silanol groups toward silylation. This effect of catalysis by amines has been reported previously [10]. The extent of amine catalysis could not be addressed directly by using **1** vs. **2** in the presence of amines, owing to the reactivity of **2** towards amines, because the assay utilized for bound **2** depends on the preservation of the epoxide group during the coupling and drying sequence. It is quite clear that the "unreactive" segment(s) of an organosilane can play an extremely important, if not central, role in determining the degree of coverage of these coupling agents in reaction with the surface hydroxyl groups on silica. Similar reaction conditions for dissimilar silanes bearing the same reactive groups will not necessarily yield comparable coverages of silane. It is hoped that the results presented above might clarify some of the idiosyncratic behavior which has been observed using materials modified with **1**.

R. J. K. acknowledges the financial support of the 3M Company in the form of a fellowship. This research was supported in part by a grant from the National Institutes of Health (grant R01-GM27581-01), and acknowledgement is made to the donors of The Petroleum Research Fund, administered by the ACS for partial support of this work (grant 10733-G3).

REFERENCES

1 P. R. Moses, L. M. Wier, J. C. Lennox, H. O. Finklea, J. R. Lenhard and R. W. Murray, Anal. Chem., 50 (1978) 576.
2 D. D. Hawn and N. R. Armstrong, J. Phys. Chem., 82 (1978) 1288.
3 F. K. Chow and E. Grushka, Anal. Chem., 49 (1977) 1756.
4 N. Becker and K. K. Unger, Chromatographia, 12 (1979) 539.
5 D. E. Leyden, G. H. Luttrell, A. E. Sloan and N. J. De Angelis, Anal. Chim. Acta, 84 (1976) 97.
6 D. E. Leyden, G. H. Luttrell, W. K. Nonidez and D. B. Werho, Anal. Chem., 48 (1976) 67.
7 F. E. Regnier and R. J. Noel, Chromatogr. Sci., 14 (1976) 316.
8 L. D. Hall and J. C. Waterton, J. Am. Chem. Soc., 101 (1979) 3697.
9 J. C. Waterton, Oxford University, personal communication, 1979.
10 L. Boksanyi, O. Liardon and E. Sz. Kovats, Adv. Coll. Interface Sci., 6 (1976) 95.

Analytica Chimica Acta, 129 (1981) 273
Elsevier Scientific Publishing Company, Amsterdam — Printed in The Netherlands

Errata

The publishers would like to apologize for the poor reproduction of the following figures.

Y. Talmi, H. P. Sieper and L. Moenke-Bankenburg, Laser-Microprobe Elemental Determinations with an Optical Multichannel Detection System.
Anal. Chim. Acta, 127 (1981) 71—85.

p. 77. Fig. 4 should have appeared as:

Fig. 4. Photograph of craters formed along the edge of a razor blade as the laser beam is gradually defocussed. Magnification, × 20.

A. M. Bond, H. A. Hudson and P. A. van den Bosch, High Flow-Rate Cells for Continuous Monitoring of Low Concentrations of Electroactive Species by Polarography and Stripping Voltammetry at the Static Mercury Drop Electrode.
Anal. Chim. Acta, 127 (1981) 121—133.

p. 126. Fig. 3(a) should have appeared as:

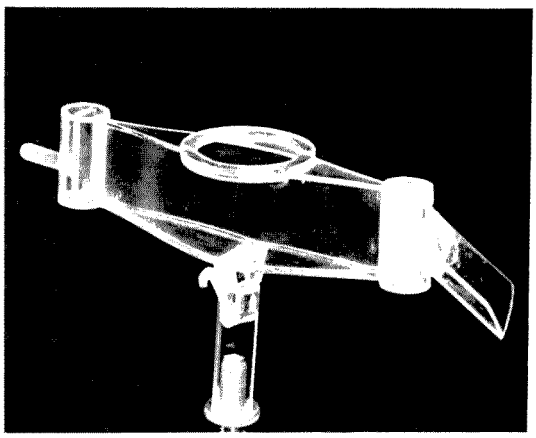

Fig. 3(a) Photograph of continuous flow cell B.

ANALYTICA CHIMICA ACTA, Vol. 129 (1981)

AUTHOR INDEX

(continued from back cover)

Short Communications

Elsevier Scientific Publishing Company, 1981

Printed in The Netherlands.

VOL. 129 ANALYTICA CHIMICA ACTA AUGUST 1. 1981

CONTENTS

(continued on inside page of cover)